SECURITY CLASSIFICATION OF THIS PAGE (When Data Entered)

REPORT DOCUMENTATION PAGE

1. REPORT NUMBER	2. GOVT AC
GRL/9301	

4. TITLE (and Subtitle)
PROOF OF THE FEASIBILITY OF COHERENT AND INCOHERENT SCHEMES FOR PUMPING A GAMMA-RAY LASER

5. TYPE OF REPORT & PERIOD COVERED
Final Report
12/24/89 - 5/31/93

6. PERFORMING ORG. REPORT NUMBER

7. AUTHOR(s)
C. B. Collins

8. CONTRACT OR GRANT NUMBER(s)
N00014-90-K-2001

9. PERFORMING ORGANIZATION NAME AND ADDRESS
University of Texas at Dallas
Center for Quantum Electronics
P.O. Box 830688
Richardson, TX 75083-0688

10. PROGRAM ELEMENT, PROJECT, TASK AREA & WORK UNIT NUMBERS

11. CONTROLLING OFFICE NAME AND ADDRESS
INNOVATIVE SCIENCE AND TECHNOLOGY DIRECTORATE
OF STRATEGIC DEFENSE INITIATIVE ORGANIZATION

12. REPORT DATE
8/31/93

13. NUMBER OF PAGES
216

14. MONITORING AGENCY NAME & ADDRESS (if different from Controlling Office)
Dr. Paul Kepple
Naval Research Laboratory
4555 Overlook Avenue, S.W.
Washington, D.C. 20375-5000
Attn: Code 4720

15. SECURITY CLASS. (of this report)
Unclassified

15a. DECLASSIFICATION/DOWNGRADING SCHEDULE

16. DISTRIBUTION STATEMENT (of this Report)
This document has been approved for public release and sale; its distribution is unlimited.

17. DISTRIBUTION STATEMENT (of the abstract entered in Block 20, if different from Report)

18. SUPPLEMENTARY NOTES

19. KEY WORDS (Continue on reverse side if necessary and identify by block number)
Gamma-ray laser, Ultrashort wavelength laser

20. ABSTRACT (Continue on reverse side if necessary and identify by block number)
The most productive approaches to the problem of the gamma-ray laser have focused upon upconversion techniques in which metastable nuclei are pumped with long wavelength radiation. At the nuclear level the storage of energy can approach tera-Joules (10^{12}J) per liter for thousands of years. However, any plan to use such a resource for a gamma-ray laser poses problems of a broad interdisciplinary nature requiring the fusion of concepts taken from relatively unrelated fields of physics. Our research group has described

(continued on next page)

DD FORM 1 JAN 73 1473 EDITION OF 1 NOV 65 IS OBSOLETE
S/N 0102-LF-014-6601

SECURITY CLASSIFICATION OF THIS PAGE (When Data Entered)

DISCLAIMER NOTICE

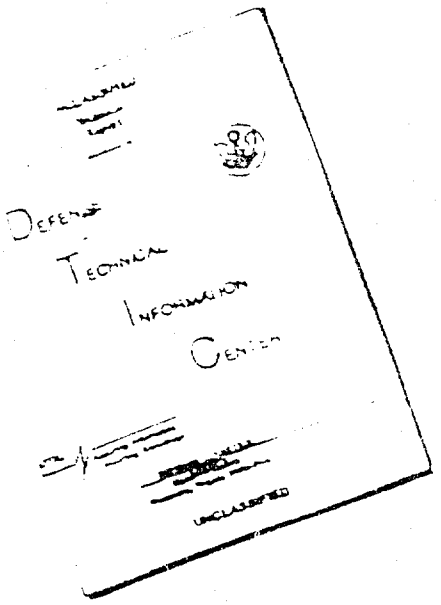

THIS DOCUMENT IS BEST QUALITY AVAILABLE. THE COPY FURNISHED TO DTIC CONTAINED A SIGNIFICANT NUMBER OF PAGES WHICH DO NOT REPRODUCE LEGIBLY.

20. Abstract (continued)

several means through which this energy might be coupled to radiation fields with cross sections for stimulated emission that could reach 10^{-17} cm^2. Such a stimulated release could lead to output powers as great as 3 x 10^{21} Watts/liter. Since 1978 we have pursued an approach for the upconversion of longer wavelength radiation incident upon isomeric nuclear populations that can avoid many of the difficulties encountered with traditional concepts of single photon pumping. Experiments have confirmed the general theory and have indicated that a gamma-ray laser is feasible if the right combination of energy levels and branching ratios exists in some real material. Of the 1,886 distinguishable nuclear materials, the present state-of-the-art has been adequate to identify 29 first-class candidates, but further evaluation cannot proceed without remeasurements of nuclear properties with higher precision. A laser-grade database of nuclear properties does not yet exist, but the techniques for constructing one have been developed and utilized under this contract. Resolution of the question of the feasibility of a gamma-ray laser now rests upon the determination of: 1) the identity of the best candidate, 2) the threshold level of laser output, and 3) the upconversion driver for that material.

This final report focuses upon our approach that is the nuclear analog to the ruby laser. It embodies the simplest concepts for a gamma-ray laser and not surprisingly, the greatest rate of achievement in the quest for a subAngstrom laser was realized in that direction. For ruby the identification and exploitation of a bandwidth funnel were the critical keys in the development of the first laser. There was a broad absorption band linked through efficient cascading to the narrow laser level.

In 1987 we reported a major milestone which showed that comparable structure existed at the nuclear scale in the first of the 29 candidate isomers available for testing, $^{180}Ta^m$. Populations of the isomer were successfully pumped down with flashes of x-rays absorbed through an astonishingly large cross section of 40,000 on the usual scale (10^{-29} cm^2 keV) where 10 describes a fully allowed process. This corresponded to a partial width for useful absorption of 0.5 eV, even better than what had been assumed for idealized nuclei.

In the course of this contract work we discovered that the giant pumping resonances occurred with a gratifying frequency throughout the table of nuclides, reaching optimal size and strength in the mass region where the better candidates lie. Nineteen isomers were successfully pumped with the bremsstrahlung from both a 4 MeV linac and a 6 MeV linac. The giant resonances for pumping the candidate isomers $^{180}Ta^m$ and $^{123}Te^m$ were found to open at gateway energies well below 4 MeV. These candidates have the largest integrated cross sections for pumping with x-rays ever found below 4 MeV in any nuclei. These two poorest of the 29 candidates are the only ones available for testing and they continue to outperform even the most optimistic expectations. The likelihood for the full feasibility of one of the better candidates continues to be raised by the successes enjoyed with the least attractive of the 29 candidates.

At the conclusion of this work we focused upon the extension of these achievements in pumping nuclei to those having laser-like transitions with microsecond lifetimes. For the test cases of Ta-181 and Hf-176 giant resonances were found for the pumping of fluorescence from levels with lifetimes of 18 and 10 microseconds, respectively. Those nuclei were pumped with the Texas-X linear accelerator installed in our facility for the dedicated use in gamma ray laser research. The importance of these first results are that the particular nuclei studied are very close neighbors in the sense of nuclear structure to the still unavailable first class candidate nuclei for a gamma ray laser. Such favorable results with these close simulations argue strongly for analogous successes with the actual candidate nuclei.

PREFACE

At first approach it would seem that the prospects for all ultrashort wavelength lasers would be vitiated by the basic υ^3 dependence of electron transition probabilities that drastically limits the storage of pump energies. However, there are some unique advantages of a gamma-ray laser that would accrue from its operation upon electromagnetic transitions of nucleons as opposed to electrons. First, the constant linking υ^3 with lifetime is more favorable by orders-of-magnitude because of the accessibility of a variety of transition moments. For example, nuclear transitions with 100 keV energies can have microsecond lifetimes so the effects pumped by an input pulse can be integrated up to larger values for longer times. Secondly, nuclear metastables store keV and even MeV for years. With upconversion schemes most of the pump power is input long before the time of use and triggering requirements are small. Nuclear transitions need not have thermal broadening and natural linewidths are routinely obtained. Without broadening, electromagnetic cross sections are large and values for 1 A transitions typically exceed the cross section for the stimulation of Nd in YAG. Finally, working metastables can be concentrated to solid densities. As candidates for ultra short wavelength media, nuclear populations clearly offer some strong advantages.

The clear attractions notwithstanding, a decade ago the difficulties in realizing a gamma-ray laser were considered to be almost insurmountable. However, in 1982 we began to emphasize an interdisciplinary concept of upconversion which ultimately launched a renaissance in the field. The essential concept was the "optical" pumping of nuclei. In this case optical meant x rays, but the fundamentals were the same. Useful, resonant absorption of pump power would occur over short distances to produce high concentrations of excited nuclei while wasted wavelengths would be degraded to heat in much larger volumes. Of all the cases considered, the nuclear analog of the ruby laser embodied the simplest concepts for a gamma-ray laser. Not surprisingly, the greatest rate of achievement has been realized in that direction.

For ruby, the identification and exploitation of a bandwidth funnel were the critical keys in the development of the first laser. There was a broad absorption band linked through efficient cascading to the narrow laser level. Our model called for a nuclear analog of this structure which was unknown in 1986 when the first phase of experiments was started. That theory was confirmed in 1988 when intense flashes of x rays were used to dump the stored energy of an isomer for the rare nuclide $^{180}Ta^{m}$ which exists naturally as 100% inverted. During the course of the research contracted over the past three years our concept for a gamma-ray laser matured to the point where it is now included in the textbooks. The first article in this final report is such a review from the CRC Handbook. It provides a convenient context into which can be placed the detailed reports of achievements realized under this contract.

Following the breakthrough in dumping populations of the $^{180}Ta^{m}$ isomer, experiments with the unique superconducting linac at Darmstadt showed that the nuclei were pumped down through two isolated resonances of extraordinary strength, about 10^{6} times larger than expected for the excitation of nuclei by x rays. Subsequent experiments used four accelerators to survey 19 isotopes for the systematic occurrence of these giant pumping resonances.

Then research focused upon the extension of the results to systems more nearly resembling actual laser materials. Fluorescent transitions with laser-like lifetimes of microseconds were found to be pumped with the same type of resonances having such extraordinary strengths. This major achievement was the synthesis of efforts to advance instrumentation, with an emphasis upon materials with microsecond lifetimes. The research was made possible by the successful installation of the Texas-X linear accelerator at our facility. Dedicated fully to this work it supported the study of these more difficult nuclei. The details of these achievements are reviewed in the following sections together with preprints and reprints of those aspects selected for publication. Results these past three years continue to enhance the feasibility of a gamma ray laser by further reducing demands upon potential pump systems.

TABLE OF CONTENTS

REPRINTS AND PREPRINTS OF MANUSCRIPTS PUBLISHED OR TO BE PUBLISHED UNDER THIS CONTRACT

Gamma-ray lasers, CRC Handbook of Laser Science and Technology, Supplement 1: Lasers (1991) p. 561 1

Resonant excitation of the reaction $^{180}Ta^{m}(\gamma,\gamma')^{180}Ta$, Physical Review C 42, R1813 (1990) 14

Excitation of $^{123}Te^{m}$ and $^{125}Te^{m}$ through (γ,γ') reactions, Physical Review C 43, 897 (1991) 18

Photoexcitation of nuclear isomers by (γ,γ') reactions, Physical Review C 43, 1238 (1991) 22

Resonant photoexcitation of isomers: $^{115}In^{m}$ as a test case, Physics Letters B 266, 9 (1991) 32

Common thresholds and the role of deformations in the photoexcitation of isomers, Physical Review C 46, 952 (1992) 37

Status and issues in the development of a gamma-ray laser, Laser Interaction and Related Plasma Phenomena 10, 151 (1992) 46

Status and issues in the development of a gamma-ray laser. II Giant resonances for the pumping of nuclei, Laser and Particle Beams 11, 43 (1993) 62

Absolute measurement of spatial and spectral characteristics of bremsstrahlung using the photoexcitation of nuclear isomers, Review of Scientific Instruments 64, 2298 (1993) 74

Low-energy conversion electron Mossbauer spectroscopy using a chevron microchannel plate detector, Review of Scientific Instruments (Sept. 1993) 82

Structure of intermediate states in the photoexcitation of the ^{89}Y isomer, Nuclear Physics A559, 253 (1993) 88

REPRINTS OF MANUSCRIPTS PUBLISHED IN CONFERENCE PROCEEDINGS UNDER THIS CONTRACT

The gamma-ray laser: Issues and progress in 1990, Proceedings of the International Conference on Lasers '90 (1991) p. 16 109

The gamma-ray laser: Issues and progress in 1991, Proceedings of the International Conference on Lasers '91 (1992) p. 63 110

Status and issues in the development of a gamma-ray laser, Proceedings of the SPIE Conference on Ultrashort-Wavelength Lasers (1992) p. 166 118

The gamma-ray laser: Issues and progress in 1992, Proceedings of the International Conference on Lasers '92 (1993) p. 73 130

UNPUBLISHED MANUSCRIPTS PREPARED UNDER THIS CONTRACT

Experimental preparations for the excitation of short-lived nuclear isomers pumped with the UTD-LINAC 138

An evaluation of nanophase diamond film doped with ^{57}Fe for use as a nuclear target 168

Installation of the Texas-X research linear accelerator 185

CRC Handbook of Laser Science and Technology

Supplement 1: Lasers

Editor

Marvin J. Weber, Ph.D.
Lawrence Livermore National Laboratory
University of California
Livermore, California

CRC Press
Boca Raton Ann Arbor Boston

Library of Congress Cataloging-in-Publication Data

Lasers/editors, Marvin J. Weber
p. cm. — (CRC handbook of laser science and technology
Supplement ; 1)
Includes bibliographical references and index
ISBN 0-8493-3506-X
1. Lasers. I. Weber, Marvin J., 1932- . II. Series.
TA1675.L378 1991
621.36'6—dc20 90-2333
CIP

Direct all inquiries to CRC Press, Inc., 2000 Corporate Blvd., N.W., Boca Raton, Florida, 33431

International Standard Book Number 0-8493-3506-X

Library of Congress Card Number 90-2333
Printed in the United States

HANDBOOK OF LASER SCIENCE AND TECHNOLOGY

VOLUME I: LASERS AND MASERS

FOREWORD — Charles H. Townes

SECTION 1: INTRODUCTION
1.1 Types and Comparisons of Laser Sources — William F. Krupke

SECTION 2: SOLID STATE LASERS
2.1 Crystalline Lasers
- 2.1.1 Paramagnetic Ion Lasers — Peter F. Moulton
- 2.1.2 Stoichiometric Lasers — Stephen R. Chinn
- 2.1.3 Color Center Lasers — Linn F. Mollenauer

2.2 Semiconductor Lasers — Henry Kressel and Michael Ettenberg
2.3 Glass Lasers — Stanley E. Stokowski
2.4 Fiber Raman Lasers — Rogers H. Stolen and Chinlon Lin
2.5 Table of Wavelengths of Solid State Lasers

SECTION 3: LIQUID LASERS
3.1 Organic Dye Lasers — Richard Steppel
3.2 Inorganic Liquid Lasers
- 3.2.1 Rare Earth Chelate Lasers — Harold Samelson
- 3.2.2 Aprotic Liquid Lasers — Harold Samelson

SECTION 4: OTHER LASERS
4.1 Free Electron Lasers
- 4.1.1 Infrared and Visible Lasers — Donald Prosnitz
- 4.1.2 Millimeter and Submillimeter Lasers — Victor L. Granatstein, Robert K. Parker, and Phillip A. Sprangle

4.2 X-Ray Lasers — Raymond C. Elton

SECTION 5: MASERS
5.1 Masers — Adrian E. Popa
5.2 Maser Action in Nature — James M. Moran

SECTION 6: LASER SAFETY
6.1 Optical Radiation Hazards — David H. Sliney
6.2 Electrical Hazards from Laser Power Supplies — James K. Franks
6.3 Hazards from Associated Agents — Robin DeVore

VOLUME II: GAS LASERS

SECTION 1: NEUTRAL GAS LASERS — Christopher C. Davis

SECTION 2: IONIZED GAS LASERS — William B. Bridges

SECTION 3: MOLECULAR GAS LASERS
3.1 Electronic Transition Lasers — Charles K. Rhodes and Robert S. Davis
3.2 Vibrational Transition Lasers — Tao-Yaun Chang
3.3 Far Infrared Lasers — Paul D. Coleman; David J. E. Knight

SECTION 4: TABLE OF LASER WAVELENGTHS — Marvin J. Weber

VOLUME III: OPTICAL MATERIALS
PART 1: NONLINEAR OPTICAL PROPERTIES/RADIATION DAMAGE

SECTION 1: NONLINEAR OPTICAL PROPERTIES

1.1 Nonlinear and Harmonic Generation Materials — Shohba Singh
1.2 Two-Photon Absorption — Walter L. Smith
1.3 Nonlinear Refractive Index — Walter L. Smith
1.4 Stimulated Raman Scattering — Fred Milanovich

SECTION 2: RADIATION DAMAGE

2.1 Introduction — Richard T. Williams and E. Joseph Friebele
2.2 Crystals — Richard T. Williams
2.3 Glasses — E. Joseph Friebele

VOLUME IV: OPTICAL MATERIALS
PART 2: PROPERTIES

SECTION 1: FUNDAMENTAL PROPERTIES

1.1 Transmitting Materials
  1.1.1 Crystals — Perry A. Miles, Marilyn J. Dodge, Stanley S. Ballard, James S. Browder, Albert Feldman, and Marvin J. Weber
  1.1.2 Glasses — James W. Fleming
  1.1.3 Plastics — Monis Manning
1.2 Filter Materials — Lee M. Cook and Stanley E. Stokowski
1.3 Mirror and Reflector Materials — David W. Lynch
1.4 Polarizer Materials — Jean M. Bennett and Ann T. Glassman

SECTION 2: SPECIAL PROPERTIES

2.1 Linear Electro-Optic Materials — Ivan P. Kaminow
2.2 Magneto-Optic Materials — Di Chen
2.3 Elasto-Optic Materials — Milton Gottlieb
2.4 Photorefractive Materials — Peter Günter
2.5 Liquid Crystals — Stephen D. Jacobs

VOLUME V: OPTICAL MATERIALS
PART 3: APPLICATIONS, COATINGS, AND FABRICATION

SECTION 1: APPLICATIONS

1.1 Optical Waveguide Materials — Peter L. Bocko and John R. Gannon
1.2 Materials for HIgh Density Optical Data Storage — Alan E. Bell
1.3 Holographic Parameters and Recording Materials — K. S. Pennington
1.4 Phase Conjugation Materials — Robert A. Fisher
1.5 Laser Crystals — L. G. DeShazer, S. C. Rand, and B. A. Wechsler
1.6 Laser Glasses — Charles F. Rapp
1.7 Infrared Quantum Counter Materials — Leon Esterowitz

SECTION 2: THIN FILMS AND COATINGS

2.1 Multilayer Dielectric Coatings — Verne R. Costich
2.2 Graded-Index Surfaces and Films — W. Howard Lowdermilk

SECTION 3: OPTICAL MATERIALS FABRICATION

3.1 Fabrications Techniques — G. M. Sanger and S. D. Fantone
3.2 Fabrication Prodedures for Specific Materials — G. M. Sanger and S. D. Fantone

HANDBOOK OF LASER SCIENCE AND TECHNOLOGY

SUPPLEMENT 1: LASERS

TABLE OF CONTENTS

SECTION 1: SOLID STATE LASERS

1.1 Crystalline Paramagnetic Ion Lasers 3
John A. Caird and Stephen A. Payne

1.2 Color Center Lasers 101
Linn F. Mollenauer

1.3 Semiconductor Lasers 127
Michael Ettenberg and Henryk Temkin

1.4 Glass Lasers 137
Douglas W. Hall and Marvin J. Weber

1.5 Solid State Dye Lasers 159
Marvin J. Weber

1.6 Fiber Raman Lasers 167
Rogers H. Stolen and Chinlon Lin

1.7 Table of Wavelengths of Solid State Lasers 179
Farolene Camacho

SECTION 2: LIQUID LASERS

2.1 Organic Dye Lasers 219
Richard N. Steppel

2.2 Liquid Inorganic Lasers 319
Harold Samelson

SECTION 3: GAS LASERS

3.1 Neutral Gas Lasers 325
Julius Goldhar

3.2 Ionized Gas Lasers 335
Alan B. Petersen

3.3.1 Electronic Transition Lasers 341
J. Gary Eden

3.3.2 Vibrational Transition Lasers 387
Tao-Yuan Chang

3.3.3 Far-Infrared CW Gas Lasers 415
David J. E. Knight

3.4 Table of Wavelengths of Gas Lasers 423
Farolene Camacho

SECTION 4: OTHER LASERS

4.1 Free-Electron Lasers 515
William B. Colson and Donald Prosnitz

4.2 Photoionization-Pumped Short Wavelength Lasers 531
David King

4.3 X-Ray Lasers 539
Dennis L. Matthews

4.4 Table of Wavelengths of X-Ray Lasers 559

4.5 Gamma-Ray Lasers 561
Carl B. Collins

SECTION 5: MASERS
5.1 Masers 571
Adrian E. Popa
5.2 Maser Action in Nature 579
James M. Moran

Index 591

Chapter 4.5

GAMMA-RAY LASERS

Carl B. Collins

UPCONVERSION IN THE NUCLEUS

At the nuclear level, the storage of excitation energies in the Mossbauer range of 1 to 1000 keV can approach tera-Joules (10^{12} J) per liter for thousands of years. If successfully coupled to the radiation field the stimulated release of such nuclear energies would occur at the rate at which resonant electromagnetic radiation passed through the laser medium and could lead to output powers as great as 3×10^{21} W/l. This is an astronomical level of intensity and has not been approached to within orders of magnitude on earth by any means previously. The peak power from a one liter device would represent about 0.03% of the total power output from the sun.

Unfortunately, the quest for a gamma-ray laser has been one of the longest unfruitful efforts in the field of laser science. Virtually all of the sustained pioneering work was done by relatively few groups in the U.S. and in the U.S.S.R. and focused upon the single photon, brute force approach to pumping. That work dealt extensively with concepts involving the use of a neutron flux for pumping the laser medium, either in situ in real-time or as a preparatory step to be followed by a rapid separation of isotopes within their natural lifetimes. All proposals were concluded to require infeasibly high levels of particle fluxes to pump the inversions, exceeding even those available from nuclear explosions, and to require neutron moderators having virtually infinite thermal capacities. By 1980, all conceivable variants of the single photon approach had been characterized as hopeless. In 1981 this traditional approach to a gamma-ray laser was virtually abandoned with the publication of Baldwin's splendid review of all classical efforts.[1]

A renaissance in feasibility studies was launched with the modernization of concepts for the upconversion in the nucleus of lower energy input radiation. In the early 1980s, processes such as the stimulated anti-Stokes scattering of intense but conventional laser radiation were introduced.[2] The theoretical implications of this renaissance were reviewed[3] in 1982. If strengthened by recent infusions of nuclear phase modulation theory,[4] that article still provides the most convenient review of the basic concepts and requirements for a viable gamma-ray laser scheme. By involving two distinct steps, the upconversion techniques for pumping a gamma-ray laser avoid the severe relationships between storage times and spontaneous powers wasted at threshold that were imposed on the single-step processes.[1] Replacement power that is required falls within a technically accessible range avoiding damage to the laser medium.

These two-step, upconversion processes can be divided further into two basic categories that correspond to the type of pumping employed: coherent and incoherent, as shown in Figure 4.5.1. The critical concept here is that both transfer the stored population to a state at the head of a cascade leading to the upper laser level. To be effective the pumping processes cannot transfer too many quanta of angular momenta from the fields, and the cascade provides a mechanism for further changes that may be necessary to reach the laser levels. Then the ultimate viability of these pump schemes will depend upon:

1. Spectroscopic studies locating a suitable configuration of nuclear energy levels, and
2. "kinetic" studies providing an efficient path of cascading from the intermediate or dressed state to the upper laser level.

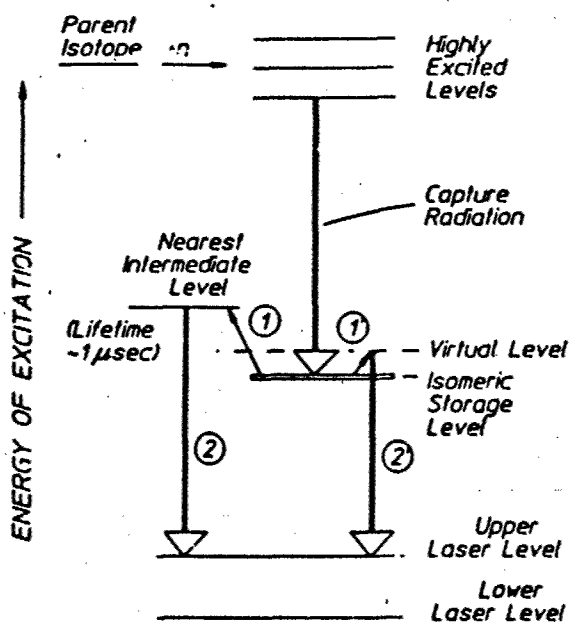

FIGURE 4.5.1 Schematic diagram showing the energetically excited levels of a typical nucleus of interest to the development of a gamma-ray laser. Life times of the stored energies in the isomeric level produced by the initial capture can range from days to hundreds of years. The first phase of the two-step process for the stimulated release of the stored energy is shown in the figure by the solid arrows. Both subsequent alternatives correspond to the use of longer wave-length radiation to lift a nucleus from the storage level to a higher level of excitation that has a much shorter lifetime. The arrow marked (1) illustrates the incoherent pumping of the storage level through the absorption of an x-ray that is resonant with the energy separation between the storage level and the next higher level of proper symmetry. The arrow marked (1'), represents the alternative process of coherent pumping through the nonresonant absorption of a photon from the radiation field in order to create a virtual or dressed state of excitation shown by the dashed level in the figure. In either case the gamma-ray output ultimately results from the upper laser level populated by a cascade occurring as a second step, as shown in the figure by either of the double arrows, (2) and (2')

Because of the interdisciplinary nature of the problem, even for an idealized nuclear material, computations of threshold levels of pumping are not without difficulty. However, under idealized conditions, the part of the pump energy which must be supplied in situ would not be large enough to represent a major impediment to the realization of a gamma-ray laser.[1] The real difficulties take peculiar forms. The use of coherent upconversion would require the location of nearly degenerate levels which could not be resolved by conventional techniques of nuclear spectroscopy. The use of incoherent pumping with X-rays would require a level of knowledge about branching ratios and transition probabilities beyond that available from current methodology. Despite the many applications of beautiful and involved techniques of nuclear spectroscopy, the current data base is inadequate in both coverage and resolution either to answer the question of whether an acceptable isotope exists or to guide in the selection of a possible candidate medium for a gamma-ray laser. In fact, the paucity of laser-grade data describing nuclear properties is so severe that one cannot say which real isotope represents the best approximation to the ideal.

For lifetimes ranging from seconds to infinity there are 1886 real nuclei to consider as candidates for a gamma-ray laser. Computer based searches of the existing data base have served to identify 29 first class candidates. Of these, 10 are known to have the necessary

(but not necessarily sufficient) arrangement of levels in which there is an isomeric storage level and at lower energies: (1) an upper laser level with lifetime between 1 nsec and 10 μs, and (2) a lower laser level of even less energy. Unfortunately, all ten are exotics having no other utility and, hence, there is no supply of samples for experimentation.

CRITICAL EXPERIMENTS

Incoherent Pumping of Nuclei

Levels of nuclear excitation which might be efficiently stimulated in a gamma-ray laser are very difficult to pump directly. To have lifetimes long enough to integrate the rates of inversion of population that can be pumped at reasonably accessible levels of input power, such levels must have very narrow widths for interaction with the radiation field. This is a fundamental attribute that has led to the general concern that absorption widths in nuclei are too narrow to permit effective pumping with X-rays. Precisely the same concerns were voiced in atomic physics before Maiman's great discovery and it is useful to pursue this analogy between ruby and gamma-ray lasers.

The nuclear analog of the ruby laser embodies the simplest concepts for a gamma-ray laser. Not surprisingly, the greatest rate of achievement in the quest for a sub-Angstrom laser has developed in that direction. For ruby the identification and exploitation of a bandwidth funnel were the critical keys in the development of the first laser. There was a broad absorption band linked through efficient cascading to the narrow laser level. Nuclei to be used in the analog of the ruby laser can start in either ground or isomeric states. However, with the latter, most of the output power can be derived from the energy stored in the isomeric state at its creation.

Whether or not the initial state being pumped is isomeric, the principal figure of merit for bandwidth funneling is the partial width for the transfer, $b_a b_o \Gamma$. The Γ is the total width of the intermediate level shown to the left of Figure 4.5.1 and the branching ratios b_a and b_o specify the probabilities that a population pumped by absorption into the broad level will decay back into the initial or fluorescent levels, respectively. It is not often that the sum of branching ratios is unity, as channels of decay to other levels are likely. However, the maximum value of partial width for a particular level occurs when $b_a = b_o = 0.5$.

The actual measurement of partial width involves the correlation of fluorescence yields excited by a pulse of continuous X-rays with those expected from the expression[5,6]

$$N_f = N_o \sum_i \xi_i \frac{\varphi_i}{A} \tag{1}$$

where No_o and N_f are the numbers of initial and fluorescent nuclei, respectively, (φ/A) is the spectral intensity of the bremsstrahlung in keV/keV/cm² at the energy E_i of the i-th pump band, and the summation is taken over all of the possible pump bands capable of cascading to the same fluorescence level of interest. The ξ_i is a combination of nuclear parameters including the partial width $b_a b_o \Gamma$ in keV,

$$\xi_i = \frac{(\pi b_a b_o \Gamma \sigma/2)_i}{E_i} \tag{2}$$

where σ is the peak of the Breit-Wigner cross section for the absorption step. The combination of parameters in the numerator of Equation 2 is termed the integrated cross section for the transfer of population in the incoherent scheme of pumping.

Of the many potential systems for a test of the formulations of Equations 1 and 2, the literature[7] supports the calculation of integrated cross sections for very few. Table 4.5.1

Table 4.5.1
SUMMARY OF NUCLIDES, ABSORPTION LINES, AND INTEGRATED CROSS SECTIONS $\pi b_e b_o \Gamma\sigma/2$ FOR THE EXCITATION OF DELAYED FLUORESCENCE SUITABLE FOR USE AS CALIBRATION STANDARDS OF X-RAY PUMP SOURCES

	Pump line (keV)	Cross section (10^{-29} cm²keV)
^{79}Br	761	6 2
^{77}Se	250	0 20
	480	0 87
	818	0 7
	1005	30 0
^{115}In	1078	18 7

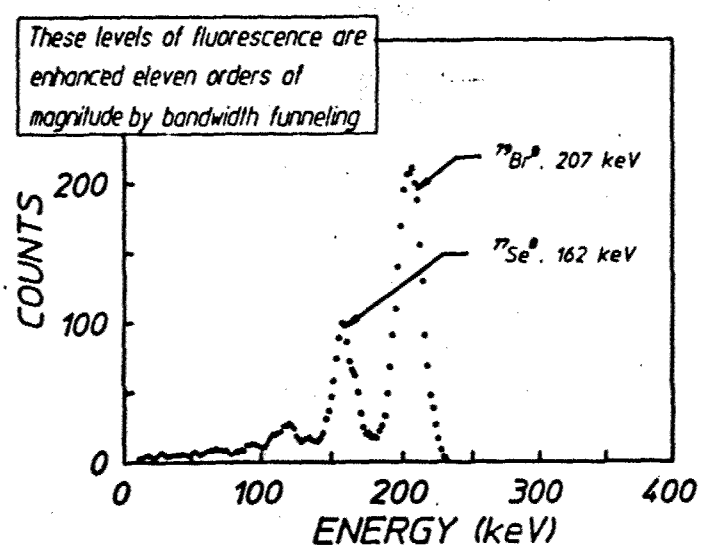

FIGURE 4.5.2. Fluorescence spectrum from a target containing 1.25 g LiBr and 1.20 g of elemental Se, both in natural abundances, excited with a single irradiation by the bremsstrahlung produced by the DNA/PITHON electron beam device. Acquisition time of this data was 80 s. Prominent lines are contributed by the isomeric transitions indicated.

summarized those which are known with sufficient accuracy to serve as standards. In the convenient units of 10^{-29} cm² keV, values range from the order of unity to a few tens for bandwidth funnels that are sufficient for demonstrations of nuclear fluorescence from reasonable amounts of material at readily accessible levels of input.

In a recently reported[5,6,8] series of experiments it was shown that bandwidth funneling works as well at the nuclear level as it had at the molecular level. In order to validate the optical pumping model of Equations 1 and 2, samples of the standard nuclei of Table 4.5.1 were pumped with intense pulses of bremsstrahlung from the DNA nuclear simulator PITHON. The clear signal-to-noise ratios that typified subsequent measurements of nuclear fluorescence exited through the pump bands of Table 4.5.1 are shown in Figure 4.5.2. The quality of such data enabled us to "invert" Equations 1 and 2 so that the spectral intensities of the pump could be obtained at three energies from the measured values of fluorescence

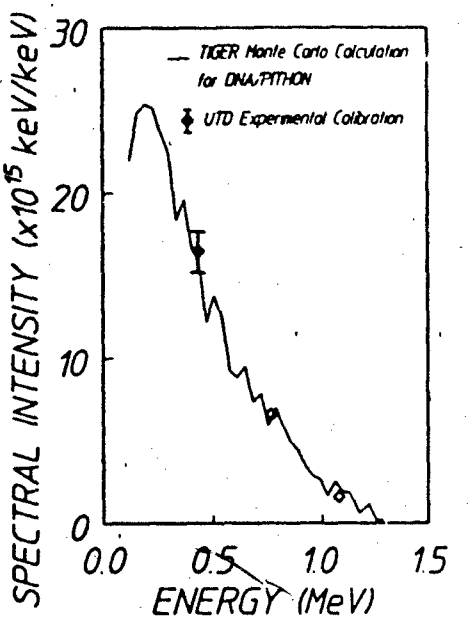

FIGURE 4.5.3 Data points plot the spectral intensities measured directly with nuclear activation techniques using the parameters of Table 4.4.1 in comparison to the spectrum computed with a coupled electron, photon transport code for a typical PITHON shot. Vertical bars show uncertainty in the measurement at the one point for which that uncertainty was larger than the plotted size of the symbol.

excited from a single pulse. Figure 4.5.3 shows a typical result[6] in comparison with a calculation of the bremsstrahlung spectrum from that particular source on that particular shot. Both measurement and calculation are absolutes with no free parameters to adjust. Such a direct measurement of the spectrum from a single intense pulse of X-ray continua had not been previously possible because of the lack of any dispersive media at these energies and the agreement with expectations is striking. The type of selective excitation of calibration nuclei is now used to establish the intensity of pump sources used to excite actual laser candidates so that fluorescence efficiencies can be determined from data with Equations 1 and 2.

Tempering expectations that these successes might be readily extended to the pumping of actual isomeric candidates for a gamma-ray laser was a concern for the conservation of various projections of the angular momenta of the nuclei. Many of the interesting isomers belong to the class of nuclei deformed from the normally spherical shape. For those systems there is a quantum number of dominant importance, K, which is the projection of individual nucleonic angular momenta upon the axis of elongation. To this is added the collective rotation of the nucleus to obtain the total angular momentum J. The resulting system of energy levels resembles those of a diatomic molecule for which

$$E_x(K,J) = E_x(K) + B_xJ(J+1) \qquad (3)$$

where $J \geq K \geq 0$ and J takes values $|K|, |K|+1, |K|+2, \ldots$ In this expression B_x is a rotational constant and $E_x(K)$ is the lowest value for any level in the resulting "band" of energies identified by other quantum numbers x. In such systems the selection rules for

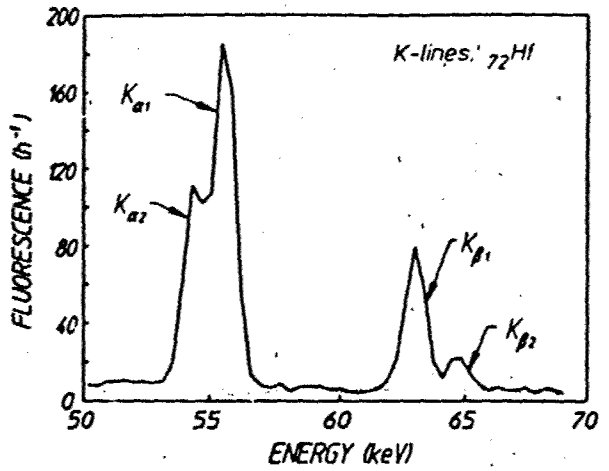

FIGURE 4.5.4 Dotted and solid curves show, respectively, the spectra obtained before and after dumping some of the isomeric $^{180}Ta^{m}$ contained in a target sample enriched to 5%. An HPGe detector was used to obtain the dotted spectrum before irradiation. The feature at 63 keV is from traces of natural activity in the counting shield. The solid curve is the spectral signature of the radioactive debris accumulated by cascading from the levels into which the isomeric population was dumped. The actual lines are the K-lines of hafnium arising from electron capture by the ^{180}Ta ground debris.

electromagnetic transitions require both $|\Delta J| \leq M$ and $|\Delta K| \leq M$, where M is the multipolarity of the transition.

In most cases of interest, the lifetime of the isomeric state is large because it has a value of K differing considerably from those of lower levels to which it would, otherwise, be radiatively connected. As a consequence, bandwidth funneling processes such as shown to the left of Figure 4.5.1 must span substantial changes in ΔK and component transitions have been expected to have large, and hence unlikely, multipolarities.

Attempts to test these rather negative expectations have generally been confounded by the rarity of the 29 candidates for a gamma-ray laser. However, very recently there has been reported[9] a major success in dumping some of the isomeric population of one of the actual candidates for a gamma-ray laser.

Not a particularly attractive candidate, *a priori*, $^{180}Ta^{m}$ was the only one for which a macroscopic sample was available in 1987. The need to span a formidably large $\Delta K = 8$ between isomer and fluorescence level supported little initial enthusiasm for this nucleus. When actually pumped, however, it showed the largest integrated cross section ever reported for interband transfer in any material, 4×10^{-22} cm^2 eV. This is an enormous value for bandwidth funneling, being about 10,000 times greater than what is characteristic of an efficient nucleus which starts in the ground state and transfers to the isomer (see, for example ^{77}Se or ^{79}Br in Table 4.5.1). The optical pumping of any isomer had never been previously reported, so nothing was available for a more direct comparison with these results.[9]

The partial width for absorption from $^{180}Ta^{m}$ isomer to fluorescence was measured to be about 0.5 eV, a value far exceeding the 1 μeV usually offered as a rule of thumb that would limit the interband transfer of nuclear population. It is a current speculation that collective oscillations of the core nucleons break the symmetries of the nuclei and provide this major windfall making it easier to dump isomers by mixing single particle states needed in the transfer process. Much more experimentation will be needed to identify whether this is the actual mechanism responsible and to understand if the lessons taught by $^{180}Ta^{m}$ are generally applicable in the pool of candidate isomers. Now, such experiments are facilitated by the

widths themselves, which have reduced the level of effort to practical dimensions. The experiments with $^{180}Ta^{m}$ have shown that clear fluorescence signals can be obtained on a scale of illuminating milligrams of material with intensities which peak in time at only a few W/cm^2, even when integrated over all wavelengths. At this level, meaningful experiments can be performed on other candidate isomers when samples become physically available.

Coherent Pumping of Nuclei

Coherent pumping, the technique depicted in the right of Figure 4.5.1, depends upon the alteration of the properties of the isomeric storage level produced by the scattering of large intensities of long wavelength radiation from the nuclei. In ferromagnetic and ferroelectric hosts the active nuclei are immersed in extremely large fields capable of developing substantial interaction energies across a nuclear volume when switched by relatively modest applied fields. If transitions to the storage level exist in the nuclei at energies comparable to that of a photon of the driving fields, the properties of the other state of the transition will be mixed into those of the storage level. It is assumed that this other state is better able to radiate gamma radiation. While the driving field need not be precisely resonant with the transition energy, the detuning, ΔE from resonance must be comparable to the interaction energy if properties are to be fully mixed. In such cases, the metastability of the storage level against gamma-ray emission is switched off by the admixture of properties from the other state of the low energy transition being driven. It is this concept which comprises the foundation of the scheme for coherently pumping a gamma-ray laser.

While precise computations of the threshold for coherent pumping are not yet available, estimates from perturbation theory[3,10-12] suggest that the threshold requirements in idealized cases are comparable to those for incoherent pumping. The principal difficulty in this case is that, again, estimates are extremely sensitive to material specifics. For coherent upconversion to be viable, a real nucleus must be found with two accidentally degenerate levels, one being a long-lived isomeric state. Such a combination would be completely invisible to current techniques of nuclear spectroscopy.

REFERENCES

1. **Baldwin, G. C., Solem, J. C., and Goldanskii, V. I.,** *Rev. Mod. Phys.*, 53, 687, 1981.
2. **Collins, C. B.,** in *Laser Techniques for Extreme Ultraviolet Spectroscopy*, McIlrath, T. J. and Freeman, R. R., Eds., AIP Conference Proceedings No. 90, New York, 1982, 454.
3. **Collins, C. B., Lee, F. W., Shemwell, D. M., DePaola, B. D., Olariu, S., and Popescu, I. I.,** *J. Appl Phys.*, 53, 4645, 1982.
4. **Sinor, T. W., Reittinger, P. W., and Collins, C. B.,** *Phys. Rev. Lett.*, 62, 2547, 1989.
5. **Anderson, J. A. and Collins, C. B.,** *Rev. Sci. Instrum.*, 58, 2157, 1987.
6. **Anderson, J. A. and Collins, C. B.,** *Rev. Sci. Instrum.*, 59, 414, 1988.
7. *Evaluated Nuclear Structure Data File* (Brookhaven National Laboratory, Upton, New York, 1986)
8. **Collins, C. B., Anderson, J. A., Paiss, Y., Eberhard, C. D., Peterson, R. J., and Hodge, W. L.,** *Phys. Rev.* 38, 1852, 1988.
9. **Collins, C. B., Eberhard, C. D., Glesener, J. W., and Anderson, J. A.,** *Phys. Rev.* 37, 2267, 1988.
10. **Collins, C. B.,** in *Advances in Laser Science-I*, Stwalley, W. C. and Lapp, M., Eds., AIP Conference Proceedings No. 146, Dallas, 1985, 40.
11. **Olariu, S., Popescu, I., and Collins, C. B.,** *Phys. Rev.*, 23, 50, 1981.
12. **Olariu, S., Popescu, I., and Collins, C. B.,** *Phys. Rev.*, 23, 1007, 1981.
13. **Ikonen, E., Helisto, P., Hietaniemi, J., and Katila, T.,** *Phys. Rev. Lett.*, 60, 643, 1988.
14. **West, P. J. and Matthias, E.,** *Z. Phys.*, 228, 369, 1978.
15. **Collins, C. B. and DePaola, B. D.,** *Optics Lett.*, 10, 25, 1985.
16. **DePaola, B. D. and Collins, C. B.,** *J. Opt. Soc. Am.*, B1, 812, 1984.

PHYSICAL REVIEW C VOLUME 42, NUMBER 5 NOVEMBER 1990

Resonant excitation of the reaction $^{180}Ta^m(\gamma,\gamma')^{180}Ta$

C. B. Collins, J. J. Carroll, T. W. Sinor, M. J. Byrd, D. G. Richmond, and K. N. Taylor
Center for Quantum Electronics, The University of Texas at Dallas, P. O. Box 830688, Richardson, Texas 75083-0688

M. Huber, N. Huxel, P. v. Neumann-Cosel, A. Richter, C. Spieler, and W. Ziegler
Institut für Kernphysik, Technische Hochschule Darmstadt, D-6100 Darmstadt, Federal Republic of Germany

(Received 17 July 1990)

Irradiation with a superconducting linear accelerator of Ta has provided data for the characterization of the reaction $^{180}Ta^m(\gamma,\gamma')^{180}Ta$. The depopulation of the isomer $^{180}Ta^m$ via an intermediate state or narrow band of states near 2.8 MeV has been found with an integrated cross section of 1.2×10^{-25} cm^2 keV. This large value exceeds, by nearly an order of magnitude, known cross sections for (γ,γ') reactions producing isomers of other species. Another intermediate state or narrow band is also indicated by the data at an energy 0.6 MeV higher.

The isotope $^{180}Ta^m$ is nature's rarest stable nuclide[1] being only 0.012% of all tantalum and the only naturally occurring isomer.[2] However, the importance of $^{180}Ta^m$ lies not in its rarity but in its abundance. The nucleus ^{180}Ta sits somewhat aside the main path of the *s* process[3,4] for cosmic nucleosynthesis and the survival of any amount into current times raises some difficult questions resulting from the presence of the isomer. The ground state of ^{180}Ta has a half-life of only 8.1 h while the isomer has an energy of 75.3 keV and a half-life[2] of 1.2×10^{15} y. The branching of nucleosynthesis to the ground and metastable states is obviously important, but even after creation populations may continue to transfer between these levels by photoexcitation, altering the effective half-life of the nucleus and the understanding of its present abundance. Either this isomer must have been singularly stable against photonuclear deexcitation, $^{180}Ta^m(\gamma,\gamma')^{180}Ta$ at the time of creation,[5,6] or the corresponding temperatures must have been too low to produce photons capable of pumping such a reaction.[7]

These latter concerns have been aggravated by the most recent experiments.[8] Not only does photonuclear deexcitation of $^{180}Ta^m$ occur, the integrated cross section reported for the process is of unprecedented size for a (γ,γ') reaction connecting ground state and isomer. However, that result was obtained by irradiating an enriched sample of $^{180}Ta^m$ with the bremsstrahlung continuum from a 5 MeV linac and so the energies of the particular photons pumping the reaction could not be determined. Reported here is the measurement of an excitation function between 2 and 5 MeV and the discovery of a very large integrated cross section in excess of 10^{-25} cm^2 keV for the deexcitation of $^{180}Ta^m$ by 2.8 MeV photons.

The energy-level diagram of ^{180}Ta and its daughters is shown in Fig. 1, together with a representation of some steps in the excitation and detection of the $^{180}Ta^m(\gamma,\gamma')^{180}Ta$ reaction. The principal means for the detection of the ^{180}Ta ground state lies in observing the $K\alpha$ lines of its daughter, ^{180}Hf following decay by electron capture. The efficiency for the emission of $K\alpha$ photons relative to the number of ^{180}Ta decays[9] is about 57%.

The time integrated yield of ground-state nuclei, N_f obtained by irradiating N_i isomers with a photon flux Φ_0 in photons/cm^2 delivered in a bremsstrahlung continuum of intensities up to an end point energy E_0 is,

$$N_f = N_i\Phi_0\int_0^{E_0}\sigma(E)F(E,E_0)dE\,, \tag{1a}$$

where $F(E,E_0)$ is the distribution of intensities within the bremsstrahlung spectrum normalized so that

$$\int_0^{E_0}F(E,E_0)dE = 1\,, \tag{1b}$$

and $\sigma(E)$ is the cross section for the reaction

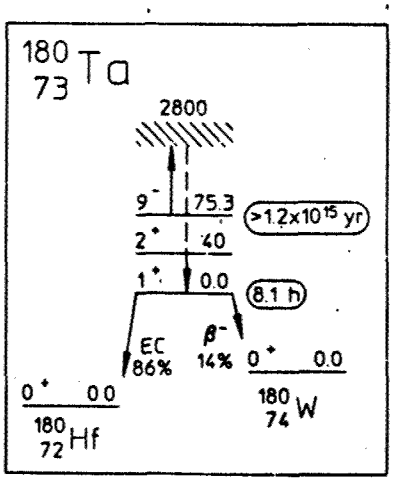

FIG. 1 Schematic energy-level diagram of ^{180}Ta and its daughters. Half-lives are shown in ovals for the ground and isomeric levels. Energies are in keV. The initial transition of the (γ,γ') reaction is shown by the arrow pointing upward to the intermediate state represented by the hatched line. Cascade through the levels of ^{180}Ta is not known, but leads finally to the ground state, which decays as indicated by the diagonal downward arrows.

$^{180}Ta^m(\gamma,\gamma)^{180}Ta$ as a function of the photon energy E.

All (γ,γ') reactions below particle threshold energies excite nuclear bound states. Therefore production or depletion of isomers by these reactions proceeds through resonant excitation of intermediate states, each with rather narrow widths. One such channel is shown in Fig. 1 at an excitation energy of $E_j = 2.8$ MeV.

The odd-odd nucleus ^{180}Ta, having a particularly high density of states, could have intermediate states lying at high energies with separations comparable to their widths, in which case the integral of Eq. (1a) could then be simplified no further. However, at lower energies where a discrete number of intermediate states contribute, the spectral intensity $F(E,E_0)$ will vary little over the narrow range of energies for which $\sigma(E)$ is nonzero around each of the E_j. Then the ground-state yield, expressed as the normalized activation per unit photon flux $A_f(E_0)$ produced with bremsstrahlung having an end point of E_0 can be written from Eq. (1a) as,

$$A_f(E_0) \equiv \frac{N_f}{N_i \Phi_0} = \sum_j (\sigma\Gamma)_{fj} F(E_j,E_0) . \tag{2a}$$

In this expression $(\sigma\Gamma)_{fj}$ is the integrated cross section for the production of ground-state N_f as a result of the excitation of the intermediate state E_j with bremsstrahlung described by the spectral function $F(E,E_0)$, so that

$$(\sigma\Gamma)_{fj} = \int_{E_j-\Delta}^{E_j+\Delta} \sigma(E)dE , \tag{2b}$$

where Δ is an energy small compared to the spacing between intermediate states and large in comparison to their widths. Levels of this type are sometimes called gateways or doorways. The integrated cross sections for such levels can be evaluated with the residue, $R_M(E_0)$ obtained by subtracting the contributions to A_f from excitations through M intermediate states,

$$R_M(E_0) = A_f(E_0) - \sum_{E_j=E_1}^{E_M} (\sigma\Gamma)_{fj} F(E_j,E_0) . \tag{3}$$

A change of the end point energy E_0 of the bremsstrahlung, as well as altering Φ_0, modulates the spectral intensity function $F(E_j,E_0)$ at all of the important energies for resonant excitation, E_j. The largest effect occurs when E_0 is increased from a value just below some intermediate state at $E_j = E_k$ to one exceeding it so that $F(E_k,E_0)$ varies from zero to some finite value.

Early work[10] on (γ,γ') reactions showed that a plot of activation, $A_f(E_0)$ as a function of bremsstrahlung end point, E_0 displayed very pronounced activation edges at the energies, E_j corresponding to the resonant excitation of new intermediate states. Unfortunately, such an excitation function was not reported previously[8] for the reaction $^{180}Ta^m(\gamma,\gamma')^{180}Ta$, so the question was unresolved as to whether or not the extraordinary size found for the integrated cross section $(\sigma\Gamma)$ was the result of many smaller $(\sigma\Gamma)_{fj}$ summing to a large value as suggested by Eq. (2a). At the time of that experiment there was no source of bremsstrahlung with a variable end point and enough intensity to provide significant excitation of samples available in such minute amounts as $^{180}Ta^m$.

In the work reported here bremsstrahlung was obtained from a Ta converter foil irradiated by the electron beam from the injector of the 130 MeV superconducting Darmstadt linear accelerator (S-DALINAC) at the Technische Hochschule Darmstadt.[11] The electrons were accelerated in three superconducting cavities in which the continuous wave rf amplitudes were varied to change the electron energy (here in the range from 2 to 5 MeV). The diameter of the electron beam was about 2 mm and this and other beam parameters were monitored and kept constant. Uncertainty in the end point was less than 50 keV.

The numbers of final-state nuclei N_f were obtained in these experiments by detecting signature photons with a Ge(Li) spectrometer. Counts in the appropriate channels were corrected for the finite durations of both irradiation and counting, for the absolute counting efficiency of the spectrometer, for the emission intensity relative to the parent, and for the opacity of the experimental sample to the escape of signature photons. The latter factor was calculated with a Monte Carlo code.

Samples used in the experiments for the deexcitation of $^{180}Ta^m$ were disks 3.8 cm in diameter and 127 μm thick. The material was 99.95% pure tantalum and contained $^{180}Ta^m$ in its natural abundance. Irradiations were made for a nominal 4 h period at a beam current of 20 μA. The actual charge passed to the bremsstrahlung converter was determined by digitizing the current and numerically integrating it during the irradiation interval. Planchettes containing nominal amounts of 2 g of SrF_2 in natural isotopic abundances were concurrently exposed in contact with the Ta foils for calibration purposes. Fourteen different end points of the bremsstrahlung were arranged to span the interval from 2 to 5 MeV.

The evaluation of $A_f(E_0)$ in Eq. (2a) requires knowledge of the particular spectral intensity functions, $F(E,E_0)$, together with the photon flux, Φ_0, incident on each sample position. These were calculated for the different end point energies, E_0 with the established EGS4 coupled electron-photon transport code developed at SLAC.[12] Verification of the calculated values of flux could only be obtained by the reaction $^{87}Sr(\gamma,\gamma')^{87}Sr^m$. This has been distinguished in the literature[10] by the comprehensive report of its excitation energies E_j and integrated cross sections $(\sigma\Gamma)_{mj}$ for production of metastable states at energies below 3 MeV and therefore serves as a benchmark for the analysis of these experiments.

The dependence of the values of $A_f(E_0)$ for $^{87}Sr^m$ upon the bremsstrahlung end point was determined from the measurements of its 388.4 keV decay signature fluorescence.[9] The dominant[10] activation edge near 2.67 MeV was well reproduced. The residue $R_3(E_0)$ was computed for the three intermediate state locations indicated in Ref. 10, leaving their integrated cross sections variable. The values of integrated cross sections best describing the data are shown in Table I. Below 4 MeV, the results of this work are in remarkable agreement with the previous measurements and thus verify the calculations of $F(E,E_0)$.

The increase of residues above 4 MeV suggested the importance of another intermediate state. The final entry in Table I records the integrated cross section found to be sufficient to describe observations of $A_f(E_0)$ over the en-

TABLE I. Values of integrated cross section $(\sigma\Gamma)_I$ for the reaction $^{87}Sr(\gamma,\gamma')^{87}Sr^m$ through gateway states indicated by the measured excitation function. The gateway excitation energies E_i for levels in Ref. 10 are given at the previously determined locations. The energy of the new state indicated by this work is given at the centroid of the appropriate spectral bin.

	$\sigma\Gamma(\times 10^{-29}$ cm^{2}keV)	
Energy (MeV)	Ref. 10	This work
1.22	8.5+4−3	8.5 ± 2
1.88	16+8−5	16 ± 4
2.67	380+200−100	430 ± 50
4.3 ± 0.1	...	1500 ± 300

ergy range up to 5 MeV.

The thermal and fast neutron fluxes in the irradiation environment were measured by standard techniques[13] and were found to give negligible contributions to the excitation function for ^{87}Sr.

The depopulation of $^{180}Ta^m$ was examined by observation of the Hf K x-ray signatures from ^{180}Ta ground-state decay. Background subtracted spectra of the data corrected for counting times shown in Fig. 2 clearly display the lowest energy activation edge for the reaction $^{180}Ta^m(\gamma,\gamma')^{180}Ta$.

Figure 3(a) plots the values of $A_I(E_0)$ obtained in this work for the deexcitation reaction $^{180}Ta^m(\gamma,\gamma')^{180}Ta$ and shows the dependence associated[14] with the increase of E_0 above an intermediate state. The measured excitation strictly excludes broad band photoabsorption such as due to the density of states or the tail of the giant dipole resonance, which must contribute at least a constant integrated cross section in each spectral bin above 2.8 MeV. The properties of the lowest energy intermediate state are the most important to the question of the survival of $^{180}Ta^m$ during cosmic nucleosynthesis. A strong level or narrow band of states near 2.8 MeV can be rather well determined by the data.[15]

Figure 3(b) shows the residue computed from Eq. (3) with $M=2$ to remove the contributions from the two lowest intermediate states or narrow bands observed in this work. The values of integrated cross section we found for deexcitation through these levels are shown in Table II.

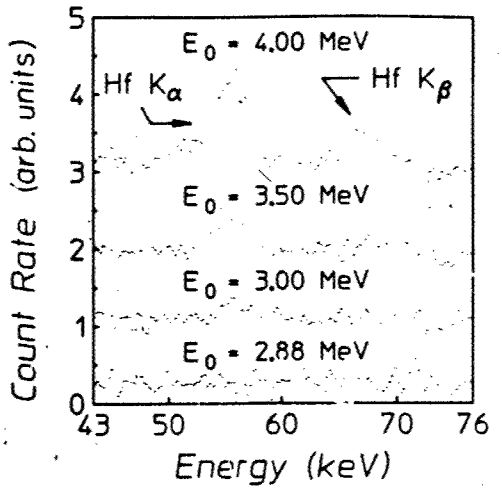

FIG. 2. Spectra of fluorescent photons from ^{180}Ta decay after irradiation with bremsstrahlung having the end points shown. The counting rate from an unexposed sample has been subtracted.

It is important to consider some likely contaminants to these data. Neutron capture is not possible since the analogous parent ^{179}Ta does not exist naturally. Also, photodissociation of ^{181}Ta can produce some $^{180}Ta^g$, but the threshold for this process is 7.576 MeV. The remaining reaction to consider is $^{181}Ta(n,\gamma)^{182}Ta$, leading to ^{182}W with a characteristic x-ray which could contribute to the broad structure attributed to Hf $K\alpha$ in Fig. 2. However, the 115 d half-life of ^{182}Ta made possible delayed measurements uncontaminated by $^{180}Ta^g$. These showed, even at the highest end point of 5 MeV, null results and indicated that no contamination could have occurred from this process.

The results of this work are in close agreement with the previous measurements[8] indicating an integrated cross section for $^{180}Ta^m(\gamma,\gamma')^{180}Ta$ of extraordinary size. However, it is now possible to report the excitation energy for the lowest strong level for the deexcitation of $^{180}Ta^m$ at 2.8 MeV. The corresponding value of the integrated

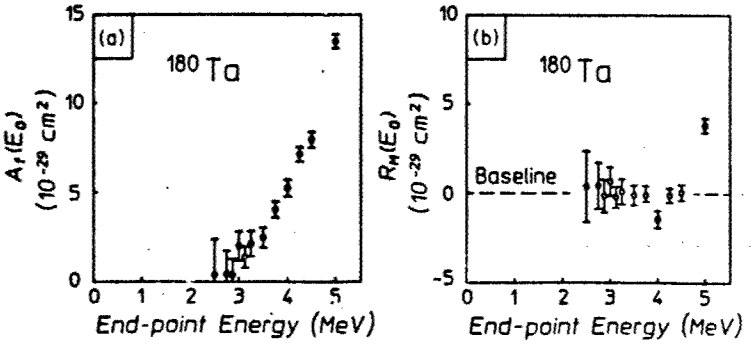

FIG. 3. (a) Linear plot of activation $A_I(E_0)$ for ^{180}Ta as a function of the bremsstrahlung end point. (b) Residue computed from Eq. (3) after removing the contributions from the two lowest energy gateways for deexcitation using parameters recorded in Table II.

TABLE II. Values of integrated cross section $(\sigma\Gamma)_{\gamma}$ for the reaction $^{180}Ta^{m}(\gamma,\gamma')^{180}Ta$ through gateway states indicated by the excitation function of Fig. 3(a). The gateway excitation energies E_{γ} for these levels are given at the centroid of the appropriate spectral bins.

Energy (MeV)	$\sigma\Gamma(\times 10^{-29}$ cm^{2}keV)
2.8 ± 0.1	12000 ± 2000
3.6 ± 0.1	35000 ± 5000

cross section is 1.2×10^{-25} cm^{2}keV and is the largest ever reported for a (γ,γ') reaction connecting a ground state and an isomer at energies below the threshold for the evaporation of neutrons. Notwithstanding the singular magnitude of this cross section, the state's energy for photodeexcitation of $^{180}Ta^{m}$ is just high enough[7] to insure the survival of this nucleus in the stellar environment and current models of cosmic nucleosynthesis are sustained.

The nuclear structure of these intermediate states for this well deformed, odd-odd nucleus also presents an interesting problem. The extraordinary $\Delta K = 8$ needed to reach the ^{180}Ta ground state implies considerable K mixing of these levels. A possible scheme which explains the large upward transition probability and the sudden onset of the depopulation would be as follows: At low energies, numerous K-allowed transitions can be constructed from the Nilsson model states of the unpaired proton and neutron. Here, K mixing is small and the states will entirely decay back to the isomer. In the simple Nilsson model a few levels with $\Delta K = 0,1$ with respect to the isomer are possible at energies near 3 MeV which can be excited by enhanced $E1$ transitions. Due to the high level density of ^{180}Ta, large K mixing would then result in depopulation of the isomer to the ground state. A detailed analysis of this process is currently underway.[16]

We thank K. Alrutz-Ziemssem, D. Flasche, H.-D. Gräf, and H. Weise for their great support in operating the superconducting electron accelerator and are grateful to P. Vogel for illuminating discussions. In addition we wish to thank our sponsors, the Department of Defense through the Naval Research Laboratory and the Bundesministerium für Forschung und Technologie, Contract No. 06DA184I.

[1] A. G. W. Cameron, in *Essays in Nuclear Astrophysics*, edited by C. A. Barnes, D. D. Clayton, and D. N. Schramm (Cambridge Univ. Press, Cambridge, 1982), p. 23.

[2] E. Browne, Nucl. Data Sheets **52**, 127 (1987).

[3] K. Yokoi and K. Takahashi, Nature (London) **305**, 198 (1983).

[4] H. Beer and R. A. Ward, Nature (London) **291**, 308 (1981).

[5] J. Law and F. A. Iddings, J. Radioanalytical Chem. **3**, 53 (1969).

[6] E. B. Norman, S. E. Kellogg, T. Bertram, S. Gil, and P. Wong, Astrophys. J. **281**, 360 (1984).

[7] J. J. Carroll, J. A. Anderson, J. W. Glesener, C. D. Eberhard, and C. B. Collins, Astrophys. J. **344**, 454 (1989).

[8] C. B. Collins, C. D. Eberhard, J. W. Glesener, and J. A. Anderson, Phys. Rev. C **37**, 2267 (1988).

[9] E. Browne and R. B. Firestone, in *Table of Radioactive Isotopes*, edited by V. S. Shirley (Wiley, New York, 1986), pp. 180–182.

[10] E. C. Booth and J. Brownson, Nucl. Phys. **A98**, 529 (1967).

[11] H.-D. Gräf and A. Richter, in *Proceedings of the 1988 Linear Accelerator Conference, Virginia* (Continuous Electron Beam Accelerator Facility Report No. CEBAF-Report-89-001, 1989), p. 231.

[12] The EGS4 Code System, Walter R. Nelson, Hideo Hirayama, and David W. O. Rogers, Stanford Linear Accelerator Center Report No. SLAC 265, 1985 (unpublished).

[13] *ASTM Standard Method for Determining Thermal Neutron Reaction and Fluence Rates by Radioactivation Techniques*, Publication No. E 262-86. (American Society for Testing and Materials, Philadelphia, 1987), and references cited there.

[14] W. T. K. Johnson, B. T. Chertok, and C. E. Dick, Phys. Rev. Lett. **25**, 599 (1970).

[15] The data below 3 MeV allow the existence of weaker intermediate states at lower energies. Reference 6 provided a null result for ground-state production at 1.3 MeV and the present work indicates that a level near 1.4 MeV would only have an integrated cross section of 500×10^{-29} cm^{2}keV.

[16] P. Vogel (private communication).

BRIEF REPORTS

Brief Reports are short papers which report on completed research or are addenda to papers previously published in the **Physical Review**. *A Brief Report may be no longer than four printed pages and must be accompanied by an abstract.*

Excitation of $^{123}Te^m$ and $^{125}Te^m$ through (γ,γ') reactions

J. J. Carroll, T. W. Sinor, D. G. Richmond, K. N. Taylor, and C. B. Collins
Center for Quantum Electronics, The University of Texas at Dallas, P. O. Box 830688, Richardson, Texas 75083

M. Huber, N. Huxel, P. v. Neumann-Cosel, A. Richter, C. Spieler, and W. Ziegler
Institut für Kernphysik, Technische Hochschule Darmstadt, D-6100 Darmstadt, Germany
(Received 5 October 1990)

Photoexcitation of the long-lived isomers $^{123}Te^m$, $T_{1/2}=119.7$ d, and $^{125}Te^m$, $T_{1/2}=58$ d, was produced with bremsstrahlung from the superconducting Darmstadt linear accelerator. The excitation function for the reaction $^{123}Te(\gamma,\gamma')^{123}Te^m$ was measured between 2 and 6 MeV. It indicated that the isomer was populated by resonant absorption through isolated intermediate states having integrated cross sections in excess of 10^{-26} cm^2 keV, i.e., values about 100 times larger than most (γ,γ') activation reactions reported previously. An excitation function was also obtained for the reaction $^{125}Te(\gamma,\gamma')^{125}Te^m$ in this energy range.

INTRODUCTION

It has been recently discovered[1] that the reaction $^{180}Ta^m(\gamma,\gamma')^{180}Ta$ occurs with an integrated cross section that is orders of magnitude larger than what could have been reasonably expected. At energies below the threshold for neutron evaporation the photoexcitation of isomers is usually characterized by values of 10^{-28}–10^{-27} cm^2 keV. Although the inverse, deexcitation of an isomer had not been previously observed, there was no *a priori* reason to expect it to be more probable, particularly since the transition requires a spin change of $\Delta K=8$. Of considerable astrophysical significance,[2,3] the result reported for $^{180}Ta^m$ approached 10^{-24} cm^2 keV and raised some interesting questions of nuclear structure. It also provided unexpected encouragement of schemes for pumping a γ-ray laser that would depend upon the sudden deexcitation of isomeric populations.[4]

Whether the deexcitation of $^{180}Ta^m$ was an isolated example limited to odd-odd nuclei with a high density of states was considered in two subsequent studies. In the first the excitation function for $^{180}Ta^m(\gamma,\gamma')^{180}Ta$ was measured with a bremsstrahlung source by varying the end point of the spectrum. It was found[5] that the (γ,γ') reactions of $^{180}Ta^m$ occurred for two discrete excitation energies of 2.8 and 3.6 MeV with integrated cross sections of 1.2×10^{-25} and 3.5×10^{-25} cm^2 keV, respectively. The high density of excited nuclear states seemed to play no particular role.

In the second experiment[6] 19 isomers were excited with the bremsstrahlung spectra from four different accelerators. Despite the relatively coarse mesh of energies at which end points could be set between 0.5 and 11 MeV, several isomers were excited through integrated cross sections that were surprisingly large at 4 MeV. One curiosity was the first report of the photoexcitation of 119.7*d*, $^{123}Te^m$, the longest-lived isomer ever populated by (γ,γ') reactions and one of the candidate nuclides for a γ-ray laser. This is a fairly light nucleus having no particularly high density of states. Also, there is little experimental or theoretical information on electromagnetic transitions between excited levels in ^{123}Te above 1 MeV.

It was the purpose of the experiment described in this Brief Report to measure the excitation function for both $^{123}Te^m$ and $^{125}Te^m$. Exploiting the precision with which the end points of the spectra could be set between 2 and 6 MeV, the (γ,γ') reactions were found to occur through relatively few gateways with large integrated cross sections approaching 10^{-25} cm^2 keV.

EXPERIMENTAL ANALYSIS AND RESULTS

Elemental tellurium samples were used in this study, and all isotopes were present in their natural abundances. Nominal amounts of 17 g were contained in plastic (Delrin) cylinders with outer diameters of 3.8 cm and heights of 1.5 cm. Calibration targets were fashioned from identical containers holding about 2 g of 99.99% pure SrF_2. Its use in calibrating bremsstrahlung spectra has been recently emphasized.[5,6]

Isomeric populations were produced by exposing the targets to bremsstrahlung from a 3-mm tantalum converter foil irradiated by the electron beam from the injector of the new 130-MeV S-DALINAC at the Technische Hochschule Darmstadt.[7] Electron energies were varied between 2 and 6 MeV with a typical step size of 250 keV. These electron energies were measured with an accuracy of 50 keV before and after each exposure. The diameter

of the beam at the converter, typically 2 mm, was also monitored. At each end point a sample stack of tellurium and strontium was irradiated axially in close proximity to the converter. The proper alignment of the beam was achieved by maximizing the dose delivered to a remote ionization chamber shielded to sample only the central 12 mrad of the bremsstrahlung cone. Variations in all beam parameters were recorded during the experiments. In particular, the charge passed to the converter was determined by digitizing the current and integrating it. Exposures were typically 4 h in duration for a beam current of about 20 μA.

The numbers of isomers produced by these irradiations were determined from the counting rates measured in distinctive fluorescence lines. The transitions responsible for the γ-ray signatures used in these measurements are indicated by bold arrows in the energy-level diagrams of Figs. 1(a) and 1(b).

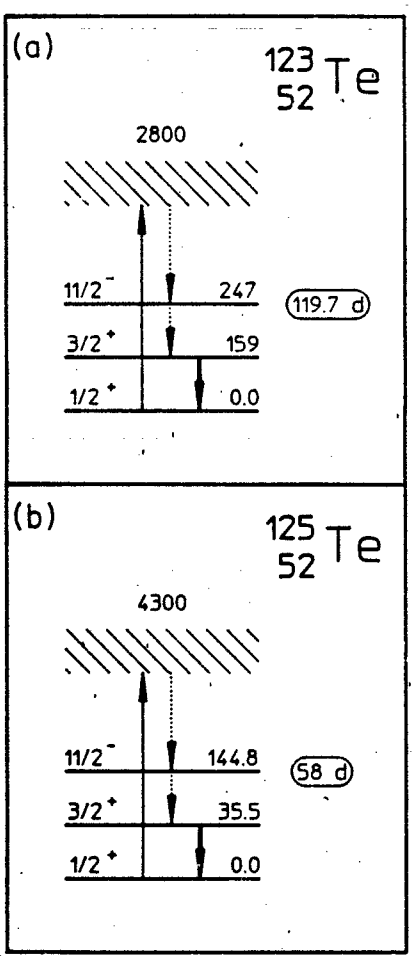

FIG. 1. Schematic energy-level diagrams for (a) ^{123}Te and (b) ^{125}Te. Half-lives of the isomers are shown in the ovals, and the energies of the levels shown are given in keV. The bold arrows show the transitions which give rise to distinctive γ-ray emissions measured in this work. The dashed arrows indicate transitions which are not directly observed.

After irradiation the tellurium samples were transported to the Center for Quantum Electronics, University of Texas at Dallas, where high-resolution spectra were collected with an HPGe detector. An example of the data obtained with a 6-MeV exposure is shown in Fig. 2. The fluorescence peak[8] at 159.0 keV from the decay of ^{123}Te^m is apparent, and even the γ rays from the strongly converted transition of ^{125}Te^m at 35.5 keV are clearly visible.

Because of the shorter isomeric lifetimes the SrF_2 calibration, samples[5,6] were counted on site with a Ge(Li) detector to measure the yield of ^{87}Sr^m. This isomer has a half-life of 2.8 h and a fluorescence signature at 388.4 keV. The raw number of counts in each peak was corrected for the finite durations of exposure and counting, the absolute counting efficiencies of the detectors, and the relative emission intensity. The opacity of the samples to the escape of the signature γ rays was compensated by a factor calculated with a Monte Carlo code for each detector geometry.

The experimentally measured yield of isomers, N_f resulting from the irradiation of N_T ground-state nuclei with bremsstrahlung is given analytically by

$$N_f = N_T \int_{E_C}^{E_0} \sigma(E) \frac{d\Phi(E)}{dE} dE \ , \tag{1}$$

where E_0 is the end-point energy, $d\Phi(E)/dE$ is the time-integrated spectral intensity in cm^{-2}keV^{-1} of the photon field, and $\sigma(E)$ is the cross section in cm^2 for the reaction. The spectral intensity is conveniently expressed as the product of a flux of all photons above a cutoff energy E_C of 1 MeV, Φ_0 incident on the target, and a relative intensity function $F(E,E_0)$, which is normalized according to

$$\int_{E_C}^{E_0} F(E,E_0) dE = 1 \ . \tag{2}$$

Equation (2) allows the definition of a normalized yield, or activation per photon, $A_f(E_0)$ given by

$$A_f(E_0) \equiv \frac{N_f}{N_T \Phi_0} = \int_{E_C}^{E_0} \sigma(E) F(E,E_0) dE \ . \tag{3}$$

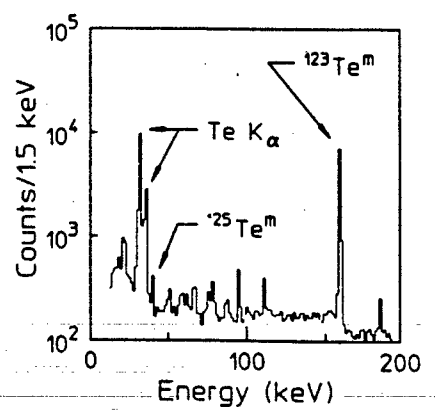

FIG. 2. Pulse-height spectrum obtained from a tellurium sample after a 6-MeV end-point irradiation. Peaks not explicitly marked are due to counting chamber background.

Plots of this quantity as a function of E_0 give the excitation functions for $^{123}Te^m$ and $^{125}Te^m$ shown in Figs. 3(a) and 3(b). This normalization makes these curves relatively insensitive to variations in isomeric population that occur simply because all the intensities increase when the end point is raised. Instead, their appearance is primarily determined by the density, location, and integrated cross sections of the states mediating the reactions.

Calculated spectra of both Φ_0 and $F(E,E_0)$ were obtained from the EGS4 electron-photon transport code developed at SLAC.[9] This Monte Carlo program is well established in the medical physics community, and its general validity has been demonstrated elsewhere.[10,11] In this work confidence in the calculated photon spectra was maintained by calibrating them with the reaction $^{87}Sr(\gamma,\gamma')^{87}Sr^m$ as discussed in Ref. 5.

At energies of interest in these experiments, gateways have widths that are small in comparison to their spacings, and Eq. (3) reduces to a summation, giving

$$A_f(E_0)=\sum_j (\sigma\Gamma)_{fj}F(E_j,E_0)\ , \tag{4}$$

where $(\sigma\Gamma)_{fj}$ is the integrated cross section and E_j is the excitation energy of the jth intermediate state feeding the isomer. It is then possible to define a quantity $R_M(E_0)$, which represents the residue of activation after subtracting contributions from the M lowest-lying intermediate states:

$$R_M(E_0)=A_f(E_0)-\sum_j^{E_M}(\sigma\Gamma)'_{fj}F(E_j,E_0)\ , \tag{5}$$

where E_M is the resonance energy of the highest-lying intermediate state contributing. Fitted values of the integrated cross sections $(\sigma\Gamma)'_{fj}$ were found by minimizing $R_M(E_0)$ for the lowest-energy state giving a break in the excitation function, and then iterating after including any new gateways suggested by the data. In the case of ^{87}Sr, the calibration procedures described earlier[5,6] were confirmed in the present work as a test of confidence. This provided experimental validation of the calculated photon spectra as well as confirming the experimental practice.

An identical analysis for $^{123}Te^m$ was based upon the excitation function of Fig. 3(a). The pronounced increase in yield beginning near 3 MeV indicates the location of an intermediate state, while the low level of activation below this energy suggests the participation of smaller gateways having $E_j<2$ MeV. The number and location of these lower-energy states could not be determined in the current work; nor does the literature provide any information. It was found that a single state near 1 MeV with an integrated cross section of $(60\pm20)\times10^{-29}$ cm^2 keV could give the activation observed below 3 MeV, but this assignment is not unique. The possible variations are indicated in Table I and do not significantly contribute to the uncertainties reported for the other gateways. Using this hypothetical state to remove the baseline yield, the residue $R_1(E_0)$ indicated two strong gateways at 2.8 and 4.2 MeV. The fitted $(\sigma\Gamma)'_{fj}$ corresponding to these states are given in Table I and are much larger than the baseline state at 1 MeV. These values were determined to within the uncertainties explicitly shown in Table I.

The excitation function obtained for population of $^{125}Te^m$ provided less detail, but the data of Fig. 3(b) were still consistent with an intermediate state located between 4.2 and 4.5 MeV, as given in Table I.

Because of the low (γ,n) threshold of the naturally occurring component of the deuterium in the plastic sample containers, it was necessary to evaluate the effects of all neutrons produced in the irradiation environment.

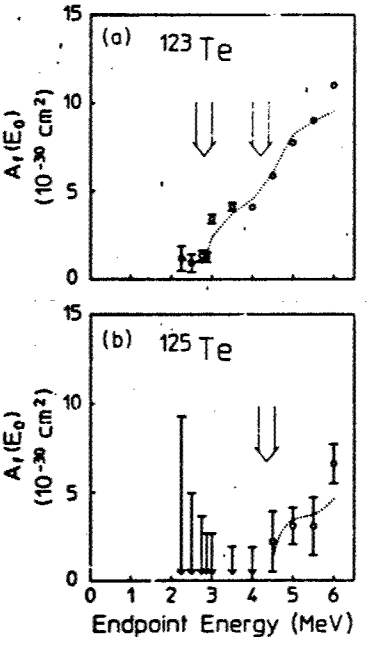

FIG. 3. Linear plots of yield normalized to the flux calculated for a low-energy cutoff of 1 MeV as functions of bremsstrahlung end-point energy for (a) ^{123}Te and (b) ^{125}Te. Where no error bars are shown, statistical errors are comparable to the symbol size. Error bars shown without symbols in (b) represent upper bounds on the activation where fluorescence was not observed above the level of background. Dotted curves plot the values calculated from the model of Eq. (4) using the results of Table I. The locations of the gateways determined in this work are indicated by the large arrows whose widths represent the available experimental resolution.

TABLE I. Values of fitted integrated cross sections $(\sigma\Gamma)'_j$ for gateway states determined from the excitation functions of Figs. 3(a) and 3(b) for the (γ,γ') reactions populating the isomers $^{123}Te^m$ and $^{125}Te^m$. The gateway excitation energies E_j for these levels are given at the centroid of the appropriate experimental bins.

Isotope	Gateway energy (MeV)	$(\sigma\Gamma)'$ (10^{-29} cm^2 keV)
^{123}Te	1.0±0.5	<60±20
	2.8±0.2	2000±300
	4.2±0.2	7600±1000
^{125}Te	4.2–4.5	7000±3000

The neutron flux was measured with standard activation techniques[12] by the inclusion of indium foils in the target stacks. Each disk was 0.0127 cm thick with a diameter of 3.8 cm and a mass of about 1 g. Epithermal neutrons were observed by detection of the 416.92-keV fluorescence from the 54.15-min isomer of ^{115}In, which is produced through neutron capture from the stable ^{115}In. At the highest photon end point of 6 MeV, there were found to be only 0.87 ± 0.05 neutrons cm^{-2} s^{-1}, and this flux decreased smoothly to zero as the end point was lowered to the deuterium (γ,n) threshold of 2.22 MeV. This low level of epithermal neutron flux produced negligible contributions to the yields of ^{123,125}Te^m and ^{87}Sr^m. The appearance of thermal neutrons was not expected because of the lack of sufficient moderators in the environment. The use of photon energies below the thresholds of all target and environmental materials excluded fast neutron production.

CONCLUSIONS

The excitation functions obtained in this work for the population of the isomers ^{125}Te^m and ^{125}Te^m indicate that their photoexcitation proceeds through absorption by isolated intermediate states. No consistent description could be obtained by assuming absorption through densely spaced levels which would have provided broadband absorption. The integrated cross sections determined for these states are about 100 times larger than most (γ,γ') activation reactions reported previously, being in excess of 10^{-26} cm^2 keV. Moreover, they are only an order of magnitude smaller than those determined in earlier measurements[4,5] for the depopulation of ^{180}Ta^m. Clearly, further investigations of the systematics of isomeric photoexcitation are needed in the range between 2 MeV and (γ,n) threshold energies in order to isolate the principal cause of the large photoexcitation rates being found. Experimental studies of a variety of different isomeric nuclei are currently underway to examine these questions. It would also be of great interest to have nuclear structure calculations illuminating the nature of the particular intermediate states through which the photoabsorption occurs.

ACKNOWLEDGMENTS

We thank K. Alrutz-Ziemssen, H.-D. Gräf, Th. Rietdorf, and H. Weise for their great support in operating the superconducting electron accelerator. In addition, we wish to thank our sponsors, the Department of Defense through the Naval Research Laboratory and the Bundesministerium für Forschung und Technologie, Contract No. 06DA1841.

[1] C. B. Collins, C. D. Eberhard, J. W. Glesener, and J. A. Anderson, Phys. Rev. C **37**, 2267 (1988).

[2] J. J. Carroll, J. A. Anderson, J. W. Glesener, C. D. Eberhard, and C. B. Collins, Astrophys. J. **344**, 454 (1989).

[3] Zs. Nemeth and F. Kaeppler, contribution to the Symposium on Nuclear Astrophysics, Baden, 1990 (unpublished).

[4] C. B. Collins, F. W. Lee, D. M. Shemwell, B. D. DePaola, S. Olariu, and I. I. Popescu, J. Appl. Phys. **53**, 4645 (1982).

[5] C. B. Collins, J. J. Carroll, T. W. Sinor, M. J. Byrd, D. G. Richmond, K. N. Taylor, M. Huber, N. Huxel, P. v. Neumann-Cosel, A. Richter, C. Spieler, and W. Ziegler, Phys. Rev. C **42**, 1813 (1990).

[6] J. J. Carroll, M. J. Byrd, D. G. Richmond, T. W. Sinor, K. N. Taylor, W. L. Hodge, Y. Paiss, C. D. Eberhard, J. A. Anderson, C. B. Collins, E. C. Scarbrough, P. P. Antich, F. J. Agee, D. Davis, G. A. Huttlin, K. G. Kerris, M. S. Litz, and D. A. Whittaker, submitted to Phys. Rev. C.

[7] H.-D. Gräf and A. Richter, in Proceedings of the 1988 Linear Accelerator Conference, Virginia, CEBAF Report No. 89-001, 1989, p. 231.

[8] E. Browne and R. B. Firestone, in *Table of Radioactive Isotopes*, edited by V. S. Shirley (Wiley, New York, 1986).

[9] Walter R. Nelson, Hideo Hirayama, and David W. O. Rogers, *The EGS 4 Code System* (SLAC Report No. 265, Stanford Linear Accelerator Center, Stanford, CA, 1985).

[10] R. Mohan, C. Chui, and L. Lidofsky, Med. Phys. **12**, 595 (1985).

[11] *Monte Carlo Transport of Electrons and Photons*, edited by T. M. Jenkins, Walter R. Nelson, and Alessandro Rindi (Plenum, New York, 1988).

[12] *ASTM Standard Method for Determining Thermal Neutron Reaction and Fluence Rates by Radioactivation Techniques*, Publication E 262-86 (American Society for Testing and Materials, Philadelphia, 1987), and references cited there.

PHYSICAL REVIEW C VOLUME 43, NUMBER 3 MARCH 1991

Photoexcitation of nuclear isomers by (γ,γ') reactions

J. J. Carroll, M. J. Byrd, D. G. Richmond, T. W. Sinor, K. N. Taylor, W. L. Hodge,* Y. Paiss,† C. D. Eberhard, J. A. Anderson,‡ and C. B. Collins
Center for Quantum Electronics, University of Texas at Dallas, Richardson, Texas 75083

E. C. Scarbrough and P. P. Antich
The University of Texas Southwestern Medical Center at Dallas, Dallas, Texas 75235

F. J. Agee, D. Davis, G. A. Huttlin, K. G. Kerris, M. S. Litz, and D. A. Whittaker
Aurora Simulator Facility, Harry Diamond Laboratories, Adelphi, Maryland 20783
(Received 21 April 1989)

Photoexcitation of the isomers of 19 nuclides was examined in this work. Four accelerators were used as sources of bremsstrahlung to expose the samples and end-point energies covered the range from 0.5 to 11 MeV. No evidence was found for nonresonant processes of excitation. However, more than half the cases showed enhanced channels for the resonant photoexcitation of isomers with integrated cross sections approaching 10^{-21} cm^2 keV. These results are three to four orders of magnitude larger than values usually characterizing (γ,γ') reactions.

INTRODUCTION

Because the photon carries relatively little momentum, (γ,γ') reactions must proceed through resonant channels for excitation with rather narrow widths. This aspect distinguishes photoexcitation from related processes such as (γ,n). The generation of an additional particle with which to conserve momentum provides a threshold of energy above which all incident photons can mediate the reaction. This facilitates the study of processes such as (γ,n) by increasing product yields and richly detailed results have been reported in the literature.[1] In contrast, the difficulties in exciting the narrow resonances for (γ,γ') reactions have inhibited investigations and relatively few results have been published in the past 50 years over which such processes have been known.[2,3]

In the region of energies from 0.1 to 10.0 MeV photon sources emit continuous spectra and the opportunity to probe (γ,γ') reactions with a tunable source of narrow width does not exist at practical levels of intensity. Even experiments designed to use γ sources are actually done with continua because of the degradation of the line spectra by Compton scattering in the real geometries employed.

The most tractable (γ,γ') reactions for study are those for the photoexcitation of isomeric states. The product lives long enough to be readily examined after termination of the input irradiation. The archetypical case has been the reaction ^{111}Cd$(\gamma,\gamma')^{111}$Cd^m exciting the 48.6 min isomer. Three of the most recent measurements of the integrated cross section $\sigma\Gamma$ were conducted in 1979, 1982, and 1987 with results of 35, 5.8, and 14 as reported in Refs. 4–6, respectively, in the usual units of 10^{-29} cm^2 keV. Probable errors were quoted as varying only from 7% to 14% and yet, no two of the measurements were even within a factor of 2 of each other. This discrepancy led to the curious suggestion[5] that some unknown mechanism for *nonresonant* nuclear absorption generally dominates the excitation step. Although fundamental considerations insist that for energies below the thresholds of neutron evaporation all (γ,γ') reactions must first excite bound nuclear states, the belief continued to spread that nonresonant processes were involved. The (γ,γ') reactions of ^{113}In, ^{87}Sr, and ^{180}Ta^m were all subsequently attributed to the unidentified nonresonant process.[7,8]

Recently, the technology has become available[9,10] to measure the spectrum of a source of pulsed bremsstrahlung, together with greatly improved computer codes[11,12] with which to calculate spectra for realistic geometries. These advances made it possible to resolve[13] the persisting controversies in the reaction ^{111}Cd$(\gamma,\gamma')^{111}$Cd^m, as well as those[14] in ^{115}In$(\gamma,\gamma')^{115}$In^m. As expected, it was found[13,14] that both ^{115}In^m and ^{111}Cd^m were excited by resonant absorption through intermediate gateway states near 1 MeV that were broadened by their short lifetimes. The sharp onset of the (γ,γ') reactions with increasing energy relegated to less than 3% any contributions from nonresonant processes and indicated that the gateway states were reasonably well connected by radiative transitions to both the ground states and the isomers. It appears that the principal cause for the large discrepancy between previous measurements was the difficulty in adequately characterizing the spectra of the irradiation. This was particularly true for radioactive sources since all spectral contributions away from the source lines were necessarily due to Compton continua generated by scattering in the irradiation environment.

The model for the photoexcitation of isomeric nuclei confirmed in recent work[13,14] is shown in Fig. 1. Only two gateway levels are drawn as examples and the number actually participating depends upon the sequence of energy levels and transition probabilities for the particu-

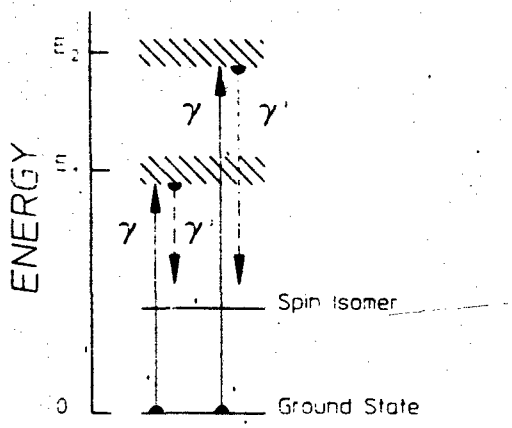

FIG. 1. Schematic representation of the (γ,γ') reactions used to populate isomeric states in these experiments. The resonant absorption of bremsstrahlung x rays, denoted as γ, excite populations of gateway states. Two are shown at excitation energies of E_1 and E_2 but the actual number will vary for each nuclide. Parts of the populations of the gateway states make transitions to the final state either directly or as part of a cascade of radiative transitions ending on the final state as indicated by the dashed arrows.

lar nucleus being considered. In the resolution of previous conflicts in ^{111}Cd and ^{115}In the values finally confirmed lay within the scatter of earlier measurements and generally agreed with nuclear parameters measured by other means.[15] However, when studies were extended to the deexcitation of an isomeric sample through the reverse of the sequence shown in Fig. 1, unexpectedly large results were obtained.[16] In contrast to values of a few 10's $\times 10^{-29}$ cm^2 keV measured for the excitation of isomers, a value of $40\,000 \times 10^{-29}$ cm^2 keV was reported[16] for the deexcitation of ^{180}Ta^m with a 6 MeV linac. The reaction ^{176}Lu$(\gamma,\gamma')^{176}$Lu^m was reported to proceed with an integrated cross section of comparable magnitude.[17] The strength of the dumping reaction ^{180}Ta$^m(\gamma,\gamma')^{180}$Ta was confirmed[18] with bremsstrahlung from the injector to the Darmstadt superconducting electron accelerator operated at 12 different end-point energies. Two gateway levels for ^{180}Ta$^m(\gamma,\gamma')^{180}$Ta were reported with integrated cross sections that totaled to $47\,000 \times 10^{-29}$ cm^2 keV.

It was the purpose of the work reported here to examine the systematics of these giant resonances for the photoexcitation of isomeric states to determine whether such results were curiosities associated only with ^{176}Lu and ^{180}Ta^m or whether they were part of more generally prevalent phenomena. A secondary objective was to learn whether the large integrated cross sections were the results of a large number of reaction channels of more conventional size or rather, a few of unprecedented magnitude.

Unfortunately, the type of electron accelerators that provided bremsstrahlung spectra with end-point energies that were chosen at will in classical investigations[19] of (γ,γ') reactions is no longer available in North America. For the experiments reported here we could arrange access only to a combination of accelerators, some with limited variability of end-point energies such as DNA/PITHON at Physics International and DNA/Aurora at Harry Diamond Laboratories. Between the ranges of energies available from those machines we used two medical linacs having fixed end points of 4 and 6 MeV. This enabled us to examine the photoexcitation of 19 isomeric nuclei, most of them over the range from 0.5 to 11 MeV. The variety of accelerators and locations minimized the possibility of introducing any systematic bias which might have been associated with any particular machine or its environment.

METHODOLOGY

Analytic approach

The normalized activation $A_f(E_0)$ of a sample per unit photon flux Φ_0 produced with a bremsstrahlung source having an endpoint E_0 can be written as

$$A_f(E_0) \equiv \frac{N_f}{N_i \Phi_0} = \sum_j (\sigma\Gamma)_{fj} F(E_j, E_0) , \qquad (1)$$

where N_i and N_f are the populations of initial and final nuclear states, respectively. In Eq. (1), $(\sigma\Gamma)_{fj}$ is the integrated cross section for the excitation of N_f through the jth gateway state as shown in Fig. 1. The function $F(E_j, E_0)$ is the spectral function describing the relative intensity at the photon energy, E_j, normalized so that

$$\int_0^{E_0} F(E, E_0)\,dE = 1 . \qquad (2)$$

The normalized activation can be useful as a sensitive indication of the opening of (γ,γ') channels whenever photons of the requisite energies E_j become available. A change of the end-point energy E_0 of the bremsstrahlung spectrum modulates the spectral intensity function $F(E_j, E_0)$ in Eq. (1) at all of the important gateway energies, E_j. The largest effect in the excitation function occurs when E_0 is increased from a value just below some gateway at $E_j = E_k$ to one exceeding it so that $F(E_j, E_0)$ varies from zero to some finite value. In earlier work[19] plots of quantities equivalent to Eq. (1) as functions of the end-point energies of the irradiating spectra showed very pronounced activation edges which appeared as sharp increases at the energies, E_j, corresponding to excitation of new gateways.

In the work reported here the ratios of activation N_f/N_i to the irradiation dose were examined as functions of E_0. The relationships between dose, which was measured directly, and Φ_0, which had to be derived from it, depended upon $F(E, E_0)$. The normalization to dose rather than Φ_0 was chosen to avoid any dependence of the features of the excitation function upon simulation models.

Experimental details

Sample materials were exposed to photons having energies up to 1.5 MeV with the DNA/PITHON nuclear simulator at Physics International. This device was a flash x-ray source using a single transmission line pulsed by a Marx generator. Since the end-point energy could be varied to some degree by changing the charging voltage of the Marx, photoexcitation from 0.5 to 1.5 MeV could be investigated with a resolution limited by the available end-point energies. The samples were placed in front of a converter foil which terminated the transmission line, and were aligned to face the photon flash. These were exposed in complex packages to activate several materials in each shot from DNA/PITHON, an important detail since the pulse repetition frequency was less than 1 h^{-1}. All the sample packages were backed with thermoluminescent dosimeters (TLD's) to measure the dosage which each target received.

The 1.5 to 6 MeV range was studied with two fixed end-point medical linacs at the Department of Radiology of the University of Texas Southwestern Medical Center at Dallas. Irradiations with nominal 4 MeV bremsstrahlung were obtained with a Varian Clinac 4/100 linac which provided a dose rate of 200 rad(H_2O) min^{-1} at 101.2 cm from the converter target. Bremsstrahlung having a nominal end point of 6 MeV was obtained with a Varian Clinac 1800 linac operating in the 6 MeV mode. This device produced 400 rad(H_2O) min^{-1} at 101.5 cm from the converter target. For both machines, the dose rate was determined by in-line ion chambers whose calibrations were directly traceable to NIST. Samples were exposed in packages confined to the region of most uniform dose distribution.

Irradiations in the 6 to 11 MeV range were provided with the DNA/Aurora nuclear simulator,[20] located at the Harry Diamond Laboratories. Powered by a Marx bank, photons were generated by converter foils which terminated four separate transmission lines. These converged on a target volume of roughly 0.1 m^3 in which the photon field was most intense. Again, the Marx charging voltage was varied to provide irradiations with different end-point bremsstrahlung. Samples were positioned in the high intensity spot and were backed by TLD's. These packages were oriented to face the centerline of the machine rather than any particular transmission line.

The spectra of these four machines have been well characterized, particularly the linacs which are committed to patient treatment. Photon spectra of the DNA/PITHON and DNA/Aurora accelerators were obtained through use of the Integrated TIGER Series (ITS) computational program.[12] They were calibrated by matching the end-point energy and the total dosage to the shape of the calculated spectrum. The DNA-PITHON device could also be cross calibrated by the activation technique described in Refs. 9 and 10. Typical spectra are given in Fig. 2, which shows the relative intensity function $F(E,E_0)$, on the meshes of energies for which data were available. For the DNA/PITHON shot shown, $\Phi_0 = 4\times10^{14}$ photons cm^{-2} and for the DNA/Aurora shot, $\Phi_0 = 5\times10^{13}$ photons cm^{-2}.

The output spectra of the medical linacs employed in this work were calculated with the EGS4 code developed at SLAC.[11] Unfortunately, the relative spectral intensity functions of these devices that were found in the literature[21] contained a computational artifact. To minimize that feature the spectra had to be modeled as part of this work. Results are shown in Fig. 3, together with the

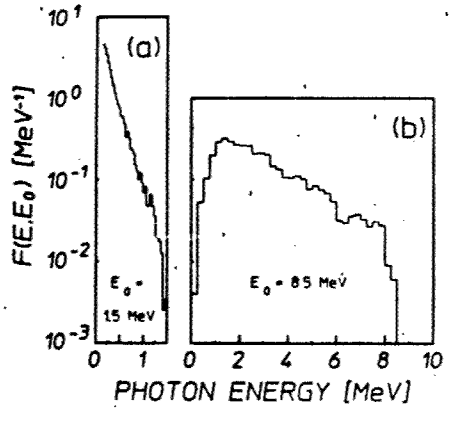

FIG. 2. Relative spectral intensities $F(E,E_0)$ of the bremsstrahlung typically produced by nuclear simulators used to irradiate samples in these experiments. The curves are normalized so that their areas are unity. The devices employed were (a) DNA/PITHON, with an end point of $E_0 = 1.5$ MeV; (b) DNA/Aurora, with an end point of $E_0 = 8.5$ MeV.

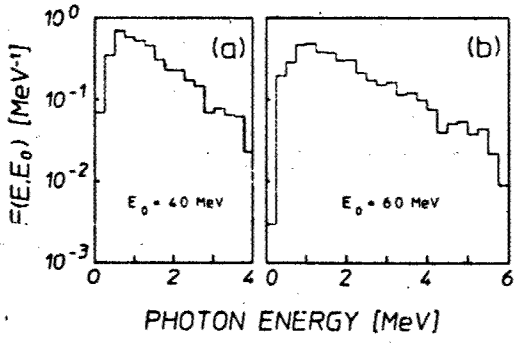

FIG. 3. Relative spectral intensities $F(E,E_0)$ of the bremsstrahlung produced by the medical linacs used to irradiate samples in these experiments. The curves are normalized so that their areas are unity. The solid lines indicate empirical fits to the calculated spectra as discussed in the text. The devices employed were as follows: (a) Varian Clinac 4/100, with a nominal end point of 4 MeV. The dotted curve shows the spectrum obtained from Ref. 21 that contains a computational artifact at about 3 MeV. (b) Varian Clinac 1800, operated in the nominal 6 MeV end-point mode.

literature values for a typical case.[21] The total fluxes at 100 cm were 3.23×10^{11} photons cm^{-2} min^{-1} for the nominally 4 MeV device, and 5.35×10^{11} photons cm^{-2} min^{-1} for the Clinac 1800 in the 6 MeV mode.

The isotopes studied in these experiments are listed in Table I along with the relevant physical parameters. The techniques employed to obtain measurements of activation depended upon the lifetimes of the isomeric states and whether or not these were long enough to transport the irradiated samples by simple means.

Isomers of the first nine nuclides listed in Table I have half-lives of less than 3 min and therefore required special treatment. These samples consisted of either powders or metallic foils enclosed in cylindrical polyethylene vials which were pneumatically transported to a well-type NaI(Tl) detector after exposure. The low energy resolution of this detector necessitated some care in the identification of the prominent features in the pulse height spectra. In all cases, confirmations that these were the fluorescence signatures of the isomers were made by determining the half-lives of the product populations. This was made possible by simultaneously acquiring data

TABLE I. Summary of isomeric nuclei studied. Nuclei marked * were present in isotopically enriched samples. In the sample column, *R* refers to samples contained in vials transferred pneumatically, *P* to flat planchettes, *F* to metallic foils, and *B* to scintillation bottles. The ^{180}Ta sample consisted of a dusting of oxide on a thin aluminum plate, referred to by *D*. In the case of the ^{176}Lu sample, β^- particles were observed instead of fluorescence photons; the NA in the transparency column indicates that this factor was not applicable for ^{176}Lu.

Nuclide	Abundance (%)	Sample form	$T_{1/2}$	Principal fluorescence (keV)	Transparency (%)
^{166}Er	91.54*	Er_2O_3	2.28	207.79	57.90
		(*R*)	sec	(41.70%)	
^{79}Br	50.69	LiBr	4.86	207.20	84.90
		(*R*)	sec	(75.80%)	
^{191}Ir	37.30	Ir	4.94	129.43	10.50
		(*R*)	sec	(25.70%)	
^{197}Au	100.00	Au	7.80	279.11	92.70
		(*R*)	sec	(73.00%)	
^{89}Y	100.00	YF_3	16.06	909.15	94.70
		(*R*)	sec	(99.14%)	
^{77}Se	94.38	Se	17.45	161.92	72.28
		(*R*)	sec	(52.40%)	
^{179}Hf	13.63	HfO	18.68	214.31	52.40
		(*R*)	sec	(94.20%)	
^{199}Hg	16.90	Hg_2Cl_2	43.20	158.40	43.96
		(*R*)	sec	(53.00%)	
^{137}Ba	11.74	BaF_2	153.12	661.66	95.50
		(*R*)	sec	(90.10)	
^{111}Cd	12.80	Cd	48.6	245.49	76.35
		(*F*)	min	(94.00%)	
^{115}In	4.30	In	1.66	391.69	98.30
		(*F*)	h	(64.20%)	
^{87}Sr	7.00	SrF_2	2.81	388.40	95.78
		(*P*)	h	(82.30%)	
^{176}Lu	2.59	$LuCl_3$	3.63	beta	NA
		(*B*)	h		
^{115}In	95.70	In	4.49	336.26	98.00
		(*F*)	h	(45.80%)	
^{180}Ta	4.00*	TaO_2	8.15	55.79	100.00
		(*D*)	h	(36.00%)	
^{135}Ba	6.60	BaF_2	1.20	268.27	94.33
		(*P*)	d	(15.60%)	
^{195}Pt	33.80	Pt	4.02	98.88	4.76
		(coin)	d	(11.40%)	
^{117}Sn	7.70	Sn	13.6	158.56	92.89
		(*F*)	d	(86.40%)	
^{123}Te	0.908	Te	119.7	158.99	62.68
		(*P*)	d	(84.00%)	

through two Ortec 918A ADCAM multichannel buffers controlled by a personal computer. While one ADCAM served to produce a pulse height spectrum, the other collected a record of the total counts received in the preset dwell interval as a function of time. A typical example of the data obtained in this way is given in Figs. 4(a) and 4(b), showing measurements for the isomer $^{167}Er^{m}$.

The remaining nuclides in Table I had half-lives longer than 48.6 min, and could be transported by hand to a nearby solid-type NaI(Tl) detector for counting. Samples containing particularly long-lived isomers like 119.7 d $^{123}Te^{m}$ and 13.61 d $^{117}Sn^{m}$ were transported to the Center for Quantum Electronics where they were counted using a high-purity, *n*-type germanium (HPGe) detector. The physical form of the materials in this slower class consisted either of thin metallic disks or flat polyethylene planchettes containing metallic chips or chemical compounds.

Since the HPGe detector provided greater resolution it was not necessary to monitor the time decay in detail. For some samples, however, energy spectra were acquired after several different elapsed times to provide additional confirmation of the product signature. For example, a pulse height spectrum of $^{123}Te^{m}$ after a 6 MeV exposure is shown in Fig. 5(a). The fluorescence line at 159 keV is well defined and gives 5% counting statistics. Since this was the longest-lived isomer ever reported to be excited by a (γ,γ') reaction, the time decay was experimentally determined from a sequence of energy spectra taken after a 6 MeV exposure. The decay of the count rate is shown in Fig. 5(b). A fit to these data gives a half-life which is in excellent agreement with the literature value.

The nuclide, ^{176}Lu, was examined with a different

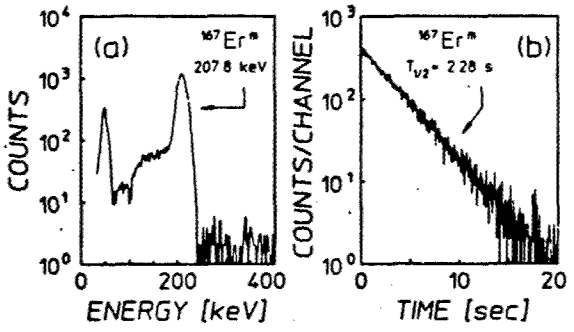

FIG. 4. Fluorescence data for the 207.8 keV line from the decay of $^{167}Er^{m}$ following a 6 MeV exposure. These were obtained with a 7.6 cm×7.6 cm diameter NaI(Tl) detector having a 5.1 cm×2.5 cm diameter well. The sample was irradiated for 25 sec. (a) Pulse height spectrum obtained with a counting period 5 sec in duration after a transport time of 2.06 sec from the end of irradiation to the start of counting. (b) Total counting rates observed in successive dwell intervals of 0.05 sec as a function of the time elapsed from the start of the counting interval following a 6 MeV exposure. The solid line indicates the literature value of the half-life, 2.28 sec.

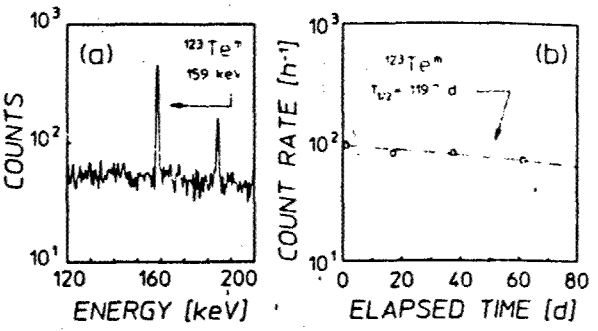

FIG. 5. Fluorescence data for the 159 keV line from the decay of $^{123}Te^{m}$ following a 6 MeV exposure. These were obtained with an *n*-type high-purity germanium detector. The sample was irradiated for 2 h. (a) Pulse height spectrum obtained with a counting period of 10 h duration after a delay from the finish of the irradiation of 22.98 h. (b) Points represent the counting rates in pulse height spectra at different elapsed times. The sizes of the symbols are comparable to one standard deviation and the counting periods were all 10 h. The dashed line shows the literature value for half-life of 119.7 d.

detection scheme. Since the isomer does not return to the ground state by a radiative transition, the number of excited nuclei must be measured by the detection of either β^- particles or the photons from the daughter nucleus. The ground state β^- decays with an end-point energy of 565 keV and the isomer β^- decays with end-point energies of 1313 keV (39.6%) and 1225 keV (60.4%). This difference allowed the use of a Cerenkov detector. Samples consisting of $LuCl_3$ dissolved in distilled water, were contained in polyethylene scintillation bottles. The Cerenkov threshold in water is about 250 keV and β^- particles emitted in the decay of the isomeric states were nearly 10 times more efficient in producing Cerenkov events than those emitted from ground state nuclei. Photons from these events were measured in coincidence, thereby recognizing only signals from the Cerenkov photons produced by single β^- particles. The detector was calibrated with ^{40}K decays from a KCl solution of known activity, since the resulting β^- particles had roughly the same end-point energy as those from $^{176}Lu^{m}$. In these measurements, the individual count rates were monitored to avoid contributions from accidental coincidences triggered by separate β^- events or by thermoluminescence from the material of the bottle. A fit to the experimental data shown in the typical spectrum of Fig. 6 produced a value for the half-life for $^{176}Lu^{m}$ of 3.58±0.05 h, which is in good agreement with the literature value of 3.63 h.

The yields of each of the final state populations were determined from the numbers of counts collected in the corresponding peaks in pulse height spectra. These raw data were then corrected in a standard manner for the photopeak detector efficiency, the fraction of fluorescence photons per decay, and the finite times of sample transport and counting. The latter factor used literature values of the half-lives.[15] It was also necessary to account

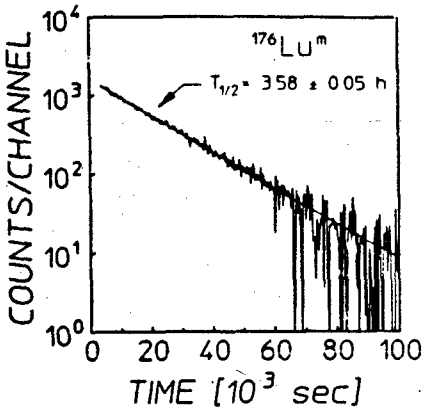

FIG. 6. Data typical of the counting rates observed in successive dwell time intervals of 320 sec for $^{176}Lu^{m}$ as a function of the time following a 6 MeV exposure. The sample was irradiated for 40 min and the delay time to the beginning of the counting was 53 min. A fit to the data is shown by the solid line for a half-life of 3.58±0.05 h, in good agreement with the literature value of 3.63 h.

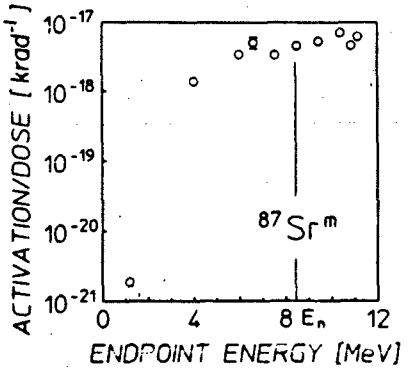

FIG. 7. Normalized activation obtained from irradiations with all four accelerators for $^{87}Sr^{m}$. The size of the symbols is comparable to one standard deviation except where error bars are explicitly shown. The point at 1.2 MeV determined from a DNA/PITHON exposure is an upper bound on the excitation since no fluorescence photons were observed above the level of background. The vertical line indicates the neutron evaporation threshold at $E_n = 8.4$ MeV.

for some attenuation of the fluorescence photons within the samples themselves because of absorption and scattering events. This effect was accommodated by Monte Carlo calculations of a transparency factor for each sample. These corrections were confirmed by comparing the activations obtained from targets containing identical materials, but in different geometries.

RESULTS

Strontium as a benchmark

Normalized activation measurements obtained from all four accelerators for $^{87}Sr^{m}$ are shown in Fig. 7, which also indicates the threshold energy for (γ,n) reactions, E_n at 8.428 MeV. The datum at 1.2 MeV represents an upper limit since no fluorescence photons were observed above the background level. Although lacking in resolution in the critical range from 1.2 to 6 MeV, the data allow several conclusions to be drawn about the photoexcitation process. First is that there is no evidence to support the participation of any nonresonant processes. This type of mechanism, if present, would be heavily dependent upon the density of nuclear states, which rises sharply at energies approaching E_n. The slow increase in the excitation function above 6 MeV relative to the change seen below 4 MeV precludes this as the dominant means of photoexcitation.

The large increase in normalized activation from 1.2 to 4 MeV indicates that at least one resonant gateway of significant magnitude lies in that range. The experimental resolution, however, does not allow a clear observation of the activation edges so the details of these states cannot be directly determined.

Fortunately, the isomer $^{87}Sr^{m}$ is distinguished by the degree to which its photoexcitation has been characterized in the literature. An early work[19] examined the production of this isomer by bremsstrahlung with end points which could be varied up to 3 MeV. The tunability of that device allowed three distinct gateways to be identified at 1.22, 1.88, and 2.66 MeV, and their integrated cross sections to be measured. In the usual units of 10^{-29} cm^2 keV, these were found to be 8.5^{+4}_{-3}, 16^{+8}_{-5}, and 380^{+200}_{-100}, respectively.

Figure 8(a) shows the ^{87}Sr data together with the nor-

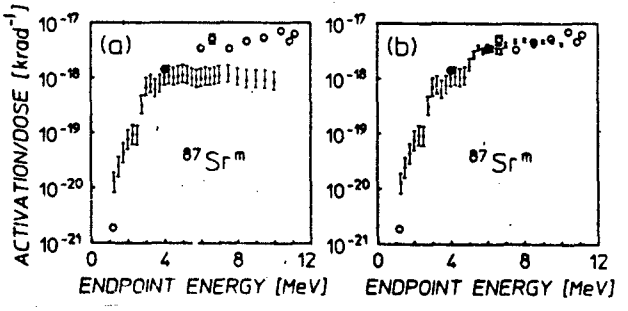

FIG. 8. Open circles plot normalized activations obtained from irradiations with all four accelerators for $^{87}Sr^{m}$ as previously shown in Fig. 7. Also displayed as solid bars are excitation functions calculated from Eq. (1) for the following: (a) Expected photoexcitation through the three known gateways of Ref. 19. The error bars indicate the uncertainties in the measurements of $(\sigma\Gamma)$ in that work. (b) Expected photoexcitation through the three known gateways plus that of a hypothetical state near 5 MeV with an integrated cross section on the order of 4000×10^{-29} cm^2 keV. The error bars indicate only the uncertainties in the measured $(\sigma\Gamma)$ of Ref. 19.

malized activations that should have been excited through the known gateways by photons with energies below 4 MeV. These values were calculated from Eq. (1) for different end-point energies by using typical bremsstrahlung spectra scaled from those shown in Fig. 3. The composite graph produced in this way exhibits the required activation edges at 1.22 and 2.66 MeV in agreement with the actual measurements. No edge is apparent at 1.88 MeV, but this is due to the comparable magnitude and proximity of this level to the one at 1.22 MeV. The correlation of the expected values near 4 MeV with the datum there indicates that no new states are required to explain all of the normalized activation obtained with the 4 MeV linac.

The data above 6 MeV in Fig. 8(a) significantly exceed the photoexcitation which could have been produced through the three known gateways. This extra activation must have therefore represented (γ,γ') reactions which proceeded through one or more unidentified levels. The simplest picture which matches the data is that of a single gateway near 5 MeV with an integrated cross section of the order of 4000×10^{-29} cm^2 keV. The normalized activation expected from this state, as well as those previously identified, is shown in relation to the experimental data in Fig. 8(b).

The nuclide ^{87}Sr provides a benchmark for other (γ,γ') studies since this is the only instance in which the current work can be compared with earlier experiments over a significant range of energies. It is apparent that the present measurements of the photoexcitation of $^{87}Sr^m$ below 4 MeV are completely explained by resonant absorption of photons through gateways already reported in the literature.[19]

Nuclide survey

All of the nuclei of Table I were irradiated with at least three of the four accelerators available. In all cases the general phenomenology seen in Fig. 7 was reproduced, but with considerable variance in the heights of the plateaus of activation reached at the higher energies. A typical example is shown in Fig. 9, which displays data obtained for the isomer $^{167}Er^m$ along with those for $^{87}Sr^m$. Several interesting aspects are apparent. Although the normalized activations achieved with ^{167}Er nuclei are nearly two orders of magnitude larger than those of the ^{87}Sr benchmark, both isomers display similarly slow increases in activation above 6 MeV. This is surprising since nonresonant processes might be expected to be more significant for the photoexcitation of a nucleus as massive as ^{167}Er. Nevertheless, resonant absorption appears to be the dominant means of isomeric production for this nucleus as it was for the benchmark nuclide. The increase in normalized activation between the 4 and 6 MeV data strongly implies that a large gateway lies in this range. The magnitude of the data near 1.2 MeV suggests that a smaller activation edge lies at lower energy.

The measurements obtained from several nuclides, ^{77}Sr, ^{79}Br, ^{111}Cd, and ^{115}In allowed the identification of resonances below 1.5 MeV. The integrated cross sections of those were found to be on the order of 1 to 10×10^{-29} cm^2 keV, and results were reported previously.[9,10,13,14] The isotope, ^{179}Hf, while not providing such detailed information, did indicate an activation edge at about 1.1 MeV for its 18.7 sec isomer $^{179}Hf^m$. Its excitation function is displayed in Fig. 10 and again the relatively slow

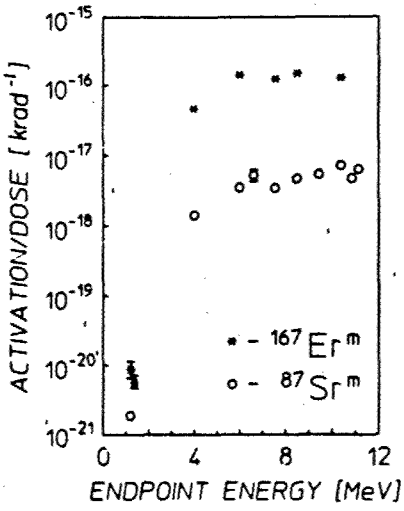

FIG. 9. Normalized activation obtained from irradiations with all four accelerators for $^{167}Er^m$. Also included for the purpose of comparison are those values for $^{87}Sr^m$. The size of the symbols is comparable to one standard deviation except where error bars are explicitly shown. The point at 1.2 MeV for $^{87}Sr^m$ determined from a DNA/PITHON exposure is an upper bound on the excitation since no fluorescence photons were observed above the level of background. The neutron evaporation thresholds for ^{167}Er and ^{87}Sr are 6.4 and 8.4 MeV, respectively.

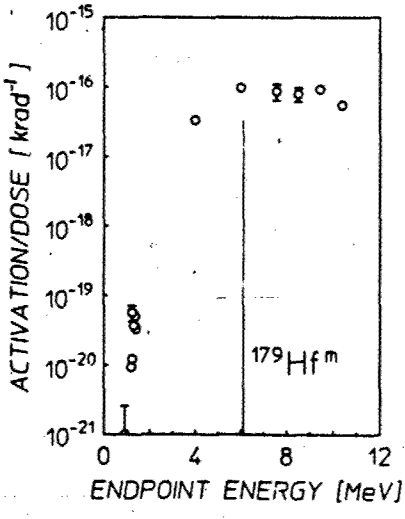

FIG. 10. Normalized activation obtained from irradiations with all four accelerators for 18.7 sec $^{179}Hf^m$. The size of the symbols is comparable to one standard deviation except where error bars are explicitly shown. The vertical line indicates the neutron evaporation threshold at $E_n = 6.1$ MeV.

rise at high energies suggests resonant photoexcitation even for this large nucleus.

The absence of any evidence for nonresonant excitation made it useful to tabulate the results of this work in terms of an effective integrated cross section $(\sigma\Gamma)$, which was a weighted average of the actual values appearing in Eq. (1),

$$(\sigma\Gamma)\equiv\sum_j(\sigma\Gamma)_{jj}\frac{F(E_j,E_0)}{F(2.125,E_0)}\ . \tag{3}$$

The choice of normalizing the relative intensities to 2.125 MeV was arbitrary. However, since the excitation enegies of all of the dominant gateways exceeded 2.125 MeV and since $F(2.125,E_0)>F(E_j,E_0)$ for those gateways, the ratio used to weight individual $(\sigma\Gamma)_{jj}$ in Eq. (3) was always less than unity. This insured that the effective $(\sigma\Gamma)$ was not greater than the sum of all integrated cross sections for a particular nuclide. Substitution of Eq. (3) into Eq. (1) gives

$$(\sigma\Gamma)=\frac{N_f}{N_i\Phi_0F(2.125,E_0)}\ , \tag{4}$$

which in turn shows the effective $(\sigma\Gamma)$ to be the value that would have been necessary for a gateway at 2.125 MeV to produce the observed activation. The results are shown in Table II for the two different values of E_0 of the bremsstrahlung from the two linacs.

Neutron excitations

All of the accelerators used, other than DNA/PITHON, were capable of evaporating neutrons from their environments. Since neutrons can also excite nuclei into their isomeric states it was important to determine the amount of normalized activation which was attributable to these particles. In principle, two types of neutron reactions could have occurred: inelastic (n,n') reactions which would have required hot neutrons and neutron capture (n,γ) processes driven by fluxes of thermal or epithermal neutrons.

Contributions to the observed activations from (n,γ) reactions could be directly determined. The thermal neutron fluxes were measured by irradiating two thin indium foils, one of which was shielded from thermal neutrons by a cadmium cover. In accordance with standard techniques,[22] energy spectra obtained from these foils were examined after exposure for photons from the isomer $^{116}In^m$, which is produced by a branch of the reaction $^{115}In(n,\gamma)^{116}In^{m,g}$. In all cases such activations were negligible. For example, the magnitudes of the fluorescence lines observed in both the bare and the shielded

TABLE II. Summary of experimental results. The quantity ΔJ is the change in spin between ground state and isomer. For both 4 and 6 MeV irradiations, the integrated cross sections of a single gateway state at the reference energy of 2.125 MeV are given as $(\sigma\Gamma)$ and have been corrected for thermal and epithermal neutron contaminations. The ratio of 6 MeV values to those at 4 MeV are given as κ_1. The ratio of integrated cross sections obtained from 10.4 MeV to 6 MeV measurements is κ_2. Also given is the fraction of thermal and epithermal neutron contamination in the total activation, A_n/A_{tot}. The comment NA is used in the column for A_n/A_{tot} when no naturally abundant parent is available for (n,γ) reactions. An entry NA in the κ_2 column indicates that this information is not currently available.

		4 MeV		6 MeV			
Nuclide	ΔJ	$(\sigma\Gamma)$ (10^{-29} cm^2 keV)	A_n/A_{tot} (%)	$(\sigma\Gamma)$ (10^{-29} cm^2 keV)	A_n/A_{tot} (%)	κ_1	κ_2
^{167}Er	3	4600±110	0.01	34000±360	0.32	7.4	1.0
^{79}Br	3	660±17	NA	1900±23	NA	2.9	1.5
^{191}Ir	4	7600±610	NA	36000±960	NA	4.7	NA
^{197}Au	4	2600±40	NA	13000±64	NA	5.0	NA
^{89}Y	4	9±5	NA	260±8	NA	29	2.9
^{77}Se	3	330±4	0.03	6500±32	0.76	20	NA
^{179}Hf	4	9400±120	0.04	25000±110	6.41	2.7	1.1
^{137}Ba	4	330±23	<0.01	1900±23	0.07	5.8	1.4
^{199}Hg	6	260±10	0.05	1400±42	5.40	5.4	NA
^{111}Cd	5	920±12	<0.01	2500±44	0.07	2.7	NA
^{113}In	4	1300±59	NA	4700±180	NA	3.6	0.71
^{87}Sr	4	390±13	<0.01	870±18	0.89	2.2	2.3
^{176}Lu	6	14000±95	0.01	35000±2300	1.51	2.5	NA
^{115}In	4	1800±16	NA	6700±14	NA	3.7	1.5
^{180}Ta	8	18000±6600	NA	35000±650	NA	1.9	NA
^{135}Ba	4	1300±62	<0.01	6000±110	0.39	4.6	4.0
^{195}Pt	4	3000±160	<0.01	14000±220	0.03	4.7	NA
^{117}Sn	5	320±47	<0.01	880±26	0.07	2.8	0.84
^{123}Te	5	4200±730	<0.01	6800±320	1.45	1.6	NA

samples allowed the determination of the thermal neutron flux of 12 neutrons cm^{-2} sec^{-1} in the 6 MeV linac environment. The contributions to the activations from thermal neutrons are summarized in Table II for each of the 19 nuclides studied.

Because of a beryllium window used in the construction of the 6 MeV linac, that environment had the largest neutron flux. Nevertheless, the results of Table II show that under no conditions did the thermal neutrons contribute more than a few percent of the activation. In most cases neutron contamination represented a few $\times 10^{-4}$ fraction of the observed activations from the 6 MeV linac. The fast neutron flux was expected to be even less important and attempts to record any flux with the (n,p) reactions of ^{46}Ti, ^{47}Ti, and ^{58}Ni were completely negative. Calculations indicated a flux of fast neutrons from the photodisintegration of environmental sources consistent with this negative and limited contamination from (n,n') reactions to tenths of a percent.

CONCLUSIONS

The principal conclusion of this work is that some of the integrated cross sections for exciting isomers can be extraordinarily large, approaching 10^{-21} cm^2 eV. This is about three to four orders of magnitude larger than what has been usually reported in the past.

Typified by the reaction ^{167}Er$(\gamma,\gamma')^{167}$Er^m, these enhanced processes seem to occur through discrete gateways or through narrow bands of gateway states. The data of Fig. 9 for ^{167}Er have a compelling resemblance to those for the excitation of ^{87}Sr which is known to occur through a few discrete levels. The same sharp jump in activation with increasing x-ray end point is followed by relatively level yield up to 11 MeV. It is possible to fit the data for ^{167}Er with a single gateway near 4 MeV but this is not a unique choice. The excitation function for the reaction ^{179}Hf$(\gamma,\gamma')^{179}$Hf^m shown in Fig. 10 also seems compelling in suggesting a single jump in activation at energies below 4 MeV. Table II shows that more than half of the 19 reactions studied had (γ,γ') reaction channels producing isomers with integrated cross sections greater than 1000×10^{-29} cm^2 keV.

The possibility that these unexpectedly large channels for the photoexcitation of isomers were the results of poor calibrations of fluxes was minimized by the use of four different accelerators in diverse environments and by the fact that the yields of the reaction ^{87}Sr$(\gamma,\gamma')^{87}$Sr^m up to 4 MeV were completely explained by the accepted values of integrated cross sections. Contamination of the products by activations from photoneutrons was shown to be generally less than 1%. It would seem that these enhanced channels for (γ,γ') reactions are the results of surprisingly favorable transitions to intermediate states that can be excited at energies less than 4 MeV. Earlier works reported in the literature were generally limited to 3 MeV and did not find activations of this magnitude, so it would be reasonable to speculate that these highly favored channels might lie between 3 and 4 MeV above the ground state.

While the ratios of activations found with 4 MeV bremsstrahlung to that produced around 1 MeV were of the order of thousands, the further increases from 4 to 6 MeV were much smaller. In Table II, the quantity κ_1 summarizes the increases in activation produced by raising the end point from 4 to 6 MeV and the quantity κ_2 records the further change resulting from an increase from 6 to 10 MeV. With a few obvious exceptions, the general trend supports the hypothesis that the principal nuclear structure responsible for the order-of-magnitude enhancement of (γ,γ') reactions lies below 4 MeV. Much smaller increases occur between 4 and 6 MeV and perhaps none between 6 and 10 MeV. Despite the care taken in reconciling the different environments, values of $0.7 \le \kappa_2 \le 1.5$ are probably not significantly different from unity. There is no persuasive evidence that additional channels opened between 6 and 10 MeV. In turn, this seems to imply that the giant dipole resonances have nothing to do with the enhancement of these (γ,γ') reactions.

The difficulties in explaining the sizes of the integrated cross sections reported in this work accrue from the large changes in angular momentum, J separating ground states from isomers. Most of the larger values belong to nuclei which are spheroidal and the projections of angular momentum, K, upon the axes of elongation differ greatly in ground and isomeric states. With an absorption transition of reasonable probability, changes in J and K are limited to $\Delta J \le 2$ and $\Delta K \le 2$. While the first might be satisfied by making a transition from the ground state to a high member of a rotational band built upon the final state, the second would be violated because K is conserved within a rotational band. What is needed is a mechanism to mix K values of nuclear levels belonging to rotational bands built upon initial and final states of the (γ,γ') reaction.

It is interesting to speculate that this might occur as a result of couplings to states built upon cores of nonfissioning shape isomers.[23] Such states show double minima in energy as functions of elongation, even at low values of spin. At some values of excitation energy the shape of such a nucleus would be unstable and projections upon its principal axes would no longer be conserved. In this way the transition from a K value characteristic of the ground state to one consistent with the isomer might occur by mixing with such a state. In any case the frequency with which giant values of integrated cross sections for photoexcitation were found in this work argues for some type of core property varying slowly with increasing nuclear size. Further work is needed to resolve the precise cause of this phenomenon.

This work was supported by the Strategic Defense Initiative Organization/Innovative Science and Technology Directorate and directed by the Naval Research Laboratory.

*Present address: High Energy Laser Associates, Oakland, CA 94611.
†Present address: Plasma Physics Department, Soreq Nuclear Research Center, Israel.
‡Present address: The University of Texas Southwestern Medical Center, Dallas, TX 75235.

[1]See, for example, the review, S. S. Dietrich and B. L. Berman, At. Data Nucl. Data Tables **38**, 199 (1988).
[2]B. Pontecorvo and A. Lazard, C. R. Acad. Sci. **208**, 99 (1939).
[3]G. B. Collins, B. Waldman, E. M. Stubblefield, and M. Goldhaber, Phys. Rev. **55**, 507 (1939).
[4]Y. Watanabe and T. Mukoyama, Bull. Inst. Chem. Res., Kyoto Univ. **57**, 72 (1979).
[5]M. Krcmar, A. Ljubicic, K. Pisk, B. Logan, and M. Vrtar, Phys. Rev. C **25**, 2097 (1982).
[6]I. Bikit, J. Slivka, I. V. Anicin, L. Marinkov, A. Ruydic, and W. D. Hamilton, Phys. Rev. C **35**, 1943 (1987).
[7]M. Krcmar, A. Ljubicic, B. A. Logan, and M. Bistrovic, Phys. Rev. C **33**, 293 (1986).
[8]E. B. Norman, S. E. Kellogg, T. Bertram, S. Gil, and P. Wong, Astrophys. J. **281**, 360 (1984).
[9]J. A. Anderson and C. B. Collins, Rev. Sci. Instrum. **58**, 2157 (1987).
[10]J. A. Anderson and C. B. Collins, Rev. Sci. Instrum. **59**, 414 (1988).
[11]Walter R. Nelson, Hideo Hirayama, and David W. O. Roger, SLAC Report 265, 1985.
[12]J. A. Halbleib and T. A. Mehlhorn, Sandia National Laboratories Report SAND84-0573, 1984.
[13]J. A. Anderson, M. J. Byrd, and C. B. Collins, Phys. Rev. C **38**, 2833 (1988).
[14]C. B. Collins, J. A. Anderson, Y. Paiss, C. D. Eberhard, R. J. Peterson, and W. L. Hodge, Phys. Rev. C **38**, 1852 (1988).
[15]*Evaluated Nuclear Structure Data File*, Information Analysis Center Report BNL-NC5-51655 (Brookhaven National Laboratory, Upton, New York, 1983).
[16]C. B. Collins, C. D. Eberhard, J. W. Glesener, and J. A. Anderson, Phys. Rev. C **37**, 2267 (1988).
[17]J. J. Carroll, J. A. Anderson, J. W. Glesener, C. D. Eberhard, and C. B. Collins, Astrophys. J. **344**, 454 (1989).
[18]C. B. Collins, J. J. Carroll, T. W. Sinor, M. J. Byrd, D. G. Richmond, K. N. Taylor, M. Huber, N. Huxel, P. v. Neumann-Cosel, A. Richter, C. Spieler, and W. Ziegler, Phys. Rev. C **42**, 1813 (1990).
[19]E. C. Booth and J. Brownson, Nucl. Phys. **A98**, 529 (1967).
[20]B. Bernstein and I. B. Smith, IEEE Trans. Nucl. Sci. **NS-20**, 294 (1973).
[21]R. Mohan, C. Chui, and L. Lidofsky, Med. Phys. **12**, 595 (1985).
[22]*ASTM Standard Method for Determining Thermal Neutron Reaction and Fluence Rates by Radioactivation Techniques*, Publication E 262-86 (American Society for Testing and Materials, Philadelphia, 1987), and references cited there.
[23]M. Girod, J. P. Delaroche, D. Gogny, and J. F. Berger, Phys Rev. **62**, 2452 (1989).

Physics Letters B 266 (1991) 9–13
North-Holland

PHYSICS LETTERS B

Resonant photoexcitation of isomers. $^{115}In^{m}$ as a test case ☆

P. von Neumann-Cosel, A. Richter, C. Spieler, W. Ziegler
Institut für Kernphysik, Technische Hochschule Darmstadt, W-6100 Darmstadt, FRG

J.J. Carroll, T.W. Sinor, D.G. Richmond, K.N. Taylor, C.B. Collins
Center for Quantum Electronics, University of Texas at Dallas, Richardson, TX 75083-0688, USA

and

K. Heyde
Institute for Theoretical Physics, Proeftuinstraat 86, B-9000 Ghent, Belgium

Received 17 April 1991

Large integrated cross sections for the photoexcitation of $^{115}In^{m}$ have been detected around $E_\gamma = 3$ MeV. Complementary nuclear resonance fluorescence studies prove that the g.s. transition strength is largely confined to the same energy region and the intermediate excited states are identified. Unified-model calculations indicate magnetic dipole $1g_{9/2} \rightarrow 1g_{7/2}$ spin-flip transitions as the major excitation mechanism.

1. Introduction

The photoactivation of isomers has a long tradition in nuclear structure studies [1]. Most investigations have concentrated on two areas, viz. the region around particle threshold and the region of low excitation energies, typically $E_x < 2$ MeV. The former reveals information like the average ratio of isomeric to total photoabsorption cross sections [2] or serves as a test of statistical aspects of γ-decay at high excitation energies [3]. In the low energy regime, the isomer population occurs via resonant photoabsorption of selectively excited intermediate states which show a finite branching for a γ-decay (or a cascade) to the isomeric level. These intermediate levels provide unique nuclear structure information, often hardly accessible by other means [4].

☆ Work supported by the German Federal Minister for Research and Technology (BMFT) under contract number 06DA1841 and the Department of Defense through the Naval Research Laboratory.

Recent studies of the little explored energy region between these two extremes have shown surprising results. Very large cross sections for the population of isomeric states at energies $E_x \gtrsim 2$–4 MeV have been observed in a variety of nuclei [5,6]. By investigating the excitation function it has been demonstrated [7] for the special case of the deexcitation of $^{180}Ta^{m}$ that the resonant photoabsorption proceeds through two intermediate states only (or closely spaced groups within the experimental resolution of ≈ 200 keV). The corresponding cross sections are three orders of magnitude larger than typical values in other isomers below 2 MeV. Similar data have been reported [8] for the 120 d isomer in ^{123}Te. Besides the obvious question of a nuclear structure interpretation, these findings provide unexpected encouragement of schemes for pumping a γ-ray laser that depend upon the sudden deexcitation of isomeric populations [9].

The experiments presented in this letter are a first effort to gain some deeper understanding of the nuclear structure phenomena responsible for the results

described above. The choice of ^{115}In was based on several considerations: (i) The photoactivation of the $E_x = 0.335$ MeV, $J^\pi = \frac{1}{2}^-$ isomer in this isotope (g.s. $J^\pi = \frac{9}{2}^+$) is probably the most extensively studied case (see refs. [4,10,11] for references) and nuclear structure data are available [12] to completely determine the contribution of all intermediate states in the region below 2 MeV which is not covered in the present experiments. (ii) The large natural abundance (95.6%) easily permits a complementary nuclear resonance fluorescence (NRF) study which characterizes the levels important in photoabsorption in more detail. (iii) The low-energy part of the ^{115}In spectrum has been successfully described [13] within the unified-model approach [14] and an extension to somewhat higher energies seems promising. Thus, a microscopic interpretation of the mixing, which distinguishes the intermediate states, can be given. (iv) The vibrational odd–even nucleus ^{115}In can be regarded as a prototype for many isotopes in this mass region containing an isomer.

2. Photoactivation experiments

Experiments were performed at the superconducting linear electron accelerator (S-DALINAC) in Darmstadt [15]. Bremsstrahlungs spectra with endpoint energies $E_0 = 2$–5 MeV were generated by irradiating a Ta converter. Disks of nominally 1 g of natural Indium (diameter 3.8 cm) were placed in the photon beam. Typical irradiation times were 4 h with an average electron current of 20 μA. The endpoint energies were varied in steps of 125 or 250 keV. The characteristic 336 keV isomeric transition of ^{115}In, measured with a Ge(Li) detector, served as a signature of the activation and the yields were determined as described in ref. [7]. The isomeric yield N_f can be expressed as

$$N_f = N_t \int_{E_c}^{E_0} \sigma(E) \frac{\mathrm{d}\phi(E, E_0)}{\mathrm{d}E} \mathrm{d}E , \qquad (1)$$

where N_t denotes the number of target atoms, $\mathrm{d}\phi/\mathrm{d}E$ describes the spectral intensity per cm^2 of the photon field for an endpoint energy E_0, and $\sigma(E)$ is the resonant absorption cross section. A description of the incident photon spectra was obtained from calculations with the electron–photon transport code EGS4 whose general validity has been demonstrated [16]. The lower integral limit in eq. (1) is defined by a cut-off energy E_c in the calculations.

The typical widths of resonant intermediate states are small enough to assume that $\mathrm{d}\sigma/\mathrm{d}E$ is constant over the resonance region. Then, eq. (1) can be simplified,

$$N_f = N_t \sum_j (\sigma\Gamma)_{j,\mathrm{iso}} \sigma(E_j, E_0) , \qquad (2)$$

with $(\sigma\Gamma)_{j,\mathrm{iso}}$ giving the integrated cross section of the jth level. We note that nonresonant cross sections, which would inhibit the use of eq. (2), are not considered. Claims of important nonresonant contributions [17] to the photoexcitation of isomers have recently been disproved [18].

Information on new intermediate states is extracted from the experimental excitation function shown in fig. 1 by including calculated $(\sigma\Gamma)_{j,\mathrm{iso}}$ values for all intermediate states below 2 MeV and then introduce a new state whenever a break in the excitation function requires additional strength. For the former, branching ratios and radiative widths are known [12] from independent experimental results. The integrated cross sections can be calculated from

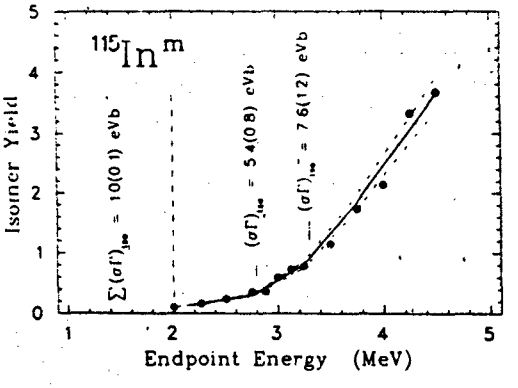

Fig. 1. Isomer yield as a function of endpoint energy. The straight line is calculated using intermediate states at 2.8 and 3.3 MeV with the strengths indicated. The contributions of states below 2 MeV are taken from the literature [12]. Statistical errors are smaller than the data point size. The error region spanned by the dashed lines additionally includes statistical errors of the photon spectra and an assumed 15% error for each individual $(\sigma\Gamma)_{\mathrm{iso}}$ value.

$$(\sigma\Gamma)_{i\omega} = \pi^2\left(\frac{\hbar c}{E_\gamma}\right)^2 g \frac{\Gamma_0 \Gamma_{i\omega}}{\Gamma} , \qquad (3)$$

with $g=(2J_i+1)/(2J_s+1)$. Here, $J_{i,s}$ are the spins of the g.s. and intermediate state, Γ_0 and $\Gamma_{i\omega}$ are the partial γ-width and the effective width to the isomer (including cascades), and Γ is the total width. A yield curve calculated in this way is presented as a solid line in fig. 1. No further states had to be included to describe the measured yields up to $E_x = 2.8$ MeV. The breaks in the theoretical excitation function, where new states were introduced, are indicated in fig. 1 and the corresponding cross sections given.

3. Nuclear resonance fluorescence experiments

The experimental setup especially designed for NRF experiments is described in ref. [19]. An absolute calibration of the photon spectra was attained by the use of In/Al and In/B sandwich targets which provide well-determined reference transitions. In order to cover an energy range $E_x \simeq 1.5$–4.5 MeV, measurements were performed at endpoint energies $E_0 = 3.1$, 4.6 and 5.2 MeV. The variation of E_0 also enables us to distinguish g.s. transitions from decays to excited states. For details of the data analysis see ref. [19].

Integrated cross sections for g.s. transitions $(\sigma\Gamma)_0$ comparable to the isomer activation results, eq. (3), can be obtained from

$$(\sigma\Gamma)_0 = \pi^2\left(\frac{\hbar c}{E_\gamma}\right)^2 g \frac{\Gamma_0^2}{\Gamma} W(\Theta) . \qquad (4)$$

The additional factor $W(\Theta)$ accounts for the nonisotropic decay characteristic which depends on the multipolarity (dipole/quadrupole) and the mixing ration δ of E2 and M1 transitions. It can be shown that due to the large g.s. spin ($J^\pi = \frac{9}{2}^+$) results obtained in the present experimental geometry are insensitive within $\pm 10\%$ to the unknown final state spin as well as an arbitrary choice of the mixing parameter and the $W(\Theta)$ dependence can be neglected.

A full account of the NRF results will be given elsewhere [20]. Here, we present only results important for the isomer population and restrict the discussion of the lower energy region to a few comments in relation to other (γ, γ') studies. The agreement with the results of Cauchois et al. [21] is good, in particular for the 1.132 and 1.463 MeV state which they obtained with the self absorption technique. The correspondence to the results of Alston [22] is reasonable for stronger transitions and mediocre for the others. Below $E_x = 2.5$ MeV, branching ratios have been measured [23] for all levels observed in the present study and assure that no significant partial width to the isomer is missed in the analysis of the excitation function.

The excitation energy region corresponding to the large $(\sigma\Gamma)_{i\omega}$ values is shown in the upper part of fig. 2. The brackets represent the experimental uncertainty of the energies of the intermediate states identified in the photoactivation. The striking result is that, except for a few moderate levels around 3.0 and 3.7 MeV, all (γ, γ') transitions are found within these energy regions. Thus, these states (or a part of them) must be responsible for the isomer population. It is further demonstrated in the lower part of fig. 2 that

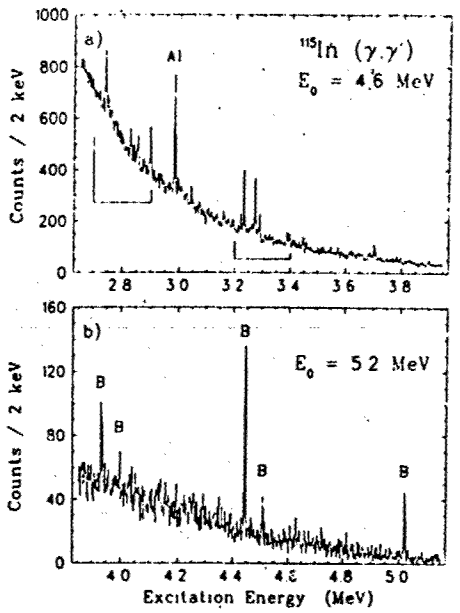

Fig. 2. Spectra of the ^{115}In(γ,γ') reaction obtained for endpoint energies $E_0 = 4.6$ and 5.2 MeV. The brackets indicate regions where significant strength for the population of the isomer is found in the excitation function (see fig. 1). The strongest lines marked B and Al are calibration lines.

no other resolved (γ, γ') state is detected up to $E_x = 5$ MeV (an upper limit of ≈ 5 eV b is estimated for possible $(\sigma\Gamma)_0$ strength above 4 MeV). These results confirm that all important intermediate states have been identified up to 4.5 meV.

4. Nuclear model calculations and discussion

In order to compare the intermediate states at low and higher energies, the isomeric ratio $R = \Gamma_{iso}/(\Gamma_0 + \Gamma_{iso})$ is introduced. The important states at low energies show typical values $R \approx 0.1$–0.2. For the observed groups around $E_1 = 2.8$ MeV and $E_1 = 3.3$ MeV, values $R_1 = 0.32$ and $R_2 = 0.27$ are obtained by averaging over all the states within the brackets. These numbers represent lower limits of R only, since not all the states necessarily show a branching to the isomer. In principle, states with $R \approx 1$ could lead to appreciable $(\sigma\Gamma)_{iso}$ values also and would eventually be missed in the (γ, γ') data because of a too small Γ_0. Such contributions, however, seem to play no important role in ^{115}In.

Further insight is attained from an analysis within the unified-model [14]. In the case of ^{115}In, the configuration space is built by proton 1h-states (relative to the semimagic ^{116}Sn nucleus) and 1p–2h states across the major shell (relative to ^{114}Cd) coupled to collective phonons (up to three quadrupole and two octupole) in the underlying cores. The two subspaces are mixed by a residual interaction which connects the pairing mode describing the 2h-core (^{114}Cd) coupled configurations with the surface model [14].

The parameters used for the calculation of energies and wavefunctions closely follow ref. [13]. For the study of M1 transitions, g-factors $g_s = 0.7 g_s^{free}$ for the quenched proton spin value and $g_R = Z/A$ for the gyromagnetic ratio were used. Alternatively, we tested the other extreme: $g_R = 0$. This variation shows some influence in detail, but the general conclusions described below are not affected. The comparison to experiment proceeds by first computing all possible E1/M1/E2 upward transitions. Then, for states with a large partial g.s. width the full decay cascade is taken into account. In this way, model values for $(\sigma\Gamma)_0$ and $(\sigma\Gamma)_{iso}$ as well as branching ratios are determined.

Some general properties of the results, which are surprisingly insensitive to details of the calculations, are summarized first. In accordance with the experimental results, intermediate states are found in a limited energy region above $E_x = 2.5$ MeV only. Also, typical $(\sigma\Gamma)_{iso}$ values at lower energies are suppressed by a factor of about 10–100. The number of important states is small, similar to the experimental NRF results.

Fig. 3 presents a comparison of both experiments and the model results. The calculations show a rough division into two groups which might be related to the experimental $(\sigma\Gamma)_{iso}$ data. A one-to-one correspondence, however, is certainly beyond the limits of the approach. Summing the model $(\sigma\Gamma)_{iso}$ strength, the isomeric ratios $R_1 = 0.25$ and $R_2 = 0.46$ compare favourably to the experimental numbers. However, an overall factor of 4 is needed to reach absolute values of integrated cross sections similar to the measured ones.

We have investigated whether this shortcoming might result from a model-inherent deviation of the average strength for the different transition types compared to experiment. Model distributions of reduced transition probabilities $B(\pi L)$ for E1/M1/E2 were produced from a complete decay study of all states up to 4 MeV and compared to the experimental systematics of Endt [24] for this mass region. The resulting patterns look very similar and experiment/model ratios $F(E1) = 0.2$, $F(M1) = 2$ and $F(E2) = 10$ are deduced from the position of the maxima. A repetition of the decay cascade calculation with each transition modified by the correction factors leads to an agreement of absolute $(\sigma\Gamma)_0$ and $(\sigma\Gamma)_{iso}$ values within a factor of two, but slightly detoriating isomeric ration results $R_1 = 0.13$ and $R_2 = 0.60$.

The overall agreement seems quite encouraging and indicates that no major part of the relevant configuration space is missed. A detailed analysis of the main decay branches reveals a clear picture of the important amplitudes in the intermediate state wavefunctions. All theoretical states shown in fig. 3 have $J^\pi = \frac{7}{2}^+$ and the g.s. coupling is dominated in *all* cases by single-particle $1g_{9/2} \rightarrow 1g_{7/2}$ spin-flip transitions. The first step of the decay to the isomer in the model calculations proceeds mainly via E1 or E2 transitions, depending on the application of the correction factors which strongly suppress E1 versus E2. In the former case, the E1 operator leads to configurations including negative parity 1h-states which effectively

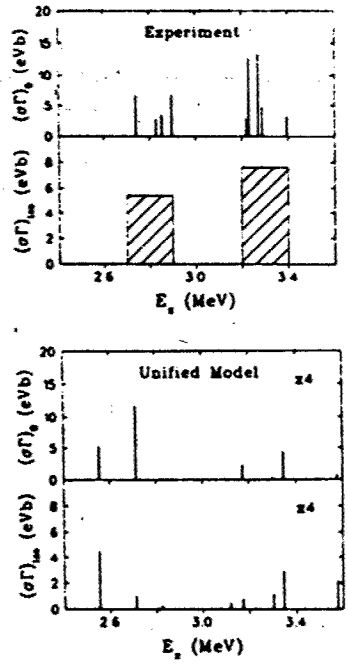

Fig. 3. Comparison of the experimental $(\sigma\Gamma)_0$ and $(\sigma\Gamma)_{\infty}$ results with unified-model calculations. The dashed histograms for the experimental $(\sigma\Gamma)_{\infty}$ strength indicate that they might be the sum of unresolved states within the experimental resolution.

populate the $J^{\pi}=\frac{1}{2}^-$ isomer. In the latter scenario, higher phonon Cd-core configurations which are admixed to a few important levels in the cascade open an efficient path for collective E2 depopulation of the intermediate states.

To summarize, large cross sections feeding the isomer in ^{115}In have been found around $E_x=3$ MeV. A complementary (γ,γ') study clearly demonstrates that the strength is induced by a small number of discrete intermediate states. A microscopic analysis within the unified-model indicates that M1 spin-flip transitions ($1g_{9/2}\rightarrow 1g_{7/2}$) are most important for the resonant absorption into excitations with a significant 1p–2h component while admixtures to the wave functions permitting E1 single-hole transitions or collective E2 strength from higher phonon Cd-core configurations are responsible for the branching to the isomer. The importance of $1g_{7/2}$ strength for the γ-decay has also been demonstrated [25] in the even-even neighbour ^{116}Sn. The combined study of isomer excitation function and nuclear resonance fluorescence turns out to be an efficient tool for further investigations in the revived field of photoexcitation of isomers.

Acknowledgement

We are indebted to Dr. H.-D. Gräf and the S-DALINAC crew for their great support in operating the accelerator. We thank M. Huber and N. Huxel for their assistance in the experiment.

References

[1] G.B. Collins et al., Phys. Rev. 55 (1939) 507.
[2] Z.M. Bigan et al., Sov. J. Nucl. Phys. 49 (1989) 567.
[3] L.Z. Dzhilavyan et al., Sov. J. Nucl. Phys. 51 (1990) 215.
[4] E.C. Booth and J. Brownson, Nucl. Phys. A 98 (1967) 529.
[5] C.B. Collins et al., Phys. Rev. C 37 (1988) 2267.
[6] J.J. Carroll et al., Phys. Rev. C 43 (1991) 1238.
[7] C.B. Collins et al., Phys. Rev. C 42 (1990) R1813.
[8] J.J. Carroll et al., Phys. Rev. C 43 (1991) 897.
[9] C.B. Collins et al., J. Appl. Phys. 53 (1982) 4645.
[10] W.J. Varhue and T.G. Williamson, Int. J. Appl. Radiat. Isot. 37 (1986) 155.
[11] C.B. Collins et al., Phys. Rev. C 38 (1988) 1852.
[12] J. Blachot and G. Marguier, Nucl. Data Sheets 52 (1987) 565.
[13] K. Heyde, M. Waroquier and R.A. Meyer, Phys. Rev. C 17 (1978) 1219.
[14] K. Heyde et al., Phys. Rep. 102 (1983) 291.
[15] K. Alrutz-Ziemssen et al., Part. Acc. 29 (1990) 53.
[16] T.M. Jenkins, W.R. Nelson and A. Rindi, eds., Monte Carlo transport of photons and electrons (Plenum, New York, 1988).
[17] A. Ljubičić et al., Phys. Rev. C 23 (1981) 2238; M. Krčmar et al., Phys. Rev. C 33 (1986) 293; C 41 (1990) 771.
[18] P. von Neumann-Cosel et al., Phys. Rev. C, in press.
[19] W. Ziegler et al., Phys. Rev. Lett. 65 (1990) 2515.
[20] C. Spieler et al., to be published.
[21] Y. Cauchois et al., J. Phys. G 7 (1981) 1539.
[22] W.J. Alston III, Phys. Rev. 188 (1969) 1837.
[23] A.B. Smith et al., J. Phys. G 11 (1985) 125.
[24] P.M. Endt, At. Data Nucl. Data Tables 26 (1981) 47.
[25] J.M. Schippers et al., KVI annual report (1988) p. 7; J.M. Schippers, Ph.D. thesis, Rijksuniversiteit Groningen (1988).

PHYSICAL REVIEW C VOLUME 46, NUMBER 3 SEPTEMBER 1992

Common thresholds and the role of deformations in the photoexcitation of isomers

C. B. Collins, J. J. Carroll, K. N. Taylor, D. G. Richmond, and T. W. Sinor
Center for Quantum Electronics, University of Texas at Dallas, P.O. Box 830688, Richardson, Texas 75083

M. Huber, P. von Neumann-Cosel, A. Richter, and W. Ziegler
Institut für Kernphysik, Technische Hochschule Darmstadt, D-6100 Darmstadt, Germany

(Received 25 October 1991)

Photoexcitations of the short-lived isomers $^{167}Er^{m}$, $T_{1/2}=2.28$ s, $^{179}Hf^{m}$, $T_{1/2}=18.68$ s, $^{191}Ir^{m}$, $T_{1/2}=4.94$ s, and $^{197}Au^{m}$, $T_{1/2}=7.8$ s, were produced with bremsstrahlung from the superconducting Darmstadt linear accelerator. Excitation functions were measured for the population of these isomers by (γ,γ') reactions between 2 and 7 MeV. They indicated that the isomers were excited by resonant absorption through isolated intermediate states having integrated cross sections in excess of 10^{-26} cm^2 keV, i.e., values about 1000 times larger than most (γ,γ') activation reactions reported previously although they were comparable to those reported earlier for the depopulating reaction $^{180}Ta^{m}(\gamma,\gamma')^{180}Ta$. In all four nuclei a common onset was observed near 2.5 MeV for intermediate states with strengths much larger than those occurring at lower energies. The summed cross sections exhibit a clear correlation with the ground state deformations.

PACS number(s): 25.20.Dc, 27.70.+q, 27.80.+w

I. INTRODUCTION

The photoexcitation of nuclear isomers by (γ,γ') reactions has been known for more than 50 years [1,2]. For most of this time, studies of this phenomenon have been concentrated either upon higher photon energies around particle thresholds or upon relatively low energies of excitation, $E \leq 2$ MeV. Results in the former case have been dominated by the photoabsorption through the giant dipole resonance and have emphasized concerns for the gross properties of the photoexcitation process [3] or for tests of statistical models of γ decay at high excitation energies [4]. At the lower energies, efforts have been characterized by the excitation of discrete intermediate states that have branched or cascaded back to an isomer with a significant probability [5]. Under those conditions the integrated cross sections for the photoexcitation of isomers have been typically 10^{-29} to 10^{-27} cm^2 keV.

Only recently have studies been extended systematically into the intermediate range of energies and then with surprising results. Initiated with the observation [6] of the deexcitation of the isomer $^{180}Ta^{m}(\gamma,\gamma')^{180}Ta$ with an unprecedented integrated cross section exceeding 10^{-25} cm^2 keV, such extraordinary values were subsequently reported [7] for $^{176}Lu(\gamma,\gamma')^{176}Lu^{m}$, also. A large survey of 19 nuclides was reported [8] that covered the broad range of end-point energies 0.5–11 MeV from four different accelerators and established that comparable integrated cross sections can be found in the majority of cases studied. However, the relatively coarse mesh over which those measurements were conducted prevented the extraction of the excitation energies and strengths of individual intermediate states (IS's).

As a next step, a series of experiments was performed in the 2–7-MeV range in order to identify and characterize the important intermediate levels. These studies were motivated by two principal aspects. First, the very efficient coupling of the ground state (g.s.) and isomer demonstrated in Refs. [6–8] provided unexpected encouragement of schemes [9] to use the resonant photoexcitation of isomers (or the reverse process, the sudden depopulation of an isomer) as a mechanism to pump a γ-ray laser. Among other conditions, the feasibility depends sensitively on the locations and coupling strengths of the resonant states. Second, the reaction mechanism selects a unique set of states with two features: a large partial g.s. width and strong admixtures in the wave function, which induce the decay into states efficiently cascading to the isomer. A schematic representation of this process which defines important parameters is shown in Fig. 1. In the excitation energy region investigated, the underlying nuclear structure is almost unexplored and theoretical interpretations are badly needed. To our knowledge, the only attempt to interpret similar data on

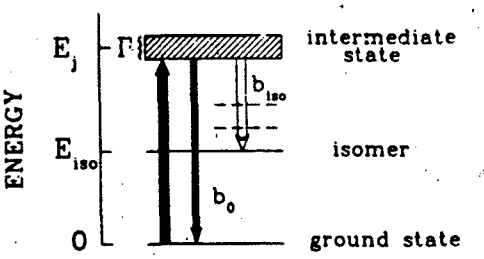

FIG. 1. Schematic representation of the resonant photoexcitation mechanism for population of an isomer with energy E_{iso}. The hatched area describes an intermediate-state IS with energy E_j and total decay width Γ. The direct branch to the ground state is denoted by b_0, and b_{iso} represents the sum of all branchings leading to the isomer. The dashed horizontal lines indicate that the decay to the isomer usually proceeds via a cascade.

a microscopic base is found in Ref. [10]. On the other hand, such data provide stringent constraints for any model calculation.

A study of the deexcitation of $^{180}Ta^m$ confirmed the striking results of Ref. [6]. It was found to occur through two intermediate states at 2.8 and 3.6 MeV with integrated cross sections of 1.2×10^{-25} and 3.5×10^{-25} cm^2 keV, respectively [11]. The excitation of isomers with large probabilities through discrete intermediate states was also established in the reactions [12,13] of $^{123,125}Te(\gamma,\gamma')^{123,125}Te^m$ and $^{115}In(\gamma,\gamma')^{115}In^m$. However, in these latter cases, integrated cross sections were of the order of 10^{-26} to 10^{-25} cm^2 keV.

Utilizing the large natural abundance of ^{115}In, complementary nuclear resonance fluorescence experiments were performed and the important intermediate states were identified [13]. Unified model [14] calculations provided a qualitative explanation of the IS as being due to fragmented $g_{9/2}\rightarrow g_{7/2}$ spin-flip strength.

The next step in understanding would require an extension of the information available on IS's in a variety of nuclei which might build a base for more systematic nuclear structure interpretations. The recent survey [8] indicates two empirical trends, viz., an average increase of yields with mass number and a correlation with the g.s. deformation. These findings are illustrated in Figs. 2(a) and 2(b) in which the integrated cross sections obtained at an electron energy of 6 MeV are plotted versus A and N_pN_n, respectively. The latter is the product of open-shell proton and neutron occupation numbers and is a well-established measure of the deformation driving proton-neutron interactions [15]. Its application is restricted to nuclei with $A>90$. While the above-mentioned trends are clearly visible, before attempting a detailed comparison one should keep in mind that these integrated cross sections have been normalized by arbitrarily assuming a single IS at 2 MeV.

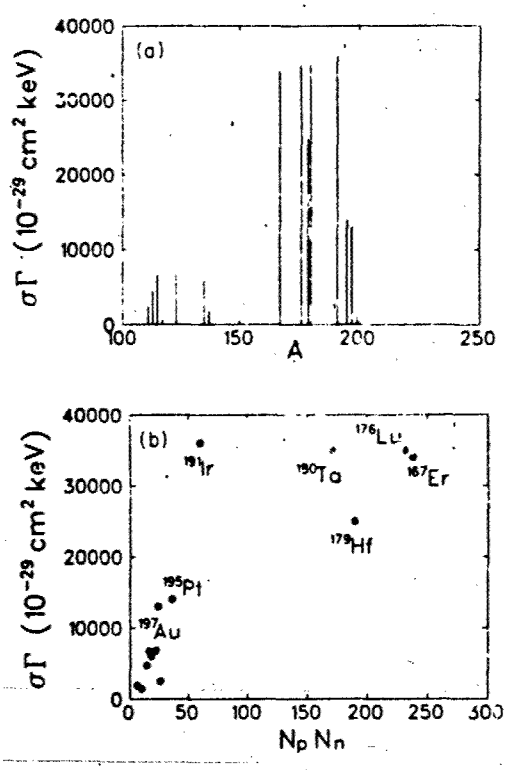

FIG. 2. Integrated cross sections of Ref. [8] for an electron energy of 6 MeV determined according to the assumption of a single hypothetical intermediate state at 2 MeV plotted versus (a) mass number A and (b) the product of open-shell proton and neutron occupation numbers N_pN_n calculated according to Ref. [15].

One purpose of the present experiments was to investigate the empirical correlation with the g.s. deformation more closely. Therefore the nuclides ^{167}Er, ^{179}Hf, ^{191}Ir, and ^{197}Au were chosen because they cover a large span of deformations ($\delta=0.09-0.32$), but lie within the same group in Fig. 2(a) and have comparable mass numbers. Furthermore, the well-deformed ^{167}Er and ^{179}Hf are prime candidates to verify that the extraordinarily large cross sections of the IS derived [11] for $^{180}Ta^m$ are indeed not uncommon. Additional results obtained in the $A=70-90$ mass region will be presented elsewhere.

II. EXPERIMENTS

A. Methods

Elemental samples of Ir, Au, and In (as a calibration standard) and the compounds HfO_2 and Er_2O_3 of typically 5–15 g served as targets. The materials were contained in hollow aluminum cylinders with 3.5 cm length and 1.4 cm outer diameter.

Isomeric populations were produced by exposing the targets to bremsstrahlung from a 3-mm tantalum converter foil irradiated by the electron beam from the injector of the new superconducting S-DALINAC accelerator at the Technische Hochschule Darmstadt [16]. Electron energies were varied from 2 to 7 MeV with a minimum step size of 125 keV. The electron energies were measured with an accuracy of 50 keV before and after each exposure. At each end point, individual samples were irradiated axially in close proximity to the converter. Each target cylinder was held in position by an aluminum stop which terminated a plastic transfer tube. The proper alignment of the beam was achieved by maximizing the dose delivered to a remote ionization chamber shielded to observe only the central 12 mrad of the bremsstrahlung cone.

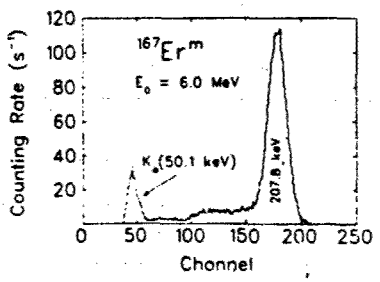

FIG. 3. Pulse-height spectrum of the γ decay of the isomer $^{167}Er^m$ pumped by bremsstrahlung from a 6-MeV electron beam.

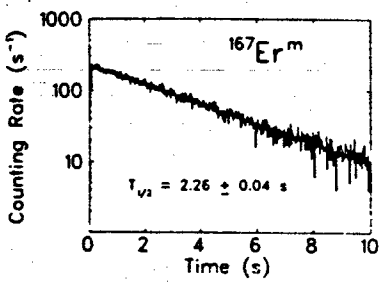

FIG. 4. Time-decay spectrum of the isomer $^{167}Er^m$. The straight line represents a best fit with $T_{1/2}=2.26\pm0.04$ s.

Variations in all beam parameters were recorded during the experiments. In particular, the charge passed to the converter was determined for each exposure by integrating the current with an analog circuit whose time constant for charging was arranged to match the lifetime of the isomer being investigated. Nominal beam currents were 5 μA. The lengths of the exposures were typically chosen to be twice the half-life of the isomer in question, while the calibration sample $T_{1/2}=4.486$ h was exposed for 5 min.

The termination of each irradiation provided a trigger signal which initiated the pneumatic transport of each sample through the plastic tube to a well-type NaI(Tl) detector for counting. This detector and all necessary electronics for the experiments were located in a room separate from the accelerator hall. A phototransistor signaled the arrival of the sample within the detector and started the simultaneous acquisition of both pulse-height and multichannel-scalar spectra. Examples of spectra obtained in this way are shown in Figs. 3 and 4. A quad counter/timer was gated by TTL signals at the start and end of irradiation, and at the arrival of the sample in the detector to measure the precise durations of exposure and transport.

The numbers of isomers produced by these irradiations were determined from the counting rates measured in distinctive fluorescence lines. The particular γ-ray signatures used in these measurements and other relevant parameters are given in Table I. The raw number of counts in each peak was corrected for the finite durations of exposure, transport, and counting, the absolute counting efficiencies of the detector, and the relative emission intensities. The opacity of the samples to the escape of the signature γ rays was compensated by a factor calculated with a Monte Carlo code specifically adapted for the well-type detector geometry.

B. Data analyses

The experimentally measured yield of isomers, N_f, resulting from the irradiation of N_T ground-state nuclei with bremsstrahlung is given analytically by

$$N_f = N_T \int_{E_c}^{E_0} \sigma(E) \frac{d\Phi(E)}{dE} dE \ , \tag{1}$$

where E_0 is the end-point energy, $d\Phi(E)/dE$ is the time-integrated spectral intensity in $cm^{-2}keV^{-1}$ of the photon field, and $\sigma(E)$ is the cross section in cm^2 for the reaction. The spectral intensity is conveniently expressed as the product of a flux Φ_0 of all photons above a cutoff energy E_c of 0.5 MeV incident on the target and a relative intensity function $F(E,E_0)$, which is normalized according to

$$\int_{E_c}^{E_0} F(E,E_0)dE = 1 \ . \tag{2}$$

Equation (2) allows the definition of a normalized yield or activation per photon, $A_f(E_0)$, given by

$$A_f(E_0) = \frac{N_f}{N_T \Phi_0} = \int_{E_c}^{E_0} \sigma(E) F(E,E_0) dE \ . \tag{3}$$

At energies of interest in these experiments, IS's have widths that are small in comparison to their spacings and it can be assumed that $d\Phi/dE$ is constant over each resonance region. Then Eq. (3) reduces to the summation

$$A_f(E_0) = \sum_j (\sigma\Gamma)_{fj} F(E_j,E_0) \ . \tag{4}$$

with $(\sigma\Gamma)_{fj}$ giving the integrated cross section of the jth IS having excitation energy E_j. We note that nonresonant cross sections which would inhibit the use of Eq. (4) are not considered. The previous claims for the significance of nonresonant contributions [17] have recently been disproven [18] and shown to have resulted merely from the omission of the importance of intense contributions to the photon fields arising in such experiments from environmental Compton scattering.

The normalized activation A_f can be useful as a sensitive indication of the opening of (γ,γ') channels whenever photons of the requisite energies E_j become available. A change of the end-point energy E_0 of the bremsstrah-

TABLE I. Summary of the literature values [20] for the relevant nuclear parameters and transparencies for the escape of fluorescence photons from samples of the nuclides. In the column for K, entries of NA indicate nuclei for which K cannot be defined or for which there are no accepted values.

Nuclide	g.s. spin J^π	g.s. spin K	E_{iso} (keV)	isomer spin J^π	isomer spin K	$T_{1/2}$ (s)	Abundance (%)	Principal fluorescence (keV)	Transparency (%)
^{167}Er	$\frac{7}{2}^+$	$\frac{7}{2}$	208	$\frac{1}{2}^-$	$\frac{1}{2}$	2.28	22.95	207.79	48
^{179}Hf	$\frac{9}{2}^+$	$\frac{9}{2}$	375	$\frac{1}{2}^-$	$\frac{1}{2}$	18.68	13.63	214.31	43
^{191}Ir	$\frac{3}{2}^+$	$\frac{3}{2}$	171	$\frac{11}{2}^-$	$\frac{11}{2}$	4.94	37.30	129.43	13
^{197}Au	$\frac{3}{2}^+$	NA	409	$\frac{11}{2}^-$	NA	7.80	100.00	279.11	11

lung spectrum modulates the spectral intensity function $F(E_j,E_0)$ in Eq. (3) at all of the important IS energies. The largest effect in the excitation function occurs when E_0 is increased from a value just below some state at E_j to one exceeding it so that $F(E_j,E_0)$ varies from zero to some finite value. In earlier work [5] plots of quantities equivalent to Eq. (3) as functions of the end-point energies of the irradiating spectra showed very pronounced activation edges, which appeared as sharp increases at the energies E_j corresponding to excitations of new intermediate states.

Calculated spectra of both Φ_0 and $F(E,E_0)$ were obtained from the EGS4 electron-photon transport code. This Monte Carlo program is well established in the medical physics community, and its general validity has been demonstrated elsewhere [19]. In this work confidence in the calculated photon spectra was maintained by calibrating them with the reaction $^{115}In(\gamma,\gamma')^{115}In^m$. This reaction is now sufficiently well characterized in the literature [13] to support its use in this way and, in this effort, was preferred over the calibration reaction $^{87}Sr(\gamma,\gamma')^{87}Sr^m$ used in other work [11,12] because of the completeness of the experimental information for it in the low-energy region not covered in the present experiments.

III. RESULTS

Figure 3 shows a typical pulse-height spectrum of the fluorescence from an isomeric population pumped by bremsstrahlung through some intermediate state(s). In this particular case, the data from $^{167}Er^m$ are shown for an electron energy of $E_0=6$ MeV. Even with the limited resolution of the NaI(Tl) well detector, the distinctive signature line of $^{167}Er^m$ is clear in the data obtained from one 10-s exposure of an erbium sample. Nevertheless, to confirm the identity of the peak, a measurement of the time decay of the fluorescent state population was taken in parallel. Such a decay curve is shown for $^{167}Er^m$ in Fig. 4 together with a fit which agrees well with the literature value [20] of the half-life, $T_{1/2}=2.28$ s.

To improve statistics, at least nine successive repetitions of the cycle for irradiation and counting were made for each nuclide at each end-point energy of the bremsstrahlung. Each was corrected for slight variations of the photon flux on that particular exposure, as well as for any variations in the transit time from the site of exposure to the counting enclosure. The resulting curves of A_f obtained from Eq. (3) as functions of the bremsstrahlung end point E_0 are shown in Figs. 5–8. The results at 6 MeV given by Carroll *et al.* [8] are included for comparison. The agreement of these values obtained in completely different experimental environments is excellent.

Values for the integrated cross sections $(\sigma\Gamma)_{fj}$ were found by fitting Eq. (4) to the data of Figs. 5–8. A useful measure of the degree of fit was provided by the residue of activation, $R_M(E_0)$, remaining after subtracting contributions from the M lowest-lying intermediate states,

$$R_M(E_0)=A_f(E_0)-\sum_{E_j=E_1}^{E_M}(\sigma\Gamma)_{fj}F(E_j,E_0)\,, \qquad (5)$$

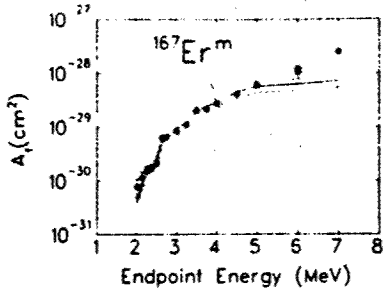

FIG. 5. Normalized yield A_f of the activation of $^{167}Er^m$ as a function of electron energy. The asterisk represents the experimental result of Ref. [8] obtained at 6 MeV. The solid line corresponds to the fit to the data, and its error bounds are given by the dotted lines.

where E_M is the resonance energy of the highest-lying intermediate state already included. Fitted values of the integrated cross sections $(\sigma\Gamma)_{fj}$ were found by minimizing $R_M(E_0)$ for the lowest-energy state giving a break in the excitation function, and then iterating after including any new gateways suggested by the data. The contribution of IS's below $E_0=2$ MeV that could not be distinguished by the present experiments was estimated by assuming a single state for which properties were adjusted to give the best description of A_f values for energies below 2.5 MeV. Because of the sudden jump of intermediate-state strength of typically more than a factor of 10 around 2.5 MeV, variations of the IS cross sections at lower energies have little effect on the results.

The results of fitting the model of Eq. (4) to the data are shown in Figs. 5–8 and are summarized in Table II. Uncertainties are shown explicitly. It should be noted

TABLE II. Values of integrated cross sections $(\sigma\Gamma)_{fj}$ and excitation energies E_j of the intermediate states most important in the production of these isomers by (γ,γ') reactions. Values needed to fit the data were determined in this work by minimizing the residues of Eq. (5).

Isomer	E_j (MeV)	$(\sigma\Gamma)_{fj}$ (10^{-29} cm^2 keV)
$^{167}Er^m$	1.9±0.1	1500±200
	2.5±0.1	8000±2000
	3.1±0.15	28 000±4000
	3.8±0.2	50 000±15 000
$^{179}Hf^m$	1.5±0.2	40±10
	2.5±0.1	1200±200
	3.0±0.15	6000±1000
	4.3±0.2	75 000±15 000
$^{191}Ir^m$	1.2±0.3	180±50
	2.5±0.1	2500±300
	3.2±0.15	5000±500
	4.3±0.2	30 000±4000
$^{197}Au^m$	1.7±0.3	70±30
	2.5±0.1	500±50
	3.2±0.15	4500±500
	4.2±0.2	20 000±4000

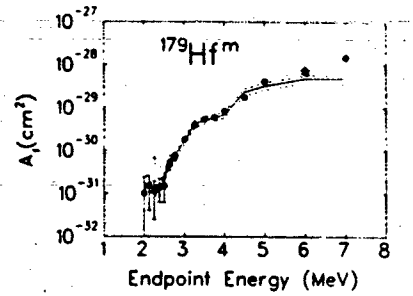

FIG. 6. Normalized yield A_f of the activation of $^{179}Hf^m$ as a function of electron energy. The asterisk represents the experimental result of Ref. [8] obtained at 6 MeV. The solid line corresponds to the fit to the data, and its error bounds are given by the dotted lines.

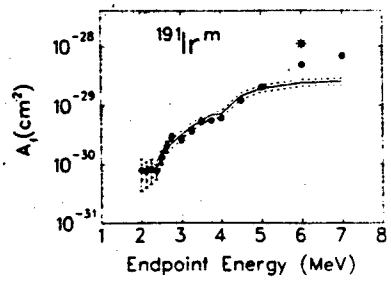

FIG. 7. Normalized yield A_f of the activation of $^{191}Ir^m$ as a function of electron energy. The asterisk represents the experimental result of Ref. [8] obtained at 6 MeV. The solid line corresponds to the fit to the data, and its error bounds are given by the dotted lines.

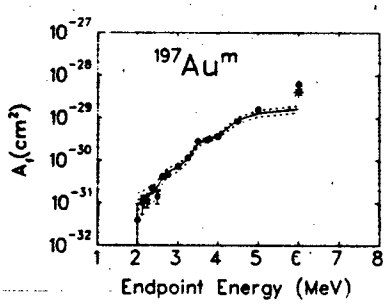

FIG. 8. Normalized yield A_f of the activation of $^{197}Au^m$ as a function of electron energy. The asterisk represents the experimental result of Ref. [8] obtained at 6 MeV. The solid line corresponds to the fit to the data, and its error bounds are given by the dotted lines.

that within the energy errors given for the IS locations the present approach cannot distinguish between single states and contributions from fragmented strength.

IV. DISCUSSION

Examination of the results presented in Table II reveals some interesting phenomena. All four nuclei show a sudden jump of very significant magnitude in the values of integrated cross sections accessed around 2.5 MeV. This same phenomenology had been reported earlier [11–13] in $^{180}Ta^m$, ^{123}Te, and ^{115}In. Confirmed for ^{115}In by both studies of resonant scattering and unified model calculations, the IS strength there accrued from $g_{9/2} \rightarrow g_{7/2}$ spin-flip transitions. However, in the present work, the chosen nuclei, together with the $^{180}Ta^m$, represent cases of both unpaired protons and unpaired neutrons in different major shells. A common mechanism independent of the details of nuclear structure would be indicated for this group of IS's.

Before attempting to find the means to explain such extraordinary strengths for these IS's, a first concern is the extent to which these measurements may be supported by prior work. Unfortunately, there are few compelling results in the literature. The only precedents are the recent measurements made over a very coarse mesh of energies [8] and the 1970 work of Johnson, Chertok, and Dick (JCD) [21]. The agreement is excellent between values of A_f obtained in the present work and those obtained with three of the four different accelerators employed previously [8]. No arbitrary factors were used to scale any of those earlier data, and the agreement seen in the Figs. 5–8 is a measure of the accuracy with which absolute measurements can be made for (γ,γ') reactions. Reference back to the original data of Ref. [8] shows that comparisons with activations produced by the fourth accelerator, a 4-MeV medical linac, were less satisfactory. With that device it was not possible either to monitor or control the end-point energy of the electrons, nominally fixed at 4.0 MeV. Because of the amount of structure now reported for activation curves near 4 MeV, the effects of small variations of end-point energy would be expected to be magnified in the resulting yields. Not surprisingly disagreements as great as a factor of 2 were obtained with that accelerator.

It is important to note that the experimental A_f value for ^{191}Ir at $E_0 = 6$ MeV in the present experiment is about a factor of 2 smaller than that in Ref. [8]. This magnitude of excitation agrees well with the empirical systematics discussed above. In addition, a corresponding reduction of the $(\sigma\Gamma)_{iso}$ value for ^{191}Ir plotted from Ref. [8] in Fig. 2(b) removes the deviation observed for this nucleus, which then fits very well into the N_pN_n systematics.

Comparisons with the JCD results are more difficult. Published in a Letter, both results and procedures were too briefly described to permit any repetition of the work. Details were promised for publication in a subsequent article which never appeared. Both the strengths and excitation energies of the IS reported by JCD disagree completely with those summarized in Table II. However, the

uniqueness of such values depends upon the degree to which inflections in curves of A_f as functions of endpoint energy can be precisely located. The fragments of data shown by JCD in the Letter are insufficient to support the uniqueness of the values they reported.

The degree to which the results of this work reported in Table II agree with prior measurements is best summarized in Fig. 9. There are plotted the values of A_f that were recently obtained in this work for the reaction ^{167}Er$(\gamma,\gamma')^{167}$Er^m together with those from Ref. [8], including the one made with the 4-MeV linac of lessened reliability. No scale factors were used and absolute measurements have been plotted. From the JCD Letter, it is possible only to calculate values of A_f which would have resulted from excitation through the IS they report by bremsstrahlung with reasonable spectra. Since they did not report IS's below 2.5 MeV, a single hypothetical intermediate state had to be included in all computations of A_f to represent contributions from those lower energies. That state was chosen to give the closest agreement with the rest of the values plotted. The results are shown in Fig. 9, which now permits a comparison of all known measurements of the activation of ^{167}Er$(\gamma,\gamma')^{167}$Er^m in the energy range from 2 to 7 MeV.

Agreement of the results of JCD from 20 years ago with the present work is at least as good as has been obtained with the 4-MeV medical linac, about a factor of 2. However, it is doubtful whether the procedures of Eq. (5) would deliver the same number and magnitudes of the IS reported by JCD if now applied to the corresponding data of Fig. 9. Values they reported were sufficient for the description of their measured A_f, but were not unique. Despite the generally favorable agreement of all of the measurements summarized in Fig. 9, we believe it reasonable to ascribe a greater weight to those from the current experiment. A primary consideration is that each exposure in the present work also included the activation of ^{115}In$(\gamma,\gamma')^{115}$In^m believed now to be well understood from a unique level of agreement of photoexcitation, resonant scattering, and model interpretation. Through this constant recalibration, the effects of experimental uncertainties were minimized.

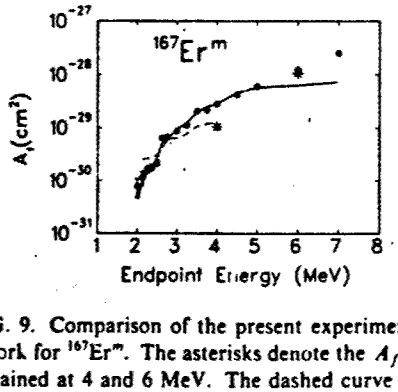

FIG. 9. Comparison of the present experiments with previous work for ^{167}Er^m. The asterisks denote the A_f results of Ref. [8] attained at 4 and 6 MeV. The dashed curve was calculated with the intermediate states given in Ref. [21] plus an arbitrary state below 2.5 MeV to account for the unknown lower-energy contributions not covered in that early work. The energy $E=1.9$ MeV and integrated cross section $\sigma\Gamma=2250\times10^{-29}$ cm^{2}keV of this state were adjusted to achieve an optimum agreement with the present data in the 2.5–3.6-MeV region accessed in both experiments. The solid line indicates the fit to the current data obtained from Eq. (5).

The resulting IS cross sections of Table II show a general tendency to increase with increasing excitation energy. We have investigated whether photoabsorption through the tail of the isovector electric giant dipole resonance (GDR) provides a quantitative explanation of the excitation functions. It is well known that the extrapolation of the GDR to lower energies describes γ-strength functions [22] and the statistical distribution of low-energy $E1$ transitions [23] reasonably well. This extrapolation might be extended down to about 4–5 MeV in nuclei far from closed shells, but nuclei near the ^{208}Pb shell closure show strong irregularities and experimental results tend to be significantly overestimated [22]. In this analysis we therefore show a comparison for both ^{167}Er and ^{197}Au as representative examples of the two groups.

The following simplifications are assumed for the calculations. The photoabsorption cross section is taken from the usual Lorentzian parametrization

$$\sigma_{\rm abs}(E)=\sum_i \sigma_{\rm max}\frac{E^2\Gamma^2}{(E^2-E_{\rm max}^2)^2+E^2\Gamma^2}\ , \tag{6}$$

with $E_{\rm max}$ and $\sigma_{\rm max}$ being the energy and cross section at maximum, respectively, and Γ is the width. For spherical nuclei, $i=1$, and for deformed nuclei, $i=1$ or 2, corresponding to oscillations with respect to the different axes. Equation (6) is substituted into Eq. (3) to obtain A_f values comparable to the experiment. In order to simplify the integral, $\sigma_{\rm abs}$ is described as a histogram with a mesh interval Δ equal to the step size of the photon intensity function $F(E,E_0)$. Then the integral can again be reduced to a simple summation

$$A_f(E_0)=\sum_{i=1}^{N} F(E_i,E_0)\sigma(E_i-\Delta/2,E_i+\Delta/2)\ , \tag{7}$$

with $E_i=E_{i-1}+\Delta$. The Lorentzian parameters were taken from Ref. [24], and the experimental results of $^{\rm nat}$Er were used for ^{167}Er.

The results are shown in Fig. 10 as hatched areas above 3.5 MeV (model A). The upper and lower borders correspond to the limits of reasonable branching ratio values of $b_0b_{\rm iso}=0.05$ and 0.25. Below 3.5 MeV, results based on the single-particle model multiplied with an average experimentally deduced [25] hindrance factor of 3×10^{-5} (model C) are displayed. This approach has been tested by Zurmühl *et al.* [26] for various well-deformed heavy nuclei. Alternatively, an extrapolation of the GDR using an energy-dependent damping width of the form $\Gamma(E)=\Gamma_{\rm max}(E/E_{\rm max})^\gamma$ has been proposed [27,28] with typical values $\gamma=1.5$–2. As an example, we adopt the approach of Kopecky and Uhl [28] (with $T=0$ since we measure the upward strength function), which is displayed as model B.

A comparison of the ^{167}Er and ^{197}Au results reveals considerable differences. In ^{167}Er, model A provides a reasonable description slightly below particle threshold, while results of model B are much too small. On the con-

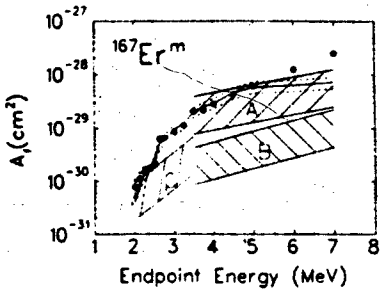

FIG. 10. Comparison of the $^{167}Er^m$ excitation function with extrapolations of the photoabsorption through the tail of the GDR assuming a Lorentzian shape (model A) or a Lorentzian with an energy-dependent damping width (model B), and with a single particle model (model C). The Lorentzian parameters were taken from Ref. [24]. The borders of the hatched regions showing the model predictions correspond to reasonable limits assumed for the unknown branching-ratio values $b_0 b_{iso}=0.25$ and 0.05. The solid line corresponds to the fit to the data, and its error bounds are given by the dotted lines.

trary, as shown in Fig. 11, model C predicts too large photoabsorption cross sections in ^{197}Au, in line with other investigations of the γ-strength function [22], while model B accounts well for the data down to about 4 MeV. It is also clear that an average $E1$ transition strength (model C) could explain the low-energy data in this case.

The extraordinary photoabsorption strength around 2.5 MeV in ^{167}Er is reflected by the failure of model C, which predicts values which are much too small. The empirical relation to the deformation parameter and IS parameters in Table II indicates that collective degrees of freedom should play a decisive role. However, recent studies of low-energy collective dipole strength in rare-earth nuclei [29–32] provide no fully satisfactory explanation. For the IS at 2.5 MeV, reduced transition probabilities $B(M1)=3.6\mu_N^2$ and $B(E1)=40\times10^{-3}$ $e^2\,fm^2$ can be extracted assuming a favorable $b_0 b_{iso}=0.2$. These numbers roughly correspond to the total experimental $M1$ and $E1$ transition strengths [31,33] typically observed below 4 MeV in the experiments. However, all the above data have been taken in even-even nuclei. Recently, a first attempt to investigate low-lying dipole transitions in an odd-even case ^{165}Ho was reported [34]. Only intrinsic single-particle transitions were excited with reasonable magnitude, and significant collective $M1$ or $E1$ strengths were not observed below 3 MeV.

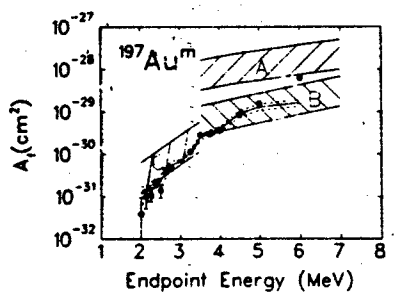

FIG. 11. Comparison of the $^{197}Au^m$ excitation function with extrapolations of the photoabsorption through the tail of the GDR assuming a Lorentzian shape (model A) or a Lorentzian with an energy-dependent damping width (model B), and with a single-particle model (model C). The Lorentzian parameters were taken from Ref. [24]. The borders of the hatched regions showing the model predictions correspond to reasonable limits assumed for the unknown branching-ratio values $b_0 b_{iso}=0.25$ and 0.05. The solid line corresponds to the fit to the data, and its error bounds are given by the dotted lines.

The importance of the quadrupole deformation already suggested in Fig. 2(b) is clearly confirmed in the present results, if one compares the cross sections of different nuclei at about equal energies. The integrated isomer cross section of the jth IS can be related to photon-scattering results via

$$(\sigma\Gamma)_{iso}=\pi^2\left(\frac{\hbar c}{E_j}\right)^2\left(\frac{2J_f+1}{2J_i+1}\right)b_0 b_{iso}\Gamma\ , \tag{8}$$

with Γ being the total decay width of the IS. Here b_0 is the direct IS to ground state branching ratio and b_{iso} stands for the sum of all branches populating the isomer, either directly or via a cascade. In order to remove the obvious excitation energy dependence contained in $(\sigma\Gamma)_{iso}$, it is useful to introduce the isomer population probabilities

$$S_j^D=\frac{(\sigma\Gamma)_{iso}^j}{E_j}\quad\text{and}\quad S_j^Q=\frac{(\sigma\Gamma)_{iso}^j}{E_j^3}\ . \tag{9}$$

These quantities are proportional to the reduced transition probabilities for excitation for the jth IS assuming either a dipole (S^D) or quadrupole (S^Q) transition, multiplied by the branching ratio to the isomer. The spin statistics factor from Eq. (8) is neglected in this approach.

This definition permits a useful comparison between the contributions of IS's at different energies in one nucleus as well as between IS's of different nuclei. In Fig. 12 the summed isomer population probability $S=\sum_j S_j$ for each nucleus is plotted versus the quadrupole deformation parameter δ of the ground state that has been derived from measured moments [35]. The circles correspond to the assumption of dipole absorption by the IS and the squares to quadrupole excitations. Since the upward transitions might be of mixed character and the sums might include transitions of both types, the results shown for pure dipole and quadrupole cases should be considered as limits. Still, regardless of the assumed character of the IS excitation, the data show a correlation between S and δ; i.e. the isomer population probability increases with the ground-state deformation.

Nuclear resonance fluorescence work [29–34] in the rare-earth region has recently suggested that for energies below 4 MeV the absorption step is most likely mediated by dipole rather than quadrupole strength. Then a very simple linear relationship is indicated in Fig. 12. A fit assuming a direct proportionality of S and δ is displayed as a solid line and describes the data very well.

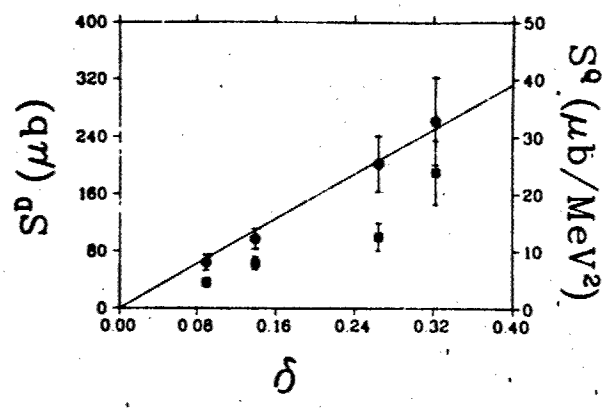

FIG. 12. Isomer excitation probability S_j calculated from Eq. (9) and summed over the energy region 2–4.5 MeV versus the ground-state deformation parameter δ. The circles correspond to the assumption of dipole excitations (S^D) and are plotted according to the left ordinate. The squares correspond to quadrupole excitations (S^Q) of the IS, plotted according to the right ordinate. The solid line is a best fit for the dipole results with a zero intercept.

At present, it remains open whether such a linear dependence is of physical significance or simply fortuitous. One should keep in mind several details: The results are a function of the excitation energy interval considered, the IS spin statistics factor might introduce variations of about a factor of 2 (see Table I), and the number of data points is certainly too small for a final conclusion. If one assumes quadrupole excitations, no simple functional form is suggested.

The extremely large integrated cross sections for the photoexcitation of well-deformed isomers are difficult to interpret in a single-particle model, and a puzzle of comparable complexity is found in the efficiency with which ΔK is transferred. Many of these isomers have values of K that differ considerably from the ground-state values [$\Delta K = 8$ (^{180}Ta), $\Delta K = 6$ (^{176}Lu), and Table I]. The extraordinary integrated cross sections can only be explained with considerable K mixing in the IS wave function. While K mixing is common at neutron threshold energies [36], evidence for violation of K selection rules around 3 MeV has also been recently gained in nuclear resonance fluorescence investigations [37] and in a detailed decay study [38] of the $K^\pi = 14^+$, 4-μs isomer at 3.312 MeV in ^{174}Hf.

It is an interesting speculation that at certain energies of excitation, collective oscillations of the core nucleons could break some of the symmetries upon which rest the identifications of the pure single-particle states. If single-particle states of differing K were mixed in this way, the possibility for transferring larger amounts of ΔK with greater partial widths might be enhanced. The similarity of results for odd-even as well as odd-odd nuclei with dissimilar single-particle structures might support the identification of this K-mixing process with some type of core property varying only slowly among neighboring nuclei.

V. CONCLUSIONS

In the present work, the main IS's between 2 and 5 MeV have been identified for ^{167}Er, ^{179}Hf, ^{191}Ir, and ^{197}Au. A sudden jump of IS cross sections of typically more than an order of magnitude is observed in all cases around 2.5 MeV. This coincides with previous results in ^{115}In [13], ^{123}Te [12], and ^{180}Ta [11], where similar phenomena were observed below 3 MeV, and indicates the presence of a common excitation mechanism.

The isomer population probability, defined as the sum of the reduced transition probabilities to the IS times the branching ratio of the IS to the isomer, reveals a correlation to the ground-state deformation regardless whether dipole or quadrupole excitations are assumed. If dipole transitions are solely responsible for the excitation (which can be justified from recent photon-scattering experiments in this mass region [29–34]), the data are well described by a linear dependence. While it is unclear at present whether this linear relation bears physical significance, the overall increase of the isomer population probability with deformation is undoubted and will be subject of further investigations, e.g., by nuclear resonance fluorescence studies.

At present, it remains an open question what might be the nuclear structure underlying the particularly strong IS below 3 MeV observed in ^{167}Er, ^{176}Lu, ^{179}Hf, and ^{180}Ta and whether a common excitation mechanism dominates or whether the detailed interplay of collective and single-particle aspects in each particular nucleus is responsible. Microscopic calculations are clearly needed.

ACKNOWLEDGMENTS

We thank H.-D. Gräf, Th. Rietdorf, P. Schardt, and H. Weise for their great support in operating the superconducting electron accelerator, and M. L. Williams for his assistance in analyzing the data. In addition, we wish to thank our sponsors, the Department of Defense through the Naval Research Laboratory and the Bundesministerium für Forschung und Technologie, Contract No. 06DA184I.

[1] B. Pontecorvo and A. Lazard, C. R. Acad. Sci. **208**, 99 (1939).
[2] G. B. Collins, B. Waldman, E. M. Stubblefield, and M. Goldhaber, Phys. Rev. **55**, 507 (1939).
[3] Z. M. Bigan, E. L. Lazarev, V. M. Mazur, and V. Sokolnyk, Yad. Fiz. **49**, 913 (1989) [Sov. J. Nucl. Phys. **49**, 567 (1989)].
[4] L. Z. Dzhilavyan, V. L. Kauts, V. I. Furman, and A. Y. Chaprikov, Yad. Fiz. **51**, 336 (1990) [Sov. J. Nucl. Phys. **51**, 215 (1990)].
[5] E. C. Booth and J. Brownson, Nucl. Phys. **A98**, 529 (1967).
[6] C. B. Collins, C. D. Eberhard, J. W. Glesener, and J. A.

Anderson, Phys. Rev. C **37**, 2267 (1988).
[7] J. J. Carroll, J. A. Anderson, J. W. Glesener, C. D. Eberhard, and C. B. Collins, Astrophys. J. **344**, 454 (1989).
[8] J. J. Carroll, M. J. Byrd, D. G. Richmond, T. W. Sinor, K. N. Taylor, W. L. Hodge, Y. Paiss, C. D. Eberhard, J. A. Anderson, C. B. Collins, E. C. Scarbrough, P. P. Antich, F. J. Agee, D. Davis, G. A. Huttlin, K. G. Kerris, M. S. Litz, and D. A. Whittaker, Phys. Rev. C. **43**, 1238 (1991).
[9] C. B. Collins, F. W. Lee, D. M. Shemwell, B. D. DePaola, S. Olariu, and I. I. Popescu, J. Appl. Phys. **53**, 4645 (1982).
[10] V. Ponomarev, A. P. Dubenskij, V. P. Dubenskij, and E. A. Boykova, J. Phys. G **16**, 1727 (1990).
[11] C. B. Collins, J. J. Carroll, T. W. Sinor, M. J. Byrd, D. G. Richmond, K. N. Taylor, M. Huber, N. Huxel, P. von Neumann-Cosel, A. Richter, C. Spieler, and W. Ziegler, Phys. Rev. C **42**, 1813 (1990).
[12] J. J. Carroll, T. W. Sinor, D. G. Richmond, K. N. Taylor, C. B. Collins, M. Huber, N. Huxel, P. von Neumann-Cosel, A. Richter, C. Spieler, and W. Ziegler, Phys. Rev. C **43**, 897 (1991).
[13] P. von Neumann-Cosel, A. Richter, C. Spieler, W. Ziegler, J. J. Carroll, T. W. Sinor, D. G. Richmond, K. N. Taylor, C. B. Collins, and K. Heyde, Phys. Lett. B **266**, 9 (1991).
[14] K. Heyde, P. van Isaker, M. Waroquier, J. L. Wood, and R. A. Mayer, Phys. Rep. **102**, 291 (1983).
[15] R. F. Casten, Nucl. Phys. **A443**, 1 (1985).
[16] K. Alrutz-Ziemssen, D. Flasche, H-D. Gräf, V. Huck, M. Knirsch, W. Lotz, A. Richter, T. Rietdorf, P. Schardt, E. Spamer, A. Staschek, W. Voigt, H. Weise, and W. Ziegler, Part. Accel. **29**, 53 (1990).
[17] A. Ljubicic, M. Pisk, and B. A. Logan, Phys. Rev. C **23**, 2238 (1981); M. Krcmar, A. Ljubicic, B. A. Logan, and M. Bistrovic, *ibid.* **33**, 293 (1986); M. Krcmar, S. Kaucic, T. Tustonic, A. Ljubicic, B. A. Logan, and M. Bistrovic, *ibid.* **41**, 771 (1990).
[18] P. von Neumann-Cosel, A. Richter, J. J. Carroll, and C. B. Collins, Phys. Rev. C **44**, 554 (1991).
[19] *Monte Carlo Transport of Photons and Electrons*, edited by T. M. Jenkins, W. R. Nelson, and A. Rindi (Plenum, New York, 1988).
[20] E. Browne and R. B. Firestone, in *Table of Radioactive Isotopes*, edited by V. S. Shirley (Wiley, New York, 1986); *Evaluated Nuclear Structure Data File* (Brookhaven National Laboratory, Upton, New York, 1986).
[21] W. T. K. Johnson, B. T. Chertok, and C. E. Dick, Phys. Rev. Lett. **25**, 599 (1970).
[22] G. A. Bartholomew, E. D. Earle, A. J. Ferguson, J. W. Knowles, and M. A. Lone, Adv. Nucl. Phys. **7**, 229 (1972).
[23] M. Schumacher, U. Zurmühl, F. Smend, and R. Nolte, Nucl. Phys. **A438**, 493 (1985).
[24] S. S. Dietrich and B. L. Berman, At. Data Nucl. Data Tables **38**, 199 (1988).
[25] P. M. Endt, At. Data Nucl. Data Tables **26**, 47 (1981).
[26] U. Zurmühl, P. Rullhusen, F. Smend, M. Schumacher, and H. G. Börner, Phys. Lett. **114B**, 99 (1982).
[27] G. Maino, A. Ventura, L. Zuffi, and F. Iachello, Phys. Rev. C **30**, 2101 (1984).
[28] J. Kopecky and M. Uhl, Phys. Rev. C **41**, 1941 (1990).
[29] C. Wesselborg, P. von Brentano, K. O. Zell, R. D. Heil, H. H. Pitz, U. E. P. Berg, U. Kneissl, S. Lindenstruth, U. Seemann, and R. Stock, Phys. Lett. B **207**, 22 (1988).
[30] H. H. Pitz, U. E. P. Berg, R. D. Heil, U. Kneissl, R. Stock, C. Wesselborg, and P. von Brentano, Nucl. Phys. **A492**, 411 (1989).
[31] A. Zilges, P. von Brentano, C. Wesselborg, R. D. Heil, U. Kneissl, S. Lindenstruth, H. H. Pitz, U. Seeman, and R. Stock, Nucl. Phys. **A507**, 399 (1990).
[32] W. Ziegler, C. Rangacharyulu, A. Richter, and C. Spieler, Phys. Rev. Lett. **65**, 2515 (1990).
[33] A. Zilges, P. von Brentano, H. Friedrichs, R. D. Heil, U. Kneissl, S. Lindenstruth, H. H. Pitz, and C. Wesselborg, Z. Phys. A **340**, 155 (1991).
[34] N. Huxel, W. Ahner, H. Diesener, P. von Neumann-Cosel, C. Rangacharyulu, A. Richter, C. Spieler, W. Ziegler, C. De Coster, and K. Heyde, Nucl. Phys. **A539**, 478 (1992).
[35] P. Raghavan, At. Data Nucl. Data Tables **42**, 189 (1989).
[36] A. Bohr and B. Mottelson, *Nuclear Structure* (Benjamin, New York, 1975), Vol. 2, p. 37.
[37] A. Zilges, P. von Brentano, A. Richter, R. D. Heil, U. Kneissl, H. H. Pitz, and C. Wesselborg, Phys. Rev. C **42**, 1945 (1990).
[38] P. M. Walker, F. Sletten, N. L. Glørup, M. A. Bentley, J. Borggreen, D. Fabricius, A. Holm, D. Howe, J. Pedersen, J. W. Roberts, and J. F. Sharpey-Schafer, Phys. Rev. Lett. **65**, 416 (1990).

STATUS AND ISSUES IN THE DEVELOPMENT OF A GAMMA-RAY LASER

C. B. Collins, J. J. Carroll, K. N. Taylor,
T. W. Sinor, C. Hong, J. Standifird, and
D. G. Richmond

Center for Quantum Electronics
University of Texas at Dallas
P.O. Box 830688
Richardson, TX 75083-0688

ABSTRACT

A gamma-ray laser would stimulate the emission of radiation at wavelengths below 1 Å from excited states of nuclei. However, the difficulties in realizing such a device were considered insurmountable when the first cycle of study ended in 1981. Nevertheless, research on the feasibility of a gamma-ray laser has taken a completely new character since then. A nuclear analog of the ruby laser has been proposed and many of the component steps for pumping the nuclei have been demonstrated experimentally. A quantitative model based upon the new data and concepts of this decade shows the gamma-ray laser to be feasible if some real isotope has its properties sufficiently close to the ideals modeled.

INTRODUCTION

At the nuclear level, long-lived excited states are known as isomers. Populations of these nuclear metastables can store energies of tera-Joules (10^{12} J) per liter at solid densities for thousands of years. Such long storage times mean that it would not be necessary to pump a gamma-ray laser medium entirely in situ. For some cases the excited nuclei could be bred in a reactor from a parent material that captures a neutron or from a specific nuclear reaction acting upon precursive elements.

The problem of suddenly assembling a critical density of prepumped nuclei to reach the threshold for stimulated emission received much attention in a first cycle of study lasting from 1963-1981 and excellent reviews are available.[1] At the end of this period, it was generally concluded that such single photon, brute force approaches were essentially hopeless. In an encyclopedic review, Baldwin and coauthors[1] concluded the general impossibility of a gamma-ray laser based upon all techniques for pumping known in 1980. That review effectively terminated all traditional lines of approach to a gamma-ray laser. However, in the earlier work the greatest emphasis had been placed upon the use of intense particle fluxes for input energy.

Laser Interaction and Related Plasma Phenomena, Vol. 10
Edited by G.H. Miley and H. Hora, Plenum Press, New York, 1992

Toward the end of the first cycle of research the precursors of a new interdisciplinary approach began to appear.[2-8] These developed rapidly and launched a renaissance in the field. The basic theory[9-11] of upconversion at the nuclear level was in-place by 1982 for the two possible variants, coherent and incoherent upconversion. Involving either multiphoton processes or multiple electromagnetic transitions to release the energy stored in isomers, many of the difficulties encountered with more traditional pumping schemes did not arise.

In the decade since 1980, research on the feasibility of a gamma-ray laser has taken a completely new character. In the first half decade a series of experiments verified that the concepts of quantum electronics could be applied at the nuclear level.[12-16] By 1986 the blueprint for a gamma-ray laser[11] had been established and substantial effort was initiated toward the demonstration of feasibility. The purpose of this article is to review the major advances of this past five years that have significantly increased the likelihood of the feasibility of a gamma-ray laser.

CONCEPTS

At first approach it would seem that the prospects for all ultrashort wavelength lasers would be vitiated by a very fundamental factor.[1] The basic ν^3 dependence of electron transition probabilities so limits the storage of pump energies that even now some of the largest pulsed-power machines are able to excite only milliJoules of x-ray laser output and then only at soft photon energies. In contrast there are four unique advantages of a gamma-ray laser that would accrue from its operation upon electromagnetic transitions of nuclei:

1) The constant linking ν^3 with lifetime is more favorable by orders-of-magnitude because of the accessibility of a variety of transition moments. The effects pumped by an input pulse can be integrated up to larger values for longer times.

2) Nuclear metastables store keV and even MeV for years. With upconversion schemes most of the pump power is input long before the time of use and triggering requirements are small.

3) Nuclear transitions need not have thermal broadening and natural linewidths are routinely obtained. Without broadening electromagnetic cross sections are large and values for 1 Å transitions typically exceed the cross section for the stimulation of Nd in YAG.

4) Working metastables can be concentrated to solid densities.

The essential concept driving the renaissance in gamma-ray laser research was the "optical" pumping of nuclei. In this case optical meant x-rays, but the fundamentals were the same. Useful, resonant absorption of pump power would occur over short distances to produce high concentrations of excited nuclei while wasted wavelengths would be degraded to heat in much larger volumes. In the blueprint[11] of 1982 for upconversions, one of several possible types of photopumping was envisioned to transfer the stored population of an isomer to a state at the head of a cascade leading to the upper laser level. Of the cases considered, the nuclear analog of the ruby laser embodied the simplest concepts for a gamma-ray laser. Not surprisingly, the greatest rate of achievement in the last five years has been realized in that direction and this review will be limited to the results along that line.

For ruby, the identification and exploitation of a bandwidth funnel were the critical keys in the development of the first laser. There was a broad absorption band linked through efficient cascading to the narrow laser level. Our theory called for a nuclear analog of this structure which was unknown in 1986 when the first phase of intensive experiments was started for SDIO. Now, that theory has been confirmed.

Whether or not the initial state being pumped is isomeric, the principal figure of merit for bandwidth funneling is the partial width for the transfer, $b_a b_0 \Gamma$. Constituent parameters are identified in Fig. 1 where it can be seen that the branching ratios b_a and b_0 specify the probabilities that a population pumped by absorption into the j-th broad level will decay back into the initial or fluorescent levels, respectively. It is not often that the sum of branching ratios is unity, as channels of decay to other levels are likely. However, the maximum value of partial width for a particular level j occurs when $b_a = b_0 = 0.5$.

Classified as (γ,γ') reactions in the literature of nuclear physics, these "optical" pumping processes have been known for over 50 years[17,18] although relatively few results have been published since that time. Practical difficulties with the calibration and availability of sources of irradiation had limited the degree of reproducibility achieved in earlier work.

The most tractable (γ,γ') reactions for study are those for the photoexcitation of stable isotopes up to isomeric levels. In some cases the product can live long enough to be readily examined after termination of the input irradiation and lessons can be learned that can be applied to the excitation of shorter-lived levels more useful in a laser. The archetypical case for basic study has been the reaction $^{111}Cd(\gamma,\gamma')^{111}Cd^m$ exciting the 48.6 min level at 396 keV. Three of the most recent measurements of the fluorescence efficiency were conducted in 1979, 1982, and 1987 as reported in Refs. 19-21, respectively. Probable errors were quoted as varying only from 7 to 14%, and yet no two of the measurements were even within a factor of 2 of each other. This discrepancy led to serious contentions over the way in which the expected fluorescence yields were calculated.[20] One of our early challenges was to place the "optical" pumping of nuclei onto a firm quantitative basis.

For a sample which is optically thin at the pump wavelength, a computation of the number of nuclei pumped into a fluorescence level in the scheme of Fig. 1 is straightforward. Most intense x-ray sources emit continua, either because bremsstrahlung is initially produced or because spectral lines are degraded by Compton scattering in the immediate environment. The time-integrated yield of final-state nuclei, N_f obtained by irradiating N_i initial targets with a photon flux Φ_0 in photons cm^{-2} delivered in a continuum of intensities up to an endpoint energy E_0 is,

$$N_f = N_i \Phi_0 \int_0^{E_0} \sigma(E) F(E,E_0) dE \quad , \qquad (1)$$

where $F(E,E_0)$ is the distribution of intensities within the input spectrum normalized so that

$$\int_0^{E_0} F(E,E_0) dE = 1 \quad , \qquad (2)$$

and $\sigma(E)$ is the effective cross section for the excitation of the final state from the initial.

All (γ,γ') reactions occurring at energies below the threshold for particle evaporation excite discrete intermediate states of nuclei as shown in Fig. 1. Although only one intermediate state appears in Fig. 1, there could be more. Each would be excited at a different pump energy but all would branch to some extent into the same fluorescence level, f. The j-th intermediate is shown in Fig. 1 as typical.

Although the width of level j is broad on a nuclear scale, it is narrow in comparison to the scale of energies, E over which $F(E,E_0)$ varies. Then, the final-state yield, expressed as the normalized activation per unit photon flux, $A_f(E_0)$ produced with bremsstrahlung having an endpoint of E_0 can be written from Eq. (1) as,

$$A_f(E_0) \equiv \frac{N_f}{N_i \Phi_0} = \sum_j (\sigma\Gamma)_{f_j} F(E_j,E_0) \quad . \tag{3a}$$

In this expression $(\sigma\Gamma)_{f_j}$ is the integrated cross section for the production of final-state N_f as, a result of the excitation of the intermediate state E_j with bremsstrahlung described by the spectral function $F(E,E_0)$, so that

$$(\sigma\Gamma)_{f_j} = \int_{E_j-\Delta}^{E_j+\Delta} \sigma(E)dE \quad , \tag{3b}$$

where Δ is an energy small compared to the spacing between intermediate states and large in comparison to their widths. Levels of this type are sometimes called gateways or doorways.

It is straightforward to show that,

$$(\sigma\Gamma)_{f_j} = (\pi b_a b_0 \Gamma \sigma_0/2)_{f_j} \quad , \tag{4a}$$

where $\sigma_0/2$ is the peak of the Breit-Wigner cross section for the absorption step, and

$$\sigma_0 = \frac{\lambda^2}{2\pi} \frac{2I_e+1}{2I_g+1} \frac{1}{\alpha_p+1} \quad , \tag{4b}$$

where λ is the wavelength of the gamma ray at the resonant energy, E_j; I_e and I_g are the nuclear spins of the excited and ground states, respectively; and α_p is the total internal conversion coefficient for the system shown in Fig. 1.

PUMP CALIBRATION

From the perspective of laser physics the most unreliable sources of energetic photons used in early studies of (γ,γ') reactions seem to have been the nuclear sources. Although assumed to emit line spectra, in actual usage they produced intensities which were dominated by the continua resulting from multiple Compton scatterings of photons by the large amounts of shielding in the irradiation environment. Such multiple scatterings are difficult to calculate and still impossible to measure in practical laboratory configurations. In contrast, the spectral intensities of

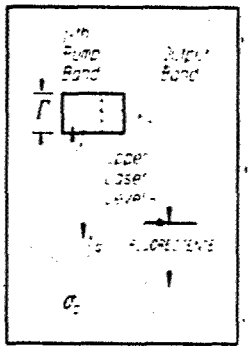

Figure 1. Schematic representation of the decay modes of a gateway state of width Γ sufficiently large to promote bandwidth funneling. The initial state from which population is excited with an absorption cross section σ_0 can be either ground or isomeric.

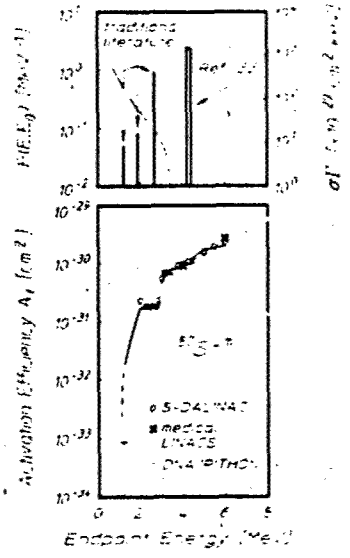

Figure 2. Activation efficiencies, A_f for the reaction $^{87}Sr(\gamma,\gamma')^{87}Sr^m$ are shown in Fig. 2b (lower) as functions of the endpoint, E_0 of the bremsstrahlung used for excitation. The solid curve in Fig. 2b plots values computed from Eq. (3a) using the gateway parameters found in the literature and plotted with the right axis in Fig. 2a (upper) together with calculated photon spectra like that given by the dashed line and plotted with the left axis in Fig. 2a. Figure 2b compares these A_f values with measurements obtained from four different accelerators.

bremsstrahlung are routinely calculated with high accuracy from measured accelerator currents and target geometries by well-established computer codes.[22]

In our experimental work of the last five years the bremsstrahlung from five accelerators in different experimental environments was used to verify the fluorescence model of Eqs. (1) - (4b) and to cross-check the accelerator intensities. The devices involved in this effort were DNA/PITHON at Physics International, DNA/Aurora at the Harry Diamond Laboratories, a 4 MeV and a 6 MeV medical linac at the University of Texas Health Sciences Center, and the superconducting injector to the storage ring at Darmstadt (S-DALINAC). Spectral intensities were calculated with the

Table I

Summary of nuclides, pump lines, and integrated cross sections for the excitation of delayed fluorescence suitable for use as calibration standards.

	PUMP LINE (keV)	$(\sigma\Gamma)_{f_j}$ (10^{-29} cm^2 keV)
^{79}Br	761	6.2
^{77}Se	250	0.20
	480	0.87
	818	0.7
	1005	30
^{115}In	1078	20

EGS4 coupled electron/photon transport code[22] adapted for each individual configuration from closely monitored values of accelerator currents. In this way both $F(E,E_0)$ and Φ_0 were obtained. In some cases Φ_0 was separately verified by in-line dosimetry.

Of the many potential systems which might be used to confirm the formulations of Eqs. (1) through (4b), the literature[23] supports the calculation of integrated cross sections for very few. Table I summarizes those which are known with sufficient accuracy to serve as standards. In the convenient units of 10^{-29} cm^2 keV, values range from the order of unity to a few tens for bandwidth funnels that are sufficient for demonstrations of nuclear fluorescence from reasonable amounts of material at readily accessible levels of input.

In our experiments samples with typical masses of grams were exposed to the bremsstrahlung from the five accelerators for times ranging from seconds to hours for the continuously operating machines and to single flashes from the pulsed devices. The activations, A_f of Eq. (3a) were determined by counting the photons spontaneously emitted from the samples after transferring them to a quieter environment. Usual corrections were made for the isotopic abundance, for the loss of activity during irradiation and transit, for the counting geometry, for the self-absorption of the fluorescence, and for the tabulated efficiencies[23,24] for the emission of signature photons from the populations, N_f. The self-absorption correction required a calculation of photon transport which was verified in some cases by confirming that the same sample masses in different geometries with different correction factors gave the same final populations.

Results were in close agreement[25] with the predictions of Eq. (3a) used with the values of $(\sigma\Gamma)_{f_j}$ shown in Table I. That work established a confidence level sufficient to support the use of nuclear activation as a means of selectively sampling spectral

intensities of single pulses of intense continua to determine absolute intensities as functions of wavelength.[26] Having calibrated the spectral sources, the persisting uncertainties in the optical pumping of $^{115}In^{m}$ and $^{111}Cd^{m}$ were resolved.[27,28]

As part of the effort to establish better calibration standards, we reexamined the reaction $^{87}Sr(\gamma,\gamma')^{87}Sr^{m}$. Particularly valuable were the data obtained with the S-DALINAC because the endpoint of the bremsstrahlung could be varied. A change of the endpoint energy, E_0 of the bremsstrahlung, as well as altering Φ_0, modulates the spectral intensity function $F(E_j,E_0)$ at all of the important energies for resonant excitation E_j. The largest effect occurs when E_0 is increased from a value just below some intermediate state at E_j to one exceeding it so that $F(E_j,E_0)$ varies from zero to some finite value as shown in Fig. 2a.

Early work[29] on (γ,γ') reactions showed that a plot of activation, $A_f(E_0)$ as a function of bremsstrahlung endpoint energy displayed very pronounced activation edges at the energies, E_j corresponding to the resonant excitation of new intermediate states. Such edges enabled new gateways to be identified for a particular reaction.

The activation efficiencies, A_f calculated from Eq. (3a) using the literature values[29] plotted in Fig. 2a are shown in Fig. 2b together with the measurements obtained with four of the accelerators. As can be seen, agreement is very good between the different accelerators and between the experimental data and the model calculations. The units of A_f in Fig. 2b are those of area because they are a type of average cross section quite different from the σ_0 of Eq. (4a) that describe individual transitions. The small plotted values are the result of averaging the large σ_0 at the resonant E_j over the broad bandwidth of $F(E,E_0)$ in which most $E \neq E_j$.

These calibration studies served to confirm both the traditional model of nuclear activation summarized in Eqs. (1) - (4b) and to validate the EGS4 code for calculating bremsstrahlung intensities from measured accelerator parameters. *Now, there can be no reasonable doubt of procedures for quantitatively measuring fluorescence efficiencies if an experiment is carefully performed with a bremsstrahlung source of pump radiation.*

GIANT PUMPING RESONANCES

If expressed as partial widths the integrated cross sections for the excitation of $^{77}Se^{m}$, $^{79}Br^{m}$, and $^{115}In^{m}$ seen in Table I corresponded to 39, 5, and 94 μeV, respectively. While among the largest values reported prior to our studies, these results still left an aura of credibility to the traditional impressions that partial widths for exciting isomers would be limited to about 1 μeV.

Tempering expectations that integrated cross sections of even this size might be expected for the dumping of actual isomeric candidates for a gamma-ray laser was a concern for the conservation of various projections of the angular momenta of the nuclei. Many of the interesting isomers belong to the class of nuclei deformed from the normally spherical shape. For those systems there is a quantum number of dominant importance, K which is the projection of individual nucleonic angular momenta upon the axis of elongation. To this is added the collective rotation of the nucleus to obtain the total angular momentum J. The resulting system of energy levels resembles those of a diatomic molecule for which

$$E_n(K,J) = E_n(K) + B_nJ(J+1) \quad , \qquad (5)$$

where $J \geq K \geq 0$ and J takes values $|K|, |K|+1, |K|+2, \ldots$. In this expression B_n is a rotational constant and $E_n(K)$ is the lowest value for any level in the resulting "band" of energies identified by other quantum numbers n. In such systems the selection rules for electromagnetic transitions require both $|\Delta J| \leq M$ and $|\Delta K| \leq M$, where M is the multipolarity of the transition.

In most cases of interest, the isomeric state has a large lifetime because its value of K differs considerably from those of lower levels to which it would otherwise be radiatively connected. As a consequence, bandwidth funneling processes such as shown in Fig. 1 must span substantial changes in ΔK and component transitions have been expected to have large, and hence unlikely, multipolarities. Initial expectations were that partial widths would decrease further as the values of ΔK needed for the transfer increased.

From this perspective the candidate isomer, $^{180}Ta^m$ was the most initially unattractive as it had the largest change of angular momentum between isomer and ground state, $8\hbar$. However, because it was the only isomer for which a macroscopic sample was readily available, $^{180}Ta^m$ became the first isomeric material to be optically pumped to a fluorescent level.

Table II

Recently measured values of integrated cross section, $(\sigma\Gamma)_{fj}$ for the reaction $^{180}Ta^m(\gamma,\gamma')^{180}Ta$. The gateway excitation energies, E_j for these levels are given at the centers of the ranges of energies that could be resolved experimentally.

Energy (MeV)	$\sigma\Gamma$ (10^{-29} cm^2 keV)
2.8 ± 0.1	12000 ± 2000
3.6 ± 0.1	35000 ± 5000

This particular isomer, $^{180}Ta^m$ carries a dual distinction. It is the rarest stable isotope occurring in nature and it is the only naturally occurring isomer. The actual ground state of ^{180}Ta is 1^+ with a halflife of 8.1 hours while the tantalum nucleus of mass 180 occurring with 0.012% natural abundance is the 9^- isomer, $^{180}Ta^m$. It has an adopted excitation energy of 75.3 keV and halflife in excess of 1.2×10^{15} years.[30]

In an experiment conducted in 1987 we exposed 1.2 mg of $^{180}Ta^m$ to the bremsstrahlung from the 6 MeV linac and obtained a large fluorescence yield.[31] This was the first time a (γ,γ') reaction had been excited from an isomeric target as needed for a gamma-ray laser and was the first evidence of the existence of giant pumping resonances. Simply the observation of fluorescence from a milligram sized target proved that an unexpected reaction channel had opened. Usually grams of material are

required in this type of experiment. Analyses[31,32] of the data indicated that the partial width for the dumping of $^{180}Ta^{m}$ was around 0.5 eV.

To determine the transition energy, E_j from the $^{180}Ta^{m}$ isomer to the gateway level, a series of irradiations was made at the S-DALINAC facility using fourteen different endpoints in the range from 2.0 to 6.0 MeV.[33] The existence of an activation edge was clearly seen in the data shown in Fig. 3b. The fitting of such data to the expression of Eq. (3a) by adjusting trial values of $(\sigma\Gamma)_{f_j}$ enabled us to determine the integrated cross sections for the dumping of $^{180}Ta^{m}$ isomeric populations into freely radiating states. Reported values[33] are summarized in Table II and shown schematically in Fig. 3a.

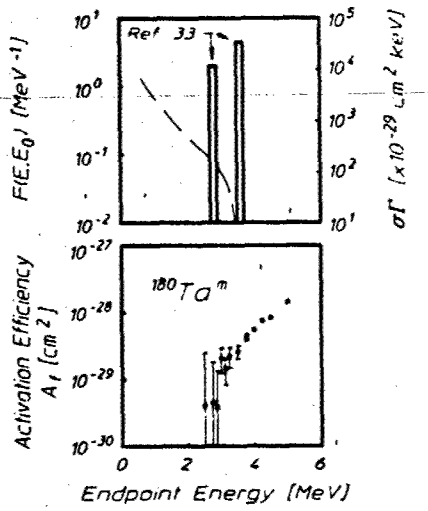

Figure 3. Activation efficiencies, A_f for the reaction $^{180}Ta^{m}(\gamma,\gamma')^{180}Ta$ are shown in Fig. 3b (lower) as functions of the endpoint, E_0 of the bremsstrahlung used for excitation. Gateway parameters obtained by fitting the data using Eq. (3a) are plotted with the right axis in Fig. 3a (upper). These parameters were determined using calculated photon spectra like that given by the dashed line and plotted with the left axis in Fig. 3a.

The integrated cross sections in Table II are enormous values exceeding anything previously reported for transfer through a bandwidth funnel by two orders of magnitude. In fact they are 10,000 times larger than the values usually measured for nuclei. With this result the restrictive guidelines customarily applied to optical pumping of nuclei are proven to be nearly 10^6 times too pessimistic.

While the width of the transfer process is difficult to interpret in a single-particle model, a puzzle of comparable complexity is found in the efficiency with which ΔK is transferred. It is an interesting speculation that at certain energies of excitation, collective oscillations of the core nucleons could break some of the symmetries upon which rest the identifications of the pure single-particle states. If single-particle states of differing K were mixed in this way, the possibility for transferring larger amounts of ΔK with greater partial widths might be enhanced. Some support for such a speculation was found in the unexpected enhancements measured very recently for the deexcitation of the $^{174}Hf^{m}$ isomer.[34] There also the decay of the isomer was found to occur primarily by transition through an intermediate state lying at 2685 keV in which K mixing occurred so that ΔK = 14 was lost between isomer and the ground-state band. This is remarkably close to the energy of the K-mixing level at 2800 ± 100 keV for ^{180}Ta shown in Table II. The close similarity of the energetics shown in Fig. 4 for nuclei with such dissimilar single-particle structures does seem to support the identification of this K-mixing process with some type of core property varying only slowly among neighboring nuclei.

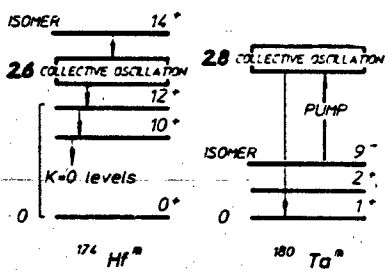

Figure 4. Energetics for the spontaneous decay of $^{174}Hf^{m}$ through an intermediate state providing ΔK=14 compared with those for the dumping of $^{180}Ta^{m}$ through a similar intermediate state. In the case of $^{180}Ta^{m}$, the dumping reaction provides ΔK=8. Both gateways are expected to be admixtures of single-particle states, thereby producing significant K mixing.

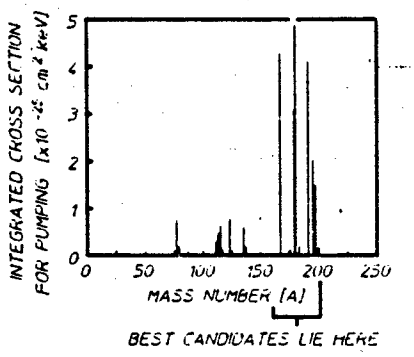

Figure 5. Integrated cross sections for pumping isomeric nuclei obtained in the survey of Ref. 35. The groupings of pumping strengths seen in the figure correspond to mass islands between magic numbers for neutrons and protons. The best candidates for a gamma-ray laser lie within the island containing the largest values of integrated cross sections corresponding to giant pumping resonances. Within each island the integrated cross sections vary only slowly with changing mass number, A.

A survey of 19 isotopes[35] conducted with the four U.S. accelerators over a fairly coarse mesh of bremsstrahlung endpoints confirmed the existence of giant resonances for breaking K in the region of masses near 180 as shown in Fig. 5.

Activation edges continued to support the identifications of integrated cross sections for pumping and dumping of isomers that were of the order of 10,000 times greater than usual values. A study with the higher resolution of the S-DALINAC[36] showed that the giant pumping resonances reappeared at lower masses near 120.

Whatever the mechanisms, the experimental fact remains that interband-transfer processes connecting to isomeric levels can be pumped through enormous partial widths reaching 0.5 eV, even when the transfer of angular momentum must be as great as $\Delta K = 8$, or even $\Delta K = 14$. It seems this is the nuclear analog of the giant resonance for pumping ruby at the atomic level. Elucidation of the process, together with identification of the gateways, has been propelled into a place of future importance.

CONCLUSIONS - A LASER MODEL

The model of a gamma-ray laser for the 1990's is not fundamentally different from the nuclear analog of the ruby laser described[11] in 1982. Envisioned as a thin film of diluent doped with isomeric nuclei and pumped with a flash of x rays in a slab geometry, the question of feasibility still rests on the degree to which the properties of some real nuclide approach those of the ideal being modeled. What has changed is that the discovery of giant pumping resonances enables some of the original constraints to be relaxed. The result is that the feasibility of a gamma-ray laser is orders-of-magnitude more probable than originally estimated in 1982. Because of this substantial improvement, it is useful to recompute the model in terms of the new data obtained in the past five years.

Since the better candidate isomers for a gamma-ray laser have never been fabricated in macroscopic amounts, the precise identity of the best nuclide to model is not known. Moreover, since feasibility is such a complex function of the nuclear parameters, the assumptions introduced into any model will critically affect the estimates of feasibility in strongly nonlinear ways. For the computation reported here the following parameters were assumed.

1) The pump band j in Fig. 1 is one of the newly discovered giant pumping resonances with a partial width of $b_a b_0 \Gamma = 1$ eV.

2) The pump transition is centered on an energy $E_j = 30$ keV.

3) The initial state is assumed to be isomeric with an excitation energy so high that 2) is possible.

4) The output transition is around 100 keV.

5) The nuclei are diluted in a thin film of diamond or Be.

6) The Borrmann effect contributes a factor of 10 to the enhancement of the ratio of cross sections for resonant to nonresonant transitions.

The most sensitive assumptions are those about the width and activation energy of the giant pumping resonance, statements 2) and 3). The range of excitation energies over which isomers can be found is very large. We have already shown that isomers can be dumped into the freely-radiating system, even through $\Delta K = 8$ or

$\Delta K = 14$, so the only doubt here is a statistical one; whether or not a giant pump resonance can be found within 30 keV of an isomer.

Following our development[11] of 1982, under small signal conditions the midrange requirement of 10^{-4} is obtained for the pumped fraction,

$$\frac{N_f}{N_i} \geq 10^{-4} \quad . \tag{6}$$

This sets the pump intensity needed for threshold, and with it the amount of waste heat to dissipate.

The essential concept in the management of the thermal economy is that the mean free path (MFP) for a photon resonant with the nuclear transition is much shorter than the MFP for nonresonant, photoelectric absorption to produce heat. Also, the MFP for a photoelectron produced in the nonresonant channel is greater in the diluent than the MPF for the photons pumping the nuclear resonance. This means that a thin film of diamond can be doped to use most of the incident photons in the bandwidth of the giant pumping resonance while the majority of the nonresonant photons will pass through the film into the substrate which can be cooled by ablation or cryogenics. Moreover, primary photoelectrons produced by the small fraction of nonresonant events in the film can escape before their energy is degraded to heat.

The quantitative expression of this strategy is obtained by substituting Eq. (3a) into Eq. (6) and assuming a single giant resonance dominates so that the sum is unnecessary. Solving for $\phi_j = \Phi_0 F(E_j, E_0)$, and using the previous assumption that each pump photon carries 30 keV gives the spectral fluence, $F_j = E_j \phi_j$ at threshold,

$$F_j \geq 177 \text{ mJ cm}^{-2} \text{ eV}^{-1} \quad . \tag{7}$$

For the likely cases of rare earth or platinide elements, the 30 keV pump energy lies below the K edge and about 15 keV above the L edge. As a result, the primary photoelectrons resulting from the nonresonant absorption in the active medium should have energies of the order of 15 keV and ranges of 6.0 and 3.0 μm in Be and C, respectively.[37] Thus, only about 10% and 20% of the primaries, respectively, should be stopped in a 0.67 μm thick host film of Be or diamond. This is the thickness corresponding to the MFP for resonant absorption at a concentration of 10%. Then the fractions of the energy from the incident pump degraded into heat in the laser film because of nonresonant absorption become

$$f(\text{Be}) = 4.8 \times 10^{-4} \quad , \tag{8a}$$

$$f(\text{C}) = 2.4 \times 10^{-4} \quad . \tag{8b}$$

Considering that edge filters or ablation layers could reduce the bandwidth of the pump radiation to 3 keV before reaching the doped layer of active medium, the incident fluence lying outside the bandwidth for resonant absorption would be 3000 times greater than the value of Eq. (7). However, only the fractions of Eqs. (8a) and (8b) are capable of being degraded into heat in the sensitive layer. The resulting energy balance can be summarized at threshold by the first two lines of Table III.

Dividing those fluences by the 0.67 μm thickness gives the energy loading of the laser film shown in Table III. These values are quite significantly below the levels of heating required to degrade the recoil-free fractions in the case of the diamond lattice. Baldwin has summarized[1] the involved dependence of the recoil-free fraction of gamma transitions upon recoil energy, lattice parameters, and temperature. He shows that even at a temperature, T equal to the Debye temperature, Θ_D the recoil-free fraction is not significantly degraded (by more than a factor of 2) for a transition even as energetic as to give a classical recoil energy of 0.14 Θ_D. In diamond with Θ_D = 2230 K this means a transition of 100 keV is little affected by a temperature increase up to T = Θ_D.

It is a textbook computation[38] to estimate that the energy content of the phonons of a material with Θ_D = 2230 K at a temperature of T = Θ_D is about 11 kJ cm^{-3}. Comparing this with the estimated loading of 3.8 kJ cm^{-3} gives a "safety factor" of almost three. A comparable margin is obtained for the Be.

Table III

Summary of the thermal economy at threshold for a laser nuclide doped into a film of 0.67 μm thickness of the materials shown.

Lattice	Be	C(diamond)
Resonant input fluence	177 mJ cm^{-2}	177 mJ cm^{-2}
Fluence degraded to heat	127 mJ cm^{-2}	255 mJ cm^{-2}
Resonant energy density	2.6 kJ cm^{-3}	2.6 kJ cm^{-3}
Thermal loading	1.9 kJ cm^{-3}	3.8 kJ cm^{-3}

To summarize, it is convenient to recast the threshold fluence of Eq. (7) into more tangible terms. The spectral fluence of 177 mJ cm^{-2} eV^{-1} corresponds to 530 J cm^{-2} if the bandwidth of the pump x rays is arranged to be 3 keV, a practical separation which might be filtered between K edges. Even if pumped instantaneously, so that no waste heat were transported away, the thermal loading would reach only 1/3 of the limit for retaining the Mössbauer effect. If derived from an x-ray line of 30 eV width, the threshold fluence would be only 5.3 J cm^{-2}. In that case the thermal loading would reach only 1/300 of the critical limit for a diamond lattice.

Even beyond this point much can be done to reduce heating further. All calculations so far were done for the instantaneous generation of the waste heat. The time for the transport of a phonon across the 0.67 μm thickness of the working layer is of the order of only 100 psec so that the transport of significant amounts of heat from that layer into a diamond heat sink is possible on a nanosecond time scale. Yet most of the fluorescent levels of interest for inversion[11] have lifetimes of tens of nanoseconds to tens of microseconds. This is many times the period for the transport of phonons out of the inverting layer so that more orders of magnitude can be realized in reducing the thermal loading further below the limits specified so

far. However, all these techniques require precise knowledge about the energy levels and absorption edges of the materials involved. Until the identity of the best candidate for a gamma-ray laser is known, the exact specifications of the solution to the disposal of the waste heat cannot be generally articulated. The examples considered here show that there are many orders-of-magnitude in the safety margin between likely amounts of heating and the much larger amounts which can be tolerated in stiff lattices such as Be and diamond.

The greatest significance is that the persistent tenets of theoretical dogma which have historically[1] inhibited the development of a gamma-ray laser are eliminated by studies of the past five years . There is no need to melt the host lattice in order to pump a nuclear system to the laser threshold. *There are no a priori obstacles to the realization of a gamma-ray laser. A gamma-ray laser is feasible if the right combination of energy levels occurs in some real material.* The overriding question to resolve is whether or not one of the better of the candidate nuclides has its isomeric level within a few tens or even hundreds of keV of one of the giant resonances for dumping angular momenta.

ACKNOWLEDGEMENT

This work was supported by SDIO/IST under direction of NRL.

REFERENCES

1. G. C. Baldwin, J. C. Solem, and V. I. Goldanskii, "Approaches to the development of gamma-ray lasers," Rev. Mod. Phys. 53:687 (1981).
2. V. S. Letokhov, Pumping of nuclear levels by x-ray radiation of a laser plasma, Sov. J. Quant. Electron. 3:360 (1974).
3. B. Arad, S. Eliezer and Y. Paiss, "Nuclear 'Anti-Stokes' transitions induced by laser radiation," Phys. Lett. 74A:395 (1979).
4. C. B. Collins, S. Olariu, M. Petrascu, and I. Popescu, "Enhancement of γ-Ray Absorption in the Radiation Field of a High Power Laser," Phys. Rev. Lett. 42:1397 (1979).
5. C. B. Collins, S. Olariu, M. Petrascu, and I. Popescu, "Laser-Induced Resonant Absorption of γ Radiation," Phys. Rev. C 20:1942 (1979).
6. S. Olariu, I. Popescu, and C. B. Collins, "Tuning of γ-Ray Processes with High Power Optical Radiation," Phys. Rev. C 23:50 (1981).
7. S. Olariu, I. Popescu, and C. B. Collins, "Multiphoton Generation of Optical Sidebands to Nuclear Transitions," Phys. Rev. C 23:1007 (1981).
8. C. B. Collins, "The Tuning and Stimulation of Gamma Radiation," Proceedings of the International Conference on Lasers '80, edited by C. B. Collins (STS Press, McLean, VA, 1981) pp. 524-531.
9. C. B. Collins, "Upconversion of Laser Radiation to γ-Ray Energies," Laser Technique for Extreme Ultraviolet Spectroscopy, edited by T. J. McIlrath and R. R. Freeman (AIP Conference Proceedings No. 90, New York, 1982) pp. 454-464.
10. C. B. Collins, "Upconversion of Laser Radiation to Gamma-Ray Energies," Proceedings of the International Conference on Lasers '81, edited by C. B. Collins (STS Press, McLean, VA, 1982) pp. 291-295.
11. C. B. Collins, F. W. Lee, D. M. Shemwell, B. D. DePaola, S. Olariu, and I. Popescu, "The Coherent and Incoherent Pumping of a Gamma Ray Laser with Intense Optical Radiation," J. Appl. Phys. 53:4645 (1982).

12. B. D. DePaola and C. B. Collins, "Tunability of radiation generated at wavelengths below 1 Å by anti-Stokes scattering from nuclear levels," J. Opt. Soc. Am. B 1:812 (1984).
13. C. B. Collins and B. D. Depaola, "Tunable Sub-Angstrom Radiation Generated by Anti-Stokes Scattering from Nuclear Levels," Laser Techniques in the Extreme Ultraviolet, edited by S. E. Harris and T. B. Lucatorto (AIP Conference Proceedings No. 119, New York, 1984) pp. 45-53.
14. C. B. Collins and B. D. DePaola, "Observation of coherent multiphoton process in nuclear states," Optics Lett. 10:25 (1985).
15. B. D. DePaola, S. S. Wagal, and C. B. Collins, "Nuclear Raman Spectroscopy," J. Opt. Soc. Am. B 2:541 (1985).
16. B. D. DePaola and C. B. Collins, "Tunability of radiation generated by wavelengths below 1 Å by anti-Stokes scattering from nuclear levels," J. Opt. Soc. Am. B 1:812 (1984).
17. B. Pontecorvo and A. Lazard, "Isomerie nucleaire produite par les rayons X du spectre continu," C. R. Acad. Sci. 208:99 (1939).
18. G. B. Collins, B. Waldman, E. M. Stubblefield, and M. Goldhaber, "Nuclear excitation of indium by x-rays," Phys. Rev. 55:507 (1939).
19. Y. Watanabe and T. Mukoyama, "Excitation of nuclear isomers by γ rays from ^{60}Co," Bull. Inst. Chem. Res., Kyoto Univ. 57:72 (1979).
20. M. Krcmar, A. Ljubicic, K. Pisk, B. Logan, and M. Vrtar, "Photoactivation of ^{111}Cd," Phys. Rev. C 25:2097 (1982).
21. I. Bikit, J. Slivka, I. V. Anicin, L. Marinkov, A. Ruydic, and W. D. Hamilton, "Photoactivation of $^{111}Cd^{m}$ without a 'nonresonant' contribution," Phys. Rev. C 35:1943 (1987).
22. "The EGS4 Code System," Walter R. Nelson, Hideo Hirayama, and David W. O. Rogers, Stanford Linear Accelerator Center Report No. SLAC 265, 1985 (unpublished).
23. Evaluated Nuclear Structure Data File (Brookhaven National Laboratory, Upton, New York, 1986).
24. E. Browne and R. B. Firestone, "Table of Radioactive Isotopes," edited by V. S. Shirley, Wiley, New York (1986) pp. 180-182.
25. J. A. Anderson and C. B. Collins, "Calibration of pulsed bremsstrahlung spectra with photonuclear reactions of ^{77}Se and ^{79}Br," Rev. Sci. Instrum. 58:2157 (1987).
26. J. A. Anderson and C. B. Collins, "Calibration of pulsed x-ray spectra," Rev. Sci. Instrum. 59:414 (1988).
27. C. B. Collins, J. A. Anderson, Y. Paiss, C. D. Eberhard, R. J. Peterson, and W. L. Hodge, "Activation of $^{115}In^{m}$ by single pulses of intense bremsstrahlung," Phys. Rev. C 38:1852 (1988).
28. J. A. Anderson, M. J. Byrd, and C. B. Collins, "Activation of $^{111}Cd^{m}$ by single pulses of intense bremsstrahlung," Phys. Rev. C 38:2833 (1988).
29. E. C. Booth and J. Brownson, "Electron and Photon Excitation of Nuclear Isomers," Nucl. Phys. A98:529 (1967).
30. E. Browne, "Nuclear data sheets for A = 180," Nucl. Data Sheets 52:127 (1987).
31. C. B. Collins, C. D. Eberhard, J. W. Glesener, and J. A. Anderson, "Depopulation of the isomeric state $^{180}Ta^{m}$ by the reaction $^{180}Ta^{m}(\gamma,\gamma')^{180}Ta$," Phys. Rev. C 37:2267 (1988).
32. J. J. Carroll, J. A. Anderson, J. W. Glesener, C. D. Eberhard, and C. B. Collins, "Accelerated Decay of $^{180}Ta^{m}$ and ^{176}Lu in Stellar Interiors through (γ,γ') Reactions," Astrophys. J. 344:454 (1989).

33. C. B. Collins, J. J. Carroll, T. W. Sinor, M. J. Byrd, D. G. Richmond, K. N. Taylor, M. Huber, N. Huxel, P. von Neumann-Cosel, A. Richter, C. Spieler, and W. Ziegler, "Resonant excitation of the reaction $^{180}Ta^{m}(\gamma,\gamma')^{180}Ta$," Phys. Rev. C 42:R1813 (1990).
34. P. M. Walker, F. Sletten, N. L. Gjørup, M. A. Bentley, J. Borggreen, B. Fabricius, A. Holm, D. Howe, J. Pedersen, J. W. Roberts, and J. F. Sharpey-Schafer, "High-K Barrier Penetration in ^{174}Hf: A Challenge to K Selection," Phys. Rev. Lett. 65:416 (1990).
35. J. J. Carroll, M. J. Byrd, D. G. Richmond, T. W. Sinor, K. N. Taylor, W. L. Hodge, Y. Paiss, C. D. Eberhard, J. A. Anderson, C. B. Collins, E. C. Scarbrough, P. P. Antich, F. J. Agee, D. Davis, G. A. Huttlin, K. G. Kerris, M. S. Litz, and D. A. Whittaker, "Photoexcitation of nuclear isomers by (γ,γ') reactions," Phys. Rev. C 43:1238 (1991).
36. J. J. Carroll, T. W. Sinor, D. G. Richmond, K. N. Taylor, C. B. Collins, M. Huber, N. Huxel, P. von Neumann-Cosel, A. Richter, C. Spieler, and W. Ziegler, "Excitation of $^{123}Te^{m}$ and $^{125}Te^{m}$ through (γ,γ') reactions," Phys. Rev. C 43:879 (1991).
37. G. Knopf and W. Paul, "Alpha, Beta and Gamma-Ray Spectroscopy," edited by Kai Siegbahn, North-Holland Co., Amsterdam (1965) pp. 1 - 25.
38. C. Kittel, "Introduction to Solid State Physics, 6th Edition," Wiley, New York (1986) pp. 106.

Laser and Particle Beams (1993), *vol.* 11, *no.* 1, *pp.* 43-54
Printed in the United States of America

Status and issues in the development of a γ-ray laser. II. Giant resonances for the pumping of nuclei

By C.B. COLLINS, J.J. CARROLL, K.N. TAYLOR, T.W. SINOR, C. HONG, J.D. STANDIFIRD AND D.G. RICHMOND

Center for Quantum Electronics, University of Texas at Dallas, Richardson, TX 75083-0688

(Received 1 May 1992; accepted 8 July 1992)

A γ-ray laser would stimulate the emission of radiation of wavelengths below 1 Å from excited states of nuclei. However, the anticipation of a need for high pump powers tended to discourage early research and the difficulties in demonstrating a device were first assumed to be insurmountable. Over the past decade, advances in pulsed-power technology have changed these perceptions and studies have built a strong momentum. A nuclear analog of the ruby laser has been proposed and many of the component steps for pumping the nuclei have been demonstrated experimentally. A quantitative model based upon the new data and concepts has shown the γ-ray laser to be feasible if some real isotope has its properties sufficiently close to the ideals modeled The greatest positive impact upon feasibility has come from the discovery of giant resonances for pumping nuclei that greatly reduce the levels of pump power needed.

1. Introduction

The basic plan for a γ-ray laser was published (Collins *et al.* 1982) in 1982 and now appears in the textbooks (Collins 1991). In the decade since then, research on this topic has been rich with achievement. The feasibility of a γ-ray laser has been substantially increased by a major breakthrough (Collins *et al.* 1988b) that has proven the basic concept. Subsequent development has focused upon applications of this breakthrough and special isotopic samples have been pumped with Bremsstrahlung X-rays in a nuclear analog of the ruby laser (Collins *et al.* 1990; Carroll *et al.* 1991a).

The greatest impediment to research on the feasibility of a γ-ray laser has come from the lack of suitable materials. There are 1,886 distinguishable nuclear isotopes, but most do not occur naturally and there have not been any reasons to produce them artificially. In 1986, a computer-based search of all nuclear properties (Evaluated Nuclear Structure Data File 1986) identified 29 isotopes as first-class candidates for a γ-ray laser (Collins *et al.* 1992) but only the 2 poorest, $^{180}Ta^{m}$ and ^{123}Te, could be acquired for testing. Those are the ones upon which the breakthrough discovery of the giant pumping resonance was made (Collins *et al.* 1988b; Carroll *et al.* 1989; Collins *et al.* 1990; Carroll *et al.* 1991b).

The better candidates for a γ-ray laser have never been available in sufficient quantities for evaluation and recent research (Carroll *et al.* 1991a) has focused instead upon 19 simulation materials that may teach the systematics for using the giant pumping resonances to excite nuclei. However, even those simulations had to be limited to physical packages in which nuclei were not bound into the hosts most likely to preserve a laser-like width for the fluorescence lines. Despite the difficulties, the results on those simulated candidates were

 0263-0346/93 $5.00 + .00

extremely encouraging as the giant resonances for pumping were found in many of them (Carroll *et al* 1991a). The significance of such resonances in reducing the demands for pump power in a hypothetical laser design were summarized in a recent review (Collins *et al.* 1992). This article reports more recent investigations into the structure and systematics of the giant pumping resonances.

2. Technical background

2.1. *Theory*

The essential concept driving the development of the γ-ray laser research has been the "optical" pumping of nuclei. In this case, optical means X-rays, but the fundamentals are the same. Useful, resonant absorption of pump power would occur over short distances to produce high concentrations of excited nuclei while wasted wavelengths would be degraded to heat only in much larger volumes. In the blueprint (Collins *et al.* 1982) of 1982, this nuclear analog of the ruby laser embodied the simplest concepts for a γ-ray laser and not surprisingly the greatest rate of achievement has been reported in that direction.

For ruby, the identification and exploitation of a bandwidth funnel were the critical keys in the development of the first laser. There was a broad absorption band linked through efficient cascading to the narrow laser level and the 1982 theory called for a nuclear analog of this structure which was unknown at that time.

Whether or not the initial state being pumped is the ground state or a long-lived isomeric level, the principal figure of merit is the integrated cross section for pumping an output transition through such a broad band, $\pi b_a b_o \Gamma \sigma_0/2$. Constituent parameters are identified in figure 1, where it can be seen that the branching ratios b_a and b_o specify the probabilities that a population pumped by absorption into the jth broad level will decay back into the initial or fluorescent levels, respectively. It is not often that the sum of branching ratios is unity, as channels of decay to other levels are likely. However, the maximum value of partial width for a particular level j occurs when $b_a = b_o = 0.5$.

For a sample that is optically thin at the pump wavelength, a computation of the num-

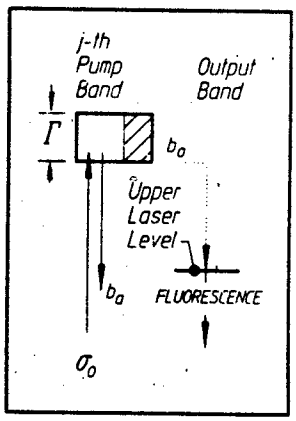

FIGURE 1. Schematic representation of the decay modes of a gateway state of width Γ sufficiently large to promote bandwidth funneling. The initial state from which population is excited with an absorption cross section σ_0 can be either ground or isomeric.

ber of nuclei pumped into a fluorescence level in the scheme of figure 1 is straightforward. Most intense X-ray sources emit continua because either Bremsstrahlung is initially produced or spectral lines are degraded by Compton scattering in the immediate environment. The time-integrated yield of final-state nuclei, N_f, obtained by irradiating N_i initial targets with a photon flux Φ_0 in photons cm^{-2} delivered in a continuum is

$$N_f = N_i \Phi_0 \int_0^{E_0} \sigma(E) F(E, E_0) \mathrm{d}E \tag{1}$$

where $F(E, E_0)$ is the distribution of intensities up to an endpoint energy E_0 within the input spectrum normalized so that

$$\int_0^{E_0} F(E, E_0) \mathrm{d}E = 1 \tag{2}$$

and $\sigma(E)$ is the effective cross section for the excitation of the final state from the initial.

All (γ, γ') reactions occurring at energies below the threshold for particle evaporation excite discrete intermediate states of nuclei as shown in figure 1. Although only one intermediate state appears in the figure, there could be more. Each would be excited at a different pump energy but all would branch to some extent into the same fluorescence level, f. The jth intermediate is shown in figure 1 as typical.

Although the width of level j is broad on a nuclear scale, it is narrow in comparison to the scale of energies, E, over which $F(E, E_0)$ varies. Then, the final-state yield, expressed as the normalized activation per unit photon flux, $A_f(E_0)$, can be written from equation (1) as

$$A_f(E_0) \equiv \frac{N_f}{N_i \Phi_0} = \sum_j (\sigma\Gamma)_{fj} F(E_j, E_0) \tag{3a}$$

In this expression, $(\sigma\Gamma)_{fj}$ is the integrated cross section for the production of final state N_f as a result of the excitation of the intermediate state E_j with Bremsstrahlung having an endpoint of E_0 described by the spectral function $F(E, E_0)$, so that

$$(\sigma\Gamma)_{fj} = \int_{E_j - \Delta}^{E_j + \Delta} \sigma(E) \mathrm{d}E \tag{3b}$$

where Δ is an energy small compared to the spacing between intermediate states and large in comparison to their widths. Levels of this type are sometimes called gateways or doorways.

It is straightforward to show that

$$(\sigma\Gamma)_{fj} = (\pi b_a b_e \Gamma \sigma_0 / 2)_{fj} \tag{4a}$$

where $2\sigma_0$ is the peak of the Breit-Wigner cross section for the absorption step and

$$\sigma_0 = \frac{\lambda^2}{2\pi} \frac{2I_e + 1}{2I_g + 1} \frac{1}{\alpha_p + 1} \tag{4b}$$

where λ is the wavelength of the γ-ray at the resonant energy, E_j; I_e and I_g are the nuclear spins of the excited and ground states, respectively; and α_p is the total internal conversion coefficient for the system shown in figure 1.

2.2. *Experimental Confirmation*

In experimental work of the last 5 years, the Bremsstrahlung from five accelerators in different experimental environments was used to verify the fluorescence model of equa-

tions (1)-(4b) and cross-check the accelerator intensities (Collins *et al.* 1992). The devices involved in those efforts were DNA/PITHON at Physics International, DNA/Aurora at the Harry Diamond Laboratories, a 4-MeV and a 6-MeV medical linac at the University of Texas Health Sciences Center, and the superconducting injector to the storage ring at Darmstadt (S-DALINAC). Spectral intensities were calculated from the EGS4 coupled electron/photon transport code (Nelson *et al.* 1985) adapted for each individual configuration from closely monitored values of accelerator currents. In this way, both $F(E,E_0)$ and Φ_0 were obtained. In some case, Φ_0 was separately verified by in-line dosimetry.

During these experiments, samples with typical masses of grams were exposed to the Bremsstrahlung from the five accelerators for times ranging from seconds to hours for the continuously operating machines and to single flashes from the pulsed devices. The activations, A_f of equation (3a), were determined by counting the photons spontaneously emitted from the samples after transferring them to a quieter environment. Usual corrections were made for the isotopic abundance, loss of activity during irradiation and transit, counting geometry, self-absorption of the fluorescence, and tabulated efficiencies (Evaluated Nuclear Structure Data File 1986) for the emission of signature photons from the populations, N_f. The self-absorption correction required a calculation of photon transport that was verified in some cases by confirming that the same sample masses in different geometries with different correction factors gave the same final populations.

Results were in close agreement (Anderson *et al.* 1987; Anderson *et al.* 1988a; Anderson *et al.* 1988b; Collins *et al.* 1988a) with the predictions of equation (3a) used with literature values of $(\sigma\Gamma)_{ff}$. That work established a confidence level sufficient to support the use of nuclear activation as a means of selectively sampling the spectra of single pulses of intense continua to determine absolute intensities as functions of wavelength. The most detailed confirmation of theory was obtained with the reaction $^{87}Sr(\gamma,\gamma')^{87}Sr^m$. Particularly valuable were the data obtained with the S-DALINAC because the endpoint of the Bremsstrahlung could be varied. A change of the endpoint energy, E_0, of the Bremsstrahlung, as well as altering Φ_0, modulates the spectral intensity function $F(E_j,E_0)$ at all of the important energies for resonant excitation E_j. The largest effect occurs when E_0 is increased from a value just below some intermediate state at E_j to one exceeding it so that $F(E_j,E_0)$ varies from zero to some finite value as shown in figure 2a.

The activation efficiencies, A_f, calculated from equation (3a) using the literature values (Booth *et al.* 1967; Collins *et al.* 1990) plotted in figure 2a are shown in figure 2b with the measurements obtained with four of the accelerators. As can be seen, agreement is good between the different accelerators and between the experimental data and the model calculations.

These calibration studies served to confirm both the traditional model of nuclear activation summarized in equations (1)-(4b) and validate the use of the EGS4 code for calculating Bremsstrahlung intensities from measured accelerator parameters.

3. Giant pumping resonances

3.1. *Discovery*

Many of the interesting isomers for a γ-ray laser belong to the class of nuclei deformed from the normally spherical shape. For those systems, there is a quantum number of dominant importance, K, which is the projection of individual nucleonic angular momenta upon the axis of elongation. To this is added the collective rotation of the nucleus to obtain the total angular momentum J. The resulting system of energy levels resembles that of a diatomic molecule.

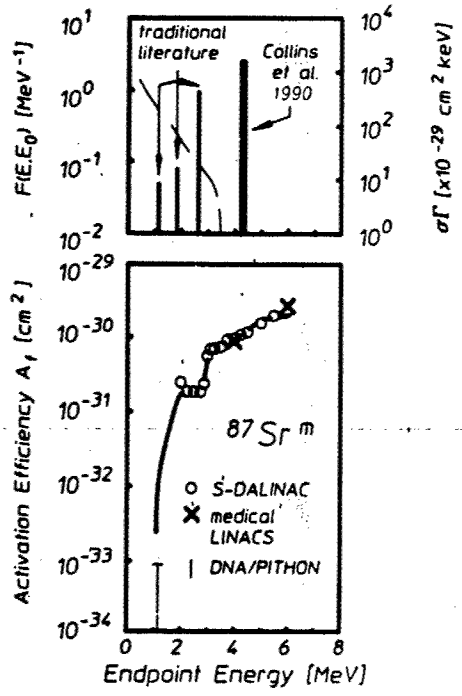

FIGURE 2. Activation efficiencies, A_f, for the reaction $^{87}Sr(\gamma,\gamma')^{87}Sr^m$ are shown (lower) as functions of the endpoint, E_0, of the Bremsstrahlung used for excitation. The solid curve in the lower panel plots values computed from equation (3a) using the gateway parameters found in the literature and plotted with the right axis in the top panel together with calculated photon spectra like that given by the broken line and plotted with the left axis in the top panel. The lower panel compares these A_f values with measurements obtained from four different accelerators.

In most cases, an isomeric state has a large lifetime because its value of K differs considerably from those of lower levels to which it would otherwise be radiatively connected. As a consequence, bandwidth funneling processes such as shown in figure 1 that start from isomeric levels must span substantial changes in K and component transitions have been expected to have large, and hence unlikely, multipolarities.

From this perspective, the candidate isomer, $^{180}Ta^m$, was the most initially unattractive as it had the largest change of angular momentum between isomer and ground state, $8\hbar$. However, because a macroscopic sample was readily available $^{180}Ta^m$ became the first isomeric material to be optically pumped to a fluorescent level.

This particular isomer, $^{180}Ta^m$, carries a dual distinction: It is the rarest stable isotope occurring in nature and the only naturally occurring isomer. The actual ground state of ^{180}Ta is 1+ with a halflife of 8.1 h while the tantalum nucleus of mass 180 occurring with 0.012% natural abundance is the 9− isomer, $^{180}Ta^m$. It has an adopted excitation energy of 75.3 keV and a halflife in excess of 1.2×10^{15} years.

In an experiment conducted in 1987, 1.2 mg $^{180}Ta^m$ was exposed to the Bremsstrahlung from the 6-MeV linac and a large fluorescence yield was obtained (Collins *et al.* 1988). This was the first time a (γ,γ') reaction had been excited from an isomeric target as needed for a γ-ray laser and was the first evidence of the existence of giant pumping resonances. Sim-

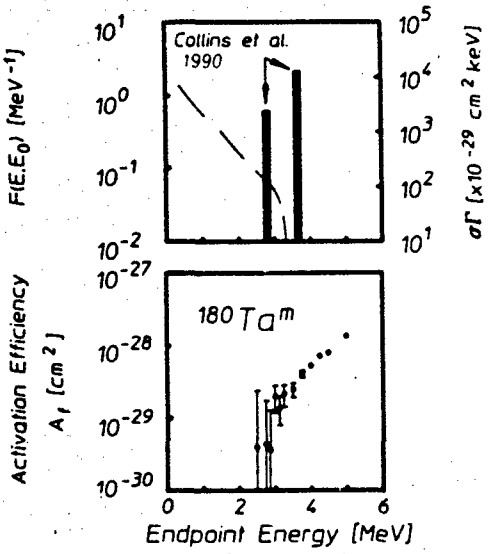

FIGURE 3. Activation efficiencies, A_f, for the reaction $^{180}Ta^m(\gamma,\gamma')^{180}Ta$ are shown (lower) as functions of the endpoint, E_0, of the Bremsstrahlung used for excitation. Gateway parameters obtained by fitting the data using equation (3a) are plotted with the right axis in the top panel. These parameters were determined using calculated photon spectra like that given by the broken line and plotted with the left axis in the top panel.

ply the observation of fluorescence from a milligram-sized target proved that an unexpected reaction channel had opened. Usually, grams of material has been required in this type of experiment. Analyses (Collins *et al.* 1988; Carroll *et al.* 1991a) of the data indicated that the partial width for the dumping of $^{180}Ta^m$ was around 0.5 eV.

To determine the transition energy, E_f, from the $^{180}Ta^m$ isomer to the gateway level, a series of irradiations (Collins *et al.* 1990) was made at the S-DALINAC facility using 14 different endpoints in the range from 2.0–6.0 MeV. The existence of an activation edge was clearly seen in the data shown in figure 3b. The fitting of such data to the expression of equation (3a) by adjusting trial values of $(\sigma\Gamma)_{ff}$ provided the integrated cross sections for the dumping of $^{180}Ta^m$ isomeric populations into freely radiating states. Reported values (Collins *et al.* 1990) are summarized in table 1 and shown schematically in figure 3a.

TABLE 1. Recently measured values (Collins *et al.* 1990) of integrated cross section, $(\sigma\Gamma)_{ff}$, for the reaction $^{180}Ta^m(\gamma,\gamma')^{180}Ta$

Energy (MeV)	$\sigma\Gamma$ (10^{-29} cm^2 keV)
2.8 ± 0.1	12,000 ± 2,000
3.6 ± 0.1	35,000 ± 5,000

The gateway excitation energies, E_f, for these levels are given at the centers of the ranges of energies that could be resolved experimentally.

The integrated cross sections in table 1 are enormous values exceeding anything previously reported for transfer through a bandwidth funnel by two orders of magnitude. In fact, they are 10,000 times larger than the values usually measured for nuclei.

3.2. *Systematics*

A survey of 19 isotopes (Carroll *et al.* 1991a) conducted with the four U.S. accelerators over a fairly coarse mesh of Bremsstrahlung endpoints confirmed the existence of giant resonances for breaking K in the region of masses near 180 as shown in figure 4. Activation edges continued to support the identifications of integrated cross sections for pumping and dumping of isomers that were of the order of 10,000 times greater than usual values. A study (Carroll *et al.* 1991b) with the higher resolution of the S-DALINAC showed that the giant pumping resonances reappeared at lower masses near 120.

3.3. *Structure*

As encouraging as were the studies showing the frequency with which giant pumping resonances occurred throughout the table of nuclides, a major concern remained. To lower pump requirements for a laser, it is necessary that the $\sigma\Gamma$ be large but not sufficient. In the ideal case (Collins *et al.* 1992), the integrated cross section, $\sigma\Gamma$, would be elevated by a strong width, Γ multiplying a cross section for absorption having the maximum value possible, $2\sigma_0$ from equation (4b). In that case, the ratio of pump power per unit volume absorbed resonantly to excite nuclei to the fraction absorbed nonresonantly and degraded to heat would be the largest possible, an important factor in thermal survival (Collins *et al.* 1992).

The density of excited states is high in the nuclei favored in figure 4, and is especially so in ^{180}Ta because that is one of the few odd-odd nuclei known to be stable. It could have been the case that the remarkable magnitude found for $\sigma\Gamma$ in the dumping of the population of ^{180}Ta^{m} was the result of a great number of adjacent but small $(\sigma\Gamma)_{fj}$ of unremarkable size adding in equation (3a) to give a surprising total yield. If so, the result would have still been exciting but much less helpful in rejecting the waste pump power degraded to heat

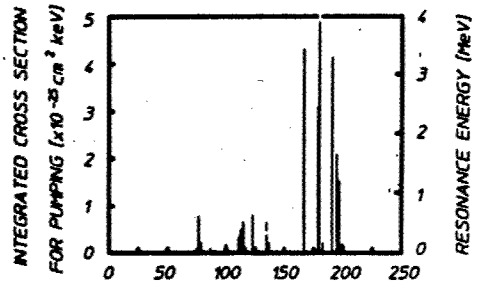

FIGURE 4. Integrated cross sections for pumping isomeric nuclei obtained in the survey of Carroll *et al.* (1991c). The groupings of pumping strengths seen correspond to mass islands between magic numbers for neutrons and protons. The best candidates for a γ-ray laser lie within the island containing the largest values of integrated cross sections corresponding to giant pumping resonances. Within each island, the integrated cross sections vary only slowly with changing mass number, A.

(Collins *et al.* 1992). To show that this unfortunate possibility was not the case required that scattering measurements be done.

From figure 1, it can be seen that photoexcitation events that do not lead to the population of different final states should be detected by the reemission or scattering of the incident photon initially absorbed by the gateway state. In analogy with the $(\sigma\Gamma)_{ff}$ of equation (4a), the integrated cross section for scattering can be written

$$(\sigma\Gamma)_{0f} = (\pi b_a^2 \Gamma\sigma_0/2)_{0f} \tag{5}$$

A large value of $(\sigma\Gamma)_{0f}$ would ensure that enough photons could be scattered for spectroscopic analysis to determine at what energies the corresponding resonances could be excited. In the event $b_a \neq 1$, some fraction of the gateway state population would also decay to the isomer to contribute to $(\sigma\Gamma)_{ff}$ and the energies for excitation of some of the giant pumping resonances could be determined.

To actually perform a scattering experiment designed to show the pumping resonances requires a nuclide with several favorable properties. It must have a final state for the process with a reasonable lifetime of seconds to hours and be available in gram quantities with isotopic purity. Beyond such practical concerns would be the desire to have the nuclear structure well characterized for energies below those at which giant resonances would be expected. With these constraints, it was relatively straightforward to identify ^{115}In as an optimal vehicle for a first test.

An experimental arrangement especially designed for nuclear resonance fluorescence (NRF) experiments has been recently described (Ziegler *et al.* 1990). The spectrum of the intense Bremsstrahlung produced by the S-DALINAC accelerator was calibrated with In/Al and In/B sandwich targets, which provided easily resolved reference transitions from the Al and B in the scattered radiation. To cover an energy range $E_j \approx 1.5$–4.5 MeV, measurements were performed at endpoint energies $E_0 = 3.1$, 4.6, and 5.2 MeV. The variation of E_0 also provided the means to distinguish ground-state transitions from decays to excited states. Detailed scattering spectra are shown in the literature (Neumann-Cosel *et al.* 1991).

The integrated cross sections obtained from the excitation of the final state, ^{115}In^m, and the photon scattering are shown in figure 5a. The excitation energy region corresponding to the large $(\sigma\Gamma)_{ff}$ values is shown in the upper part of figure 5a. The widths of the histograms represent the experimental uncertainty in the energies of the intermediate states identified in the photoactivation. The striking result is that, except for a few moderate levels around 3.0 and 3.7 MeV, all (γ,γ') transitions are found within these energy regions. Thus, these states (or a part of them) must have been responsible for the isomer population. No other (γ,γ') state is resolved in the lower part of figure 5a up to $E_j = 5$ MeV. Together, these results confirm that all important intermediate states in this range have been identified.

Further insight was attained (Neumann-Cosel *et al.* 1991) from an analysis within the unified model. In the case of ^{115}In, the configuration space is built by proton $1h$-states (relative to the semimagic ^{116}Sn nucleus) and $1p$-$2h$ states across the major shell (relative to ^{114}Cd) coupled to collective phonons (up to three quadrupole and two octupole) in the underlying cores. The two subspaces are mixed by a residual interaction that connects the pairing mode describing the $2h$-core (^{114}Cd) coupled configurations with the surface model. The comparison to experiment was accomplished by first computing all possible $E1/M1/E2$ upward transitions in such a system. Then, for states with a large partial width for transitions to the ground state the full decay cascade was taken into account. In this way, model values for $(\sigma\Gamma)_{0f}$ and $(\sigma\Gamma)_{ff}$ as well as branching ratios were determined (Neumann-Cosel *et al.* 1991). In accordance with the experimental results, intermediate states were found in a limited energy region above $E_j = 2.5$ MeV only. Also, typical $(\sigma\Gamma)_{ff}$

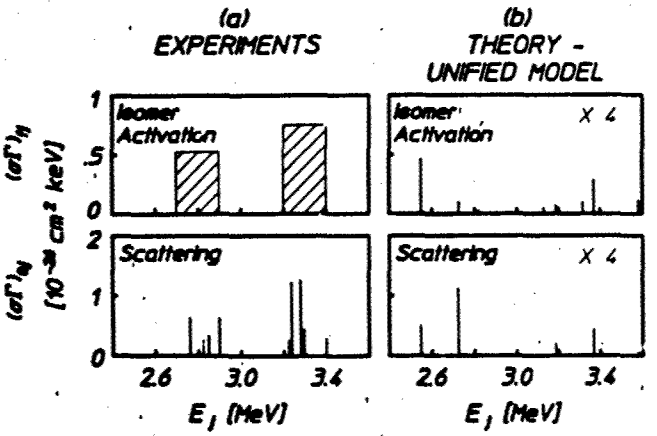

FIGURE 5. Comparison of integrated cross sections for ^{115}In as functions of intermediate state energy, E_j, obtained from (a) experiments and (b) unified model calculations reported in Neumann-Cosel *et al.* (1991). In each case, the upper panel shows values of $(\sigma\Gamma)_{fj}$ from equation (4a) for photoexcitation, $^{115}\text{In}(\gamma,\gamma')^{115}\text{In}^m$, while the lower panel describes $(\sigma\Gamma)_{0j}$ from equation (5) for photon scattering, $^{115}\text{In}(\gamma,\gamma')^{115}\text{In}$.

values at lower energies were suppressed by a factor of about 10–100. The total number of important states was small, in agreement with the experimental NRF results.

Figure 5b presents the model results for comparison with the experiments. The calculations show a rough division into two groups that might be related to the experimental $(\sigma\Gamma)_{fj}$ data. A one-to-one correspondence, however, seemed beyond the limits of the approach. Simply summing the model $(\sigma\Gamma)_{fj}$ strength compared favorably to the experimental numbers. The overall agreement seemed encouraging and indicated that no major part of the relevant configuration space was missed.

A detailed analysis of the main decay branches revealed a clear picture of the important amplitudes in the intermediate state wavefunctions. All theoretical states had $J^\pi = 7/2+$ and the ground-state coupling was dominated in all cases by single-particle $1g_{9/2} \rightarrow 1g_{7/2}$ spin-flip transitions. The first step of the decay of the isomer in the model calculations proceeded mainly via $E1$ or $E2$ transitions.

The critical conclusions of these scattering studies is that nuclear structure theory, scattering measurements, and the photoactivation experiments all agree in the first case tested. The giant pumping transitions in ^{115}In occurred through discrete intermediate states. Absorption cross sections approached those ideals of equation (4b) needed to separate the wasted deposition of heat from the excitation of nuclei in a sample pumped with intense X-rays.

4. Conclusions

The significance to laser feasibility of these favorable developments from scattering studies may be appreciated with the help of analogs from the atomic scale. There is to be found the familiar increase in the density of levels available for excitation as transition energies approach the limit for photoionization. The number of such Rydberg states is in general of the order of n^3, where n is a principal quantum, and this makes it difficult to pump

energy into a selected one of them with a continuum source of modest spectral width. The general difficulty in scaling X-ray lasers is a clear illustration of this problem. It seems that it is only the rigor of coupling schemes for angular momenta that allow the few cases demonstrated to work at all.

At the nuclear level, the situation could have been even worse. Because of the fundamentally different potentials, the likelihood is much greater for what would be considered multiply excited states from the atomic perspective. The level density is more difficult to specify quantitatively, but an approximation of $\exp(\sqrt{n})$ is reasonably indicative as excitation energies approach what is needed to remove the first particle in a photonuclear reaction.

Because the coupling schemes were shown to be weaker in the nuclei by the striking efficiency with which $\Delta K = 8\hbar$ could be lost in ^{180}Ta, there was a clear hazard that highly excited nuclear levels could not be selectively excited. Sum rules limit the strength per unit bandwidth available at a particular transition energy, and there was the possibility that the sum would be smoothly distributed over the great number of levels in any interval of high-excitation energy. Then, the deposition of pump energy into nuclear excitation would have been diluted into a much larger volume by the small cross sections available to any component transition. That did not happen and this constitutes a second breakthrough of importance comparable to the first achieved by dumping the population of ^{180}Ta^{m}.

The giant pumping resonances found in the ^{115}In study show the transition strength is concentrated into relatively few discrete lines. The nuclear structure model identified this particular case as an example of fragmented spin-flip transition strength, but the point critical to laser feasibility is the fragmentation. Relatively few transitions to gateway states collected all of that type of transition strength available over the range of energies from 2–5 MeV. The actual mechanism of the fragmentation was less clear, having arisen from detailed unified model calculations.

Although only resonances for the ^{115}In excitation have been studied to date, the systematics of data such as shown in figure 4 suggests parallels that make it useful to speculate about the possible origin of such a pervasive phenomenon. Recent calculations (Girod *et al.* 1989) have shown the tendency of heavy but nonfissile nuclei to develop multiple potential energy minima in configuration space as shown schematically in figure 6. Second minima of this type would contain fission isomers for even higher mass numbers, but

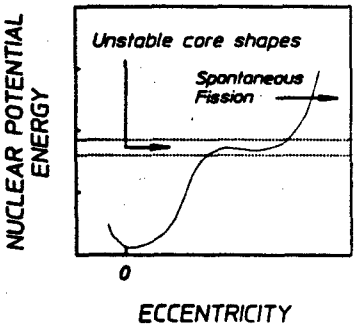

FIGURE 6. Schematic representation of a dependence of potential energy upon nuclear eccentricity that would tend to produce a second local minimum. Shape isomers have been predicted to lie in such auxiliary minima. For large mass numbers, spontaneous fission can occur when populations tunnel out of the secondary well.

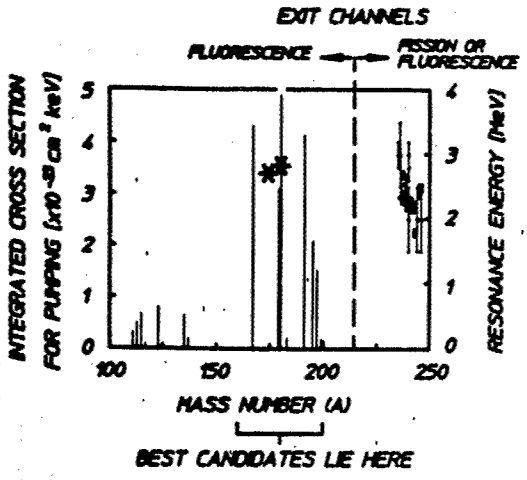

FIGURE 7. Integrated cross sections from figure 4 shown together with the excitation energies, E_j, of the giant pumping resonances for nuclides of the mass numbers plotted as abscissae. Asterisks locate the energies for dumping $^{108}Ta^m$ and $^{174}Hf^m$ for comparison with the energies of fission isomers from Evaluated Nuclear Structure Data File (1986), given with their error bars. These energies are plotted using the rightmost ordinate.

for cases of interest here the Coulomb barrier would be too great to allow a decay from an auxiliary minimum to fission. Although purely speculative at this time; it is interesting to note that contributions from several minima might tend to bunch level densities while at the same time break selection rules on K by failing to provide a fixed core shape onto which K-projections of angular momentum might be conserved. Coincidentally, the excitation energies of auxiliary minima is of the order of a few MeV in even–even nuclei, which might serve as cores upon which would be built the single-particle states of interest.

Some first support for such speculations has been found in the unexpected enhancements measured recently for the deexcitation of the $^{174}Hf^m$ isomer (Walker *et al.* 1990). There, also, the decay of the isomer was found to occur primarily by transition through an intermediate state lying at 2,685 keV in which K mixing occurred so that $\Delta K = 14$ was lost between isomer and the ground-state band. This is remarkably close to the energy of the K-mixing level at 2,800 ± 100 keV for ^{180}Ta shown in figure 7. The close similarity of the energetics seen for nuclei with such dissimilar single-particle structures does seem to support the identification of this K-mixing process with some type of core property varying only slowly among neighboring nuclei. Of great curiosity is the extent to which the excitation energies of these two K-mixing states found to date agree with energies of the known fission isomers shown in figure 7. Such correlation would be expected if these phenomena had a common origin in shape isomerism.

It seems reasonable to conclude that the first breakthrough in determining the feasibility of a γ-ray laser has been followed by a second. The proof that isomeric populations can be dumped by pumping them with intense pulses of X-rays has been followed by this demonstration that the transition strengths for doing so are fragmented into relatively few discrete transitions of great intensity. These are precisely the necessary conditions for the concentration of useful pump power into the selective excitation of nuclear populations while dissipating power degraded to heat in much larger volumes.

Acknowledgment

The authors gratefully acknowledge the support of this work by SDIO/TNI through NRL.

REFERENCES

ANDERSON, J.A. *et al.* 1988a *Phys. Rev. C* **38**, 2833.

ANDERSON, J.A. & COLLINS, C.B. 1987 *Rev. Sci. Instrum.* **58**, 2157.

ANDERSON, J.A. & COLLINS, C.B. 1988b *Rev. Sci. Instrum.* **59**, 414.

BOOTH, E.C. & BROWNSON, J. 1967 *Nucl. Phys.* A **98**, 529.

CARROLL, J.J. *et al.* 1989 *Astrophys. J.* **344**, 454.

CARROLL, J.J. *et al.* 1991a *Phys. Rev. C* **43**, 1238.

CARROLL, J.J. *et al.* 1991b *Phys. Rev. C* **43**, 879.

COLLINS, C.B. 1991 *Handbook of Laser Science and Technology* (CRC Press, Boca Raton, FL), pp. 561–567.

COLLINS, C.B. *et al.* 1982 *J. Appl. Phys.* **53**, 4645.

COLLINS, C.B. *et al.* 1988b *Phys. Rev. C* **37**, 2267.

COLLINS, B.B. *et al.* 1990 *Phys. Rev. C* **42**, R1813.

COLLINS, C.B. *et al.* 1992 *Laser Interaction and Related Plasma Phenomena*, G.H. Miley and H. Hora, eds. (Plenum, New York) Vol. 10, pp. 151–166.

Evaluated Nuclear Structure Data File. 1986 Information Analysis Center Report BNL-NC5-51655 (Brookhaven National Laboratory, Upton, NY).

GIROD, M. *et al.* 1989 *Phys. Rev. Lett.* **62**, 2452.

NELSON, W.R. *et al.* 1985 *The EGS4 Code System*, Stanford Linear Accelerator Center Report No. SLAC 265 (Stanford Linear Accelerator Center, Stanford, CA).

NEUMANN-COSEL, P. VON *et al.* 1981 *Phys. Lett. B* **226**, 9.

WALKER, P.M. *et al.* 1990 *Phys. Rev. Lett.* **65**, 416.

ZIEGLER, W. *et al.* 1990 *Phys. Rev. Lett.* **65**, 2515.

Absolute measurement of spatial and spectral characteristics of bremsstrahlung using the photoexcitation of nuclear isomers

J. J. Carroll, D. G. Richmond, T. W. Sinor, K. N. Taylor, C. Hong, J. D. Standifird, and C. B. Collins
Center for Quantum Electronics, The University of Texas at Dallas, P.O. Box 830688, Richardson, Texas 75083-0688

N. Huxel, P. von Neumann-Cosel, and A. Richter
Institut fur Kernphysik, Technische Hochschule Darmstadt, Schlossgartenstrasse 9, DW 64289 Darmstadt Germany

(Received 25 March 1993; accepted for publication 27 April 1993)

A method of obtaining absolute, direct measurements of the spatial and spectral characteristics of bremsstrahlung is discussed. This technique, called x-ray activation of nuclei (XAN) is based on the use of well-known photonuclear reactions which populate long-lived nuclear isomers. These populations sample incident photon continua at discrete excitation energies and effectively store this information for convenient retrieval following the irradiation of gram-sized targets. Recently a series of experiments has been conducted which has significantly expanded the available data for the photoexcitation of a wide range of isomers at higher energies. Thus it has become feasible to extend the use of XAN to energies approaching 4 MeV. The utility of this technique is demonstrated by the characterization of bremsstrahlung from the newly installed research linac at the University of Texas at Dallas.

I. INTRODUCTION

Linear electron accelerators (linacs) and pulsed power e-beam devices have become indispensable as sources of bremsstrahlung for a wide variety of applications. Linacs are now common in medical radiology,[1] nuclear physics[2] and industry[3] for the irradiation of a broad range of materials. The uses of e-beam devices are less familiar but no less important and large machines are employed extensively as nuclear simulators[4] to test the effects of radiation on electronics and other hardware. They have also been used for nuclear physics research.[5,6] These diverse applications and their procedures have been established over a period of years yet there remains a common impediment to the use of such intense photon sources. This is the difficulty in accurately and directly measuring the spectral properties of the bremsstrahlung needed to calibrate the output of the accelerator or pulsed-power machine.

Many techniques have been developed for the characterization of bremsstrahlung, the most prevalent of which is based upon traditional measurements of the dose of absorbed radiation. This quantity is routinely and accurately measured[1] with ionization chambers or thermoluminescent dosimeters (TLDs) for either flash or continuous exposures. Since the dose can be a useful indicator of the overall photon flux it is the basis of calibration procedures employed in most medical and industrial applications and in monitoring the radiation produced by nuclear simulators.[7] However, dose is a convolution of the photon spectrum with appropriate absorption coefficients which depend continuously upon wavelength[1] so it is not possible to explicitly determine the energy distribution of the bremsstrahlung. Instead the usual practice[8] is to use dose measurements to normalize spectra computed with sophisticated Monte Carlo codes[9-11] such as EGS4, GEANT, or TIGER. The utility of these programs has been extensively examined and the accuracy of their results has been demonstrated experimentally even when modeling relatively complex geometries.[12,13] Still this procedure may be suspect when used for e-beam devices[7] since the simulations rely heavily upon time-resolved values of voltage and current which are needed as input parameters, but which are very difficult or even impossible to measure.

An improvement on traditional dose methods has been devised[14] in which a set of TLDs is irradiated, the TLDs being enclosed within small spheres of assorted materials like aluminum and depleted uranium. The dosimeters register various measurements attenuated by the shielding provided by the "differential absorbers" and these values are deconvolved to give the spectrum of the incident radiation. This method has been effectively[14] used to characterize bremsstrahlung flashes from e-beam devices but it cannot provide information for photon energies above about 1 MeV, for which there is little variation in the transparency of the absorber materials. The form of the spectra obtained is also quite sensitive to the initial shape assumed in the calculation.

Other techniques are available which provide spectral characterizations of MeV bremsstrahlung but even the simplest of these is seriously limited in its usefulness. The most straightforward approach[15] is to allow a well-shielded detector placed at a large distance from the photon source to observe a very small fraction of the total flux through a pinhole collimator. With this arrangement the energy distribution can be directly measured as a pulse-height spectrum of the photons that are individually detected. However, in addition to the requirement of a large working environment, long exposures are needed for the accumulation of reasonable statistics that cannot be achieved with most low duty cycle e-beam devices.

 0034-5748/93/64(8)/2298/8/$6.00

A more complex method[16] is that of nuclear resonance fluorescence (NRF) which provides an excellent means of calibrating bremsstrahlung spectra by using (γ,γ') reactions to resonantly scatter large numbers of photons from gram-sized targets. The incident spectral distribution is obtained at discrete excitation energies from known reaction cross sections. Yet NRF procedures are limited by the large amount of shielding needed for detectors that observe the scattered photons in real time and by the necessity for long continuous exposures. Compton spectrometers are also quite useful but require simple irradiation geometries[17] and are often large and expensive.[18] Finally there are photoactivation methods that rely on the detection of fluorescence from (γ,n) reaction products. Samples are irradiated with either continuous bremsstrahlung or flashes of x rays and are transported to a quieter environment for counting. However, only two isotopes permit this type of reaction at incident photon energies[19] below 4 MeV so this method has no utility for calibrating many bremsstrahlung sources. Despite the variety of characterization techniques available there is a clear and present need for a new approach which is equally applicable for the calibration of linacs and e-beam devices. It should also be sensitive to photon energies up to several MeV and be simple and portable in its implementation.

The x-ray activation of nuclei (XAN) procedure is ideally suited to meet this need while avoiding the problems inherent in other methods. The fundamental concept[20] was first suggested in the 1940's but has only been applied in the quantitative fashion of XAN since 1987, primarily for the characterization of flashes of x rays from large pulsed-power machines.[21–25] This basic idea is similar to that of NRF in that nuclear transitions are used to measure the spectral intensity of bremsstrahlung at discrete excitation energies. However, in NRF scattered gamma rays are detected in real time at intensities that are only slightly above a dominant Compton background. In XAN the focus is on the detection of fluorescence from long-lived nuclear states called isomers which are produced by (γ,γ') reactions so it is not necessary to count samples *in situ*. Instead targets containing isomeric nuclei in their ground state are irradiated and then transported either pneumatically or by hand to a simple gamma-spectrometer system. With useful halflives ranging from seconds to hours, populations of nuclear isomers sample bremsstrahlung spectra and effectively store the information for convenient retrieval. The equipment and samples needed to implement XAN are relatively inexpensive, portable, and reusable and the target package occupies very little space in the irradiation environment.

In the past XAN has been primarily applied[22–25] to the characterization of bremsstrahlung with photon energies no higher than about 1.5 MeV due to the paucity of information on (γ,γ') reactions which populate isomers. Recently the nuclear database has been expanded by a series of investigations[26–31] of the photoexcitation of a wide range of isomers. Thus it has been feasible to extend the applicability of XAN up to energies approaching 4 MeV, making it possible to calibrate a wider range of photon sources.

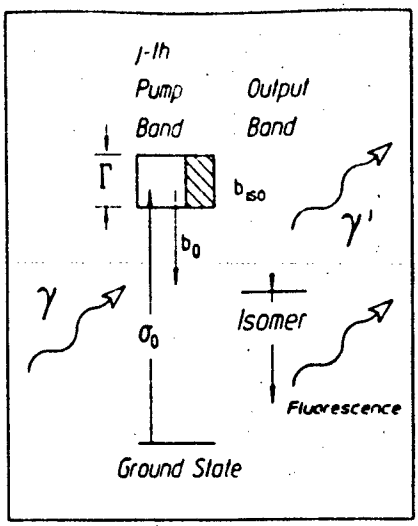

FIG. 1. Schematic representation of the population of a nuclear isomer by a (γ,γ') reaction. The incident photon γ is absorbed with a cross section σ_0 by the j^{th} gateway shown having a natural width Γ. The probabilities that the intermediate state decays directly back to the ground state and either directly or by cascade to the isomer are b_0 and b_{iso}, respectively. Photons promptly emitted during the population of the isomer are the γ'.

The utility of this approach is demonstrated by the measurement of spatial and spectral distributions for bremsstrahlung produced by the recently installed Texas-X research linac at the University of Texas at Dallas.

II. THEORETICAL BACKGROUND

The irradiation of a sample containing N_T target nuclei in some initial state by bremsstrahlung results in a population of N_f nuclei in a given final state according to

$$N_f = N_T \int_0^{E_0} \sigma(E) \frac{d\Phi(E)}{dE} dE, \qquad (1)$$

where the photon continuum is described by an endpoint E_0 that equals the electron energy and a time-integrated spectral intensity, $d\Phi(E)/dE$ that gives the photon fluence per unit energy bandwidth. The excitation reaction is described by the energy-dependent cross section $\sigma(E)$.

The XAN technique is based on the photoexcitation of nuclear isomers which are metastable due to the large multipolarities required for their electromagnetic decay to levels at lower energies.[32] This also inhibits the inverse process so isomers are not significantly excited by direct absorption transitions from the ground state. Instead at energies below the photoneutron threshold, isomers are produced by the two-step process illustrated in Fig. 1 in which an incident photon designated by γ is resonantly absorbed by a higher-lying level. The metastable level is then populated by a branch of the decay cascade from the intermediate, or "gateway" state with promptly emitted photons being the γ'. This process is equivalent to bandwidth funneling which is so familiar in laser physics. The

standard notation for this reaction is $X(\gamma,\gamma')X^m$, in which X and X^m represent the participating nucleus in its ground and isomeric states, respectively.

It has been demonstrated experimentally[28,30] that gateways are well separated and have widths that are large on a nuclear scale but small compared to the structure of broad bremsstrahlung continua. Since the spectral intensity is a constant over each gateway, Eq. (1) reduces to

$$A=\frac{N_I}{N_T}=\sum_j (\sigma\Gamma)_j \frac{d\Phi(E_j)}{dE}, \tag{2}$$

where the fractional activation, A has been introduced and

$$(\sigma\Gamma)_j=(\pi b_{iso} b_0 \sigma_0 \Gamma/2)_j, \tag{3}$$

is the integrated cross section for production of the isomer through the j^{th} gateway having an excitation energy E_j. For each intermediate state the integration is performed over a Lorentzian line shape having the natural width of the level, $\Gamma=(\hbar \ln 2)/T_{1/2}$ with $T_{1/2}$ being its halflife. The summation in Eq. (2) includes all gateways whose excitation energies are less than the bremsstrahlung endpoint. In the process depicted in Fig. 1 the probabilities that a gateway will decay directly back to the ground state and either directly or by cascade to the isomer are b_0 and b_{iso}, respectively. The quantity σ_0 is one half of the peak cross section for the absorption resonance and is given by the Breit–Wigner formula[33]

$$\sigma_0=\frac{\lambda^2}{2\pi}\frac{2I_j+1}{2I_0+1}\frac{1}{\alpha+1}, \tag{4}$$

in which λ is the wavelength of the incident photon, I_j and I_0 are the angular momenta of the gateway and ground states, respectively, and α is the internal conversion coefficient for the absorption transition.

In the most ideal implementation of XAN several isomeric nuclides would be chosen, each of which possessed only one gateway which satisfied the condition $E_j<E_0$. The summation of Eq. (2) would then reduce to a single term. If integrated cross sections were available in the literature for these gateways either as direct evaluations or from the quantities in Eqs. (3) and (4), it would be a simple matter to obtain the incident spectral intensity at each of the E_j from measured activations. Unfortunately the nuclear data only support the identification of one isotope, ^{137}Ba which fulfills this criterion for $E_0<4$ MeV within experimental limits. Other isomeric nuclei whose lifetimes and fluorescence energies are convenient for measurements and whose gateway structures are well known all possess multiple intermediate states. Thus it is necessary to employ a more complex procedure to determine the spectral distribution of bremsstrahlung. In this demonstration of the XAN method, the calibration isotopes ^{79}Br, ^{87}Sr, ^{115}In, and ^{137}Ba were chosen since gram-sized samples were readily available. The gateway parameters and additional relevant quantities for their isomers are listed in Table I. Other isomeric nuclides such as ^{77}Se, ^{179}Hf, ^{191}Ir, ^{197}Au, and ^{89}Y are also sufficiently well characterized[29–31] to support their use for XAN, and in some cases may provide additional spectral resolution.

TABLE I. Relevant quantities for the isomeric nuclides employed in this work. Gateway energies, E_j, and integrated cross sections, $(\sigma\Gamma)_j$, were obtained from the literature as either direct evaluations (Refs. 26, 28, 31, 41) or calculated from the parameters (Ref. 40) of Eqs. (3) and (4). Uncertainties in the E_j were on the order of 3% while those for the $(\sigma\Gamma)_j$ were on the order of 15%. The fluorescence energies, E_{fluor}, are the primary signatures (Ref. 35) of the decay of the isomers.

Isomer	$T_{1/2}$	E_{fluor} (keV)	E_j (MeV)	$(\sigma\Gamma)_j$ (10^{-26} cm^2 keV)
^{79}Br^m	4.9 s	207	0.761	5.9
			1.8	65
^{87}Sr^m	2.8 h	388	1.2	8.5
			1.9	16
			2.7	430
^{115}In^m	4.5 h	336	1.1	18.7
			1.4	64
			1.6	101
			2.8	540
			3.3	760
^{137}Ba^m	2.6 min	662	3.2	220

III. EXPERIMENTAL DETAILS AND RESULTS

A. General

Irradiations were performed with bremsstrahlung from the Texas-X research linac recently installed at the University of Texas at Da.... The Texas-X was designed to produce nominal 4-MeV electrons in pulses of 2.78-μs duration with a repetition rate of 360 Hz. This gave a duty cycle of 1/1000 and a time-integrated current of 150 μA for the exposures used in this work. The accelerator was emplaced in an underground facility with internal dimensions of 2.6 m height, 7.3 m length, and 2.9 m width. Only the magnetron/waveguide assembly resided in the chamber and this was oriented such that the electron beam propagated horizontally along the long dimension of the room at a height of 1.4 m from the floor. The electrons exited the modified Varian waveguide through a 2 mil (51 μm) window composed of a 49:1 alloy of Cu and Be. Bremsstrahlung was produced by electrons that impinged normally on a 2.5 cm×2.5 cm, 3-mm-thick tantalum converter held within a large water-cooled copper jacket. The converter was located 2.7 cm from the exit window. For energies near 4.0 MeV the range[34] of electrons in naturally dense tantalum is about 3 g cm^{-2} or 0.17 cm. Thus x rays produced from the converter constituted thick-target bremsstrahlung.

B. Electron beam properties

Measurements were made of the properties of the electron beam prior to irradiating nuclear targets. Stopping range experiments were performed using aluminum, copper, and graphite sheets of different thicknesses as attenuators. Electrons passing through these filters were collected by an aluminum block and the excess charge was recorded from the voltage across a 50-Ω load using an oscilloscope and trace digitizing software. Typical data obtained using aluminum attenuators are shown in Fig. 2(a) and plot the charge delivered to the collector during each pulse as a

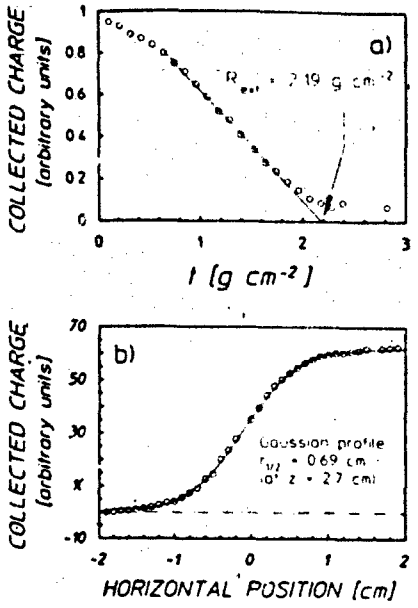

FIG. 2. (a) Electron stopping measurements obtained using aluminum attenuators. The symbols plot the relative charge delivered to the aluminum collector during each linac pulse as a function of attenuator mass thickness. The extrapolated range was found to be $R_{ext}=2.19$ g cm^{-2} and tables in the literature indicated (Ref. 34) that this corresponded to an electron energy of 3.55 MeV. (b) Horizontal profile of the electron beam determined at a distance of 2.7 cm from the CuBe exit window. The symbols plot the charge collected by a large aluminum plate as it was moved across the beam. Values ranged from zero when no part of the beam was intercepted to a maximum when all electrons were stopped. The best fit to the data was a Gaussian having a half radius $r_{1/2}=0.69$ cm. This defined the spot size of the electron beam at a distance corresponding to the entrance to the converter foil.

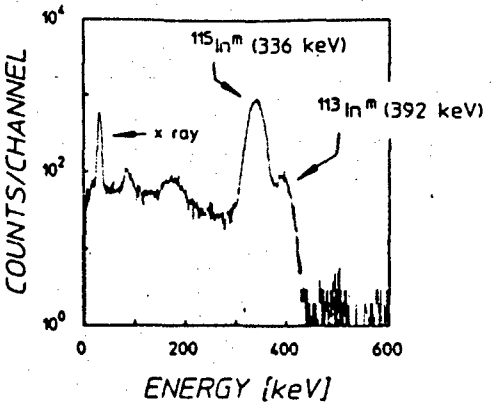

FIG. 3. Typical pulse-height spectrum obtained from an ^{115}In sample using a standard NaI(Tl) spectrometer. The sample had been irradiated for 15 min and was counted for 5 min. The peak at 336 keV was the fluorescence signature (Ref. 35) of the decay of $^{115}In^m$ while that at 392 keV resulted from the decay of another indium isomer, $^{113}In^m$.

function of filter mass thickness. An extrapolated range of 2.19 g cm^{-2} was obtained from these data and tables in the literature[34] indicated that this corresponded to an electron energy of 3.55 MeV. The average of values determined from stopping experiments conducted with different materials gave $E_0=3.6\pm0.1$ MeV.

The spatial profile of the electron was measured by using a 10 cm×10 cm, 2-cm-thick aluminum plate to scan across the beam. This plate was oriented so that its large area faced the exit window at a distance of 2.7 cm. Figure 2(b) plots the collected charge as a function of its relative horizontal position and this varied from zero when no part of the beam was intercepted to a maximum when all electrons were stopped. The best fit to these and similar data obtained by vertical scans at this distance was a Gaussian having a radial half width of 0.69 cm. This defined the electron spot size at the entrance plane to the converter and the half angle for the electron divergence, $\theta_e=13.5°$. The beam axis was determined from scans conducted at various distances from the exit window and a small HeNe laser affixed to a stable platform was used to identify the axis for further experiments.

C. Bremsstrahlung spatial distribution

Although the strength of XAN lies in its ability to provide spectral characterizations of bremsstrahlung, spatial distributions can also be obtained. In this work the axial dependence of x rays from the Texas-X was investigated by using metallic indium disks 1.0 cm in diameter and 0.127 mm thick as well as plastic planchettes 5.0 cm in diameter and 0.8 cm thick containing BaF_2 in powder form. In each case the calibration isotopes of ^{115}In and ^{137}Ba were present in their natural abundances. The samples were oriented to face the beam and were placed at various distances along the beam axis. Following their irradiation the targets were transported by hand to a standard NaI(Tl) spectrometer system to obtain pulse-height spectra. A typical example is shown in Fig. 3 for an indium sample exposed for 15 min and counted for 5 min. The fluorescence signature[35] of the decay of $^{115}In^m$ was the large photopeak at 336 keV while the smaller peak to its right resulted from the decay of a less well-characterized isomer, $^{113}In^m$. Fractional activations were determined from the measured numbers of counts in the full-energy peaks using standard corrections for the finite lifetimes of the isomers, the detection and emission efficiencies, and the transparencies of the samples to the fluorescence gamma rays. This last correction factor was computed by a simple Monte Carlo code that was tested to insure that samples of identical mass but in different configurations would give the same activation.

Fractional activations normalized to irradiation time for the indium and barium samples are shown in Fig. 4. The data are plotted as functions of R^{-2}, where $R=z-z_0$, z is the axial distance from the converter and z_0 is an offset included to account for the extended nature of the photon source. The expected behavior was observed in the measurements and in the results of EGS4 simulations of the photon flux passing through the sample areas. The offset was found to be $z_0=-(2.5\pm0.5)$ cm which coincided with the location of the CuBe exit window.

The radial dependence of the bremsstrahlung was determined by irradiating a set of thin (0.127 mm) indium samples at several axial distances. These foils were fash-

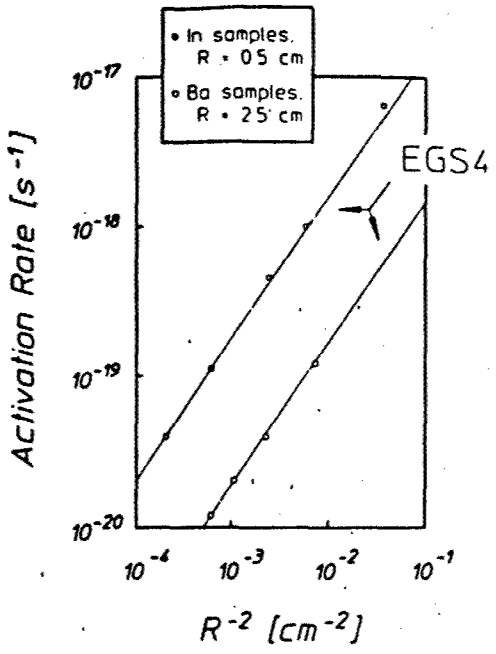

FIG. 4. Axial dependence of the bremsstrahlung determined from measured fractional activations A normalized to irradiation time for the calibration isotopes ^{115}In and ^{137}Ba. The symbols are plotted as functions of R^{-2} where $R=z-z_0$ and $z_0=-(2.5\pm0.5)$ cm. This offset corresponded to the spacing between converter and exit window. The expected behavior was observed in the measurements and in the curves which resulted from EGS4 simulations.

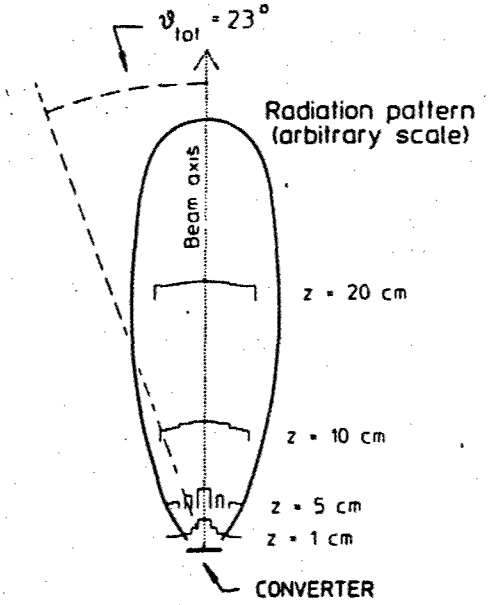

FIG. 5. Radial dependence of the bremsstrahlung determined from fractional activations A normalized to irradiation time of indium annular samples exposed at various distances along the beam axis. Radial profiles are plotted at each distance and demonstrate the spread of the radiation lobe. Data for some of the annuli at $z=5$ cm could not be obtained due to instrumentation problems. The shape of the lobe was obtained by connecting values of a given relative intensity in the radial profiles and evidenced the expected qualitative behavior. The half angle for the bremsstrahlung was found to be $\theta_{tot}=23°$.

ioned in the form of concentric annuli in radial increments of 0.5 cm and a circular central target 1.0 cm in diameter. A total diameter of 8.0 cm was covered by the set of eight samples. The total photon flux striking each annulus was taken to be well represented by the fractional activation of each sample due to the division by N_T in Eqs. (1) and (2). This was justified because the number of target nuclei was directly proportional to the mass and therefore to the area of each sample. It was assumed that there was no significant variation in spectral content across the annuli. Radial distributions mapped in this way are shown in Fig. 5 and indicate the beam profiles at each axial position at which samples were irradiated. Profiles at $z>5$ cm were described by Gaussians whose halfwidths were proportional to R^{-2}. To display the information in a more familiar form the radiation lobe was obtained by connecting values of a given relative intensity in the radial profiles. The shape of this lobe evidenced the expected qualitative behavior for thick target bremsstrahlung[36] and a half angle for the photon intensity was found to be $\theta_{tot}=23°$. This was in excellent agreement with the sum of θ_e and the mean angle for the emission of thick-target bremsstrahlung from collinear relativistic electrons[36]

$$\theta_m=\gamma^{-1}=(29°)/E_0. \tag{5}$$

Here γ is the relativistic gamma factor and the electron energy is expressed in MeV. For 3.6-MeV electrons, $\theta_m=8.06°$ giving $\theta_{tot}=21.6°$.

Spatial distributions were also obtained from dose measurements made with an ionization chamber whose calibration was traceable to NIST and are shown in Fig. 6. Again the expected axial dependence was observed and the angular dose profile determined at a distance of 60 cm from the converter was in good agreement with that given by fractional activations and by a Gaussian function with a half angle of 22°.

D. Bremsstrahlung spectral distribution

The spectral distribution was examined by irradiating the full set of the calibration nuclides listed in Table I. Planchettes containing the compounds BaF_2 and SrF_2 in powder form and an indium disk were exposed for times on the order of 15 min and transported by hand from the linac chamber to the spectrometer system. In the case of the bromine isotope the short lifetime (4.9 s) necessitated the pneumatic transfer of a cylindrical sample 5.0 cm in length and 1.0 cm in diameter containing LiBr through a plastic tube to a NaI(Tl) well scintillator. The "rabbit" was irradiated axially for 20 s. Additional electronics were used to initiate its transport by turning on a standard shop vacuum and to signal its arrival in the detector well, thereby beginning the acquisition of a pulse-height spectrum. As outlined before, fractional activations normalized to the exposure times were determined from the fluorescence observed. These values are listed in Table II and were normalized to an axial position of $z=30$ cm.

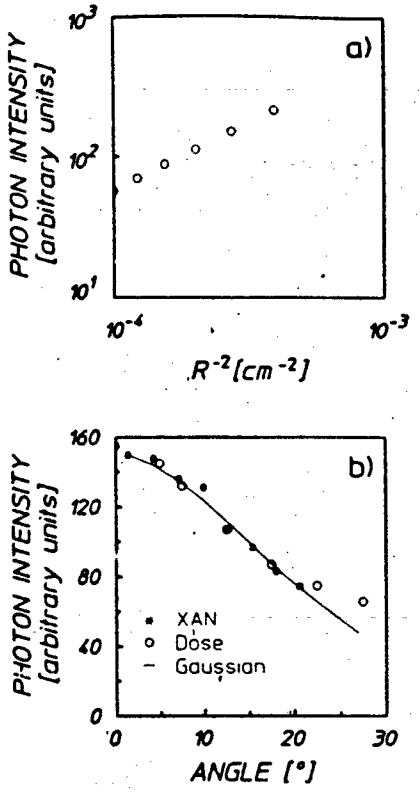

FIG. 6. Photon intensities determined from dose measurements made with a calibrated ionization chamber showing (a) axial dependence and (b) angular dependence of the bremsstrahlung. In both cases the data evidenced the expected behavior observed in the results of isomeric activations. In (b) both dose and photoactivation measurements are included as well as a curve given by a Gaussian distribution with half angle of 22°.

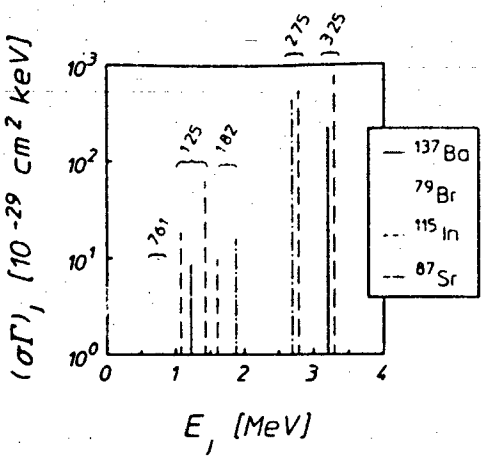

FIG. 7. Integrated cross sections and excitation energies for the gateways listed in Table I for the population of the four calibration isomers. The simplified mesh used to determine the spectral distribution of the bremsstrahlung was obtained by grouping the gateways into the bands shown. The energy representing each band was the average of the E_j for the enclosed states weighted by their integrated cross sections.

The application of Eq. (2) to the ^{137}Ba datum yielded a spectral intensity of $(8.96 \pm 0.62) \times 10^6$ cm^{-2} s^{-1} keV^{-1} at $E_j = 3.2$ MeV. Prior to proceeding with the complete analysis it was instructive to see to what degree the endpoint could be determined by a simple approach. Assuming that only the large gateway at 2.7 MeV produced the measured activation for ^{87}Sr^m, the spectral intensity at that energy was found to be 2.1×10^7 cm^{-2} s^{-1} keV^{-1}. An uncertainty was not assigned to this value due to the nature of the approximation. It was expected that the energy dependence near the endpoint of the spectrum could be described as a linear function since photons in this region were for the most part due to single interactions within the converter. This is the basis of the traditional Kuhlenkampff approach[37] and has been proven to be applicable even for thick-target bremsstrahlung.[38] Following this idea, a linear fit was made to the spectral intensities obtained above and gave an endpoint energy of 3.58 MeV, in remarkable agreement with the results of electron stopping measurements.

TABLE II. Fractional activations normalized to exposure time obtained from samples containing the four calibrations isomers used in this work. These values were employed for the determination of the spectral intensity of the irradiating bremsstrahlung and have been normalized to $z = 30$ cm.

Isomer	Normalized fractional activation (10^{-19} s^{-1})
^{79}Br^m	1.46 ±0.03
^{87}Sr^m	0.889 ±0.03
^{115}In^m	1.77 ±0.01
^{137}Ba^m	0.197 ±0.013

The determination of bremsstrahlung spectral intensity in XAN is equivalent to solving a system of equations. Unfortunately in this application the nuclides of Table I possessed a total of 11 gateways giving an equal number of unknowns (at each of the E_j) while there were only four equations available from the measured activations. Although this could not be solved exactly, an iterative procedure was used to obtain the spectrum. The basic strategy was to employ a simplified gateway mesh to arrive at successive approximations, working from the known value fixed by the ^{137}Ba activation towards lower energies. Convergence was tested at each step by using a fitted energy distribution to calculate expected values for the fractional activations of the calibration isomers and comparing these with the measurements. The only assumption made regarding the spectral shape was that the natural logarithm of the energy distribution was smoothly and slowly varying and could be represented well by a low-order polynomial above about 0.5 MeV where self absorption in the Ta target would not be significant.

The simplified gateway mesh was defined by the five bands shown in Fig. 7. The choice of the groupings was obvious for those intermediate states lying near 3.25, 2.75, and 0.76 MeV but the remaining gateways were more evenly spaced and were simply divided into two bands at 1.25 and 1.82 MeV. These energies were averages of the E_j for the included states, weighted by the relative sizes of their integrated cross sections which were summed to give the $(\sigma\Gamma)$ for each group. Using these bands an approxi-

mate system of three equations in three unknowns was obtained by neglecting the lower band at 0.76 MeV. The known spectral intensity at 3.2 MeV was also used to remove contributions to the activations due to that band. Expressed in matrix form this was (suppressing units for convenience)

$$\overline{(\sigma\Gamma)}\cdot\varphi = \mathbf{A}, \tag{6a}$$

where

$$\overline{(\sigma\Gamma)} = \begin{pmatrix} 8.5 & 16 & 430 \\ 0 & 65 & 0 \\ 92.8 & 0 & 540 \end{pmatrix}, \tag{6b}$$

$$\varphi = \begin{pmatrix} d\Phi(1.25)/dE \\ d\Phi(1.82)/dE \\ d\Phi(2.75)/dE \end{pmatrix}, \tag{6c}$$

and

$$\mathbf{A} = \begin{pmatrix} 0.889 \\ 0.639 \\ 1.09 \end{pmatrix} \times 10^{10}, \tag{6d}$$

and having the solution

$$\varphi = \begin{pmatrix} 2.30 \\ 10.8 \\ 1.62 \end{pmatrix} \times 10^{7}. \tag{7}$$

In this first approximation the result obtained at 1.25 MeV was unphysical since no significant self absorption should occur at that energy and this indicated that the spectral intensity was seriously overestimated between 1.82 and 2.75 MeV. Therefore an upper bound on the energy distribution was found by fitting the natural logarithm of intensity to a quadratic function of E expressed in MeV using the values of Eq. (7) above 1.25 MeV and the known value at 3.2 MeV,

$$\varphi_1(E) = (8.41\times10^{10})\exp(-4.74E+0.592E^2). \tag{8}$$

The form of Eq. (8) is shown in Fig. 8 as the curve labeled "Step 1."

Fractional activations were calculated with this function and the full set of gateways listed in Table I. These were found to be larger than the measured values by factors of 2.45, 1.61, and 3.22 for ^{79}Br, ^{87}Sr, and ^{115}In, respectively. The next approximation was to lower the upper bound accordingly. To diminish the magnitude of the fit more at lower energies than near the fixed value at 3.2 MeV, $\varphi_1(1.82) = 1.08\times10^8$ was reduced by the average overestimation of the activations, 2.43. A new fit was obtained using spectral intensities of 4.43×10^7, 1.62×10^7, and 8.96×10^6 at 1.82, 2.75, and 3.25 MeV. This gave

$$\varphi_2(E) = (2.17\times10^8)\exp(-0.737E-0.0753E^2). \tag{9}$$

Fractional activations computed using Eq. (9) differed from the measurements by 0.838, 1.01 and 1.21 for ^{79}Br, ^{87}Sr, and ^{115}In, respectively, with an average factor of 1.02. Since this was well within the fractional uncertainty introduced by the integrated cross sections of Table I, the fitting procedure was terminated. Therefore the second-order fit

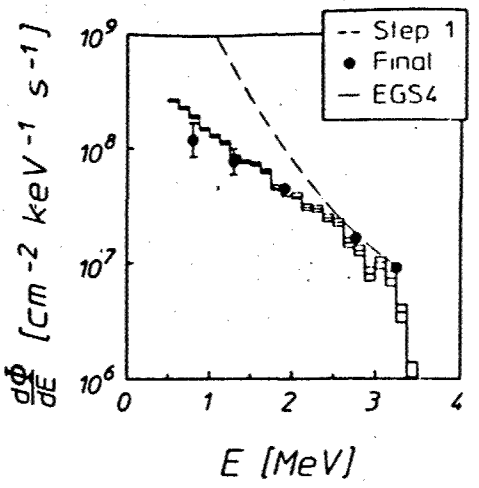

FIG. 8. Spectral intensity of the bremsstrahlung determined from fractional activations of the calibration isomers. The dashed curve plots the result of the first iteration of the analytical procedure and represented an overestimation of the flux which worsened at energies away from the fixed value at 3.25 MeV. The symbols plot the result of the second and final iteration at the five band energies of Fig. 7. Error bars estimate the uncertainty introduced by the procedure since the size of the symbols is comparable to the statistical error. For comparison a spectrum calculated using EGS4 for the experimental geometry and materials and $E_0 = 3.6$ MeV is shown as the histogram and includes statistical errors. Good agreement was in evidence between the results of XAN, EGS4, and measurements of the dose delivered by the photon continuum of the figure.

of Eq. (9) provided the final spectral measurements shown in Fig. 8 along with a spectrum computed with EGS4 for the experimental geometry and materials and for an endpoint of 3.6 MeV. Despite the good agreement seen in the figure, the weakness of the approach was that it required an extrapolation outside the better determined region of 1.25–3.25 MeV in order to obtain spectral intensities at lower energies. Generally such an extrapolation is suspect but in this case was justified by the assumption of slow variation for the natural logarithm of the energy distribution.

As confirmation of the spectrum of Fig. 8, a calculation was made of the dose that corresponded to the EGS4 result. Normalized to a distance of $z = 1$ m this was found to be 269 rad min^{-1}, agreeing within 4% of the measured value of 280 rad min^{-1}.

The fractional activations measured for the calibration isotopes could have contained contributions from any neutron flux present within the linac chamber during the irradiations. To test for the presence of thermal neutrons, each indium spectrum like that shown in Fig. 3 was inspected for evidence of fluorescence from the isomer ^{116}In^{m2}, having a halflife[35] of 54.15 min. This isotope does not occur naturally and therefore if present its isomer could only have resulted from neutron capture by the stable ^{115}In. No photopeaks were observed in the spectra which would have indicated the presence of ^{116}In^{m2} and an upper bound on the ambient thermal neutron flux was found to be $\Phi_n < 5$ cm^{-2} s^{-1} from the known cross section.[39] In instances where a stable parent was available for neutron capture (^{86}Sr and ^{136}Ba), this flux was sufficient to have produced

less than 0.001% of the measured activations. Fast neutrons were not expected to be present in significant numbers due to the limited photon energies.

It is important to note that the photoexcitation of nuclear isomers can provide a valuable tool for the characterization of bremsstrahlung even if XAN is not fully implemented with a set of calibration isotopes. As discussed in Ref. 13 the activation measured for the population of a single isomer such as $^{115}In^{m}$ can serve to quite effectively test and normalize computed spectra. That procedure can provide a considerable improvement over traditional dose-normalization techniques since bremsstrahlung is sampled as a discrete rather than a continuous convolution of the spectral shape. However, a spectrum computed with a Monte Carlo code is still required as a starting point in those alternative approaches.

IV. DISCUSSION

The XAN technique provides an ideal method for obtaining absolute measurements of the spectral and spatial distributions of bremsstrahlung while requiring relatively simple and proven equipment and samples that avoid problems inherent in other methods. The target package used is also small, portable, and reusable. Although its utility was demonstrated by the characterization of x rays from a linear accelerator, XAN is equally well suited to the calibration of e-beam devices. However, the present accuracy of the technique is limited to about 15% due to the available nuclear data and the nature of the approach employed to analyze the measured activations. Still it was not necessary to introduce any *a priori* assumptions regarding the spectral shape other than that the natural logarithm of the intensity was slowly varying above about 0.5 MeV. What remains for the future is the refinement of the analytical approach and its extension to higher energies as further improvements are made to the nuclear database.

ACKNOWLEDGMENT

The authors gratefully acknowledge the support of this work by SDIO/TNI through NRL.

[1] H. E. Johns and J. R. Cunningham, *The Physics of Radiology, 4th ed.* (Thomas, Springfield, Ill, 1983).
[2] See, e.g., M. Promé, *Proceedings of the Third European Particle Accelerator Conference* (Edition Frontieres, Gif-sur-Yvette, 1992), Vol. 1, p. 27.
[3] E. A. Abramyan, *Industrial Electron Accelerators and Applications* (Hemisphere, New York, 1988).
[4] B. Bernstein and I. B. Smith, IEEE Trans. Nucl. Sci. NS-20, 294 (1973).
[5] C. B. Collins, J. A. Anderson, Y. Paiss, C. D. Eberhard, R. J. Peterson, and W. L. Hodge, Phys. Rev. C 38, 1852 (1988).
[6] J. J. Carroll, M. J. Byrd, D. G. Richmond, T. W. Sinor, K. N. Taylor, W. L. Hodge, Y. Paiss, C. D. Eberhard, J. A. Anderson, C. B. Collins, E. C. Scarbrough, P. P. Antich, F. J. Agee, D. Davis, G. A. Huttlin, K. G. Kerris, M. S. Litz, and D. A. Whittaker, Phys. Rev. C 43, 1238 (1991).
[7] K. G. Kerris, The Aurora Bremsstrahlung Environment, Harry Diamond Laboratories Report No. HDL-TM-81-18 (unpublished).
[8] R. Mohan, C. Chui, and L. Lidofsky, Med. Phys. 12, 592 (1985).
[9] W. R. Nelson, H. Hirayama, and D. W. O. Rogers, The EGS4 Code System, Stanford Linear Accelerator Center Report No. SLAC 265, 1985 (unpublished).
[10] R. Brun, F. Bruyart, M. Marie, A. C. McPherson, and P. Zanarini, GEANT 3, CERN Report DD/EE/84-1, 1987 (unpublished).
[11] J. A. Halbleib and T. A. Mehlhorn, ITS The Integrated TIGER Series of Coupled Electron/Photon Monte Carlo Transport Codes, Sandia National Laboratories Report SAND84-0573, 1984 (unpublished).
[12] T. M. Jenkins, W. R. Nelson, and A. Rindi, eds., *Monte Carlo Transport of Photons and Electrons* (Plenum, New York, 1988).
[13] P. von Neumann-Cosel, N. Huxel, A. Richter, C. Spieler, J. J. Carroll, and C. B. Collins, Nucl. Instrum. Methods A (unpublished).
[14] D. A. Whittaker, K. G. Kerris, M. Litz, S. G. Gorbics, and N. R. Pereira, J. Appl. Phys. 58, 1034 (1985).
[15] R. Abrose, D. L. Kahler, H. E. Lehnhet, and C. A. Quarles, Nucl. Instrum. Methods B 56, 327 (1991).
[16] F. R. Metzger, Prog. Nucl. Phys. 7, 54 (1959).
[17] D. J. Landry and D. W. Anderson, Med. Phys. 18, 527 (1991).
[18] G. T. Baldwin and J. R. Lee, IEEE Trans. Nucl. Sci. NS-33, 1298 (1986).
[19] S. S. Dietrich and B. L. Berman, Atomic Data Nucl. Data Tables 38, 199 (1988).
[20] W. C. Miller and B. Waldman, Phys. Rev. 75, 425 (1949).
[21] Y. Paiss, C. D. Eberhard and C. B. Collins, J. de Phys. C9, 131 (1987).
[22] J. A. Anderson and C. B. Collins, Rev. Sci. Instrum. 58, 2157 (1987).
[23] J. A. Anderson and C. B. Collins, Rev. Sci. Instrum. 59, 413 (1988).
[24] J. A. Anderson, C. D. Eberhard, K. N. Taylor, J. M. Carroll, J. J. Carroll, M. J. Byrd, and C. B. Collins, IEEE Trans. Nucl. Sci. NS-36, 241 (1989).
[25] J. A. Anderson, J. M. Carroll, K. N. Taylor, J. J. Carroll, M. J. Byrd, T. W. Sinor, C. B. Collins, F. J. Agee, D. Davis, G. A. Huttlin, K. G. Kerris, M. S. Litz, D. A. Whittaker, N. R. Pereira and S. G. Gorbics, Nucl. Instrum. Methods B 40, 1189 (1989).
[26] C. B. Collins, J. J. Carroll, T. W. Sinor, M. J. Byrd, D. G. Richmond, K. N. Taylor, M. Huber, N. Huxel, P. von Neumann-Cosel, A. Richter, C. Spieler, and W. Ziegler, Phys. Rev. C 42, 1813 (1990).
[27] J. J. Carroll, T. W. Sinor, D. G. Richmond, K. N. Taylor, C. B. Collins, M. Huber, N. Huxel, P. von Neumann-Cosel, A. Richter, C. Spieler, and W. Ziegler, Phys. Rev. C 43, 897 (1991).
[28] P. von Neumann-Cosel, A. Richter, C. Spieler, W. Ziegler, J. J. Carroll, T. W. Sinor, D. G. Richmond, K. N. Taylor, C. B. Collins, and K. Heyde, Phys. Lett. B 266, 9 (1991).
[29] C. B. Collins, J. J. Carroll, K. N. Taylor, D. G. Richmond, T. W. Sinor, M. Huber, P. von Neumann-Cosel, A. Richter, and W. Ziegler, Phys. Rev. C 46, 952 (1992).
[30] M. Huber, P. von Neumann-Cosel, A. Richter, C. Schlegel, R. Schulz, J. J. Carroll, K. N. Taylor, D. G. Richmond, T. W. Sinor, C. B. Collins, and V. Yu. Ponomarev, Nucl. Phys. A (to be published).
[31] J. J. Carroll, C. B. Collins, K. Heyde, M. Huber, P. von Neumann-Cosel, V. Yu. Ponomarev, D. G. Richmond, A. Richter, C. Schlegel, T. W. Sinor, and K. N. Taylor, Phys. Rev. C (unpublished).
[32] E. Segre, *Nuclei and Particles, 2nd ed.* (Benjamin/Cummings, Menlo Park, CA, 1982), p. 369 ff.
[33] G. Breit and E. Wigner, Phys. Rev. 49, 519 (1936).
[34] F. H. Attix, *Introduction to Radiological Physics and Radiation Dosimetry* (Wiley, New York, 1986), Appendix E.
[35] E. Browne and R. B. Firestone, in *Table of Radioactive Isotopes*, edited by V. S. Shirley (Wiley, New York, 1986).
[36] W. Heitler, *The Quantum Theory of Radiation, 3rd ed.* (Dover, New York, 1984), p. 242 ff.
[37] H. Kuhlenkampff, Ann. der Phys. 69, 548 (1922).
[38] S. Lindenstruth, A. Degener, R. D. Heil, A. Jung, U. Kneissl, J. Margraf, H. H. Pitz, P. Schacht, U. Seemann, R. Stock, and C. Wesselborg, Nucl. Instrum. Methods A 300, 293 (1991).
[39] *Nuclides and Isotopes, 14th ed.* (General Electric Company, San Jose, CA, 1989), p. 33.
[40] For ^{79}Br see Nucl. Data Sheets 37, 393 (1982); for ^{87}Sr see Nucl. Data Sheets 62, 327 (1991); for ^{115}In see Nucl. Data Sheets 52, 565 (1987), for ^{137}Ba see Nucl. Data Sheets 59, 767 (1990).
[41] E. C. Booth and J. Brownson, Nucl. Phys. A 98, 529 (1967).

Low-energy conversion electron Mössbauer spectroscopy using a chevron microchannel plate detector

T. W. Sinor, J. D. Standifird, K. N. Taylor, C. Hong, J. J. Carroll, and C. B. Collins
Center for Quantum Electronics, University of Texas at Dallas, P. O. Box 830688, Richardson, Texas 75083-0688

(Received 2 March 1993; accepted for publication 12 June 1993)

A detection system for conversion electron Mössbauer spectroscopy is described. A chevron microchannel plate assembly attached to a two-stage electrostatic lens is used to preferentially detect electrons with energies ≤15 eV. Mössbauer spectra collected with these electrons can provide information about a variety of solid-state surface phenomena.

I. INTRODUCTION

Conversion electron Mössbauer spectroscopy[1-4] (CEMS) is a low-noise spectroscopic technique based on the detection of conversion, Auger, and secondary electrons emitted from a material as a result of the de-excitation of Mössbauer nuclei. It provides information about the environment in which these sensitive nuclei are embedded. However, the range which can be probed with the method is limited by the escape depth of the electrons in the material. For ^{57}Fe the mean electron range in metallic iron has been reported to be 57 and 36 nm for the 7.3 and 5.4 keV conversion and Auger electrons, respectively.[1] It has been shown that the component with energies ≤15 eV comprises about 50% of the total signal and provides information from the top 5 nm of the sample.[5-7] Because the range of those electrons is so short, they can provide specific information about a variety of solid-state surface phenomena and aid in the characterization of implanted layers.[8-10]

In this article we discuss the design and construction of a relatively simple spectrometer that was used to selectively and efficiently detect this low-energy component. It was based upon a chevron microchannel plate (MCP) assembly with an active diameter of 25 mm that served as the detector. A two-stage electrostatic lens was used to preferentially focus and accelerate low-energy electrons from the target to the detector. This acceleration increased the energy of the electrons to a level more compatible with the sensitivity of the input ~~to a~~ microchannel plate.

The detection of higher energy signal electrons, which escape from and provide information about deeper regions of the target, could serve as a source of "contamination" to the signal in that they carry little or no information about the surface effects being investigated. The number of these electrons detected was reduced to negligible levels by minimizing the geometrical solid angle between the Mössbauer target and the MCP assembly. This was possible since the trajectories of the more energetic electrons were not significantly focused by the relatively weak electrostatic fields of the lens.

II. EXPERIMENTAL DETAIL

A. Apparatus

Figure 1 shows the experimental arrangement used in these measurements. A ^{57}Co(Pd) source with a nominal activity of 10 mCi was mounted on a Doppler motor external to the vacuum chamber containing the sample and electron detector and provided the 14.4-keV Mössbauer radiation. To optimize the passage of resonant γ rays into the target chamber a thin entrance window was constructed from titanium. The 14.4-keV γ rays were only slightly attenuated ~~by~~ but the window efficiently filtered out a significant number of the lower energy x rays that were produced by the decay of source nuclei. Without filtering, these x rays would have seriously degraded the performance of the detection system.

Low-energy electrons emitted from the target were collected with a two-stage aperture lens. The MCP, target, electrical feedthrough, and electrostatic lens were mounted as an integral unit on a 6-in. vacuum flange. This provided for convenient mounting and removal of the entire assembly from the vacuum chamber for adjustments to the target geometry. The angular position of the Mössbauer target with respect to the direction of the source γ rays was adjusted by rotating it about the vertical axis. Data were typically collected with the target at a 45° angle with respect to the detector axis and the incident radiation.

The chamber was initially evacuated with an Alcatel CFF-450 turbomolecular pump (TMP) to a pressure of about 3×10^{-7} Torr. However, vibrations from the TMP seriously degraded the resonant absorption in the absorber and could not be used to maintain the vacuum necessary to operate the chevron. To provide for vibrationless pumping, a 140 *l*/s Varian diode VacIon pump was used to maintain the required pressure of 2×10^{-6} Torr. It is important to note that such pumps operate by ionizing gas in a magnetically confined cold-cathode discharge. Thus proper precautions had to be taken to prevent neutral and charged particles, as well as hard ultraviolet radiation from escaping from the VacIon pump and degrading the performance of the detector. To avoid this difficulty a line-of-sight baffle was used that consisted of six successive aperture plates. This was inserted between the VacIon pump and target chamber with the apertures staggered in a helical pattern.

16.6p

FIG. 1. Schematic diagram of the experimental arrangement.

B. Lens design

The structure and dimensions of the lens used in this work are shown in Fig. 2. The steering of the electrons was performed primarily by the potential gradients established between two annular rings mounted inside a wire cylinder. The rings had a common outer diameter of 12.7 cm and inner diameters of 2.5 and 6.4 cm, respectively. The overall length of the lens was 14 cm. It not only served to focus and accelerate electrons to the detector, but also as a Faraday shield isolating the lens elements from the ground potential of the chamber walls due to the inclusion of endcaps on the assembly. This minimized the number of noise

15.6p

FIG. 2. Drawing of the two-element electron lens designed to efficiently collect electrons having energies ≤ 5 eV. The steering of the electrons was performed primarily by the potential gradients established between R_1 and R_2. With the inclusion of the endcaps on the assembly, the lens system not only served to focus and accelerate electrons to the detector input plate, but also as a Faraday cage in shielding the lens elements from the ground potential and noise electrons of the chamber walls. The optimum operating biases for the lens were found to be $V_{R_1} = -2817$ V, $V_{R_2} = -1967$ V, and $V_{\text{cone}} = -2757$ V when the chevron was operated at -1616 V and the MCP grid at -1870 V.

17p

FIG. 3. Circuit diagram of the supporting electronics for the chevron microchannel plate assembly.

photoelectrons produced inside the chamber that entered the sensitive region of the detector.

To model the lens and to determine the optimum potentials for the various elements the program EGN2C was employed which is traceable to SLAC.[11] This program is designed to calculate trajectories of charged particles in electrostatic and magnetostatic fields and is capable of including effects due to space-charge and self-magnetic fields. In this work these effects were not investigated. Input to the program included electrode boundary conditions and initial conditions for electrons emitted from the surface of the target.

Various electron emission configurations including plane waves and point sources were simulated for electrons with energies ranging from 15 eV to 7.3 keV. Biases were found that achieved an effective solid angle for collection of nearly 2π steradians for electrons with energies below 15 eV and are indicated in Fig. 2. A circuit diagram of the supporting electronics for the MCP assembly is shown in Fig. 3. Simulations indicated that the lens had a negligible effect on the trajectories of electrons with energies greater than about 100 eV for the biases used. The detection efficiency for these electrons was then solely defined by the geometrical solid angle between the detector and the target.

C. Noise reduction

To obtain Mössbauer spectra with large signal-to-noise ratios, proper collimation of the source was critical to reduce nonresonant scattering inside the chamber. Various collimator designs were used in these experiments but the best performance was realized with a 1.25-cm-thick lead plate that had a circular aperture at its center. The aperture was tapered so that its diameter increased in the direction of propagation of the radiation to reduce scattering from the collimator walls.

Radiation scattering inside the chamber was minimized by providing an exit window diametrically opposite

FIG. 4. Conversion electron Mössbauer spectra for a 93.55% enriched ^{57}Fe target. (a) Lens in a focusing or active mode and collected for 3.4 h with a counting rate of 2.47 cps. (b) With the lens in a passive, field-free mode possessing no focusing or accelerating properties the signal counting rate dropped to 0.087 cps. The data were collect five times longer than in (a). The geometrical collection of the lens accounted for less than 3.5% of the signal when the lens was operated at optimum biases.

the entrance window. This window had a diameter of 10 cm and was constructed of mylar to avoid significant backscattering of photons and photoelectrons. The beam size of γ rays from the ^{57}Co source was optimized by proper collimation to illuminate the entire target without expanding to a diameter that would impede its exit from the output window.

To further reduce scattering in the system the lens was constructed from a copper mesh which had an open area of 69% and a wire diameter of 250 μm. Perturbations of the electric field resulting from the use of a mesh instead of a continuous sheet of metal have been shown to be negligible at distances greater than the wire separation.[12] The percentage of open area was further increased by alternately removing wires in the region of the lens that were in the direct path of the input radiation.

III. RESULTS

The target foil used to evaluate the effectiveness of the lens was a $5.0 \times 5.0 \times 2 \times 10^{-4}$ cm iron foil with ^{57}Fe nuclei enriched to 93.55%. For purposes of comparison, data were collected with the electron lens operating in an "active" mode at the optimum potentials for low-energy electrons and in a passive mode where there were no accelerating fields. Data collected with the lens in the focusing or active mode are shown in Fig. 4(a). The total collection time for the data was 3.44 h and the total signal counting rate was 2.47 counts per second. The data with the lens in the passive, field-free mode are shown in Fig. 4(b). There the signal counting rate was 0.087 counts per second. The data were collected five times longer than the corresponding data with the lens active to obtain reasonable statistics.

Operation of the lens in a passive mode helped determine the geometrical collection efficiency for the system. In this geometry it was concluded from the data of Fig. 4 that the lens increased the signal count rate by a factor of 28 while the background signal increased by only a factor of 11. For the biases used in the active mode the trajectories of the higher energy signal electrons were defined solely by the geometrical solid angle between the target and MCP assembly and were the same for both bias configurations. This contribution to the signal counting rate could have been reduced further by simply increasing the distance between the target and detector assembly.

IV. DISCUSSION

Detection of electrons with energies ≤ 15 eV can provide detailed information about a variety of surface phenomena in the top 5 nm of a material. In this article we have described the design and construction of a detection system for conversion electron Mössbauer spectroscopy. This device preferentially detects electrons with energies ≤ 15 eV and has the potential for providing a simple alternative to more complex and expensive electron detectors which are currently used in energy-resolved Mössbauer spectroscopy.

It was shown that the detection efficiency of higher energy conversion and Auger electrons can be minimized by choosing an appropriate geometry. Numerous computer simulations using plane-wave and point-source electron configurations showed that the electrostatic lens gave an effective solid angle of almost 2π steradians for the signal electrons having appropriately low energies.

Although not pursued in this work, it is possible with the current design to collect virtually all the electrons emitted from the target. This could be accomplished if the potential difference between the input of the chevron and target foil is made sufficiently large. Furthermore, if a retarding field analyzer is positioned between the target and MCP, the lower energy electrons can be efficiently filtered out.[13] In this manner it is possible to obtain energy-resolved Mössbauer spectra over a wide range of electron energies.

ACKNOWLEDGMENTS

The authors gratefully acknowledge the support of this work by SDIO/TNI through NRL.

[1] For a good review see, J. A. Sawicki, in *Industrial Applications of the Mössbauer Effect*, edited by G. J. Long and J. G. Stevens (Plenum, New York, 1986), p. 83.
[2] Z. Boschev, A. Jordanov, and A. Minkova, Nucl. Instrum. Methods 70, 36 (1969).
[3] J. Fenger, Nucl. Instrum. Methods 69, 268 (1969).
[4] K. R. Swanson and J. J. Spijkerman, J. Appl. Phys. 41, 3155 (1970).
[5] W. Jones, J. M. Thomas, R. K. Thorpe, and M. J. Tricker, Appl. Surf. Sci. 1, 388 (1978).

[8] J. A. Sawicki and T. Tyliszczak, Nucl. Instrum. Methods 216, 501 (1983)
[9] J. S. Zabinski and B. J. Tatarchuk, Nucl. Instrum. Methods B 42, 379 (1989)
[8] J. S. Zabinski and B. J. Tatarchuk, Nucl. Instrum. Methods B 31, 576 (1988)
[9] G. Klingelhöfer and E. Kankeleit, Hyperfine Interactions 57, 1905 (1990)
[10] J. S. Zabinski and B. J. Tatarchuk, Thin Solid Films 166, 213 (1988)
[11] W. B. Herrmannsfeldt, *EGUN, An Electron Optics and Gun Design Program*, Stanford Linear Accelerator Center, Stanford, CA, SLAC Report-331 (1988)
[12] See, for example, R. P. Feynman, R. B. Leighton, and M. Sands, *The Feynman Lectures in Physics* (Addison-Wesley, Reading, MA, 1964), Vol II, p. 7–10
[13] H. Sato and M. Mitsuhashi, Hyperfine Interactions 58, 2535 (1990)

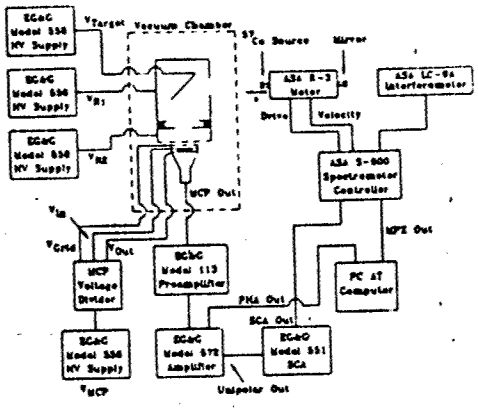

RSI/scar/07309/661/501

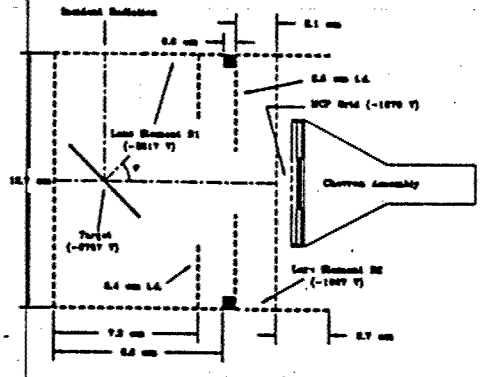

RSI/scar/07309/662/501

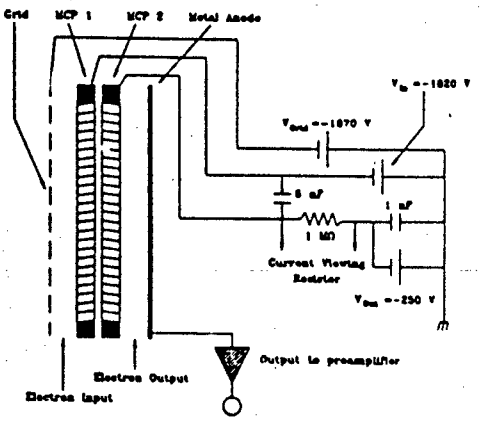

RSI/SEPT/047304/fig3/501

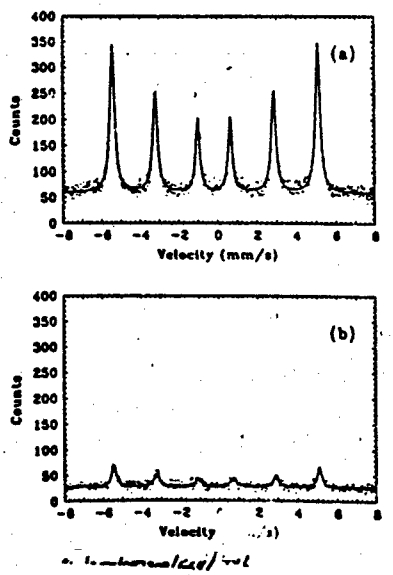

Structure of intermediate states in the photoexcitation of the ^{89}Y isomer*

M. Huber, P. von Neumann-Cosel, A. Richter, C. Schlegel and R. Schulz
Institut für Kernphysik, Technische Hochschule Darmstadt, D-6100 Darmstadt, Germany

J.J. Carroll, K.N. Taylor, D.G. Richmond, T.W. Sinor and C.B. Collins
Center for Quantum Electronics, The University of Texas at Dallas, TX 75083-0688 Richardson, Texas, USA

V. Yu. Ponomarev
Laboratory of Theoretical Physics, Joint Institute for Nuclear Research, Dubna, Head Post Office, P.O. Box 79, Moscow, Russia

Abstract: Resonant photon scattering off ^{89}Y was investigated in a measurement of the $^{89}Y^{m}$ excitation function for bremsstrahlung endpoint energies $E_0 = 2 - 5$ MeV and in a nuclear resonance fluorescence experiment with $E_0 = 5$ MeV. The results are compared to a quasiparticle-phonon model calculation. Besides a well known single particle M1 transition at low energies, the photoexcitation spectrum is governed by transitions to states built by coupling of the dominant $p_{1/2}$ hole ground state configuration to collective quadrupole phonons in the neighbouring ^{90}Zr. The detailed decay cascade to the isomer reproduces the experimental finding of only two intermediate states with about equal strength and explains the suppression of other possible transitions due to the nature of the particular E1 matrix element. The theoretical isomer branching ratios are small compared to the experiment, but depend critically on details of the model.

NUCLEAR REACTIONS ^{89}Y$(\gamma,\gamma')^{89}Y^{m}$, $E_0 = 2 - 5$ MeV; ^{89}Y(γ,γ'), $E_0 = 5$ MeV. Deduced ground state and isomer activation transition strengths, $t_{1,2}$. Quasiparticle-phonon model calculations.

* Work supported by the German Federal Minister for Research and Technology (BMFT) under contract number 06DA641I and by the Department of Defense through the Naval Research Laboratory.

1. Introduction

The photoactivation of isomers has recently attracted considerable interest [1-5]. These studies have been motivated by several sources of interest. It has been proposed to use the population or depopulation of isomers by resonant photoabsorption as the basic mechanism for driving a γ-ray laser [6]. For feasibility studies, a much improved experimental data base is needed. Photon coupling between ground state (g.s.) and isomer plays an important role in nuclear astrophysics. As examples, photoactivation [7] of ^{176}Lu and the depopulation [1] of ^{180}Ta^{m} provide critical tests of the present understanding of the s-process element production [8-9]. An understanding of the nuclear structure of intermediate states (IS) responsible for the isomer feeding is not only of interest by itself, but also a prerequisite for progress in the above described problems.

Most experimental photoactivation work has concentrated either on the low-energy area [see e.g. refs. [10-11] and references therein] $E \leq 2$ MeV, or on the giant resonance region [12-14], where the statistical γ-decay properties and the competition with other emission channels can be tested. The work described in refs. [1-5] focused on the energy region in between and produced a number of unexpected results, viz. very large integrated cross sections (ICS) in heavy deformed nuclei implying considerable K mixing at low energies [15], a threshold of ICS at excitation energies E_x = 2.5 - 3 MeV and a close correlation of absolute magnitudes of isomer population with the g.s. deformations [5].

A first attempt to reach a detailed understanding of the IS nuclear structure was made in the investigation of ^{115}In. Here, photoactivation and complementary nuclear resonance fluorescence (NRF) experiments were performed and the combined information turned out to be a powerful tool to constrain microscopic model descriptions [4]. In the present work we have extended this combined experimental method to another example, $^{89}Y^{m}$. The isomeric transition is of M4 type $1/2^- \rightarrow 9/2^+$, but complementary to the ^{115}In case, ^{89}Y has a $J^\pi = 1/2^-$ g.s. and a $J^\pi = 9/2^+$ isomer (E_{iso} = 0.909 MeV). It provides an interesting case because of its semimagic nature. The reduced configuration space should facilitate the identification of the important nuclear structure aspects. Furthermore, additional information from spectroscopic studies with a variety of methods is available [16] up to relatively high excitation energies. Photoactivation of $^{80}Y^{m}$ was observed in the survey of ref. [3] and the yields turned out to be very small compared to other isomers in this mass region.

The results are compared to calculations with the quasiparticle-phonon model [17]. It has already been successfully applied [18]) to explain the structure of IS in the photoactivation of ^{81}Br. The properties of the the ^{89}Y low-energy spectrum have been tested in a variety of other models [19-22]), but the study of electromagnetic transitions has been restricted to the lowest states only.

2. Experiments and data analysis

The experiments were performed with the 10 MeV injector of the superconducting continuous wave electron accelerator S-DALINAC in Darmstadt [23]). Figure 1 displays the experimental area for both measurements in more detail. The electron beam traversed through a 100 μm Al exit window and impinged on a rotating 3 mm Ta converter disk for bremsstrahlung production. The electron beam alignment could be sensitively monitored with the dose delivered to an ionization chamber 2 m downstream which is shielded against background radiation and covers only 12 mrad around 0°.

2.1 NUCLEAR RESONANCE FLUORESCENCE EXPERIMENT

For the NRF experiment, a metallic Y powder target of 2.55 g sealed in a 0.1 mg/cm^2 polyethylene foil was placed behind the 60 cm lead collimator which has a conical opening. The bremsstrahlung converter was moved to the position close to the collimator entrance indicated in fig. 1. The collimator defines a beam spot of 2.5 cm^2 at the target position. The resonantly scattered photons were detected with a Ge(Li) and a HPGe detector, both 150 ccm, placed at 90° and 127°, respectively, relative to the beam axis. In the present experiment, only the 127° diode was used (see sect. 3). A graded shield of 9 mm Pb + 5 mm Cu was placed between target and detector in order to suppress the strong nonresonant low-energy background. Data were taken at E_0 = 5 MeV with a typical average current of 25 μA. The total measuring time was 32 h.

The energy calibration and relative efficiency of the Ge detector were determined off line with a ^{56}Co source with a geometry identical to the target. During the measurement, thin disks of 1.05 g Al were sandwiched around the yttrium target. In ^{27}Al a number of extremely well determined transitions [24]) are excited in the energy region of interest and serve as standards for the determination of the total photon flux.

The shape of the bremsstrahlung spectrum was taken from a Monte Carlo calculation with the code EGS4 [25]). From fig. 1 it is obvious that the experimental geometry is simple and reliable results from the Monte Carlo calculations can be expected. The calculated spectral shapes compare very well [26,27]) to the results for strong transitions in ^{27}Al and ^{11}B which are commonly used as standards. Further details of the data analysis are given in ref. [26]).

From the line contents of identified transitions one obtains the ICS of the g.s. transitions $(\sigma\Gamma)_0^i$ which are related to the characteristic properties of the excited state i by

$$(\sigma\Gamma)_0^i = \pi^2 \left(\frac{\hbar c}{E_i}\right)^2 \frac{2J_i + 1}{2J_0 + 1} \frac{(\Gamma_0^i)^2}{\Gamma} W(\Theta) \quad . \tag{1}$$

Here, J_0 and J_i are the spins of the g.s. and excited state, respectively, Γ_0^i is the partial width directly to the g.s., Γ is the total width and E_i is the energy of the transition. The angular distribution $W(\Theta)$ accounts for the nonisotropic decay which depends on the multipolarity (dipole/quadrupole) and the mixing ratio δ of E2/M1 transitions.

2.2 ISOMER ACTIVATION EXPERIMENT

The experiment was performed as close as possible to the bremsstrahlung converter in order to maximize the photon flux. The target consisted of an Al cylinder (diameter 1.4 cm, height 2.7 cm, walls 0.1 cm) filled with 4.8 g of YF_3 powder. The cylinder was aligned to the beam direction with the front side in a distance of 1.3 cm to the converter. The sample was typically irradiated for a time duration of two half lives ($t_{1/2}$ = 16.06 s) and then transported with a high compression rabbit system to a 3.5" NaI bore hole detector outside of the accelerator hall. Typically 5 to 9 cycles were performed per electron endpoint energy. Details of the measurement with this shuttle system are described in refs. [5,28]).

The absolute efficiency of the NaI detector was calculated with a Monte Carlo program which included the geometry of target cylinder and detector, the nonuniform distribution of activation over the length of the target and the self absorption of the signature transition in the target material.

Following the method described in ref. [5]), ICS for the states populating the isomer can be derived from the yields and the photon spectral intensities which

were taken again from EGS4 calculations. The integrated cross sections $(\sigma\Gamma)^i_{int}$ are related to eq. (1) by

$$(\sigma\Gamma)^i_{int} = \pi^2 \left(\frac{\hbar c}{E_i}\right)^2 \frac{2J_i + 1}{2J_0 + 1} \frac{\Gamma^i_0 \Gamma^i_{ps}}{\Gamma} = (\sigma\Gamma)^i_0 \frac{\Gamma^i_{ps}}{\Gamma^i_0 W(\Theta)} \quad (2)$$

Here, Γ^i_{ps} represents the sum of all partial widths of level i which decay to the isomer, either directly or via a cascade.

The validity of the data analysis procedures was tested with a measurement of ^{115}In. It was shown in ref. [1]) that the isomeric yield below 2.8 MeV provides an absolute calibration of the total photon flux, since all activation levels are completely characterized in the literature [5]). The present results agree within 5% with those of ref. [1]), which were measured in a completely different geometry with a thin disk target, as well as with the 6 MeV endpoint energy result of ref. [1]).

3. Results and discussion

3.1. NUCLEAR RESONANCE FLUORESCENCE OF ^{89}Y

A (γ,γ') spectrum taken at an endpoint energy $E_0 = 5$ MeV is displayed in fig. 2. Except those levels marked as Al calibration lines, all visible transitions are assumed to be ^{89}Y g.s. transitions. The observation of transitions to excited states can be excluded in the present case. Since NRF is restricted to dipole or quadrupole excitations, the lowest level which could be effectively populated would be at 1.507 MeV. Because of the correspondingly reduced γ-energy, such a transition is lost in the Compton background which rises exponentially towards lower energies.

A summary of all observed transitions is given in table 1 together with the available information [16]) on spins and g.s. branching ratios. In cases where both quantities are known, the resulting half life is presented in the last column. For previously unknown levels, the partial g.s. width is given as $g\Gamma^2_0/\Gamma$ with $g = 2J + 1/2J_0 + 1$.

Unlike the case of even-even nuclei where a two-point angular distribution allows a clear distinction between dipole and quadrupole transitions [26]) the possible angular distributions in an odd-even nucleus are much more isotropic. Therefore only measurements with the 127° detector which has a more favourable peak-to-background ratio were evaluated. For the angular correlations of ^{89}Y g.s. transitions $1/2 \rightarrow 1/2, 3/2, 5/2 \rightarrow 1/2$ the value of $W(\Theta)$ at 127° averaged over the

detector solid angle varies by less than 15% from $W(\Theta) = 1$. Thus, the $W(\Theta)$ factor is omitted and for previously unknown levels an additional systematic error should be included. For an assigned $5/2^-$ spin, the values in table 1 are corrected with a factor $W(\Theta) = 0.856$. In the case of a $3/2^-$ state, the maximum deviation from unity for an arbitrary E2/M1 mixing ratio is less than 4.5%.

The strongest transition observed in NRF is to a state at 1.508 MeV which has $J^\pi = 3/2^-$. Its almost pure $p_{1/2}$ hole character is well established in single nucleon pick-up [30]) and (e,e') reaction [31,32]) studies. In an early (γ,γ') experiment [31]) a total width $\Gamma = 22(3)$ meV was observed which compares favourably with the present value.

The 2.881 MeV and 3.067 MeV levels correspond to M1/E2 transitions. From a combination of the $L = 1$ result in the (^{3}He,d) reaction [34]) and $L = 2$ from inelastic (p,p') and (n,n') scattering [35,36]), $J^\pi = 3/2^-$ is clear. The refs. [37,38]) show that the 2.881 MeV state decays to the g.s. with a branching ratio $b_o \simeq 1$. Including the results from sect. 3.2, we infer $b_o = 0.96$.

The 3.107 MeV and 3.139 MeV states are likely $J^\pi = 5/2^-$ candidates. The excitation of the 3.139 MeV state in the present experiment is very weak at the threshold of the detection sensitivity. It is, however, of interest because of its significant branch [37,38]) into a cascade to the isomer. It is noted that the B(E2) value of 145 e^2fm^4 reported in ref. [31]) for the sum of the 3.067, 3.107 and 3.139 MeV levels unresolved in their (e,e') experiment is in good agreement with the present results, if one assumes a dominant E2 transition for the $3/2^-$ state.

The strong 3.992 and 4.108 MeV states are again observed in inelastic nucleon scattering as $L = 2$ states. From the available data one cannot distinguish between $J^\pi = 3/2^-$ and $5/2^-$. A g.s. branching ratio of $b_o \simeq 1$ can be deduced for both states from refs. [37,38]).

No candidate for an E1 transition is seen in the (γ,γ') data. For those $3/2^-$ levels which are simultaneously observed in the (p,p') and (n,n') experiments, dominant E2 transition strength is suggested from the collective character of inelastic nucleon scattering reactions.

3.2 PHOTOACTIVATION OF $^{89}Y^m$

The isomer yield resulting from the bremsstrahlung irradiation is shown in fig. 3 as a function of the endpoint energy. Up to 2.875 MeV no isomer activity

is detected. Towards higher energies, breaks of the excitation function are clearly visible just below 3 and around 4 MeV. The solid line results from a calculation assuming IS at 2.9 and 4.0 MeV with the ICS given in table 2.

The good agreement with the energies of states excited strongly in the (γ,γ') reaction together with the model results described in sect. 4 clearly suggests that the 2.881 MeV state is the first IS. The ICS of the weakly excited 3.139 MeV level is in any case too small to explain the first break. Because of the small number of data points the energy of the second IS is more uncertain and we cannot distinguish whether the 3.992 or the 4.170 MeV level provides the isomer population.

Compared to typical values of ICS in the energy region 2 - 4 MeV observed in refs. [1,2,4,5]), the isomer population in ^{89}Y is weak. This finding is also in qualitative agreement with the yield values at 4 and 6 MeV deduced in ref. [1]). While the average $(\sigma\Gamma)_0$ strength is even slightly higher than observed for ^{115}In in ref. [1]), the isomeric ratio $\Gamma_{\gamma\gamma'}/\Gamma_0 + \Gamma_{\gamma\gamma'}$ is about an order-of-magnitude smaller.

4. Quasiparticle-phonon model calculations

4.1 DETAILS OF THE CALCULATIONS

To understand the structure of states observed in the present experiments microscopic calculations within the quasiparticle-phonon model have been performed. A detailed description of treating odd nuclei within this theoretical framework can be found in ref. [17]).

The present calculations have been performed with the wave function

$$\Psi_\nu(JM) = C_I^\nu \left\{ \alpha^+_{JM} + \sum_{\lambda\mu i} D_j^{\lambda i}(J\nu) \left[\alpha^+_{jm} Q^+_{\lambda\mu i}\right]_{JM} \right\} \Psi_0 \qquad (3)$$

of the ground or excited states with angular momentum J and projection M. In this equation α^+_{jm} is a quasiparticle creation operator, $Q^+_{\lambda\mu i}$ is a phonon creation operator with the momentum λ, projection μ and the RPA-root number i, Ψ_0 is the ground state wave function of the even-even core and ν is the number within a sequence of states with given J^π. For phonons we consider both collective, such as 2^+_1 or 3^-_1, and pure two-quasiparticle excitations of the core.

Numerically, equations for ^{89}Y have been solved by use of the computer code PHOQUS [39]). The QPM effective Hamiltonian includes an average field, pairing

interaction and residual interaction between quasiparticles. The average field was treated by a Woods-Saxons potential with parameters from ref. [10]). Parameters of the residual interaction were adjusted to reproduce the experimental position and the B(Eλ) values of the 2_1^+ and 3_1^- states for ^{90}Zr while dealing with hole excitations and for ^{88}Sr in case of particle excitations. Natural parity phonons with $\lambda^\pi = 1^- \cdot 6^+$ have been included in the second term of the wave function eq. (3). We have taken into account "quasiparticle⊗phonon" configurations up to an excitation energy of 12 MeV. Nevertheless, actual calculations show that only collective 2^+ phonons play an important role in description of photoexcitation of states up to 5 MeV, since the interaction between different phonon configurations is not strong in this nucleus.

4.2 COMPARISON TO NUCLEAR RESONANCE FLUORESCENCE RESULTS

The calculated (γ,γ') excitation strength is presented in fig. 4 together with the experimental $(\sigma\Gamma)_0$ data. In the QPM only 6 sizeable transitions are found below 4.5 MeV. Due to the restriction of the model space to one-phonon coupled states the degree of fragmentation is less than indicated by the experimental results. However, since higher phonon configurations do not contribute additional photoexcitation strength, the main features of the (γ,γ') results can already be explained in the one-phonon approximation.

The two lowest states in the calculation at 1.540 and 1.838 MeV correspond to the well known lowest $J^\pi = 3/2^-$ and $5/2^-$ states which have been shown [11]) to be of dominant $p_{3/2}$ and $f_{5/2}$ single-hole structures, repectively. The model result for the $3/2^-$ level $(\sigma\Gamma)_0$ = 70.2 eVb is in excellent agreement with experiment. The $5/2^-$ state was not observed in the experiment. One can calculate from the g.s. transition strength of $(\sigma\Gamma)_0$ = 4.67 eVb from the data available [16]) and show that the experimental count rate is smaller than the background fluctuations.

The next transitions are in two groups of nearly degenerate levels which result from the coupling of the g.s. configuration to the lowest collective phonons [11]) in the neighbouring even-even nucleus ^{90}Zr, i.e. dominant $[p_{1/2} \otimes 2^+_{1,3}]_{3/2^-,5/2^-}$ structure. The near degeneracy is a result of the neglection of more complex configurations and would probably be removed if one included two-phonon states.

The 3.147 MeV, $J^\pi = 3/2^-$ model state corresponds to the experimental 2.881 MeV and probably the 3.067 MeV state. The magnitudes of ICS support this

assignment. The 5/2 model state can be reasonably compared to the more fragmented experimental strength up to 3.5 MeV. The levels resulting from coupling to the 2_1^+ state can be identified with the experimental levels at 3.992 and 4.170 MeV.

The structure of these states implies that the phonon transitions are responsible for the (γ,γ') strength. The general dominance of collective E2 strength in the NRF data explains the close correspondence to inelastic nucleon scattering results discussed in sect. 3.

4.3 COMPARISON TO ISOMER ACTIVATION RESULTS

Since the relevant excitation spectrum is entirely explained assuming M1 and E2 transitions, for a total M4 transfer the intermediate state decay must proceed in a two-step cascade including an E1 transition for the parity change. Figure 5 presents a calculated level scheme according to this condition. The first step in the cascade to the isomer is limited to $5/2^+$ final states and two are found in the energy region considered.

While the g.s. partial widths are comparable for $3/2^-$ and $5/2^-$ states, large differences are observed in the population of the $5/2^+$ states. The decay to the higher model state at 3.308 MeV is extremely weak due to its almost pure $[p_{1/2} \otimes 3_1^-]_{5/2^+}$ character which restricts to a strongly suppressed $2_1^+ \rightarrow 3_1^-$ phonon transition. The decay widths of the $5/2^-$ states to the lower $5/2^+$ state are much weaker compared to the transitions from the $3/2^-$ levels, since the reduced E1 transition matrix elements are about an order of magnitude smaller. The lowest $5/2^+$ state is strongly coupled to the isomer via a large $[g_{9/2} \otimes 2_1^+]_{5/2^+}$ component in the wave function, so the transitions from the $3/2^-$ states are responsible for the isomer population. This result is in full agreement with the experimental finding of only two IS with about equal strength as well as with the deduced energies.

However,here the description depends on weak quasiparticle configurations of both, initial and final state, which are sensitive to details such as basis truncation and collectivity of phonons. This aspect of the calculations could certainly be improved by the inclusion of the "quasiparticle⊗2-phonon" states where configurations like $[p_{3/2} \otimes [2_1^+ \otimes 3_1^-]_{1^-}]$ are expected to contribute. Also, an extension of the model space by summation over the principle quantum number N for the

quasiparticle configuration [12]) could be important.

5. Conclusions

The photoexcitation of ^{89}Y was investigated with two different methods. NRF data were measured at E_0 = 5 MeV and states up to excitation energies of 4.2 MeV could be identified. The $^{89}Y^m$ excitation function for E_0 = 2 - 5 MeV revealed no activity up to 2.9 MeV and only two IS were found up to 5 MeV.

The (γ,γ') transitions can be explained with a QPM calculation as the coupling of collective phonons in the neighbouring ^{90}Zr with the $p_{1/2}$ hole g.s. configuration leading to groups of $3/2^-$, $5/2^-$ states. While the total electromagnetic transition strength agrees favourably, the experimental fragmentation is underestimated due to the model's restriction to one-phonon coupled states. The omission of more complex configurations is justified for the present problem, since they do not add electromagnetic strength. Besides a well known low-lying single particle M1 transition, the excitation is governed by E2 phonon transitions.

The calculations demonstrate that the cascade needed for the activation of $^{89}Y^m$ proceeds via the lowest $5/2^+$ state which decays almost exclusively to the isomer. The experimental finding of only two IS at about 2.9 and 4.0 MeV is verified and the coupling to the $5/2^+$ state is of single particle E1 character. Due to the nature of the transition matrix elements the $5/2^- \rightarrow 5/2^+$ transitions are suppressed by more than two orders of magnitude with respect to the $3/2^- \rightarrow 5/2^+$ transitions. The calculated branching ratios are small compared to the experiment. However, they depend critically on weak quasiparticle components of the initial and final state wave functions.

One can conclude that up to energies of about 5 MeV the main features of the electromagnetic excitation as well the decay of the excited states to the ^{89}Y isomer are now understood. The usefulness of a combination of NRF and isomer activation experiments has again been proven as a powerful method for nuclear structure studies.

We thank H.-D. Gräf and H. Weise for their great support in operating the accelerator. We are indebted to W. Ziegler for his help in the experiment. One of us (V.Yu.P.) would like to thank the members of the S-DALINAC group for their hospitality during his stay in Darmstadt.

References

[1] C.B. Collins, J.J. Carroll, T.W. Sinor, M.J. Byrd, D.G. Richmond, K.N. Taylor, M. Huber, N. Huxel, P. von Neumann-Cosel, A. Richter, C. Spieler and W. Ziegler, Phys. Rev. **C42** (1990) R1813

[2] J.J. Carroll, T.W. Sinor, D.G. Richmond, K.N. Taylor, C.B. Collins, M. Huber, N. Huxel, P. von Neumann-Cosel, A. Richter, C. Spieler and W. Ziegler, Phys. Rev. **C43** (1991) 897

[3] J.J. Carroll, M.J. Byrd, D.G. Richmond, T.W. Sinor, K.N. Taylor, W.L. Hodge, Y. Paiss, C.D. Eberhard, J.A. Anderson, C.B. Collins, E.C. Scarbrough, P.P. Antich, F.J. Agee, D. Davis, G.A. Huttlin, K.G. Kerris, M.S. Litz and D.A. Whittacker, Phys. Rev. **C43** (1991) 1238

[4] P. von Neumann-Cosel, A. Richter, C. Spieler, W. Ziegler, J.J. Carroll, T.W. Sinor, D.G. Richmond, K.N. Taylor, C.B. Collins and K. Heyde, Phys. Lett. **B266** (1991) 9

[5] C.B. Collins, J.J. Carroll, K.N. Taylor, D.G. Richmond, T.W. Sinor, M. Huber, P. von Neumann-Cosel, A. Richter and W. Ziegler, Phys. Rev. **C46** (1992) 952

[6] C.B. Collins, F.W. Lee, D.M. Shemwall, B.D. DePaola, S. Olariu and I.I. Popescu, J. Appl. Phys. **53** (1982) 4645

[7] N. Klay, F. Käppeler, H. Beer and G. Schatz, Phys. Rev **C44** (1991) 2839;
K.T. Lesko, E.B. Norman, R.-M. Larimer, B. Sur and C.B. Beausang, *ibid* 2850

[8] F. Käppeler, H. Beer and K. Wisshak, Rep. Prog. Phys. **52** (1989) 945

[9] J.J. Carroll, J.A. Anderson, J.W. Glesener, C.D. Eberhard and C.B. Collins, Astroph. J. **344** (1989) 454

[10] E.C. Booth and J. Brownson, Nucl. Phys. **A98** (1967) 529

[11] Á. Veres, At. Energy Rev. **18** (1980) 281

[12] Z.M. Bigan, E.L. Lazarev, V.M. Mazur and V. Sokolnyk, Sov. J. Nucl. Phys. **49** (1989) 567

[13] L.Z. Dzhilavyan, V.L. Kauts, V.I. Furman and A.Y. Chaprikov, Sov. J Nucl. Phys. 51 (1990) 215

[14] J. Sáfár, H. Kaji, K. Yoshihara, L. Lakosi and A. Veres, Phys. Rev. C44 (1991) 1086

[15] J.J. Carroll, C.B. Collins, P. von Neumann-Cosel, D.G. Richmond, A Richter, T.W. Sinor and K.N. Taylor, Phys. Rev. **C45** (1992) 470

[16] H. Sievers, Nucl. Data Sheets **58** (1989) 351

[17] S. Galès, Ch. Stoyanov and A.I. Vdovin, Phys. Rep. **166** (1988) 125

[18] V.Yu. Ponomarev, A.P. Dubenskij, V.P. Dubenskij and E.A. Boykova, J. Phys. **G16** (1990) 1727

[19] P. Hofstra and K. Allaart, Z. Phys. **A292** (1979) 159

[20] S.M. Abecasis, J. Davidson and M. Davidson, Phys. Rev. **C22** (1980) 2237

[21] C.A. Heras and S.M. Abecasis, Phys. Rev. **C27** (1983) 1765

[22] X. Ji and B.H. Wildenthal, Phys. Rev. **C38** (1988) 2849

[23] K. Alrutz-Ziemssen, D. Flasche, H.-D. Gräf, V. Huck, M. Knirsch, W. Lotz, A. Richter, T. Rietdorf, P. Schardt, E. Spamer, A. Staschek, W. Voigt, H. Weise and W. Ziegler, Part. Acc. **29** (1990) 53

[24] P.M. Endt, Nucl. Phys. **A521** (1990) 200

[25] W.R. Nelson, H. Hirayama and D.W.O. Rogers, Stanford Linear Accelarator Report 265 (1985)

[26] W. Ziegler, Dissertation, Technische Hochschule Darmstadt (1990)

[27] N. Huxel, Diploma thesis, Technische Hochschule Darmstadt (1992)

[28] M. Huber, Diploma thesis, Technische Hochschule Darmstadt (1992)

[29] J. Blachot and G. Marguier, Nucl. Data Sheets **52** (1987) 565

[30] A. Stuitbank, G.J. Wagner, K.T. Knöpfle, L.K. Pao, G. Mairle, H. Riedesel, K. Schindler, V. Bechtold and L. Friedrich, Z. Phys. **A297** (1980) 307

[31] S.P. Fivozinskij, S. Penner, J.W. Lightbody Jr. and D. Blum, Phys. Rev. **C9** (1974) 1533

[32] J.E. Wise, F.W. Hersman, J.H. Heisenberg, T.E. Milliman, J.P. Connelly, J.R. Calarco and C.N. Papanicolas, Phys. Rev. **C42** (1990) 1077

[33] W.J. Alston III, H.H. Wilson and E.C. Booth, Nucl. Phys. **A116** (1968) 281

[34] G. Vourvopoulos, R. Shoup and B.A. Brown, Nucl. Phys. **A174** (1971) 581

[35] J. Hulstman, H.P. Blok, J. Verburg, J.G. Hoogteyling, C.B. Nederveen, H.T. Vijlbrief, E.J. Kapstein, S.W. Milo and J. Blok, Nucl. Phys. **A251** (1975) 269

[36] Y. Yiming, C.E. Brient, R.W. Finlay, G. Randers-Pehrson, A. Marcinkowski, R.C. Taylor and J. Rapaport, Nucl. Phys. **A390** (1982) 419

[37] C. Nardelli, P. Pavan and G. Tornielli, Lett. Nuovo. Cim. **38** (1983) 129

[38] C. Budtz-Jørgensen, P. Guenther, A. Smith, J. Whalen, W.C. McMurray, M.J. Renan and I.J. van Heerden, Z. Phys. **A319** (1984) 47

[39] Ch. Stoyanov and C.Z. Khuong, Preprint JINR Dubna P-4-81-234 (1981)

[40] V.Yu. Ponomarev, V.G. Soloviev, Ch. Stoyanov and A.I. Vdovin, Nucl. Phys. **A323** (1979) 446

[41] P.M. Endt, At. Data Nucl. Data Tables **23** (1979) 547

[42] P. von Neumann-Cosel, A. Richter, H.-J. Schmidt-Brücken, G. Schrieder, H. Lenske, H.H. Wolter, J. Carter, R. Jahn, B. Kohlmeyer and D. Schüll, Nucl. Phys. **A516** (1990) 385

Table 1

TABLE 1. Transitions in $^{89}Y(\gamma,\gamma')$.

E_γ (keV)	$(\sigma\Gamma)_0$ (eVb)	$g\Gamma_0^2/\Gamma$ (meV)	J^π [from ref. [16]]	b_0	$t_{1/2}$ (fs)
1507.2(1)	64.5(36)		$3/2^-$	1.00	$23.9^{+2.5}_{-2.1}$
2881.6(1)	19.6(12)		$3/2^-$	0.96 [a]	$19.9^{+2.1}_{-1.9}$
3067.0(3)	8.2(17)		$3/2^-$	1.00	$45.0^{+4.5}_{-4.1}$
3106.9(6)	4.0(22)		$5/2^-$	0.87	100^{+190}_{-55}
3139.0(5)	2.9(11)		$5/2^-$	0.78	110^{+70}_{-40}
3396.1(3)	11.7(19)	35(6)			
3445.3(3)	5.8(9)	18(3)			
3480.3(5)	6.8(24)	21(8)			
3515.6(6)	2.4(11)	8(4)	$3/2^-, 5/2^-$		
3660.0(5)	6.7(18)	23(6)			
3898.6(5)	6.1(12)	24(5)			
3991.8(3)	22.4(25)	93(10)	$3/2^-, 5/2^-$	0.95 [b], 1.00 [c]	$9.3^{+1.1}_{-1.0}$ [b], $12.6^{+1.6}_{-1.3}$ [c]
4069.8(8)	1.0(6)	4(3)			
4170.2(4)	25.5(31)	115(14)	$3/2^-, 5/2^-$	0.95 [b], 1.00 [c]	$7.5^{+1.0}_{-0.8}$ [b], $10.1^{+1.5}_{-1.1}$ [c]

[a]) Isomeric branching ratio from sect. 3.2

[b]) If $J^\pi = \frac{3}{2}^-$ with isomeric branching ratios from sect. 3.2

[c]) If $J^\pi = \frac{5}{2}^-$

Table 2

TABLE 2. Intermediate states in the photoactivation of $^{89}Y^{m}$.

E_x (MeV)	$(\sigma\Gamma)_{int}$ (eVb)
2.9(1)	0.8(1)
4.0(2)	1.2(5)

Figure Captions

Fig. 1. Schematic, but in scale view of the experimental area for nuclear resonance fluorescence and photoactivation studies. Note the different positions of the bremsstrahlung converter (close to the collimator for NRF) for the two types of experiments.

Fig. 2. Spectrum of the $^{89}Y(\gamma,\gamma')$ reaction at an endpoint energy $E_0 = 5$ MeV.

Fig. 3. The ^{89}Y isomer yield as a function of the bremsstrahlung endpoint energy. The solid line represents calculated values [3]) using the intermediate states of table 2.

Fig. 4. Comparison of the experimental integrated cross sections ($\sigma\Gamma$)$_0$ of g.s. transitions in the $^{89}Y(\gamma,\gamma')$ reaction with QPM calculations. The experimental spin assignments are from ref. [16]).

Fig. 5. Selected scheme of levels and partial decay widths from the QPM results for ^{89}Y. The graph is restricted to states relevant to the photoexcitation of $^{89}Y^m$. The levels are split in $J^\pi = 3/2^-$ states in the left column, $J^\pi = 5/2^-$ states in the right column and positive parity states in the middle. The decay widths are given in meV. Weak transitions are denoted by dashed lines.

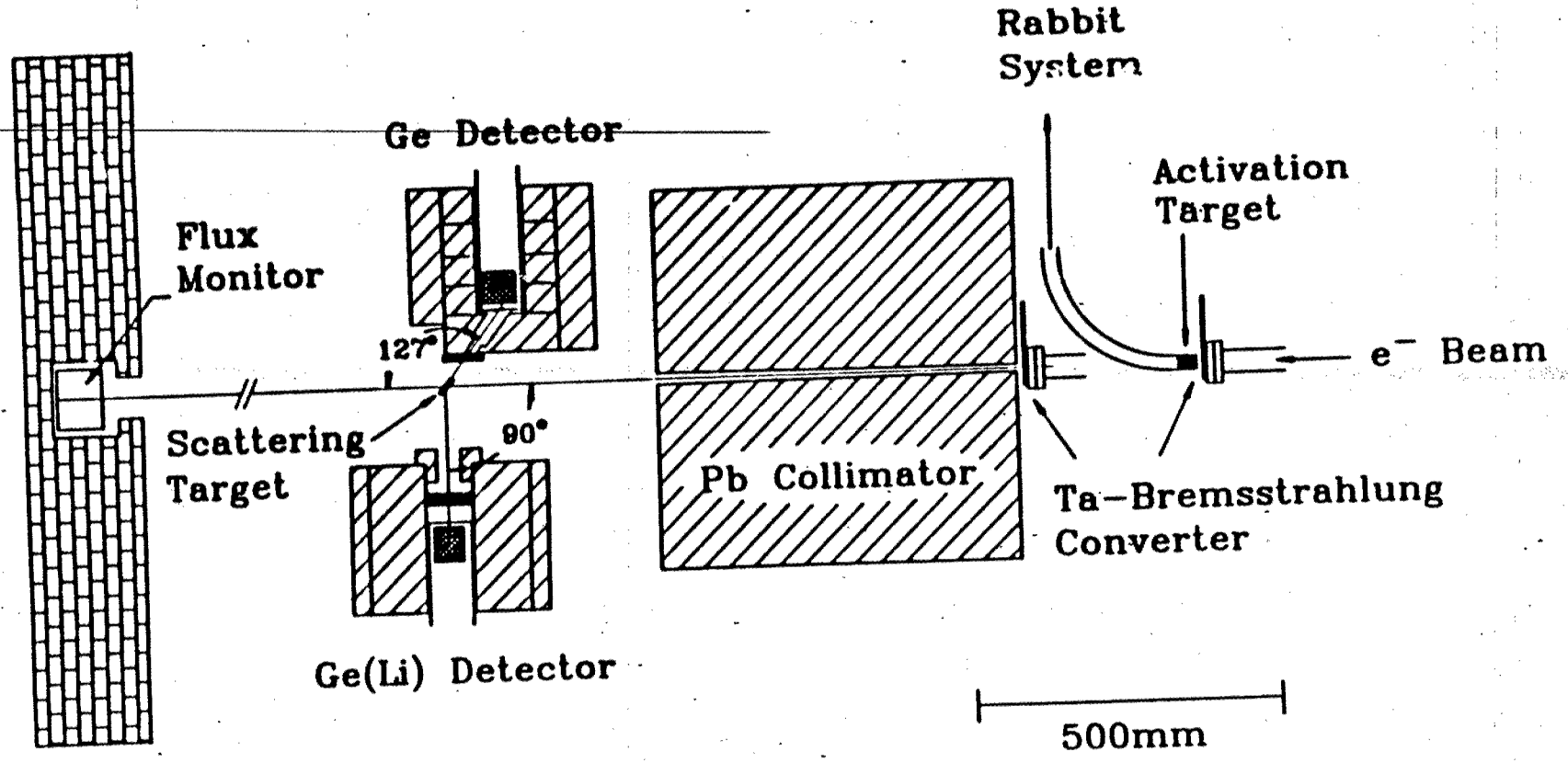
Rabbit
System
Ge Detector
Activation
Target
Flux
Monitor
127°
e⁻ Beam
Scattering
Target
90°
Pb Collimator
Ta–Bremsstrahlung
Converter
Ge(Li) Detector
500mm

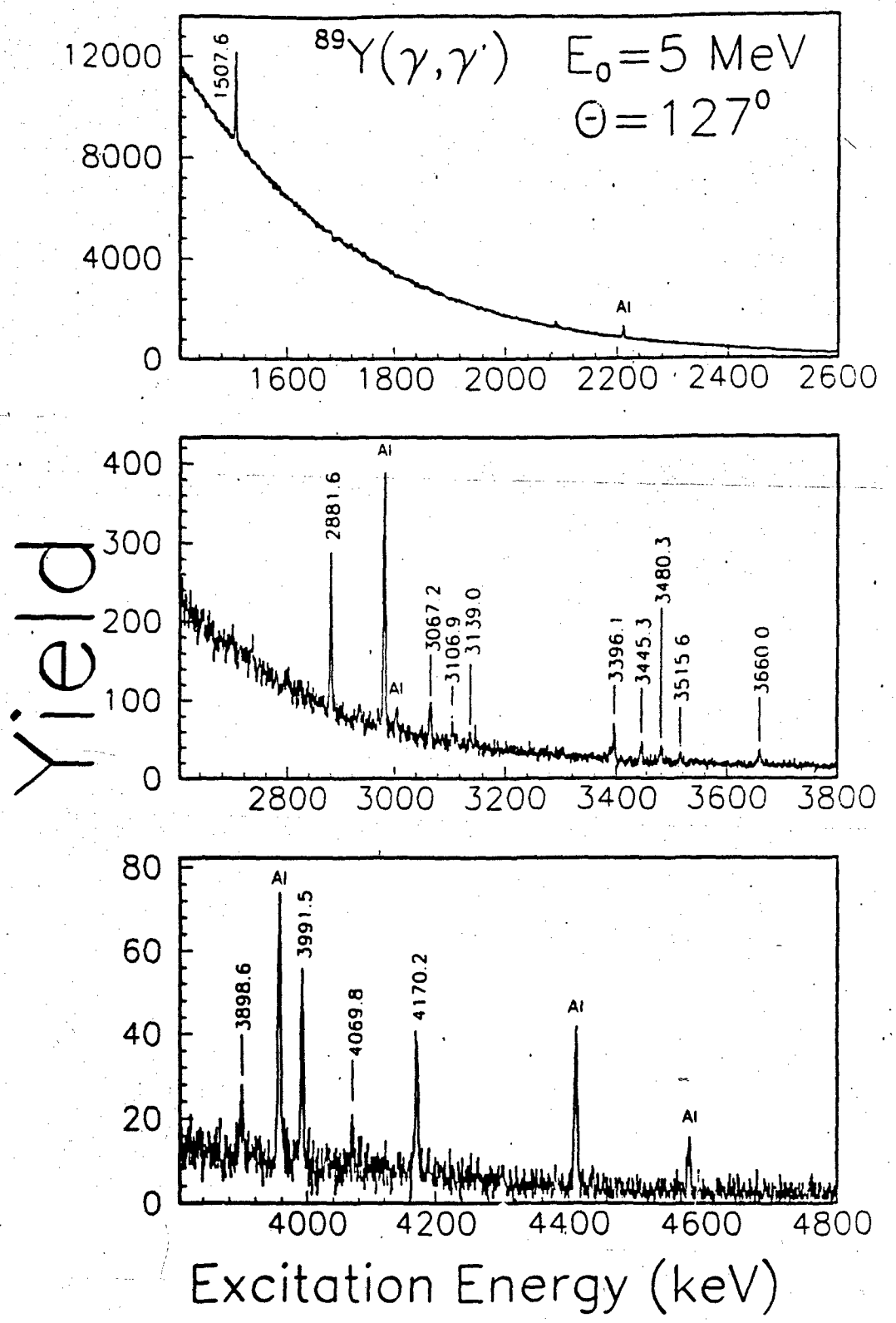
$^{89}Y(\gamma,\gamma')$ E_0=5 MeV
Θ=127°
1507.6
Al
2881.6
3067.2
3106.9
3139.0
3396.1
3445.3
3480.3
3515.6
3660.0
3898.6
3991.5
4069.8
4170.2
Yield
Excitation Energy (keV)

Fig. 2

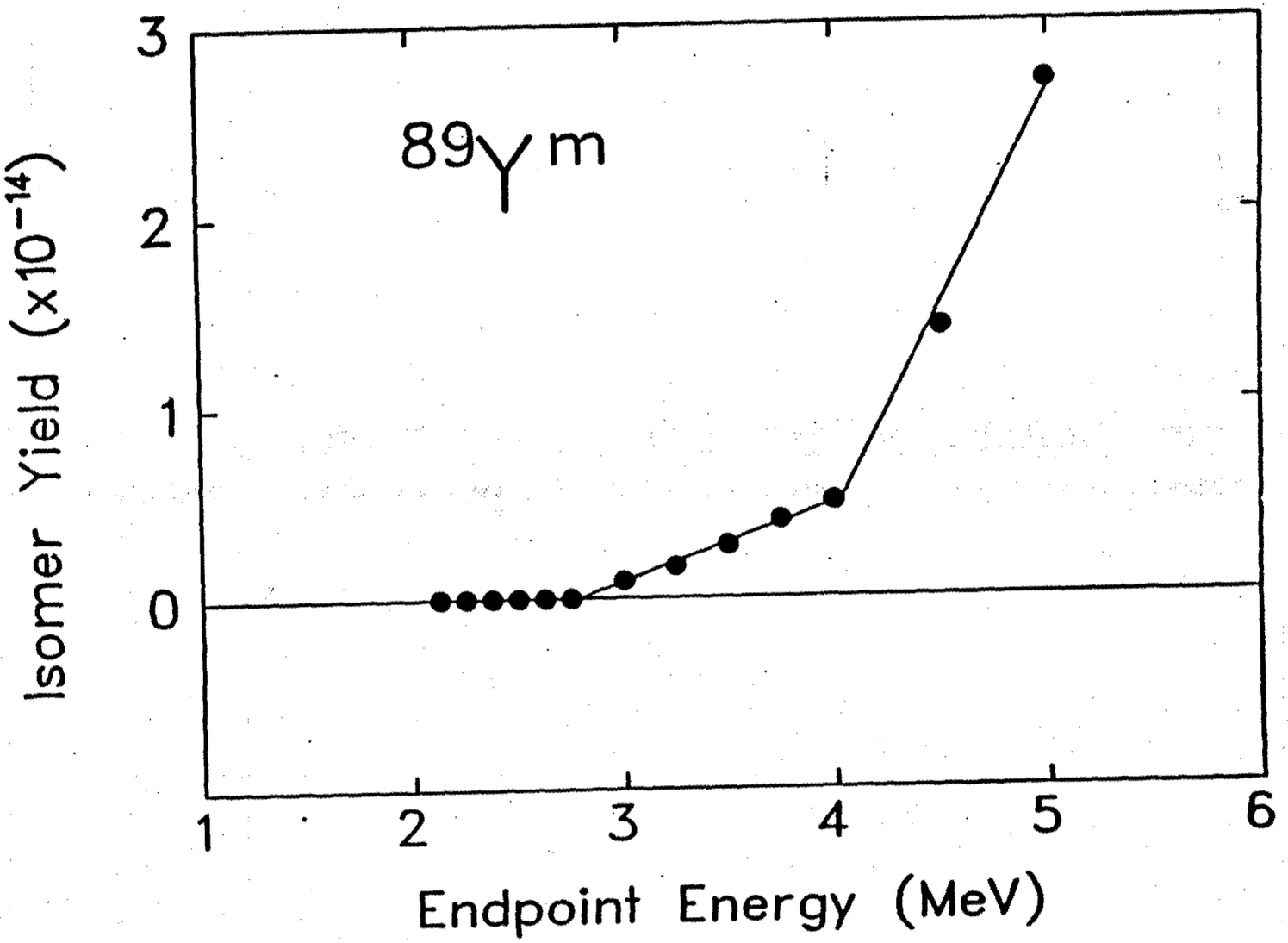

Fig. 3

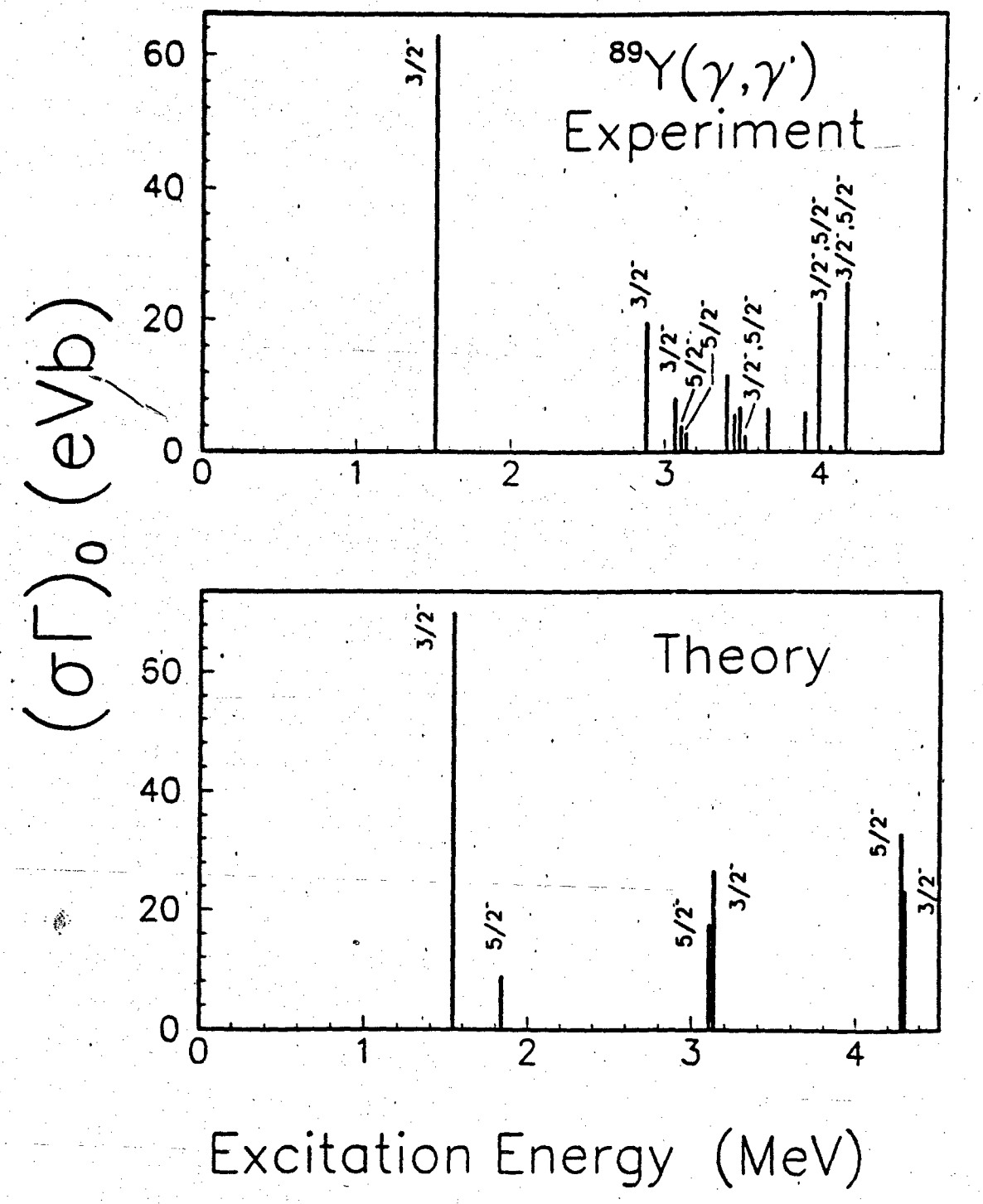
$^{89}Y(\gamma,\gamma')$
Experiment
Theory
$(\sigma\Gamma)_0$ (eVb)
Excitation Energy (MeV)
3/2⁻
5/2⁻
0
20
40
60
1
2
3
4

Fig. 4

^{89}Y

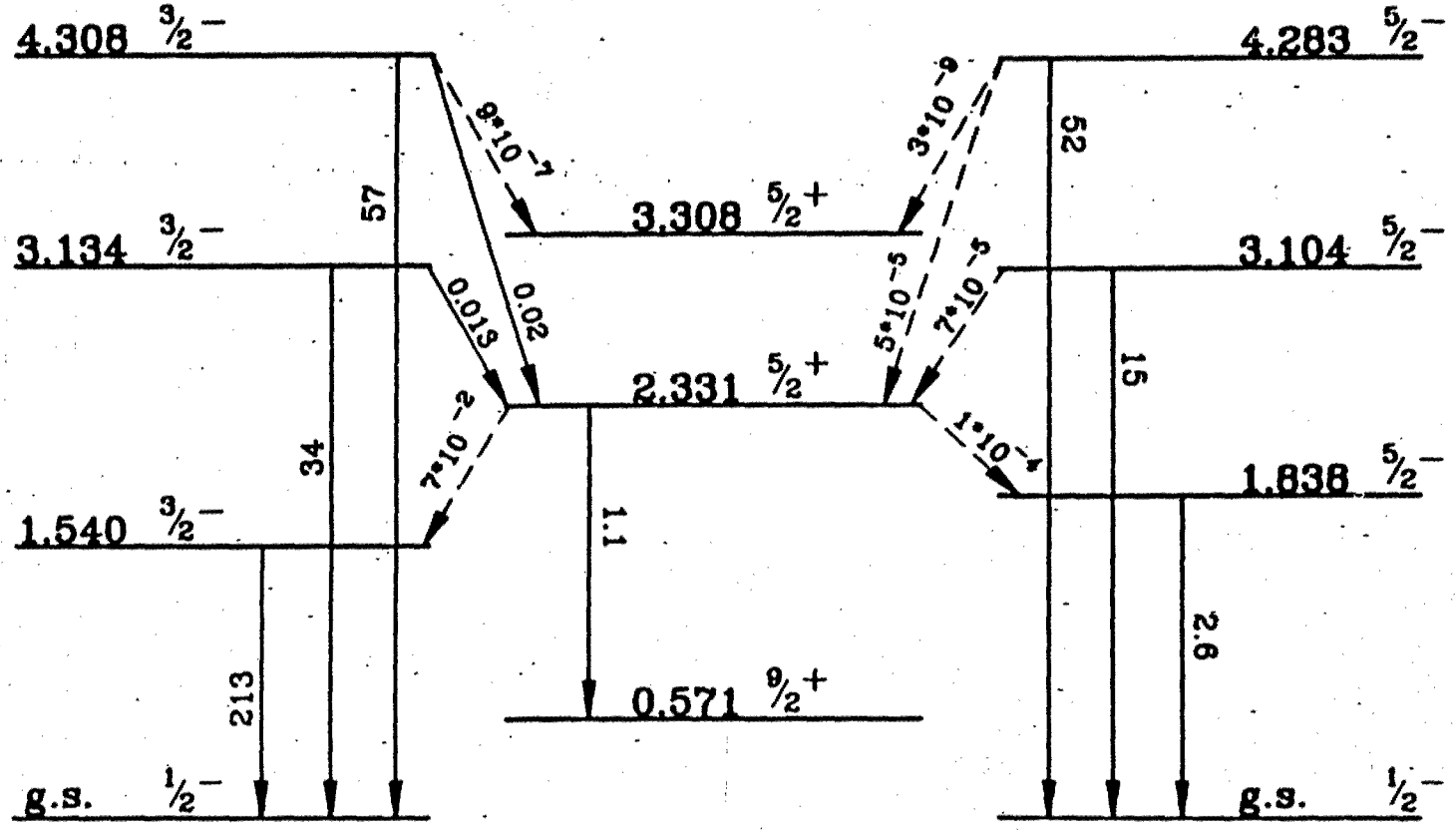
4.308 3/2−
3.134 3/2−
1.540 3/2−
g.s. 1/2−
3.308 5/2+
2.331 5/2+
0.571 9/2+
4.283 5/2−
3.104 5/2−
1.838 5/2−
g.s. 1/2−
57
34
213
0.02
0.013
11
52
15
2.6
9*10−7
7*10−2
3*10−9
5*10−5
7*10−5
1*10−4

Fig. 5

MANUSCRIPT SHEET This 11 x 14 sheet will be reduced to 77% of its present size, making maximum type area 6½ x 9". CODE NO.

Start typing all but Title Page on Line 1. Type up to, but not beyond, the blue margin lines at left and right. Do not type on printed guide numbers above the lines.

THE GAMMA-RAY LASER: ISSUES AND PROGRESS IN 1990

J. J. Carroll, C. B. Collins, T. W. Sinor, K. N. Taylor and D. G. Richmond
The University of Texas at Dallas, Center for Quantum Electronics
P. O. Box 830688, Richardson, Texas 75083-0688

A gamma-ray laser would produce shorter wavelengths than x-ray lasers and with much greater output due to the unique advantages of nuclear systems. In nuclei, a variety of electromagnetic transition moments occur and thus the constant linking ν^3 with the spontaneous lifetime is orders of magnitude more favorable than at the atomic level. Input pump energy can therefore be integrated for longer times to larger values. These γ-ray transitions routinely have natural linewidths which would insure large cross sections for stimulated emission. Finally, nuclear metastable states, called isomers, can store keV to MeV for years, giving teraJoules per liter at solid densities.

Despite this impetus, traditional research on the gamma-ray laser had reached an impasse in 1981. Those failed approaches required nuclei to be pumped with particle fluxes which would deposit unmanageable amounts of heat in the host material. The impossibility of a gamma-ray laser based on those schemes was detailed in the encyclopedic review of Ref. 1.

A new concept of optical pumping was introduced[2] in 1982 and showed a way to proceed. The theory predicted a clear feasibility of the gamma-ray laser if a nucleus could be found whose properties were sufficiently close to the models of Fig. 1. The simplest of the new schemes is the nuclear analog to the ruby laser shown in Fig. 1 a). The pumping process, called a (γ,γ') reaction, has been known to nuclear physicists for over 50 years, although poorly characterized when compared to particle reactions. Since 1986 precision measurements of these reactions have demonstrated nuclear bandwidth funneling with large effective widths, $b_c b_s \Gamma$ for populating isomers.

The most attractive pumping scheme is that of Fig. 1 b) where upconversion is made possible by pumping isomers with lifetimes of years. In this case most input energy is in place long before use and in-situ pump requirements would be small. However, these favorable half-lives for energy storage result from the large difference in angular momentum between isomers and freely radiating states so the initial perception was that transitions like that of Fig. 1 b) could not occur.

The dumping of the stored energy of an isomer by a (γ,γ') reaction was first shown in 1988 for the rare nuclide $^{180}Ta^m$, which exists naturally as 100% inverted. A milligram sample was irradiated with bremsstrahlung and fluorescence due to decay of the ground state was observed.[3] This represented a useful absorption width of nearly 0.5 eV. More recent experiments[4] with an x-ray source tunable between 2 and 5 MeV have pinpointed the energies for two isolated pump states with integrated cross sections each in excess of 10^4 in the usual units of 10^{-29} cm^2 keV. These are more than an order of magnitude larger than values previously observed for any (γ,γ') reaction and are 10^4 larger than usual values for populating isomers.

Absorption through funneling states like these takes place at resonances which are narrow with respect to the broad pump continua. The cross sections within these widths are much larger than those for excitation of these transitions by particles and are comparable to values for photoelectric absorption. Therefore an optically pumped gamma-ray laser could be constructed from suitable nuclei diluted in a thin lattice of low Z atoms such as C. The technology for producing thin diamond films is now advanced to the point of commercialization.[5] Useful energy would then be absorbed by the active nuclei even in a one micron layer while little heat could be deposited by the primary electrons produced by nonresonant absorption.

The study of (γ,γ') reactions has shown that there are no a priori obstacles to a gamma-ray laser. More important, the results of Refs. 3 and 4 have increased the feasibility of the optically pumped gamma-ray laser by 10^4 over that envisioned in 1982. The primary problem remaining is to identify which nucleus has the right combination of energy levels and this defines the direction of future research. An extensive review of the progress towards the gamma-ray laser can be found in Ref. 6.

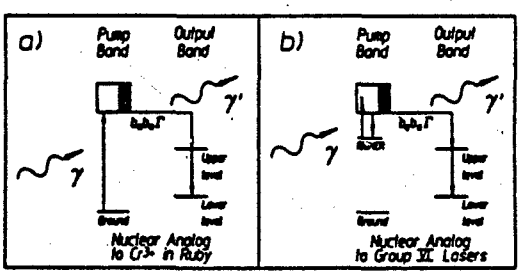

Figure 1. Schematic representation of the priority schemes for pumping a gamma-ray laser with flash x-rays.
a) Three-level laser (nuclear analog to ruby laser)
b) Three-level laser with upconversion.

References

1. Baldwin G. C., Solem J. C., and Goldanskii V. I., Rev. Mod. Phys. 1981, 53, p 687.
2. Collins C. B., Lee F. W., Shemwell D. M., DePaola B. D., Olariu S., and Popescu I., J. Appl. Phys. 1982, 53, p 4645.
3. Collins C. B., Eberhard C. D., Glesener J. W., and Anderson J. A., Phys. Rev. C 1988, 37, p 2267.
4. Collins C. B., Carroll J. J., Sinor T. W., Byrd M. J., Richmond D. G., Taylor K. N., Huber M., Huxel N., v. Neumann-Cosel P., Richter A., Spieler C., and Ziegler W., Phys. Rev. C 1990, 42, p R1813.
5. Davanloo F., Juengerman E. M., Jander D. R., Lee T. J., and Collins C. B., J. Appl. Phys. 1990, 67, p 2081.
6. Collins C. B., Carroll J. J., Sinor T. W., Taylor K. N., and Richmond D. G., J. Appl. Optics (pending).

Do not type or paste anything below this line.

Do not type anything on this line.

Do not type anything on this line.

Write Author's Last Name

THE GAMMA-RAY LASER: ISSUES AND PROGRESS IN 1991

J. J. Carroll, C. B. Collins, K. N. Taylor, T. W. Sinor,
C. Hong, J. D. Standifird, and D. G. Richmond
The University of Texas at Dallas, Center for Quantum Electronics
P.O. Box 830688, Richardson, Texas 75083-0688

ABSTRACT

A gamma-ray laser would stimulate the emission of radiation at wavelengths below 1 Å from excited states of nuclei. The difficulties in realizing such a device were considered insurmountable when the first cycle of study ended in 1981. Since then, research on the feasibility of a gamma-ray laser has taken a completely new character. A nuclear analog of the ruby laser has been proposed and many of the component steps for pumping the nuclei have been demonstrated experimentally. A computation based upon the new data and concepts of this decade shows the gamma-ray laser to be feasible if some real isotope has its properties sufficiently close to the ideals modeled.

INTRODUCTION

At the nuclear level, long-lived excited states are known as isomers. Nuclear metastable populations can store tera-Joules (10^{12} J) per liter at solid densities for thousands of years meaning that it would not be necessary to pump a gamma-ray laser medium entirely in situ. For some cases the excited nuclei could be bred in a reactor by neutron capture or other nuclear reactions acting upon precursive elements.

The problem of suddenly assembling a critical density of prepumped nuclei to reach the threshold for stimulated emission received much attention in a first cycle of study (1963-1981). It was generally concluded that such single photon brute force approaches were essentially hopeless and the encyclopedic review of Baldwin, et al.[1] described the general impossibility of a gamma-ray laser based upon all techniques for pumping known in 1980. That review effectively terminated all traditional lines of approach to a gamma-ray laser. However, those lines had emphasized the use of intense particle fluxes for input energy.

The precursors of a new interdisciplinary approach[2-8] appeared near the end of this first cycle and launched a renaissance in the field. The basic theory[9-11] for pumping at the nuclear level was in-place by 1982 for the two possible variants, coherent and incoherent upconversion. Either multiphoton processes or multiple electromagnetic transitions could be used to release the energy stored in isomers to avoid many of the difficulties encountered with more traditional pumping schemes.

In the decade since 1980, research on the feasibility of a gamma-ray laser has taken a completely new character. The first half decade verified that the concepts of quantum electronics could be applied at the nuclear level.[12-16] By 1986 the blueprint for the a gamma-ray laser[11] had been established and substantial effort was initiated toward the demonstration of feasibility. This article reviews the major advances of the past five years that have significantly increased the likelihood of the feasibility of a gamma-ray laser.

CONCEPTS

The basic ν^3 dependence of electron transition probabilities so limits the storage of pump energies[1] that even now some of the largest pulsed-power machines are able to excite only milliJoules of x-ray laser output at soft photon energies. In contrast there are four unique advantages of a gamma-ray laser arising from its operation upon electromagnetic transitions of nuclei:

1) The constant linking ν^3 with lifetime is more favorable by orders-of-magnitude because of the accessibility of a variety of transition moments. Thus input pulses can be integrated for longer times to greater values.
2) Nuclear metastables store keV and even MeV for years. With upconversion schemes most of the pump power is input long before the time of use and triggering requirements are small.
3) Nuclear transitions routinely exhibit natural linewidths. Without broadening electromagnetic cross sections are large and values for 1 Å transitions typically exceed the cross section for the stimulation of Nd in YAG.
4) Working metastables can be concentrated to solid densities.

The essential concept driving the renaissance in gamma-ray laser research was the "optical" pumping of nuclei with x rays. Useful, resonant absorption of pump power would occur over short distances while wasted wavelengths would only be degraded to heat in much larger volumes. Of the cases considered,[11] the nuclear analog of the ruby laser embodied the simplest concepts for a gamma-ray laser. Not surprisingly, the greatest rate of achievement in the last five years has been realized in that direction and this review will be limited to the results along that line.

For ruby, bandwidth funneling was the critical key to the development of the first laser. A broad absorption band was linked through efficient cascading to the narrow laser level. Our theory[11] proposed a nuclear analog of this structure which was unknown in 1986 when intensive experiments were started for SDIO. Now, that theory has been confirmed.

The principal figure of merit for any bandwidth funnel is the partial width for the transfer, $b_e b_0 \Gamma$. Figure 1 identifies the branching ratios b_e and b_0 which specify the probabilities that a population pumped by absorption into the j-th broad level

will decay back into the initial or fluorescent levels, respectively. The sum of branching ratios is seldom unity but the maximum value of partial width for a particular level j occurs when $b_a = b_o = 0.5$.

These "optical" pumping processes have been known in nuclear physics as (γ,γ') reactions for over 50 years[17,18] although relatively few results have been published since that time. Practical difficulties with the calibration and availability of sources of irradiation had limited the degree of reproducibility achieved in earlier work even for the most tractable (γ,γ') reactions for study, those for the photoexcitation of stable isotopes up to isomeric levels. Fluorescence can then be observed after the termination of the input irradiation and lessons can be learned that can be applied to the excitation of shorter-lived, more laser-like levels. The archetypical case for study has been the reaction $^{111}Cd(\gamma,\gamma')^{111}Cd^m$ exciting the 48.6 min level at 396 keV. Three of the most recent measurements[19-21] of the fluorescence efficiency were conducted in 1979, 1982, and 1987. Probable errors were quoted as varying only from 7 to 14%, and yet no two of the measurements were even within a factor of 2 of each other. This discrepancy led to serious contentions over the way in which the expected fluorescence yields were calculated[20] so one of our early challenges was to place the "optical" pumping of nuclei onto a firm quantitative basis.

Most intense x-ray sources emit continua, either as bremsstrahlung or as spectral lines degraded by Compton scattering in the immediate environment. The time-integrated yield of final-state nuclei, N_f obtained by irradiating N_i initial targets with a photon flux Φ_o in photons cm^{-2} delivered in a continuum of intensities up to an endpoint energy E_o is,

$$N_f = N_i \Phi_o \int_0^{E_o} \sigma(E) F(E,E_o) dE \quad . \tag{1}$$

where $F(E,E_o)$ is the distribution of input intensities normalized to integrate to one over the range of photon energies, and $\sigma(E)$ is the effective cross section for the excitation of the final state from the initial. All (γ,γ') reactions occurring at energies below the threshold for particle evaporation excite discrete intermediate states or gateways like the level j shown in Fig. 1 which branches to some extent into the fluorescence level, f.

Although broad on a nuclear scale, the width of level j is narrow compared to the broad input continuum. The final-state yield is then expressed as the normalized activation per unit photon flux, $A_f(E_o)$.

$$A_f(E_o) = N_f / (N_i \Phi_o) = \sum_j (\sigma\Gamma)_{fj} F(E_j,E_o) \quad . \tag{2a}$$

The $(\sigma\Gamma)_{fj}$ is the integrated cross section for the production of final-states through the excitation of the intermediate state with energy E_j so that

$$(\sigma\Gamma)_{fj} = \int_{E_j-\Delta}^{E_j+\Delta} \sigma(E) dE \quad . \tag{2b}$$

where Δ is an energy small compared to the spacing between intermediate states and large in comparison to their widths. The integrated cross section can be written as

$$(\sigma\Gamma)_{fj} = (\pi b_a b_o \Gamma \sigma_o/2)_{fj} \quad . \tag{3}$$

where $\sigma_o/2$ is the peak of the Breit-Wigner cross section for the absorption step, and $\sigma_o \sim \lambda^2$ where λ is the wavelength of the gamma ray at the resonant energy, E_j.

PUMP CALIBRATION

The most unreliable sources of x rays used in early studies of (γ,γ') reactions seem to have been the nuclear sources. Although assumed to emit line spectra, they actually produced continua dominated by multiple Compton scatterings of photons in the irradiation environment. Such multiple scatterings are difficult to calculate and still impossible to measure in practical laboratory configurations. In contrast, bremsstrahlung spectra are routinely calculated with high accuracy from measured accelerator currents and target geometries by well-established computer codes.[22]

In our experimental work of the last five years the bremsstrahlung from five accelerators was used to verify the model of Eqs. (1) - (3) and to cross-check the accelerator calibrations. These devices were DNA/PITHON at Physics International, DNA/Aurora at the Harry Diamond Laboratories, a 4 MeV and a 6 MeV medical linac at the University of Texas Health Sciences Center, and the superconducting injector to the storage ring at Darmstadt (S-DALINAC). Spectra were calculated with the EGS4 coupled electron/photon transport code[22] adapted for each experiment, giving both $F(E,E_o)$ and Φ_o. In some cases Φ_o was verified by in-line dosimetry.

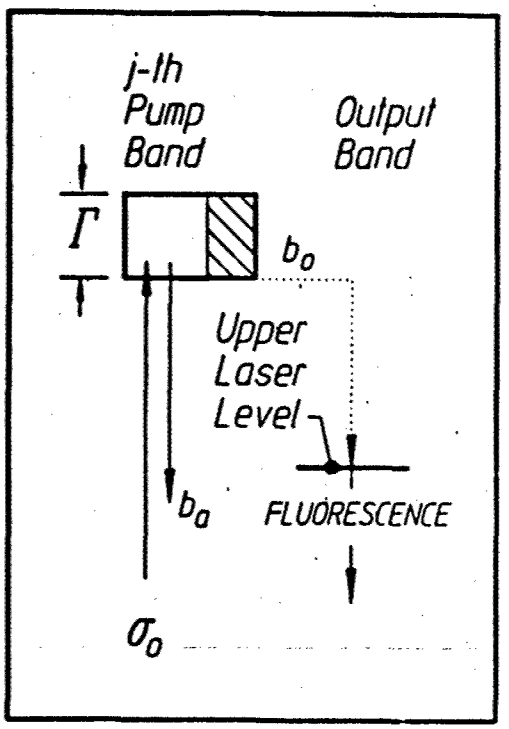

Figure 1: Schematic representation of the decay modes of a gateway state of width Γ sufficiently large to promote bandwidth funneling. The initial state from which population is excited with an absorption cross section σ_0 can be either ground or isomeric.

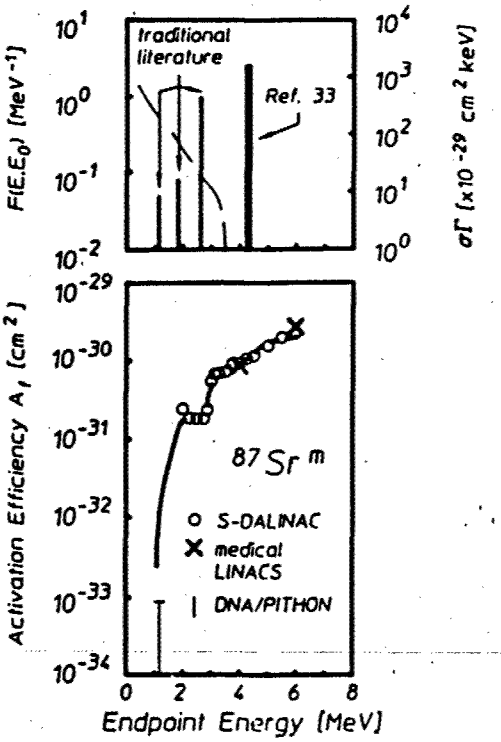

Figure 2: Activation efficiencies, A_f for the reaction $^{87}Sr(\gamma,\gamma')^{87}Sr^m$ are shown in Fig. 2b (lower) as functions of the endpoint, E_0 of the bremsstrahlung used for excitation. The solid curve in Fig. 2b plots values computed from Eq. (2a) using the gateway parameters found in the literature and plotted with the right axis in Fig. 2a (upper) together with calculated photon spectra like that given by the dashed line and plotted with the left axis in Fig. 2a. Figure 2b compares these A_f values with measurements obtained from four different accelerators.

Table I

Summary of nuclides, pump lines, and integrated cross sections for the excitation of delayed fluorescence suitable for use as calibration standards.

	PUMP LINE (keV)	$(\sigma\Gamma)_{fj}$ (10^{-29} cm^2 keV)
^{79}Br	761	6.2
^{77}Se	250	0.20
	480	0.87
	818	0.7
	1005	30
^{115}In	1078	20

The literature[23] supports the calculation of integrated cross sections for very few systems useful for validating Eqs. (1) through (3). Table I summarizes those which are known with sufficient accuracy to have served as standards for the first studies. In units of 10^{-29} cm^2 keV, values range from the order of unity to a few tens for bandwidth funnels that are sufficient to demonstrate nuclear fluorescence from grams of material at readily accessible levels of input.

In our experiments samples were exposed to the bremsstrahlung from the five accelerators. The activations, A_f of Eq. (2a) were determined by counting fluorescence photons emitted from the samples after transferring them to a quieter environment.

Usual corrections were made for the isotopic abundances, the finite isomer lifetimes, the counting geometry, the self-absorption of the fluorescence, and the tabulated efficiencies[23,24] for the emission of signature photons per decay. The self-absorption correction was verified in some cases by examining the fluorescence yield arising from samples of the same mass and material in different geometries.

Results were in close agreement[25] with the predictions of Eq. (2a) used with the values of $(\sigma\Gamma)_{ij}$ shown in Table I. That work established a confidence level supporting the use of nuclear activation as a means of selectively sampling spectral intensities.[26] Having calibrated the spectral sources, the persisting uncertainties in the optical pumping of nuclei like $^{115}In^{m}$ and $^{111}Cd^{m}$ were resolved.[27,28]

To establish even better calibration standards, we reexamined the reaction $^{87}Sr(\gamma,\gamma')^{87}Sr^{m}$, principally with the S-DALINAC because the endpoint of its bremsstrahlung could be varied. Changing the endpoint energy, E_0 of the bremsstrahlung modulates the spectral intensity $F(E_j,E_0)$ at all the resonant excitation energies E_j. The largest effect occurs when E_0 is increased from a value just below a gateway at E_j to a value exceeding it as shown in Fig. 2a.

Early work[29] on the ^{87}Sr reaction showed that a plot of $A_f(E_0)$ vs. bremsstrahlung endpoint energy displayed pronounced activation edges at the energies, E_j corresponding to the resonant excitation of new intermediate states. These edges identified new gateways for the particular reaction.

The activation efficiencies, A_f calculated from Eq. (2a) using the literature values[29] plotted in Fig. 2a are shown in Fig. 2b together with the measurements obtained with four accelerators. The agreement is very good between the different accelerators and between the experimental data and the model calculations. The units of A_f are those of area but they are a type of average cross section quite different from the σ_0 of Eq. (3) that describe individual transitions. The small values are the result of the broad bandwidth of the pump continuum in which most $E \neq E_j$.

These calibration studies confirmed both the model of nuclear activation of Eqs. (1) - (3) and validated the EGS4 code for calculating bremsstrahlung intensities from measured accelerator parameters. *Now, there can be no reasonable doubt of procedures for quantitatively measuring fluorescence efficiencies if experiments are carefully performed with bremsstrahlung sources.*

GIANT PUMPING RESONANCES

Expressed as partial widths the integrated cross sections for the excitation of the isomers seen in Table I range from 5 to nearly 100 μeV. These results left an aura of credibility to the traditional impressions that partial widths for exciting isomers would be limited to about 1 μeV.

Tempering expectations that integrated cross sections of even this size might occur for dumping of isomeric candidates for a gamma-ray laser were concerns for the conservation of projections of the nuclear angular momenta. Many of the candidates belong to the class of nuclei deformed from the normally spherical shape for which the dominant quantum number is K, the projection of individual nucleonic angular momenta upon the axis of elongation. To this is added the collective rotation of the nucleus to obtain the total angular momentum J. The resulting system of energy levels resembles those of a diatomic molecule for which

$$E_n(K,J) = E_n(K) + B_n J(J+1) \quad , \qquad (4)$$

where $J \geq K \geq 0$ and J takes values $|K|, |K|+1, |K|+2, \ldots$. In this expression B_n is a constant and $E_n(K)$ is the lowest energy for any level in the resulting "band" identified by other quantum numbers n. The selection rules for electromagnetic transitions require $|\Delta J| \leq M$ and $|\Delta K| \leq M$, where M is the multipolarity of the transition.

For deformed nuclei, the isomer has a large lifetime because its value of K differs considerably from those of lower, freely-radiating levels. Thus bandwidth funneling like that shown in Fig. 1 must span substantial ΔK and component transitions have been expected to have large, and hence unlikely, multipolarities.

From this perspective the candidate isomer, $^{180}Ta^{m}$ was the most initially unattractive as it had the largest change of angular momentum between isomer and ground state, 8ħ. However, because it was the only isomer for which a macroscopic sample was readily available, $^{180}Ta^{m}$ became the first isomeric material to be optically dumped to a fluorescent level.

This isomer carries a dual distinction. It is the rarest stable isotope occurring in nature and it is the only naturally occurring isomer. The actual ground state of ^{180}Ta is 1^{+} with a halflife of 8.1 hours while the tantalum nucleus of mass 180 occurring with 0.012% natural abundance is the 9^{-} isomer, $^{180}Ta^{m}$. The isomer has an adopted excitation energy of 75.3 keV and halflife in excess of 1.2×10^{15} years.[30]

In 1987 we exposed 1.2 mg of $^{180}Ta^{m}$ to the bremsstrahlung from the 6 MeV linac and obtained a large fluorescence yield.[31] This was the first time an isomer had been dumped by a (γ,γ') reaction as needed for a gamma-ray laser and was the first evidence of the existence of giant pumping resonances. Simply the observation of fluorescence from a milligram sized target proved that an unexpected reaction channel had opened since grams of material are usually required in this type of experiment. Analyses[31,32] of the data indicated that the partial width for the dumping of $^{180}Ta^{m}$ was around 0.5 eV.

The gateway energies, E_j for the $^{180}Ta^m$ dumping reaction were determined from experiments using the S-DALINAC.[33] An activation edge was clearly seen in the data shown in Fig. 3b. Values for $(\sigma\Gamma)_{fj}$ were obtained from Eq. (2a) to determine the integrated cross sections for the dumping of $^{180}Ta^m$ isomeric populations into freely-radiating states. Reported values[33] are summarized in Table II and shown schematically in Fig. 3a.

Table II

Recently measured values of integrated cross section, $(\sigma\Gamma)_{fj}$ for the reaction $^{180}Ta^m(\gamma,\gamma')^{180}Ta$. The gateway excitation energies, E_j for these levels are given at the centers of the ranges of energies that could be resolved experimentally.

Energy (MeV)	$(\sigma\Gamma)_{fj}$ (10^{-29} cm^2 keV)
2.8 ± 0.1	12000 ± 2000
3.6 ± 0.1	35000 ± 5000

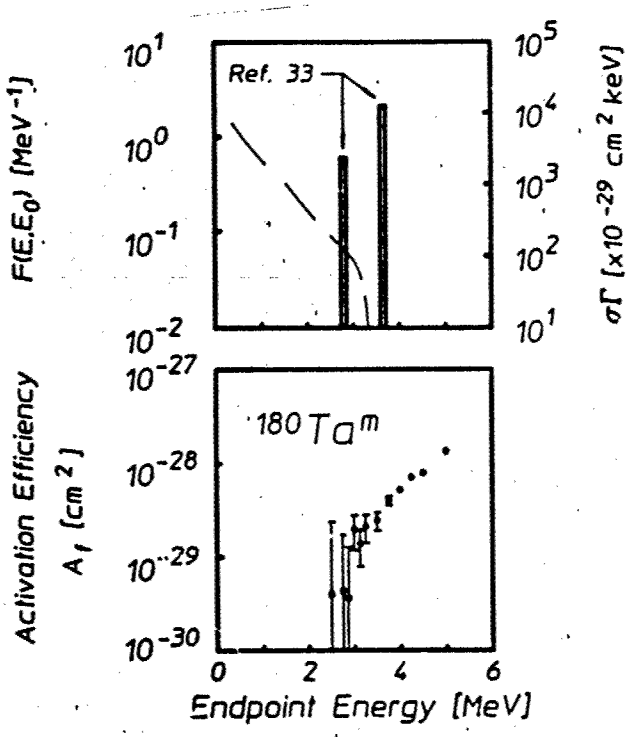

Figure 3: Activation efficiencies, A_f for the reaction $^{180}Ta^m(\gamma,\gamma')^{180}Ta$ are shown in Fig. 3b (lower) as functions of the endpoint, E_0 of the bremsstrahlung used for excitation. Gateway parameters obtained by fitting the data using Eq. (2a) are plotted with the right axis in Fig. 3a (upper). These parameters were determined using calculated photon spectra like that given by the dashed line and plotted with the left axis in Fig. 3a.

The values in Table II are enormous, exceeding anything previously reported for transfer through a bandwidth funnel by two orders of magnitude. In fact they are 10,000 times larger than the values usually measured for nuclei. This proves that the restrictive guidelines customarily applied to optical pumping of nuclei are nearly 10^6 times too pessimistic.

The width of the transfer process is difficult to interpret and a complex puzzle is also found in the efficiency with which ΔK is transferred. An interesting speculation is that at certain excitation energies, collective core oscillations break some of the symmetries by which pure single-particle states are identified. Admixtures of single-particle states of differing K would enhance the transfer of larger amounts of ΔK with greater partial widths. Support for this idea was found in recent measurements for the deexcitation of the $^{174}Hf^m$ isomer.[34] The decay of that isomer to the ground state was found to occur primarily through an intermediate state lying at 2685 keV in which K mixing occurred so that $\Delta K = 14$ was lost. This is remarkably close to the energy of the K-mixing level at 2800 ± 100 keV for ^{180}Ta. The close similarity of the energetics shown in Fig. 4 for nuclei with

such dissimilar single-particle structures supports the identification of this K-mixing process as a core property varying only slowly among neighboring nuclei.

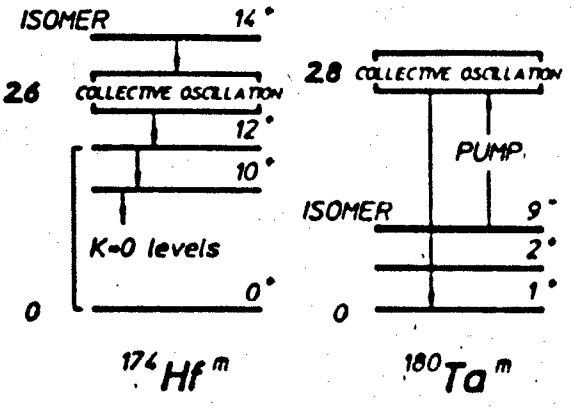

Figure 4: Energetics for the spontaneous decay of $^{174}Hf^{m}$ through an intermediate state providing $\Delta K=14$ compared with those for the dumping of $^{180}Ta^{m}$ through a similar intermediate state. In the case of $^{180}Ta^{m}$, the dumping reaction provides $\Delta K=8$. Both gateways are expected to be admixtures of single-particle states, thereby producing significant K mixing.

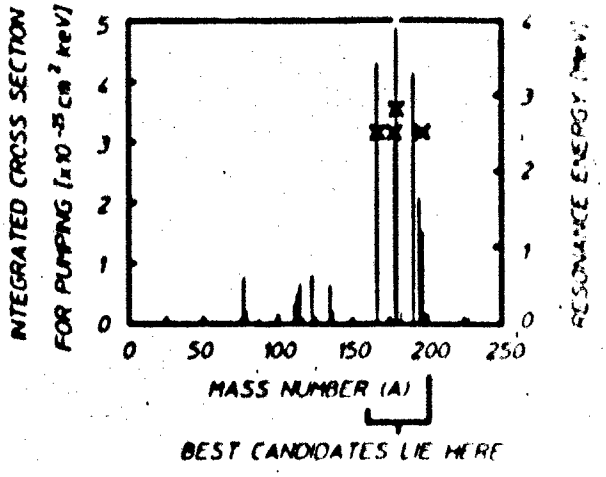

Figure 5: Integrated cross sections for pumping isomeric nuclei obtained in the survey of Refs. 35 and 37. The groupings correspond to mass islands between magic numbers for neutrons and protons. The best candidates for a gamma ray laser lie within the mass 180 island. Within each island the integrated cross sections and the excitation energies of the giant pumping resonances, indicated by the X symbols, vary only slowly with changing mass number, A.

A survey of nineteen isotopes[35] conducted with the four U.S. accelerators over a fairly coarse mesh of bremsstrahlung endpoints demonstrated that giant pumping resonances for breaking K were common among nuclei neighboring ^{180}Ta. Figure 5 shows how the integrated cross sections for pumping or dumping isomers vary slowly with changing A in this mass region and continue to be on the order of 10,000 times greater than usual values. Large pumping resonances were also indicated for masses near 120 and this was confirmed by a higher resolution study using the S-DALINAC.[36] More importantly, improved systematics[37] were recently obtained with the S-DALINAC for four isotopes near mass 180. The excitation energies of the pumping resonances were determined as given in Fig. 5. The locations of those resonances as well as their integrated cross sections were shown to vary little among neighboring masses.

Whatever the mechanisms, the experimental fact remains that interband-transfer processes connecting to isomeric levels can be pumped through enormous partial widths reaching 0.5 eV, even when the transfer of angular momentum must be as great as $\Delta K = 8$, or even $\Delta K = 14$. It seems this is the nuclear analog of the giant resonance for pumping ruby at the atomic level. Elucidation of the process has been propelled into a place of future importance.

CONCLUSIONS - A LASER MODEL

The 1990's model of a gamma-ray laser is fundamentally identical to the nuclear analog of the ruby laser described[11] in 1982. A thin film of diluent would be doped with isomeric nuclei and pumped with a flash of x rays. For this model the question remains whether or not the properties of some real nuclide approach those of the ideal. The discovery of giant pumping resonances relaxes some of the original constraints and improves the feasibility of a gamma-ray laser by orders-of-magnitude over the estimate of 1982. Thus the model can be recomputed in terms of the new data of the past five years.

Since the better candidate isomers for a gamma-ray laser have never been fabricated in macroscopic amounts, the precise identity of the best nuclide to model is not known. Therefore the assumptions introduced for this model critically affect the estimates of feasibility in strongly nonlinear ways. These were:

1) The pump band is one of the newly discovered giant pumping resonances with a partial width of $b_e b_o \Gamma = 1$ eV.
2) The pump transition is centered on an energy $E_j = 30$ keV.
3) The initial state is assumed to be isomeric with an excitation energy so high that 2) is possible.
4) The output transition is around 100 keV.
5) The nuclei are diluted in a thin film of diamond or Be.
6) The Borrmann effect enhances the ratio of resonant to nonresonant absorption by 10 x.

The most sensitive assumptions are those of statements 2) and 3) but there is a large range of excitation energies for isomers. We have already shown that isomers can be dumped into freely radiating states even though $\Delta K > 8$ so there is only a statistical doubt whether or not a giant pump resonance can be found within 30 keV of an isomer.

Under small signal conditions[11] the mid-range requirement is obtained for the pumped fraction $N_f / N_o = 10^{-4}$. This sets the pump intensity needed for threshold and with it the amount of waste heat to dissipate. To manage the thermal economy the mean free path (MFP) for a photon resonant with the nuclear transition must be much shorter than the MFP for nonresonant photoelectric absorption to produce heat. Also the MFP for a photoelectron produced in the nonresonant channel must be greater in the diluent than the MFP for the pump photons. This means that a thin film of diamond can be doped to use most of the incident photons in the bandwidth of the giant pumping resonance while the majority of the nonresonant photons will pass through the film into the substrate which can be cooled by ablation or cryogenics. Any primary photoelectrons will then escape before their energy is degraded to heat.

Assuming a single giant resonance dominates so that the sum is unnecessary in Eq. (2a) and solving for $\phi_t = \phi_o F(T, E_o)$, 30 keV pump photons would give a spectral fluence at threshold of $F_t = E_t \phi_t \geq 177$ mJ cm^{-2} eV^{-1}. For the likely cases of rare earth or platinide elements, the 30 keV pump energy lies below the K edge and about 15 keV above the L edge. As a result, primary photoelectrons should have energies of the order of 15 keV and ranges of 6.0 and 3.0 μm in Be and C respectively[38]. Thus, only about 10% and 20% of the primaries, respectively, should be stopped in a host film of Be or diamond with a thickness of 0.67 μm corresponding to the MFP for resonant absorption at a concentration of 10%. Then the fractions of the incident pump energy which are degraded into heat in the laser film because of nonresonant absorption are $f(Be) = 4.8 \times 10^{-4}$ and $f(C) = 2.4 \times 10^{-4}$.

Edge filters or ablation layers could reduce the pump bandwidth to 3 keV so the incident fluence lying outside the bandwidth for resonant absorption would be 3000 times greater than the value found above. However, only the fractions f(Be) and f(C) can be degraded into heat. The resulting fluences degraded to heat for Be and diamond are 127 mJ cm^{-2} and 255 mJ cm^{-2}, respectively.

The thermal energy loading of the laser film is 1.9 kJ cm^{-3} for Be and 3.8 kJ cm^{-3} for diamond. These values are quite significantly below the levels of heating required to degrade the recoil-free fractions for the host lattice. Baldwin has summarized[1] the dependence of the recoil-free fraction of gamma transitions upon recoil energy, lattice parameters, and temperature. He shows that even at a temperature, $T=\Theta_D$, the Debye temperature, the recoil-free fraction is not significantly degraded (by more than a factor of 2) even for a transition giving a classical recoil energy of $0.14\ \Theta_D$. In diamond with $\Theta_D = 2230$ K this means a transition of 100 keV is little affected by a temperature increase up to $T = \Theta_D$. The energy content of the phonons of a material with $\Theta_D = 2230$ K at a temperature of $T = \Theta_D$ is estimated[39] to be about 11 kJ cm^{-3}. The estimated loading of 3.8 kJ cm^{-3} gives a "safety factor" of almost three for C with a comparable margin for Be.

The spectral fluence of 177 mJ cm^{-2} eV^{-1} corresponds to 530 J cm^{-2} for a pump bandwidth of 3 keV. Ever if pumped instantaneously the thermal loading would reach only 1/3 of the limit for retaining the Mössbauer effect. If derived from an x-ray line of 30 eV width, the threshold fluence would be only 5.3 J cm^{-2} and the thermal loading would reach only 1/300 of the critical limit for a diamond lattice.

Much can be done to reduce heating further. The above calculations assumed the instantaneous generation of the waste heat. The time for the transport of a phonon across the 0.67 μm film is of the order of only 100 psec so that significant amounts of heat could be transported into a diamond heat sink on a nanosecond time scale. Yet most of the fluorescent levels of interest for inversion[11] have lifetimes of tens of nanoseconds to tens of microseconds. Thus more orders of magnitude can be realized in reducing the thermal loading further below the limits specified so far. However, all these techniques require precise knowledge about the energy levels and absorption edges of the materials involved. Until the identity of the best candidate for a gamma-ray laser is known, the exact specifications of the solution to the disposal of the waste heat cannot be generally articulated. The examples considered here show that there are many orders-of-magnitude in the safety margin between likely amounts of heating and the much larger amounts which can be tolerated in stiff lattices such as Be and diamond.

The greatest significance is that the persistent tenets of theoretical dogma which have historically[1] inhibited the development of a gamma-ray laser are eliminated by studies of the past five years. There is no need to melt the host lattice in order to pump a nuclear system to the laser threshold. *There are no a priori obstacles to the realization of a gamma-ray laser. A gamma-ray laser is feasible if the right combination of energy levels occurs in some real material.* The overriding question to resolve is whether or not one of the better of the candidate nuclides has its isomeric level within a few tens or even hundreds of keV of one of the giant resonances for dumping angular momenta.

This work was supported by SDIO/IST under direction of NRL.

REFERENCES

1. G. C. Baldwin, J. C. Solem, and V. I. Goldanskii, Rev. Mod. Phys. 53, 687 (1981).
2. V. S. Letokhov, Sov. J. Quant. Electron. 3, 360 (1974).
3. B. Arad, S. Eliezer and Y. Paiss, Phys. Lett. 74A, 395 (1979).
4. C. B. Collins, S. Olariu, M. Petrascu, and I. Popescu, Phys. Rev. Lett. 42, 1397 (1979).
5. C. B. Collins, S. Olariu, M. Petrascu, and I. Popescu, Phys. Rev. C 20, 1942 (1979).
6. S. Olariu, I. Popescu, and C. B. Collins, Phys. Rev. C 23, 50 (1981).
7. S. Olariu, I. Popescu, and C. B. Collins, Phys. Rev. C 23, 1007 (1981).
8. C. B. Collins, in Proceedings of the International Conference on Lasers '80, edited by C. B. Collins (STS Press, McLean, VA, 1981) pp. 524-531.
9. C. B. Collins, in Laser Technique for Extreme Ultraviolet Spectroscopy, edited by T. J. McIlrath and R. R. Freeman (AIP Conference Proceedings No. 90, New York, 1982) pp. 454-464.
10. C. B. Collins, in Proceedings of the International Conference on Lasers '81, edited by C. B. Collins (STS Press, McLean, VA, 1982) pp. 291-295.
11. C. B. Collins, F. W. Lee, D. M. Shemwell, B. D. DePaola, S. Olariu, and I. Popescu, J. Appl. Phys. 53, 4645 (1982).
12. B. D. DePaola and C. B. Collins, J. Opt. Soc. Am. B 1, 812 (1984).
13. C. B. Collins and B. D. Depaola, in Laser Techniques in the Extreme Ultraviolet, edited by S. E. Harris and T. B. Lucatorto (AIP Conference Proceedings No. 119, New York, 1984) pp. 45-53.
14. C. B. Collins and B. D. DePaola, Optics Lett. 10, 25 (1985).
15. B. D. DePaola, S. S. Wagal, and C. B. Collins, J. Opt. Soc. Am. B 2, 541 (1985).
16. B. D. DePaola and C. B. Collins, J. Opt. Soc. Am. B 1, 812 (1984).
17. B. Pontecorvo and A. Lazard, C. R. Acad. Sci. 208, 99 (1939).
18. G. B. Collins, B. Waldman, E. M. Stubblefield, and M. Goldhaber, Phys: Rev. 55, 507 (1939).
19. Y. Watanabe and T. Mukoyama, Bull. Inst. Chem. Res., Kyoto Univ. 57, 72 (1979).
20. M. Krcmar, A. Ljubicic, K. Pisk, B. Logan, and M. Vrtar, Phys. Rev. C 25, 2097 (1982).
21. I. Bikit, J. Slivka, I. V. Anicin, L. Marinkov, A. Ruydic, and W. D. Hamilton, Phys. Rev. C 35, 1943 (1987).
22. *The EGS4 Code System*, Walter R. Nelson, Hideo Hirayama, and David W. O. Rogers, Stanford Linear Accelerator Center Report No. SLAC 265, 1985 (unpublished).
23. *Evaluated Nuclear Structure Data File* (Brookhaven National Laboratory, Upton, New York, 1986).
24. E. Browne and R. B. Firestone, Table of Radioactive Isotopes, edited by V. S. Shirley (Wiley, New York, 1986) pp. 180-182.
25. J. A. Anderson and C. B. Collins, Rev. Sci. Instrum. 58, 2157 (1987).
26. J. A. Anderson and C. B. Collins, Rev. Sci. Instrum. 59, 414 (1988).
27. C. B. Collins, J. A. Anderson, Y. Paiss, C. D. Eberhard, R. J. Peterson, and W. L. Hodge, Phys. Rev. C 38, 1852 (1988).
28. J. A. Anderson, M. J. Byrd, and C. B. Collins, Phys. Rev. C 38, 2833 (1988).
29. E. C. Booth and J. Brownson, Nucl. Phys. A98, 529 (1967).
30. E. Browne, Nucl. Data Sheets 52, 127 (1987).
31. C. B. Collins, C. D. Eberhard, J. W. Glesener, and J. A. Anderson, Phys. Rev. C 37, 2267 (1988).
32. J. J. Carroll, J. A. Anderson, J. W. Glesener, C. D. Eberhard, and C. B. Collins, Astrophys. J. 344, 454 (1989).
33. C. B. Collins, J. J. Carroll, T. W. Sinor, M. J. Byrd, D. G. Richmond, K. N. Taylor, M. Huber, N. Huxel, P. von Neumann-Cosel, A. Richter, C. Spieler, and W. Ziegler, Phys. Rev. C 42, R1813 (1990).
34. P. M. Walker, F. Sletten, N. L. Gjørup, M. A. Bentley, J. Borggreen, B. Fabricius, A. Holm, D. Howe, J. Pedersen, J. W. Roberts, and J. F. Sharpey-Schafer, Phys. Rev. Lett. 65, 416 (1990).
35. J. J. Carroll, M. J. Byrd, D. G. Richmond, T. W. Sinor, K. N. Taylor, W. L. Hodge, Y. Paiss, C. D. Eberhard, J. A. Anderson, C. B. Collins, E. C. Scarbrough, P. P. Antich, F. J. Agee, D. Davis, G. A. Huttlin, K. G. Kerris, M. S. Litz, and D. A. Whittaker, Phys. Rev. C 43, 1238 (1991).
36. J. J. Carroll, T. W. Sinor, D. G. Richmond, K. N. Taylor, C. B. Collins, M. Huber, N. Huxel, P. von Neumann-Cosel, A. Richter, C. Spieler, and W. Ziegler, Phys. Rev. C 43, 879 (1991).
37. C. B. Collins, J. J. Carroll, K. N. Taylor, D. G. Richmond, T. W. Sinor, M. Huber, P. von Neumann-Cosel, A. Richter and W. Ziegler, Phys. Rev. C (pending).
38. G. Knopf and W. Paul, in Alpha, Beta and Gamma-Ray Spectroscopy, edited by Kai Siegbahn (North-Holland Co., Amsterdam, 1965) pp. 1 - 25.
39. C. Kittel, Introduction to Solid State Physics, 6th Edition (Wiley, New York, 1986) p. 106.

PROCEEDINGS REPRINT

SPIE—The International Society for Optical Engineering

Reprinted from

Ultrashort-Wavelength Lasers

22–23 July 1991
San Diego, California

Volume 1551

Invited Paper

Status and issues in the development of a gamma-ray laser

C. B. Collins, J. J. Carr II, T. W. Sinor, and K. N. Taylor

University of Texas at Dallas, Center for Quantum Electronics
P.O. Box 830688, Richardson, TX 75083-0688

ABSTRACT

A gamma-ray laser would stimulate the emission of radiation at wavelengths below 1 Å from excited states of nuclei. However, the difficulties in realizing such a device were considered insurmountable when the problem was last reviewed in 1981. Nevertheless, research on the feasibility of a gamma-ray laser has taken a completely new character since then. A nuclear analog of the ruby laser has been proposed and many of the component steps for pumping the nuclei have been demonstrated experimentally. A quantitative model based upon the new data and concepts of this decade shows the gamma-ray laser to be feasible if some real isotope has its properties sufficiently close to the ideals modeled.

1. INTRODUCTION

At the nuclear level, long-lived excited states are known as isomers. Populations of these nuclear metastables can store energies of tera-Joules (10^{12} J) per liter at solid densities for thousands of years. Such long storage times mean that it would not be necessary to pump a gamma-ray laser medium entirely in situ. For some cases the excited nuclei could be bred in a reactor from a parent material that captures a neutron or from a specific nuclear reaction acting upon precursive elements.

The problem of suddenly assembling a critical density of prepumped nuclei to reach the threshold for stimulated emission received much attention in the early literature and excellent reviews are available.[1] Unhappily, it was generally concluded that such single photon, brute force approaches were essentially hopeless. In an encyclopedic review, Baldwin and coauthors[1] concluded the general impossibility of a gamma-ray laser based upon all techniques for pumping known in 1980. That review effectively terminated all traditional lines of approach to a gamma-ray laser. However, in the earlier work the greatest emphasis had been placed upon the use of intense particle fluxes for input energy.

In 1979 we began the introduction[2-14] of a new interdisciplinary concept of upconversion which launched a renaissance in the field. The basic theory[9] of upconversion at the nuclear level was in-place by 1982 for the two possible variants, coherent and incoherent upconversion. Involving either multiphoton processes or multiple electromagnetic transitions to release the energy stored in isomers, many of the difficulties encountered with more traditional pumping schemes did not arise.

In the decade since 1980, research on the feasibility of a gamma-ray laser has taken a completely new character. The purpose of this article is to review the advances of this past decade that have significantly increased the likelihood of the feasibility of a gamma-ray laser.

2. CONCEPTS

At first approach it would seem that the prospects for all ultrashort wavelength lasers would be vitiated by a very fundamental factor.[1] The basic ν^3 dependence of electron transition probabilities so limits the storage of pump energies that even now some of the largest pulsed power machines are able to excite only milliJoules of x-ray laser output and then only at soft photon energies of little applicability. In contrast there are four unique advantages of a gamma-ray laser that would accrue from its operation upon electromagnetic transitions of nuclei:

0-8194-0679-1/92/$4.00

each other. This discrepancy led to serious contentions over the way in which the expected fluorescence yields were calculated.[18] One of the early challenges of the renaissance period was to place the "optical" pumping of nuclei onto a firm quantitative basis.

For a sample which is optically thin at the pump wavelength, a computation of the number of nuclei pumped into a fluorescence level in the scheme of Fig. 1 is straightforward. Most intense x-ray sources emit continua, either because bremsstrahlung is initially produced or because spectral lines are degraded by Compton scattering in the immediate environment. The time integrated yield of final-state nuclei, N_f obtained by irradiating N_i initial targets with a photon flux Φ_o in photons cm^{-2} delivered in a continuum of intensities up to an end point energy E_o is,

$$N_f = N_i \Phi_o \int_0^{E_o} \sigma(E) F(E, E_o) dE \quad , \tag{1}$$

where $F(E,E_o)$ is the distribution of intensities within the input spectrum normalized so that

$$\int_0^{E_o} F(E, E_o) dE = 1 \quad , \tag{2}$$

and $\sigma(E)$ is the effective cross section for the excitation of the final state from the initial.

All (γ,γ') reactions occurring at energies below the threshold for particle evaporation excite bound intermediate states of nuclei as shown in Fig. 1. Although only one intermediate state appears in Fig. 1, there could be more. Each would be excited at a different pump energy but all would branch to some extent into the same fluorescence level, f. The j-th intermediate is shown in Fig. 1 as typical.

Although the width of level j is broad on a nuclear scale, it is narrow in comparison to the scale of energies, E over which $F(E,E_o)$ varies. Then, the final-state yield, expressed as the normalized activation per unit photon flux $A_f(E_o)$ produced with bremsstrahlung having an end point of E_o can be written from Eq. (1) as,

$$A_f(E_o) \equiv \frac{N_f}{N_i \Phi_o} = \sum_j (\sigma\Gamma)_{fj} F(E_j, E_o) \quad . \tag{3a}$$

In this expression $(\sigma\Gamma)_{fj}$ is the integrated cross section for the production of final-state N_f as a result of the excitation of the intermediate state E_j with bremsstrahlung described by the spectral function $F(E,E_0)$, so that

$$(\sigma\Gamma)_{fj} = \int_{E_j-\Delta}^{E_j+\Delta} \sigma(E) dE \quad , \tag{3b}$$

where Δ is an energy small compared to the spacing between intermediate states and large in comparison to their widths. Levels of this type are sometimes called gateways or doorways.

It is straightforward to show that,

$$(\sigma\Gamma)_{fj} = (\pi b_a b_o \Gamma \sigma_o/2)_{fj} \quad , \tag{4a}$$

where $\sigma_o/2$ is the peak of the Breit-Wigner cross section for the absorption step, and

$$\sigma_o = \frac{\lambda^2}{2\pi} \frac{2I_e+1}{2I_g+1} \frac{1}{\alpha_p+1} \quad , \tag{4b}$$

where λ is the wavelength of the gamma ray at the resonant energy, E_j; I_e and I_g are the nuclear spins of the excited and ground states, respectively; and α_p is the total internal conversion coefficient for the system shown in Fig. 1.

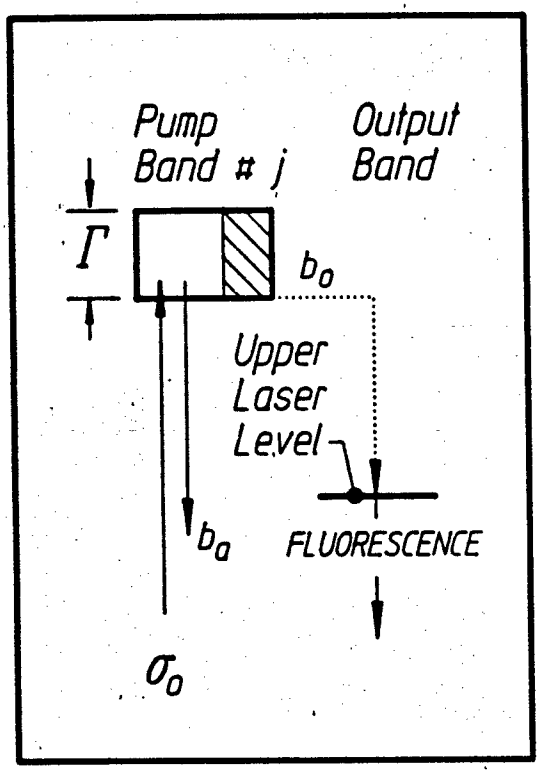

Figure 1: Schematic representation of the decay modes of a gateway state of width Γ sufficiently large to promote bandwidth funneling. The initial state from which population is excited with an absorption cross section σ_0 can be either ground or isomeric.

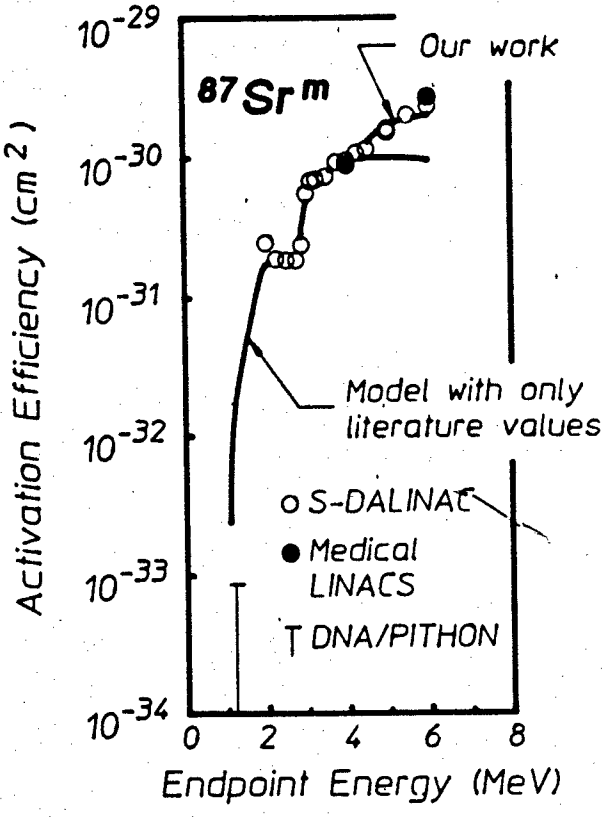

Figure 2: Activation efficiencies, A_f for the reaction $^{87}Sr(\gamma,\gamma')^{87}Sr^m$ as functions of the end point, E_0 of the bremsstrahlung used for excitation. Dotted and solid curves plot values computed from Eq. (3a) using Ref. 27 for comparison with measurements obtained from the accelerators indicated by the type of symbol shown.

3. PUMP CALIBRATION

From the perspective of laser physics the most unreliable sources of energetic photons used in early studies of (γ,γ') reactions seem to have been the nuclear sources. Although assumed to emit line spectra, in actual usage they produced intensities which were dominated by the continua resulting from multiple Compton scatterings of photons by the large amounts of shielding in the irradiation environment. Such multiple scatterings are difficult to calculate and still impossible to measure in practical laboratory configurations. In contrast, the spectral intensities of bremsstrahlung are routinely calculated with high accuracy from measured accelerator currents and target geometries by well-established codes.[20]

In our experimental work of the last five years the bremsstrahlung from five accelerators in different experimental environments was used to verify the fluorescence model of Eqs. (1) - (4b) and to cross-check the accelerator intensities. The

devices involved in this effort were DNA/PITHON at Physics International, DNA/Aurora at the Harry Diamond Laboratories, a 4 MeV and a 6 MeV medical linac at the University of Texas Health Sciences Center, and the superconducting injector to the storage ring at Darmstadt (S-DALINAC). Spectral intensities were calculated with the coupled electron/photon transport code[20] EGS4 adapted for each individual configuration from closely monitored values of accelerator currents. In this way both $F(E,E_o)$ and Φ_o were obtained. In some cases Φ_o was separately verified by in-line dosimetry.

Table I

Summary of nuclides, pump lines, and integrated cross sections for the excitation of delayed fluorescence suitable for use as calibration standards.

	PUMP LINE (keV)	$\pi b_a b_o \Gamma \sigma_o/2$ (10^{-29} cm^2 keV)
^{79}Br	761	6.2
^{77}Se	250	0.20
	480	0.87
	818	0.7
	1005	30
^{115}In	1078	20

Of the many potential systems which might be used to confirm the formulations of Eq. (1) through (4b), the literature[21] supports the calculation of integrated cross sections for very few. Table I summarizes those which are known with sufficient accuracy to serve as standards. In the convenient units of 10^{-29} cm^2 keV, values range from the order of unity to a few tens for bandwidth funnels that are sufficient for demonstrations of nuclear fluorescence from reasonable amounts of material at readily accessible levels of input.

In our experiments samples with typical masses of grams were exposed to the bremsstrahlung from the five accelerators for times ranging from seconds to hours for the continuously operating machines and to single flashes from the pulsed devices. The activations, A_f of Eq. (3a) were determined by counting the photons spontaneously emitted from the samples after transferring them to a quieter environment. Usual corrections were made for the isotopic abundance, for the loss of activity during irradiation and transit, for the counting geometry, for the self-absorption of the fluorescence, and for the tabulated efficiencies[22] for the emission of signature photons from the populations, N_f. The self-absorption correction required a calculation of photon transport which was verified in some cases by confirming that the same sample masses in different geometries with different correction factors gave the same final populations.

Results were in close agreement[23] with the predictions of Eq. (3a) used with the values of $(\sigma\Gamma)_{fj}$ shown in Table I. That work established a confidence level sufficient to support the use of nuclear activation as a means of selectively sampling spectral intensities of single pulses of intense continua to determine absolute intensities as functions of wavelength.[24] Having calibrated the spectral sources the persisting uncertainties in the optical pumping of ^{115}In^m and ^{111}Cd^m were resolved.[25,26]

As part of the calibration effort reported here, we reexamined the reaction ^{87}Sr$(\gamma,\gamma')^{87}$Sr^m. Particularly valuable were the data obtained with the S-DALINAC because the end point of the bremsstrahlung could be varied. A change of the end point energy, E_o of the bremsstrahlung, as well as altering Φ_o, modulates the spectral

intensity function $F(E_j,E_o)$ at all of the important energies for resonant excitation E_j. The largest effect occurs when E_o is increased from a value just below some intermediate state at E_j to one exceeding it so that $F(E_j,E_o)$ varies from zero to some finite value.

Early work[27] on (γ,γ') reactions showed that a plot of activation, $A_f(E_o)$ as a function of bremsstrahlung end point energy displayed very pronounced activation edges at the energies, E_j corresponding to the resonant excitation of new intermediate states. Such edges enabled new gateways to be identified for a particular reaction.

The activation efficiencies, A_f calculated from Eq. (3a) using the literature values[27] are shown in Fig. 2 together with the measurements obtained with four of the accelerators. As can be seen, agreement is very good between the different accelerators and between the experimental data and the model calculations. The units of A_f in Fig. 2 are those of area because they are a type of average cross section quite different from the σ_o of Eq. (4a) that describe individual transitions. The small plotted values are the result of averaging the large σ_o at the resonant E_j over the broad bandwidth of $F(E,E_o)$ in which most $E \neq E_j$.

These calibration studies served to confirm both the traditional model of nuclear activation summarized in Eq. (1) - (4b) and to validate the EGS4 code for calculating bremsstrahlung intensities from measured accelerator parameters. *Now, there can be no reasonable doubt of procedures for quantitatively measuring fluorescence efficiencies if an experiment is carefully performed with a bremsstrahlung source of pump radiation.*

4. GIANT PUMPING RESONANCES

If expressed as partial widths the integrated cross sections for the excitation of $^{77}Se^m$, $^{79}Br^m$, and $^{115}In^m$ seen in Table I corresponded to 39, 5, and 94 μeV, respectively. While technically breaking the rule-of-thumb these results still left an aura of credibility to the traditional impressions that partial widths for exciting isomers would be limited to 1 μeV.

Tempering expectations that integrated cross sections of even this size might be expected for the dumping of actual isomeric candidates for a gamma-ray laser was a concern for the conservation of various projections of the angular momenta of the nuclei. Many of the interesting isomers belong to the class of nuclei deformed from the normally spherical shape. For those systems there is a quantum number of dominant importance, K which is the projection of individual nucleonic angular momenta upon the axis of elongation. To this is added the collective rotation of the nucleus to obtain the total angular momentum J. The resulting system of energy levels resembles those of a diatomic molecule for which

$$E_n(K,J) = E_n(K) + B_nJ(J+1) \quad , \qquad (5)$$

where $J \geq K \geq 0$ and J takes values $|K|$, $|K|+1$, $|K|+2$,.... In this expression B_n is a rotational constant and $E_n(K)$ is the lowest value for any level in the resulting "band" of energies identified by other quantum numbers n. In such systems the selection rules for electromagnetic transitions require both $|\Delta J| \leq M$ and $|\Delta K| \leq M$, where M is the multipolarity of the transition.

In most cases of interest, the isomeric state has a large lifetime because its value of K differs considerably from those of lower levels to which it would, otherwise, be radiatively connected. As a consequence, bandwidth funneling processes such as shown in Fig. 1 must span substantial changes in ΔK and component transitions have been expected to have large, and hence unlikely, multipolarities. Initial expectations were that partial widths would decrease further as the values of ΔK needed for the transfer increased.

From this perspective the candidate isomer, $^{180}Ta^m$ was the most initially unattractive as it had the largest change of angular momentum between isomer and ground state, 8$\hbar$. However, because it was the only isomer for which a macroscopic

sample was readily available, $^{180}Ta^{m}$ became the first isomeric material to be optically pumped to a fluorescent level.

Table II

Recently measured values of integrated cross section $(\sigma\Gamma)_{fj}$ for the reaction $^{180}Ta^{m}(\gamma,\gamma')^{180}Ta$. The gateway excitation energies, E_j for these levels are given at the centers of the ranges of energies that could be resolved experimentally.

Energy (MeV)	$\sigma\Gamma$ (10^{-29} cm^2 keV)
2.8 ± 0.1	12000 ± 2000
3.6 ± 0.1	35000 ± 5000

This particular isomer, $^{180}Ta^{m}$ carries a dual distinction. It is the rarest stable isotope occurring in nature and it is the only naturally occurring isomer. The actual ground state of ^{180}Ta is 1^+ with a half-life of 8.1 hours while the tantalum nucleus of mass 180 occurring with 0.012% natural abundance is the 9^- isomer, $^{180}Ta^{m}$. It has an adopted excitation energy of 75.3 keV and half-life in excess of 1.2×10^{15} years.[28]

In an experiment conducted in 1987 we exposed 1.2 mg of $^{180}Ta^{m}$ to the bremsstrahlung from the 6 MeV linac and obtained a large fluorescence yield.[29] This was the first time a (γ,γ') reaction had been excited from an isomeric target and was the first evidence of the existence of giant pumping resonances. Simply the observation of fluorescence from a milligram sized target proved that an unexpected reaction channel had opened. Usually grams of material are required in this type of experiment. Analyses[29,30] of the data indicated that the partial width for the dumping of $^{180}Ta^{m}$ was around 0.5 eV.

To determine the transition energy, E_j from the $^{180}Ta^{m}$ isomer to the gateway level, a series of irradiations was made at the S-DALINAC facility using fourteen different end points in the range from 2.0 to 6.0 MeV.[31] The existence of an activation edge was clearly seen even in the raw data[31] shown in Fig. 3. The fitting of such data to the expression of Eq. (3a) by adjusting trial values of $(\sigma\Gamma)_{fj}$ enabled us to determine the integrated cross sections for the dumping of $^{180}Ta^{m}$ isomeric populations into freely radiating states. Reported values[31] are summarized in Table II.

The integrated cross sections in Table II are enormous values exceeding anything previously reported for interband transfer through a bandwidth funnel by two orders of magnitude. In fact they are 10,000 times larger than the values usually measured for nuclei. With this result the restrictive guidelines customarily applied to optical pumping of nuclei are proven to be nearly 10^6 times too pessimistic.

While the width of the transfer process is difficult to interpret in a single particle model, a puzzle of comparable complexity is found in the efficiency with which ΔK is transferred. It is an interesting speculation that at certain energies of excitation collective oscillations of the core nucleons could break some of the symmetries upon which rest the identifications of the pure single particle states. If single particle states of differing K were mixed in this way, the possibility for transferring larger amounts of ΔK with greater partial widths might be enhanced. Some support for such a speculation was found in the unexpected enhancements measured very recently for the deexcitation of the $^{174}Hf^{m}$ isomer.[32] There also the decay of the isomer was found to occur primarily by transition through an intermediate state lying at 2685 keV in which K-mixing occurred so that $\Delta K = 14$ was lost between isomer and the ground state band. This is remarkably close to the energy of the K-mixing level at 2800 ± 100 keV for ^{180}Ta shown in Table II. The similarity of results for nuclei with such dissimilar single particle structures does seem to support the identifica-

tion of this K-mixing process with some type of core property varying only slowly among neighboring nuclei.

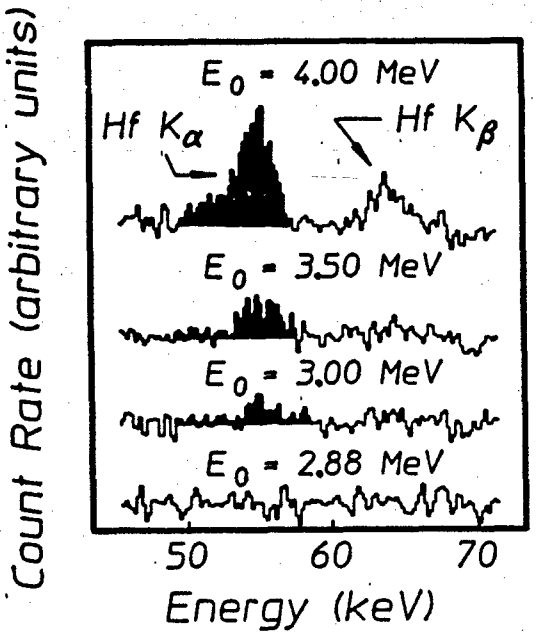

Figure 3: Spectra of fluorescent photons from ^{180}Ta decay after irradiation with bremsstrahlung having the end points shown. The counting rate from an unexposed sample has been subtracted and the curves have been offset vertically for clarity. The total fluorescence signal is given by the shaded area.

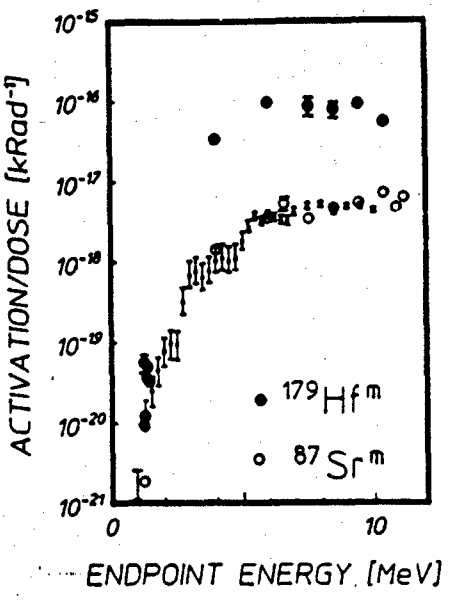

Figure 4: Activation edge for the excitation of ^{179}Hf^{m} through a giant pumping resonance in comparison to the excitation of the calibration nuclide ^{87}Sr^{m} and the fit of the calibration data to literature values of integrated cross sections. Data plot activation per unit dose of irradiation in contrast to activation per unit photon flux as described in Eq. (3a).

A survey of 19 isotopes[33] conducted with the four U.S. accelerators over a fairly coarse mesh of bremsstrahlung endpoints, confirmed the existence of giant resonances for breaking K in the region of masses near 180. Activation edges such as shown in Fig. 4 continued to support the identifications of integrated cross sections for pumping and dumping of isomers that were of the order of 10,000 times greater than usual values. A study with the higher resolution of the S-DALINAC[34] showed the giant pumping resonances reappeared at lower masses near 120.

Whatever the mechanisms, the experimental fact remains that interband transfer processes connecting to isomeric levels can be pumped through enormous partial widths reaching 0.5 eV, even when the transfer of angular momentum must be as great as $\Delta K = 8$, or even $\Delta K = 14$. It seems this is the nuclear analog of the giant resonance for pumping ruby at the atomic level. Elucidation of the process, together with identification of the gateways, has been propelled into a place of future importance.

5. CONCLUSIONS - A LASER MODEL

The 1990 model of a gamma-ray laser is not fundamentally different from the nuclear analog of the ruby laser described[9] in 1982. Envisioned as a thin film of diluent doped with isomeric nuclei and pumped with a flash of x-rays in a slab geometry, the question of feasibility still rests on the degree to which the properties of some real nuclide approach those of the ideal being modeled. What has

changed is that the discovery of giant pumping resonances enables some of the original constraints to be relaxed. The result is that the feasibility of a gamma-ray laser is orders-of-magnitude more probable than originally estimated in 1982. Because of this substantial improvement, it is useful to recompute the model in terms of the new data obtained in the past decade.

Since the better candidate isomers for a gamma-ray laser have never been fabricated in macroscopic amounts, the precise identity of the best nuclide to model is not known. Moreover, since feasibility is such a complex function of the nuclear parameters, the assumptions introduced into any model will critically affect the estimates of feasibility in strongly nonlinear ways. For the computation reported here the following parameters were assumed.

1) The pump band j in Fig. 1 is one of the newly discovered giant pumping resonances with a partial width of $b_a b_o \Gamma = 1$ eV.

2) The pump transition is centered on an energy $E_j = 30$ keV.

3) The initial state is assumed to be isomeric with an excitation energy so high that 2) is possible.

4) The output transition is around 100 keV.

5) The nuclei are diluted in a thin film of diamond or Be.

6) The Borrmann effect contributes a factor of 10 to the enhancement of the ratio of cross sections for resonant to nonresonant transitions.

The most sensitive assumptions are those about the width and activation energy of the giant pumping resonance, statements 2) and 3). The range of excitation energies over which isomers can be found is very large. We have already shown that isomers can be dumped into the freely radiating system, even through $\Delta K = 8$ or $\Delta K = 14$, so the only doubt here is a statistical one; whether or not a giant pump resonance can be found within 30 keV of an isomer.

Following our development[9] of 1982, under small signal conditions the midrange requirement of 10^{-4} is obtained for the pumped fraction,

$$\frac{N_f}{N_i} \geq 10^{-4} \qquad (6)$$

This sets the pump intensity needed for threshold, and with it the amount of waste heat to dissipate.

The essential concept in the management of the thermal economy is that the mean free path (MFP) for a photon resonant with the nuclear transition is much shorter than the MFP for nonresonant, photoelectric absorption to produce heat. Also, the MFP for a photoelectron produced in the nonresonant channel is greater in the diluent than the MPF for the photons pumping the nuclear resonance. This means that a thin film of diamond can be doped to use most of the incident photons in the bandwidth of the giant pumping resonance while the majority of the nonresonant photons will pass through the film into the substrate which can be cooled by ablation or cryogenics. Moreover, primary photoelectrons produced by the small fraction of nonresonant events in the film can escape before their energy is degraded to heat.

The quantitative expression of this strategy is obtained by substituting Eq. (3a) into Eq. (6) and assuming a single giant resonance dominates so that the sum is unnecessary. Solving for $\phi_j = \Phi_0 F(E_j, E_0)$, and using the previous assumption that each pump photon carries 30 keV gives the spectral fluence, $F_j = E_j \phi_j$ at threshold,

$$F_j \geq 177 \text{ mJ cm}^{-2} \text{ eV}^{-1} \qquad (7)$$

For the likely cases of rare earth or platinide elements the 30 keV pump energy lies below the K-edge and about 15 keV above the L-edge. As a result, the primary photoelectrons resulting from the nonresonant absorption in the active medium should have energies of the order of 15 keV and ranges of 6.0 and 3.0 μm in Be and C, respectively.[35] Thus, only about 10% and 20% of the primaries, respectively, should be stopped in a 0.67 μm thick host films of Be or diamond, the thickness corresponding to the MFP for resonant absorption at a concentration of 10%. Then the fractions of the energy from the incident pump degraded into heat in the laser film because of nonresonant absorption become

$$f\,(Be) = 4.8 \times 10^{-4} \quad , \tag{8a}$$

$$f\,(C) = 2.4 \times 10^{-4} \quad . \tag{8b}$$

Considering that edge filters or ablation layers could reduce the bandwidth of the pump radiation to 3 keV, before reaching the doped layer of active medium, the incident fluence lying outside the bandwidth for resonant absorption would be 3000 times greater than the value of Eq. (7). However, only the fractions of Eqs. (8a) and (8b) are capable of being degraded into heat in the sensitive layer. The resulting energy balance can be summarized at threshold by the first two lines of Table III.

Dividing those fluences by the 0.67 μm thickness gives the energy loading of the laser film shown in Table III. These values are quite significantly <u>below</u> the levels of heating required to degrade the recoil free fractions in the case of the diamond lattice. Baldwin has summarized[1] the involved dependence of the recoil free fraction of gamma transitions upon recoil energy, lattice parameters, and temperature. He shows that even at a temperature, T equal to the Debye temperature, Θ_D the recoil free fraction is not significantly degraded (by more than a factor of 2) for a transition even as energetic as to give a classical recoil energy of 0.14 Θ_D. In diamond with $\Theta_D = 2230°$ K this means a transition of 100 keV is little affected by a temperature increase up to $T = \Theta_D$.

It is a textbook computation[36] to estimate that the energy content of the phonons of a material with $\Theta_D = 2230°$ K at a temperature of $T = \Theta_D$ is about 11 kJ cm^{-3}. Comparing this with the estimated loading of 3.8 kJ cm^{-3} gives a "safety factor" of almost three. A comparable margin is obtained for the Be.

To summarize, it is convenient to recast the threshold fluence of Eq. (7) into more tangible terms. The spectral fluence of 177 mJ cm^{-2} eV^{-1} corresponds to 530 J cm^{-2} if the bandwidth of the pump x-rays is arranged to be 3 keV, a practical separation which might be filtered between K-edges. Even if pumped instantaneously, so that no waste heat were transported away, the thermal loading would reach only 1/3 of the limit for retaining the Mössbauer effect. If derived from an x-ray line of 30 eV width, the threshold fluence would be only 5.3 J cm^{-2}. In that case the thermal loading would reach only 1/300 of the critical limit for a diamond lattice.

Even beyond this point much can be done to reduce heating further. All calculations so far were done for the instantaneous generation of the waste heat. The time for the transport of a phonon across the 0.67 μm thickness of the working layer is of the order of only 100 psec so that the transport of significant amounts of heat from that layer into a diamond heat sink is possible on a nanosecond time scale. Yet most of the fluorescent levels of interest for inversion[9] have lifetimes of tens of nanoseconds to tens of microseconds. This is many times the period for the transport of phonons out of the inverting layer so that more orders of magnitude can be realized in reducing the thermal loading further below the limits specified so far. However, all these techniques require precise knowledge about the energy levels and absorption edges of the materials involved. Until the identity of the best candidate for a gamma-ray laser is known, the exact specifications of the solution to the disposal of the waste heat cannot be generally articulated. The examples considered here show that there are many orders of magnitude in the safety margin between likely amounts of heating and the much larger amounts which can be tolerated in stiff lattices such as Be and diamond.

Table III

Summary of the thermal economy at threshold for a laser nuclide doped into a film of 0.67 μm thickness of the materials shown.

Lattice	Be	C(diamond)
Resonant input fluence	177 mJ cm^{-2}	177 mJ cm^{-2}
Fluence degraded to heat	127 mJ cm^{-2}	255 mJ cm^{-2}
Resonant energy density	2.6 kJ cm^{-3}	2.6 kJ cm^{-3}
Thermal loading	1.9 kJ cm^{-3}	3.8 kJ cm^{-3}

The greatest significance is that the persistent tenents of theoretical dogma inhibiting the development of a gamma-ray laser are eliminated by studies of the past decade. There is no need to melt the host lattice in order to pump a nuclear system to the laser threshold. *There are no a priori obstacles to the realization of a gamma-ray laser. A gamma-ray laser is feasible if the right combination of energy levels occurs in some real material.* The overriding question to resolve is whether or not one of the better of the candidate nuclides has its isomeric level within a few tens or even hundreds of keV of one of the giant resonances for dumping angular momenta.

This work was supported by SDIO/IST under direction of NRL.

6. REFERENCES

1. G. C. Baldwin, J. C. Solem, and V. I. Goldanskii, "Approaches to the development of gamma-ray lasers," Rev. Mod. Phys. 53, 687-744 (1981).
2. C. B. Collins, S. Olariu, M. Petrascu, and I. Popescu, "Enhancement of γ-Ray Absorption in the Radiation Field of a High Power Laser," Phys. Rev. Lett. 42, 1397-1400 (1979).
3. C. B. Collins, S. Olariu, M. Petrascu, and I. Popescu, "Laser-Induced Resonant Absorption of γ Radiation," Phys. Rev. C 20, 1942-1945 (1979).
4. S. Olariu, I. Popescu, and, C. B. Collins, "Tuning of γ-Ray Processes with High Power Optical Radiation," Phys. Rev. C. 23, 50-63 (1981).
5. S. Olariu, I. Popescu, and, C. B. Collins, "Multiphoton Generation of Optical Sidebands to Nuclear Transitions," Phys. Rev. C 23, 1007-1014 (1981).
6. C. B. Collins, "The Tuning and Stimulation of Gamma Radiation," Proceedings of the International Conference on Lasers '80, edited by C. B. Collins (STS Press, McLean, VA, 1981) p. 524-531.
7. C. B. Collins, "Upconversion of Laser Radiation to γ-Ray Energies," Laser Technique for Extreme Ultraviolet Spectroscopy, edited by T. J. McIlrath and R. R. Freeman (AIP Conference Proceedings No. 90, New York, 1982) p. 454-464.
8. C. B. Collins, "Upconversion of Laser Radiation to Gamma-Ray Energies," Proceedings of the International Conference on Lasers '81, edited by C. B. Collins (STS Press, McLean, VA, 1982) p. 291-295.
9. C. B. Collins, F. W. Lee, D. M. Shemwell, B. D. DePaola, S. Olariu, and I. Popescu, "The Coherent and Incoherent Pumping of a Gamma Ray Laser with Intense Optical Radiation," J. Appl. Phys. 53, 4645-4651 (1982).
10. B. D. DePaola and C. B. Collins, "Tunability of radiation generated at wavelengths below 1 Å by anti-Stokes scattering from nuclear levels," J. Opt. Soc. Am. B 1, 812-817 (1984).
11. C. B. Collins, and B. D. Depaola, "Tunable Sub-Angstrom Radiation Generated by Anti-Stokes Scattering from Nuclear Levels," Laser Techniques in the Extreme Ultraviolet, edited by S. E. Harris and T. B. Lucatorto (AIP Conference Proceedings No. 119, New York, 1984) p. 45-53.
12. C. B. Collins and B. D. DePaola, "Observation of coherent multiphoton process in nuclear states," Optics Lett. 10, 25-27 (1985).

13. B. D. DePaola, S. S. Wagal, and, C. B. Collins, "Nuclear Raman Spectroscopy," J. Opt. Soc. Am. B 2, 541-543 (1985).
14. B. D. DePaola and C. B. Collins, "Tunability of radiation generated by wavelengths below 1 Å by anti-Stokes scattering from nuclear levels," J. Opt. Soc. Am. B 1, 812-817 (1984).
15. B. Pontecorvo and A. Lazard, "Isomerie nucleaire produite par les rayons X du spectre continu," C. R. Acad. Sci. 208, 99-101 (1939).
16. G. B. Collins, B. Waldman, E. M. Stubblefield, and M. Goldhaber, "Nuclear excitation of indium by x-rays," Phys. Rev. 55, 507 (1939).
17 Y. Watanabe and T. Mukoyama, "Excitation of nuclear isomers by γ rays from ^{60}Co," Bull. Inst. Chem. Res., Kyoto Univ. 57, 72 - 82 (1979).
18. M. Krcmar, A. Ljubicic, K. Pisk, B. Logan, and M. Vrtar, "Photoactivation of ^{111}Cd," Phys. Rev. C 25, 2097-2099 (1982).
19. I. Bikit, J. Slivka, I. V. Anicin, L. Marinkov, A. Ruydic, and W. D. Hamilton, "Photoactivation of $^{111}Cd^m$ without a 'nonresonant' contribution," Phys. Rev. C. 35, 1943-1945 (1987).
20. The EGS4 Code System, Walter R. Nelson, Hideo Hirayama, and David W. O. Rogers, Stanford Linear Accelerator Center Report No. SLAC 265, 1985 (unpublished).
21. Evaluated Nuclear Structure Data File (Brookhaven National Laboratory, Upton, New York, 1986).
22. E. Browne and R. B. Firestone, in Table of Radioactive Isotopes, edited by V. S. Shirley (Wiley, New York, 1986), pp. 180-182.
23. J. A. Anderson and C. B. Collins, "Calibration of pulsed bremsstrahlung spectra with photonuclear reactions of ^{77}Se and ^{79}Br," Rev. Sci. Instrum. 58, 2157 - 2160 (1987).
24. J. A. Anderson and C. B. Collins, "Calibration of pulsed x-ray spectra," Rev. Sci. Instrum 59, 414 - 419 (1988).
25. C. B. Collins, J. A. Anderson, Y. Paiss, C. D. Eberhard, R. J. Peterson, and W. H. Hodge, "Activation of $^{115}In^m$ by single pulses of intense bremsstrahlung," Phys. Rev. C 38, 1852 - 1856 (1988).
26. J. A. Anderson, M. J. Byrd, and C. B. Collins, "Activation of $^{111}Cd^m$ by single pulses of intense bremsstrahlung," Phys. Rev. C 38, 2833 - 2842 (1988).
27. E. C. Booth and J. Brownson, "Electron and Photon Excitation of Nuclear Isomers," Nucl. Phys. A98, 529 - 541 (1967).
28. E. Browne, "Nuclear data sheets for A = 180," Nucl. Data Sheets 52, 127 - 169 (1987).
29. C. B. Collins, C. D. Eberhard, J. W. Glesener, and J. A. Anderson, "Depopulation of the isomeric state $^{180}Ta^m$ by the reaction $^{180}Ta^m(\gamma,\gamma')^{180}Ta$," Phys. Rev. C. 37, 2267 - 2269 (1988).
30. J. J. Carroll, J. A. Anderson, J. W. Glesener, C. D. Eberhard, and C. B. Collins, "Accelerated Decay of $^{180}Ta^m$ and ^{176}Lu in Stellar Interiors through (γ,γ') Reactions," Astrophys. J. 344, 454 - 459 (1989).
31. C. B. Collins, J. J. Carroll, T. W. Sinor, M. J. Byrd, D. G. Richmond, K. N. Taylor, M. Huber, N. Huxel, P. v. Neumann-Cosel, A. Richter, C. Spieler, and W. Ziegler, "Resonant excitation of the reaction $^{180}Ta^m(\gamma,\gamma')^{180}Ta$," Phys. Rev. C. 42, R1813 - R1816 (1990).
32. P. M. Walker, F. Sletten, N. L. Gjørup, M. A. Bentley, J. Borggreen, B. Fabricius, A. Holm, D. Howe, J. Pedersen, J. W. Roberts, and J. F. Sharpey-Schafer, "High-K Barrier Penetration in ^{174}Hf: A Challenge to K Selection," Phys. Rev. Lett. 65, 416 - 419 (1990).
33. J. J. Carroll, M. J. Byrd, D. G. Richmond, T. W. Sinor, K. N. Taylor, W. L. Hodge, Y. Paiss, C. D. Eberhard, J. A. Anderson, C. B. Collins, E. C. Scarbrough, P. P. Antich, F. J. Agee, D. Davis, G. A. Huttlin, K. G. Kerris, M. S. Litz, and D. A. Whittaker, "Photoexcitation of nuclear isomers by (γ,γ') reactions," Phys. Rev. C. 43, 1238-1247 (1991).
34. J. J. Carroll, T. W. Sinor, D. G. Richmond, K. N. Taylor, C. B. Collins, M. Huber, N. Huxel, P. v. Neumann-Cosel, A. Richter, C. Spieler, and W. Ziegler, "Excitation of $^{123}Te^m$ and $^{125}Te^m$ through (γ,γ') reactions," Phys. Rev. C. 43, 879-900 (1991).
35. G. Knopf and W. Paul, in: Alpha, Beta and Gamma-Ray Spectroscopy (ed. Kai Siegbahn, North-Holland Co., Amsterdam, 1965), p. 1 - 25.
36. C. Kittel, Introduction to Solid State Physics, 6th ed. (Wiley, New York, 1986), p. 106.

THE GAMMA-RAY LASER: ISSUES AND PROGRESS IN 1992

J. J. Carroll, T. W. Sinor, K. N. Taylor, C. Hong,
J. D. Standifird, B. W. Johnson and C. B. Collins
The University of Texas at Dallas, Center for Quantum Electronics
P. O. Box 830688, Richardson, Texas 75083-0688

Abstract

A gamma-ray laser would provide the stimulated emission of radiation at wavelengths shorter than 1 Å from excited states of nuclei. Unique advantages provided by nuclear transitions would also enable the integration of pump energy over longer times and thus to larger values than are possible with x-ray lasers. However, in the first cycle of study ending in 1981 it was concluded that the difficulties were insurmountable for achieving a gamma-ray laser using traditional approaches of pumping with particle fluxes. Since then research has take an entirely new character with the introduction of the concept of "optical" pumping of a gamma-ray laser as a nuclear analog to the ruby laser. In the past six years the components of this concept have been demonstrated experimentally by the main line project at the Center for Quantum Electronics and three major breakthroughs have been realized. Computations based upon this new data show that a gamma-ray laser is feasible if some isotope has its properties sufficiently close to the ideals modeled

Introduction

Studies of the feasibility of a gamma-ray laser have been motivated by the unique advantages presented in nuclear systems. Many nuclei possess particularly long-lived excited states called isomers with energies of keV to MeV. Populations of these metastable states can store tera-Joules per liter at solid densities for up to thousands of years so it would not be necessary to provide all the pump energy for a gamma-ray laser in situ. Electromagnetic transitions in nuclei provide a variety of transition moments for which the constant linking spontaneous lifetime with the ν^3 factor is orders-of-magnitude more favorable than might otherwise be expected for such short wavelengths. Thus lasing levels in nuclei can have lifetimes as long as μs and pump pulses can be integrated for longer times than for x-ray lasers. Also, gamma-ray transitions routinely have natural linewidths, as in the Mössbauer effect, which would insure large cross sections for stimulated emission. Without broadening, values for 1 Å nuclear transitions typically exceed the cross section for the stimulation of Nd in YAG.

Despite this impetus, there was little real progress towards a gamma-ray laser prior to 1982. This was a result of the concentration on the traditional approach of pumping nuclei with intense particle fluxes and then suddenly assembling a critical density to reach the threshold for stimulated emission. The general impossibility of those brute force, single (output) photon schemes was concluded due to the unmanageable amounts of heat expected to be deposited in the host matrix as discussed in the encyclopedic review of Baldwin, et al.[1] This effectively served to define the termination of the traditional approaches to a gamma-ray laser and demonstrated that the critical test for any new approach must be the efficacy of pumping to release the energy stored in isomers.

A new interdisciplinary approach[2] to a gamma-ray laser emerged in 1982 following precursive work[3-9] that appeared near the end of the first cycle of research. The basic plan[10,11] called for the "optical" pumping of nuclei using coherent or incoherent processes. Either multiphoton processes or multiple electromagnetic transitions would be used to release the energy stored in nuclear isomers while avoiding many of the problems encountered by the traditional approach. In the most straightforward application,[2] incoherent pumping simply represents a nuclear analog to the ruby laser in which "optical" refers to x rays. A way was also indicated by which to manage wasted pump energy using a thin film of low Z material as a host matrix.

Driven by this blueprint for a gamma-ray laser which now appears in the textbooks,[12] in the past decade the main line project at the Center for Quantum Electronics has been rich with achievement. The fundamental concepts of coherent pumping have been demonstrated[13-17] but not surprisingly the greatest rate of progress has been realized in the simpler direction of incoherent pumping.[18-28] In fact the feasibility of a gamma-ray laser has been increased orders-of-magnitude by major breakthroughs in the pumping of nuclear isomers with bremsstrahlung.

At the present the most significant impediment to study of the feasibility of a gamma-ray laser continues to be the lack of suitable materials. Of the 1886 distinguishable isotopes,[29,30] 29 have been identified as first class candidates, but only the two poorest, ^{180}Ta and ^{123}Te were available in sufficient amounts for testing. Still the discovery of giant pumping resonances for these nuclides[22-24] and others[25-27] greatly strengthened the feasibility. It is upon such pumping processes that the realization of a gamma-ray laser depends, rather than on refinements like superradiance which may simply serve to reduce threshold requirements

In the absence of better candidates, research by the main line continues to focus upon the pumping of simulation isomers that may teach the structure and systematics for these giant resonances. This study has also been recently extended with encouraging results to the examination of the pumping of laserlike states with lifetimes on the order of tens of μs. The present paper will review these developments and the major breakthroughs which have significantly increased the feasibility of a gamma-ray laser.

Concepts

The critical key to the development of the ruby laser was the identification and exploitation of a bandwidth funnel in which a broad absorption band was linked through efficient cascading to a narrow laser level. This an essential element as well to the blueprint for a nuclear analog to the ruby laser and is depicted by the schematic diagram of Fig. 1. Whether the initial state being pumped is the ground state or an isomer, the principal figure of merit is the integrated cross section, $\pi b_e b_o \sigma_o \Gamma/2$, for populating the upper laser level through the absorption state. Only one such state, or gateway, is shown in the figure but there could be more. The probabilities that the gateway will decay directly back to the initial level and either directly or by cascade to the laser level are b_e and b_o, respectively. These quantities together with the natural width of the absorption level, Γ give the useful, partial-width describing the transfer of population, $b_e b_o \Gamma$. The parameter σ_o is the one half of the peak value of the Breit-Wigner cross section and is proportional to the square of the wavelength of the pump photon. This means that the cross section for useful absorption of pump energy will be much larger for photons than for particles of the same energy. This is another crucial element to the feasibility of a gamma-ray laser as discussed in detail later.

Optical pumping processes like that depicted in Fig. 1 have been known in nuclear physics for more than 50 years[31] and are called (γ,γ') reactions where γ and γ' refer to the incident and scattered photons, respectively. Values of integrated cross section for these reactions typically range[18-21,32] from 1's to 10's in the usual units (uu.) of 10^{-29} cm^2 keV. However, the need for intense photon sources in the study of these reactions led to practical difficulties in accurately calibrating the incident flux. In particular the most difficult sources of x rays to characterize proved to be radionuclides for which all intensity away from the spectral lines resulted from environmentally sensitive Compton scattering. Thus little quantitative agreement could be found in the literature between values of integrated cross section obtained in different experiments. Even as late as 1987 there were serious contentions[33] over the mechanism by which these reactions occurred and the way in which expected fluorescence yields were calculated. Still the qualitative analysis of (γ,γ') experiments clearly showed that bandwidth funneling did occur in nuclei.

The earliest challenge to the gamma-ray laser project was to place the optical pumping of nuclei on a firm quantitative basis, beginning with a model for the reaction. The time-integrated yield of final-state nuclei, N_f obtained by irradiating a population of initial-state nuclei, N_i with a continuum of photons extending up to a maximum "endpoint" energy, E_o is given by

$$N_f = N_i \Phi_o \int_0^{E_o} \sigma(E)\, F(E,E_o)\, dE \quad . \tag{1}$$

where Φ_o is the total flux of incident photons integrated over the lifetime of the final state, $F(E,E_o)$ is the distribution of energies within the continuum and $\sigma(E)$ is the energy-dependent cross section for the reaction. It is now well known that all (γ,γ') reactions occurring at energies below the threshold for photoneutron production resonantly excite discrete states like that shown in Fig. 1. Although the widths of these gateways may be large on the nuclear scale, at this level there is little structure to most incident photon continua. If the gateways are well-spaced compared to their widths Eq. 1 becomes

$$A_f(E_o) = N_f / (N_i \Phi_o) = \sum_j (\sigma\Gamma)_j\, F(E_j,E_o) \quad . \tag{2}$$

where the yield has been expressed as the fractional activation per unit photon flux, $A_f(E_o)$ and $(\sigma\Gamma)_j = (\pi b_e b_o \sigma_o \Gamma/2)_j$ is the cross section for population of the final state through the j^{th} gateway integrated over a Lorentzian lineshape. The Breit-Wigner formula gives

$$\sigma_o = \frac{\lambda^2}{2\pi}\,\frac{2I_j+1}{2I_g+1}\,\frac{1}{\alpha_p+1} \quad . \tag{3}$$

where λ is the wavelength of the pump photon, I_j and I_g are the angular momenta of the gateway and ground states, respectively, and α_p is the internal conversion coefficient for the pump transition.

Model Validation

The model of Eq. 2 was validated by using bremsstrahlung from five different accelerators to irradiate targets containing the few isomeric nuclei for which reliable gateway data was available in the literature. These devices were two nuclear simulators, DNA/PITHON and DNA/Aurora, two medical linacs and one research linac, the injector to the superconducting Darmstadt linear accelerator (S-DALINAC). This approach, rather than that of using radionuclides as x-ray sources, was chosen due to the relative insensitivity of the intense, broad continua of bremsstrahlung to Compton scattering. Also, due to the wide use of electron accelerators in a variety of fields well-established computer codes have been developed for the accurate calibration of their photon output from measured currents and target geometries.

Gram sized samples were exposed for times ranging from seconds to hours for the cw machines and to single flashes from the pulsed-power devices. The yield of isomers produced by each irradiation were obtained by detecting fluorescence photons emitted after transferring the samples to a quieter environment. Standard corrections were made for the isotopic abundance, isomer lifetime, detection and emission efficiencies, and transparency of the samples to the fluorescence. Photon spectra were calculated with the EGS4 electron/photon transport code[34] adapted for each experiment to give both Φ_0 and $F(E,E_0)$. In some cases Φ_0 was verified by in-line dosimetry.

The results of these experiments[18-21,23] were in excellent agreement with the predictions of Eq. 2 using literature values[29,30,32] of gateway energies and integrated cross sections. A typical example is given in Fig. 2 which shows a composite excitation function obtained for the calibration isomer $^{87}Sr^m$ using the above mentioned accelerators[23,25] and the newly installed Texas-X research linac at the University of Texas at Dallas. It is important to note that the yield of the ^{87}Sr isomer was orders-of-magnitude enhanced by nuclear bandwidth funneling over that which could have been accounted for by direct excitation of the metastable level from the ground state.

An important consequence of the confidence level established by these experiments was the development of a new method[35] for selectively sampling the energy distribution of intense photon fluxes and providing absolute measurements using isomeric photoexcitation reactions. Even more important for the present work, *there could no longer be any reasonable doubt of the model or procedures for quantitatively measuring fluorescence efficiencies using bremsstrahlung*. This methodology was then applied to the examination of candidate nuclei for a gamma-ray laser.

Giant Pumping Resonances

Many of the candidate isotopes for a gamma-ray laser are deformed nuclei whose energy levels are built upon rotational bands like those of diatomic molecules. For a spheroidal nucleus an additional quantum must be conserved in reactions, K which is the projection of the total angular momentum, J on the major axis of symmetry. The selection rules for electromagnetic transitions are therefore $|\Delta J| \leq M$ and $|\Delta K| \leq M$ where M is the multipolarity of the transition. In general, isomeric levels of these deformed nuclei have quite long lifetimes since they lie in bands whose values of K differ greatly from those of bands containing lower-lying states to which they would otherwise be radiatively connected. Such isomers would be ideal as an initial state in the pumping of a gamma-ray laser since much energy is already stored in the nucleus. However, this same property means that a bandwidth funnel like that of Fig. 1 would have to span substantial ΔK and the integrated cross section for such a transfer of population could have been expected to be very small.

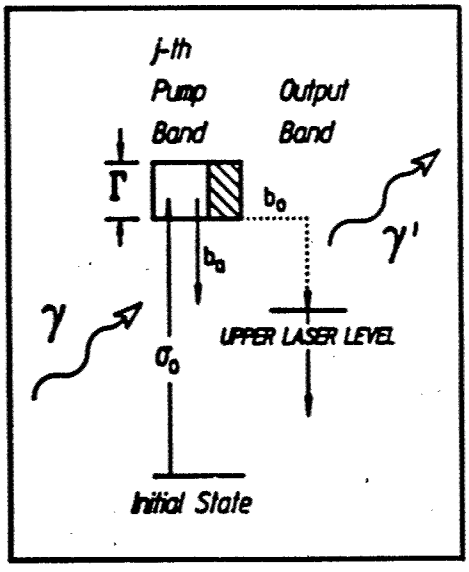

Figure 1: Schematic representation of the bandwidth funneling of population to a laser level through a gateway state with natural width Γ. The incident photon γ is absorbed with a cross section σ_0 by the initial level which may be either a ground state or an isomer. The cascade from gateway to laser level is shown by the dotted line with promptly emitted photons being the γ'.

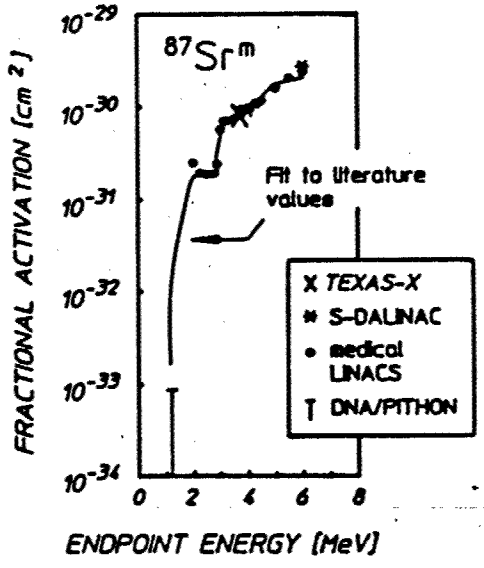

Figure 2: Fractional activations, A_f for the reaction $^{87}Sr(\gamma,\gamma')^{87}Sr^m$ as a function of bremsstrahlung endpoint, E_0 obtained with 5 different accelerators. The solid curve plots values computed from Eq. 2 using gateway parameters found in the literature and calculated photon spectra. The agreement of these values with the measurements is excellent, validating the procedures.

From this perspective the nuclide ^{180}Ta was considered to be among the poorest candidates since its isomer stores only 75 keV and requires the largest change in angular momentum, 8ħ for transitions to the ground state.[29,30] However, this isotope carries the distinction of being the only naturally occurring isomer in nature, having a lifetime in excess of 10^{12} years while its ground state has a halflife of only 8.1 hours. Since a macroscopic sample was readily available, ^{180}Ta^{m} became the first candidate tested.

An experiment was conducted[22] in 1987 in which 1.2 mg of ^{180}Ta^{m} was irradiated with bremsstrahlung from a 6 MeV medical linac and a large fluorescence yield was observed. This was the first demonstration that the energy stored in a nuclear isomer could be dumped to freely-radiating states by a (γ,γ') reaction as needed for a gamma-ray laser. Simply the observation of any fluorescence from a mg sized target when grams of material were needed for the calibration isotopes was evidence of pumping of unexpected magnitude and analysis[22] of the data indicated that the partial width for the dumping of ^{180}Ta^{m} was about 0.5 eV.

The gateway excitation energy for this isomer was determined by a series of irradiations[23] made with the variable energy S-DALINAC. Fourteen different endpoints in the range from 2.0 to 5.5 MeV were used to obtain the excitation function shown in Fig. 3. As in the case of the calibration isomer, ^{87}Sr^{m}, sharp increases in the yield as a function of endpoint, called activation edges, were observed indicating the location of the gateways. Using these locations and incident photon spectra computed with EGS4, Eq. 2 was used to iteratively fit the excitation by using trial values for the $(\sigma\Gamma)_j$. The lowest-lying gateway identified[23] for the dumping of the ^{180}Ta isomer was at 2.8 MeV with an integrated cross section of 12000 uu. The demonstration that populations of nuclear isomers can be dumped with bremsstrahlung, and with integrated cross sections 10^4 times larger than could have been expected stands as the first major breakthrough towards a gamma-ray laser and has enhanced its feasibility by four orders-of-magnitude.

These "giant pumping resonances" were also observed[24] for the second poorest candidate, ^{123}Te. However, no other candidates were available in sufficient amounts for testing so research focused on the pumping of simulation isomers in order to learn more about the systematics and structure of these gateways. A preliminary survey[25] of the pumping of 19 isomeric nuclei was conducted over a fairly coarse mesh of bremsstrahlung endpoints using the nuclear simulators and the medical linacs. Again, giant pumping resonances for transferring large ΔK were observed for nuclei in a region of masses near A = 180. A refined survey[26] was obtained using the S-DALINAC and served to locate the gateways and measure integrated cross sections for four isotopes neighboring ^{180}Ta. The results of these studies are shown in Fig. 4 which indicates that both the excitation energies and integrated cross sections for pumping isomers vary slowly between neighboring masses. The integrated cross sections were also correlated[26] with the ground state deformation, a property of the nuclear core.

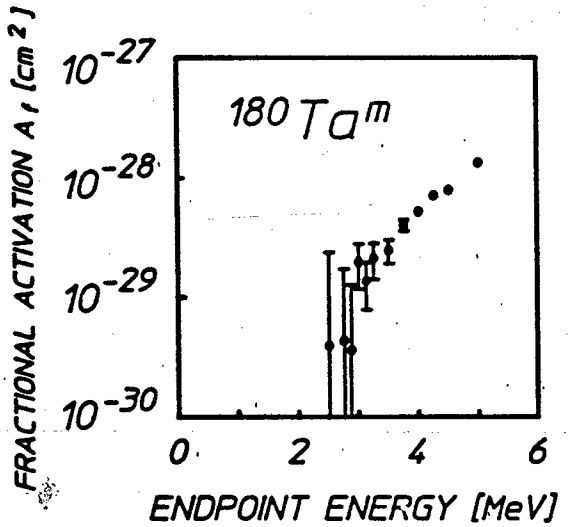

Figure 3: Fractional activations, A_f for the reaction ^{180}Ta$^{m}(\gamma,\gamma')^{180}$Ta as a function of bremsstrahlung endpoint, E_0 obtained with the S-DALINAC. Gateway parameters were determined by fitting the measured excitation function using Eq. 2 with trial values for the $(\sigma\Gamma)_j$ which were found to be 10^4 larger than those usually measured for (γ,γ') reactions. These data demonstrate the dumping of an isomeric population with x rays.

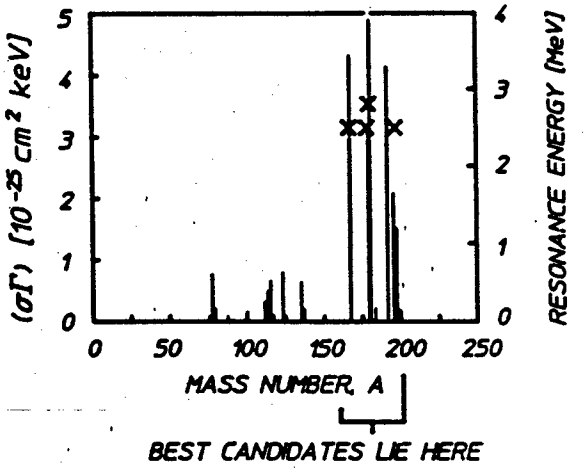

Figure 4: Systematics for integrated cross sections and gateway locations for pumping nuclear isomers with photons. The groupings correspond to mass islands between magic numbers for neutrons and protons. The best candidates for a gamma-ray laser lie in the mass-180 island. Within each island the integrated cross sections and excitation energies, indicated by the X symbols plotted by the right-hand ordinate, vary only slowly with changing mass number, A.

The unexpected magnitudes measured for pumping resonances in the mass 180 region have been difficult to interpret in the single-particle model and the apparent ease with which such large ΔK is transferred has been a mystery. However, an understanding of the basic principle has taken form which identifies these gateway locations with energies that excite collective oscillations of the nuclear core for which there would be no fixed shape by which K could be conserved. This would break the selection rule for K through strong admixtures of single-particle states. It is interesting to speculate that these giant pumping resonances may parallel the appearance of double minima shown to occur in the potential energy of heavy but nonfissile nuclei.[36] These minima are expected to lie at excitation energies of a few MeV while the gateways identified in the mass-180 region lie between 2.5 and 3 MeV.

Support for this idea comes not only from the systematics of the giant resonances for pumping isomers but also from experimental results which demonstrated[37] that the spontaneous electromagnetic decay of the isomer $^{174}Hf^{m}$ proceeded through a level at 2.65 MeV which provided an even larger degree of K transfer, $\Delta K = 14$. This is remarkably close to the energy of the K-mixing gateway at 2.8 $\pm$ 0.1 MeV found for ^{180}Ta. The understanding of giant pumping resonances as coupling to core oscillations means that the behavior of candidate isotopes lying near those nuclides tested can be reasonably be interpolated from the systematics data. Thus it can be expected that if an isomer starts with enough energy, little additional pump would be needed to reach a giant pumping resonance which lay 2.5 - 3.0 MeV above the ground state, but perhaps only a few hundred keV above the metastable state. This understanding constitutes a second breakthrough towards the feasibility of a gamma-ray laser.

The above described discoveries have significantly improved the feasibility of a gamma-ray laser by lowering pump requirements for a gamma-ray laser, primarily because of the large sizes of the integrated cross sections measured. However, the resolution of those experiments only permitted the gateways to be located to within $\pm$ 0.1 MeV. The possibility was therefore left open that the reaction strength might not be concentrated in a few transitions with relatively large widths, but instead might be spread over a great number of closely spaced levels with considerably reduced widths. This was of particular concern for the nuclei favored in Fig. 4 which have large excited state densities, and even more so for ^{180}Ta which is a rare odd-odd nucleus. Such behavior would seriously degrade the ratio of useful pump energy absorbed resonantly by the active nuclei to the energy absorbed nonresonantly, making the management of waste heat more difficult. A series of experiments were performed to explore this possibility.

Isomeric excitation functions reflect only one specific reaction channel of the process depicted in Fig. 1, that is the strong absorption of incident photons in a transition from the ground state to the gateway followed by a decay cascade leading to the metastable level. However, another important channel is that of absorption followed by a direct decay of the gateway back to the ground state. From Fig. 1 it can be seen that a large $(\sigma\Gamma)$ for the population of an isomer will be accompanied by elastic scattering of significant numbers of photons with an analogous integrated cross section, $(\sigma\Gamma)_{el} = \pi b_e^2 \sigma_0 \Gamma/2$. The detection of these photons in real time during an irradiation permits the direct measurement of excitation energies and widths for nuclear transitions and forms the basis for nuclear resonance fluorescence (NRF) experiments.

An experimental arrangement especially designed for NRF measurements was used to investigate[27,28] two isomeric nuclides, ^{89}Y and ^{115}In which were chosen for their large natural isotopic abundances and the degree to which their structure could be characterized within the unified model. Gram-sized samples were sandwiched between aluminum and boron calibration targets and were irradiated with well-collimated bremsstrahlung. Endpoint energies were used which permitted the observation of photons scattered by strong transitions with excitation energies in the range from 1.5 to 4.5 MeV. These photons were measured with carefully shielded detectors placed off-axis and appeared in pulse-height spectra as peaks superimposed on a large Compton background. Isomeric excitation functions were also measured for these isotopes.

Detailed spectra are available in the literature[27,28] but the relevant points are illustrated in schematic form for ^{115}In in Fig. 5. The excitation function data[27] of Fig. 5a indicated two giant pumping resonances located at 2.8 $\pm$ 0.1 MeV and at 3.2 $\pm$ 0.1 MeV. The striking discovery is in the NRF data of Fig. 5b which only exhibits strong transitions with energies lying within the experimental resolution of the gateways. Thus these few levels, or a subset thereof, were responsible for the population of the isomer. This conclusion was confirmed by unified-model calculations which showed that the absorption strength was concentrated into a small number of E1 or E2 transitions with excitation energies near those measured. Similar results[28] were obtained for ^{89}Y. Although a one-to-one correspondence was beyond the limits of the theoretical approach, the correlation between calculations and experiments clearly showed that the gateways in ^{89}Y and ^{115}In correspond to a small number of levels having relatively large widths. This is the third major breakthrough in the feasibility of a gamma-ray laser.

Recent Developments

The feasibility of a gamma-ray laser has been greatly enhanced by the discovery of giant resonances for the pumping and dumping of nuclear isomers. Such a metastable state would be used as a high-lying storage level from which a modest pump would populate a lasing level. Thus the next step in the project was to examine the pumping of more laserlike excited nuclear states with lifetimes on the order of μs, a task which required new research tools and techniques.

A milestone for the gamma-ray laser project was reached in 1992 with the construction of an underground facility dedicated to the pumping of nuclear materials and the installation of the Texas-X research linear accelerator at the University of Texas at Dallas. This 4 MeV linac was designed to produce pulses of bremsstrahlung of 2.78 μs duration with a repetition rate of up to 360 Hz, characteristics which were ideal for the study of the pumping of states with lifetimes greater than 1 μs. After an initial emplacement and testing period, the output spectrum of the Texas-X was calibrated absolutely by photoactivation measurements.[38] A survey of previously tested isotopes was then conducted as a test of consistency. The agreement with earlier measurements was excellent as evidenced in the data for the calibration isomer $^{87}Sr^{m}$ in Fig. 2.

To investigate the pumping of laserlike levels a new technique was developed which allowed a NaI(Tl) detector to observe fluorescence on a μs timescale emitted from samples irradiated with bremsstrahlung from the Texas-X. In brief, this required rapid and stable gating of the photomultiplier tube to avoid "blinding" the detector during each exposure pulse and the management of electromagnetic noise effects in the associated electronics. Further efforts are underway to refine the technology but preliminary results were quite encouraging as shown in Fig. 6 for the 615 keV, 18 μs state in ^{181}Ta. The detector was gated on 8 μs after each linac pulse and a time-to-amplitude converter (TAC) was used to obtain a decay spectrum for the level which was collected for a total of 7×10^5 cycles. The agreement between the measured halflife and the literature value[29] was excellent and the data analysis indicated that the integrated cross section for pumping was comparable to those for the population of isomers. Extensive studies of this type are now in progress.

Another development was the implantation by a local small business of isotopically pure ^{57}Fe nuclei within a thin diamond film deposited on a titanium substrate. The sample represented a realistic simulation of a host material capable in principle of preserving a natural width for the stimulated-emission cross section, a necessary condition for a gamma-ray laser. In fact Mössbauer spectra showed this to be the case and the quality of the data obtained from the 4.5 μg of ^{57}Fe within the film was not significantly degraded from that obtained from a milligram enriched ^{57}Fe sample.

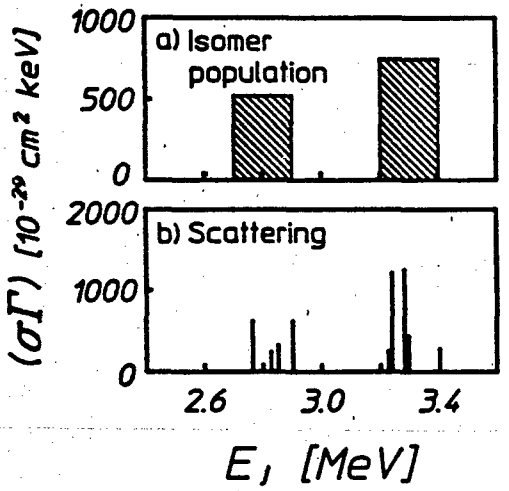

Figure 5: Schematic representing integrated cross sections for a) population of the isomer $^{115}In^{m}$ obtained from excitation function measurements and for b) elastic scattering by absorption transitions obtained from NRF measurements. Gateway locations of a) were determined only within ± 0.1 MeV and strongly scattering levels were only observed within these bands. Thus a subset of the transitions of b) are respc sible for the population of the isomer. This was confirmed by unified model calculations.

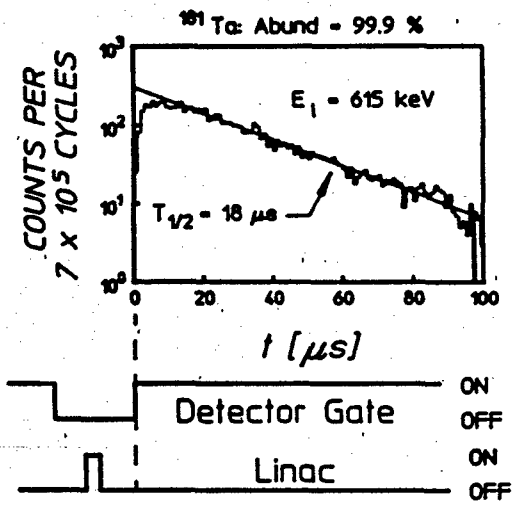

Figure 6: Fluorescence detected from the 18 μs, 615 keV level in ^{181}Ta following its excitation by bremsstrahlung from the Texas-X research linac. These preliminary data were collected for nearly 10^6 cycles using a new technique which allowed a NaI(Tl) detector to be gated off during pulses of x rays from the linac and then turned on to observe fluorescence from the sample between pulses, as shown in schematic form. The integrated cross section obtained was comparable to that for pumping nuclear isomers with x rays.

A Laser Model

The 1990's model for a gamma-ray laser is fundamentally identical to the nuclear analog of the ruby laser presented[2] in 1982. Isomeric nuclei would be doped into a thin, low-Z diluent and would be pumped by a flash of x rays. However, the discovery of giant pumping resonances has relaxed some of the original constraints, improving the feasibility of a gamma-ray laser by orders-of-magnitude over that originally projected. Thus it is instructive to recompute the model in terms of this new data. Of course the precise identity of the best nuclide to model is unknown so it is necessary to begin with certain assumptions:

1) There is a single pump transition with an excitation energy of E_j = 30 keV.
2) The initial state is an isomer with a sufficiently energy high that 1) is possible.
3) The gateway is a giant pumping resonance having a partial width of $b_a b_o \Gamma$ = 1 eV.
4) The output transition is around 100 keV.
5) The active nuclei are implanted in a thin film of diamond.
6) The Borrmann effect enhances the ratio of resonant to nonresonant absorption by a factor of 10.

The most critical assumptions are those of 1) and 2). However, isomers can be found over a large range of excitation energies from 10's of keV to several MeV so there is only a statistical question whether a giant pumping resonance can be found within 30 keV of an isomer. The remaining conditions are based on recent discoveries, the present state-of-the-art technology for producing thin diamond films[39] and projections for its development in the near future.

Following the development[2] of 1982, under small signal conditions the threshold for amplification in a single pass down the length of the film requires the fraction of active nuclei pumped to be $N_x/N_i \geq \sigma_{NR}/\sigma_R$. The σ_{NR} and σ_R are the cross sections for nonresonant and resonant absorption, respectively, of the 100 keV output photons. It can be shown[1,40] that with the assumed Borrmann enhancement a midrange value for this fraction is 10^{-4} although even more favorable values are possible. It is also conceivable that refinement effects like superradiance may serve to reduce the threshold requirement further. Using the required pump fraction and the Breit-Wigner cross section of Eq. 3 for a 30 keV photon with $I_j = I_g$ and $\alpha_p = 0$, Eq. 2 gives the needed spectral flux of $\Phi_0 F(E_j, E_0) = 5.9 \times 10^{13}$ cm^{-2} eV^{-1}, or a spectral fluence of 177 mJ cm^{-2} eV^{-1}. If edge filters or ablation layers are used prior to the doped layer the pump bandwidth could be limited to 3 keV, yielding a total fluence of 530 J cm^{-2}.

The essential concept for the management of the thermal economy of a gamma-ray laser is that the mean free path (MFP) for useful, resonant absorption of the 30 keV pump must be much smaller than the MFP for nonresonant, photoelectric absorption. Also the MFP for resonant absorption must be smaller than the MFP for any primary photoelectrons produced by nonresonant events in the film. Primary photoelectrons are the dominant source of heating since relatively few conversion electrons will be produced by energetic gamma transitions in the pump cascade. These conditions can be met by doping a thin diamond film with a 10 % concentration of active nuclei. In order to maximize the absorption of the pump in this example, the thickness of the film is chosen to equal one MFP for 30 keV photons, that is 0.67 μm.

In the case of isotopes which are rare earths or platinides, the 30 keV pump would lie below the K edge and about 15 keV above the L edge, giving primary photoelectrons with energies near 15 keV. In diamond the range of these electrons would be about 3.0 μm so only 20 % of the primaries would be stopped in the host film.[40] The fraction of the incident pump fluence which would be stopped in the laser medium by nonresonant absorption is 2.4×10^{-3} so the total fraction of input fluence which would be converted to heat would be 4.8×10^{-4}. The total fluence degraded to heat would then be 255 mJ cm^{-2} and the thermal loading of the film would be 3.8 KJ cm^{-3}. For comparison, the energy density due to useful, resonant absorption would be 2.6 KJ cm^{-3}.

To have stimulated emission the host lattice must preserve the natural width of the output transition through the Mössbauer effect. The complex dependence of the recoil-free-fraction upon materials and gamma transition energies was discussed in Ref. 1 and it was shown that little degradation of this factor occurred for temperatures even as high as the Debye temperature, Θ_D. In diamond the Debye temperature is Θ_D = 2230 K and the energy content of a film at a temperature $T = \Theta_D$ is computed[41] to be about 11 KJ cm^{-3}. Thus the estimated instantaneous thermal loading of 3.8 KJ cm-3 gives a "safety factor" of nearly three for preserving the stimulated emission cross section. A similar calculation for a host film of beryllium gives comparable results.[40]

Much can be done to reduce the heating further since phonons can be transported across the 0.67 mm film in about 100 ps while lasing levels would have lifetimes ranging from 10's of ns to 10's of μs. Thus over the duration of the pump flash the cooling of the film could be improved significantly over that of the example above. However, the techniques available depend upon precise knowledge of the actual isotope and the absorption edges of the materials used. Still the model demonstrates that there is a large safety margin between likely amounts of thermal loading and the amounts which can be tolerated in stiff lattices like diamond or beryllium.

Conclusions

The discovery of giant resonances for pumping and dumping populations coupled with the development of the technology for producing thin diamond films have enhanced the feasibility of a gamma-ray laser by orders-of-magnitude over that projected in the blueprint of 1982. All of the component concepts have now been demonstrated experimentally and the persistent but false tenets of theoretical dogma which have historically inhibited the development of a gamma-ray laser have been eliminated. In particular it is not necessary to melt the host lattice in order to optically pump a nuclear system to threshold. *There are no a priori obstacles to the realization of a gamma-ray laser. A gamma-ray laser is feasible if the right combination of energy levels occurs in some real material.* The remaining question to resolve is whether or not one of the better candidates has its isomeric level located sufficiently close to a giant resonance for dumping angular momenta.

This work was supported by SDIO/TNI under the direction of NRL.

References

1. G. C. Baldwin, J. C. Solem and V. I. Goldanskii, Rev. Mod. Phys. 53, 687 (1981).
2. C. B. Collins, F. W. Lee, D. M. Shemwell, B. D. DePaola, S. Olariu and I. Popescu, J. Appl. Phys. 53, 4645 (1982).
3. V. S. Letokhov, Sov. J. Quant. Electron. 3, 360 (1974).
4. B. Arad, S. Eleizer and Y. Paiss, Phys. Lett. 74A, 395 (1979).
5. C. B. Collins, S. Olariu, M. Petrascu and I. Popescu, Phys. Rev. Lett. 42, 1397 (1979).
6. C. B. Collins, S. Olariu, M. Petrascu and I. Popescu, Phys. Rev. C 20, 1942 (1979).
7. S. Olarui, I. Popescu and C. B. Collins, Phys. Rev. C 23, 50 (1981).
8. S. Olariu, I. Popescu and C. B. Collins, Phys. Rev. C 23, 1007 (1981).
9. C. B. Collins, in Proceedings of the International Conference on Lasers '80, ed. C. B. Collins (STS Press, McLean, VA, 1981) p 524.
10. C. B. Collins, in Laser Technique for Extreme Ultraviolet Spectroscopy, ed. T. J. McIlrath and R. R. Freeman (AIP Conference Proceedings No. 90, New York, 1982) p 454.
11. C. B. Collins, in Proceedings of the International Conference on Lasers '81, ed. C. B. Collins (STS Press, McLean, VA, 1982) p 291.
12. C. B. Collins, in CRC Handbook of Laser Science and Technology, Supplement 1: Lasers, ed. by M. J. Weber (CRC Press, Boca Raton, Fl., 1991) p 561.
13. B. D. DePaola and C. B. Collins, J. Opt. Soc. Am. B 1, 812 (1984).
14. C. B. Collins and B. D. DePaola, Optics Lett. 10, 25 (1985).
15. B. D. DePaola, S. S. Wagal and C. B. Collins, J. Opt. Soc. Am. B 2, 541 (1985).
16. B. D. DePaola and C. B. Collins, J. Opt. Soc. Am. B 1, 812 (1984).
17. T. W. Sinor, P. W. Reittinger and C. B. Collins, Phys. Rev. Lett. 62, 2547 (1989).
18. J. A. Anderson and C. B. Collins, Rev. Sci. Instrum. 58, 2157 (1987).
19. J. A. Anderson and C. B. Collins, Rev. Sci. Instrum. 59, 313 (1988).
20. C. B. Collins, J. A. Anderson, Y. Paiss, C.D. Eberhard, R.J. Peterson and W. L. Hodge, Phys. Rev. C 38, 1852 (1988).
21. J. A. Anderson, M. J. Byrd and C. B. Collins, Phys. Rev. C 38, 2833 (1988).
22. C. B. Collins, C. D. Eberhard, J. W. Glesener and J. A. Anderson, Phys. Rev. C 37, 2267 (1988).
23. C. B. Collins, J. J. Carroll, T. W. Sinor, M. J. Byrd, D. G. Richmond, K. N. Taylor, M. Huber, N. Huxel, P. v. Neumann-Cosel, A. Richter, C. Spieler and W. Ziegler, Phys. Rev. C 42, R1813 (1988).
24. J. J. Carroll, T. W. Sinor, D. G. Richmond, K. N. Taylor, C. B. Collins, M. Huber, N. Huxel, P. v. Neumann-Cosel, A. Richter, C. Spieler and W. Ziegler, Phys. Rev. C 43, 1238 (1991).
25. J. J. Carroll, M. J. Byrd, D. G. Richmond, T. W. Sinor, K. N. Taylor, W. L. Hodge, Y. Paiss, C. D. Eberhard, J. A. Anderson, C. B. Collins, E. C. Scarbrough, P. P. Antich, F. J. Agee, D. Davis, G. A. Huttlin, K. G. Kerris, M. S. Litz and D. A. Whittaker, Phys. Rev. C 43, 1238 (1991).
26. C. B. Collins, J. J. Carroll, K. N. Taylor, D. G. Richmnond, T. W. Sinor, M. Huber, P. v. Neumann-Cosel, A. Richter and W. Ziegler, Phys. Rev. C 46, 952 (1992).
27. P. v. Neumann-Cosel, A. Richter, C. Spieler, W. Ziegler, J. J. Carroll, T. W. Sinor, D. G. Richmond, K. N. Taylor, C. B. Collins and K. Heyde, Phys. Lett. B266, 9 (1991).
28. M. Huber, P. v. Neumann-Cosel, A. Richter, C. Schlegel, R. Schulz, J. J. Carroll, K. N. Taylor, D. G. Richmond, T. W. Sinor, C. B. Collins and V. Y. Ponomarev, submitted to Nucl. Phys. (pending).
29. *Evaluated Nuclear Structure Data File* (Brookhaven National Laboratory, Upton, New York, 1986). Sheets.
30. E. Browne and R. B. Firestone, Table of Radioactive Isotopes, ed. by V. S. Shirley (Wiley, New York, 1986).
31. B. Pontecorvo and A. Lazard, C. R. Acad. Sci. 208, 99 (1939).
32. E. C. Booth and J. Brownson, Nucl. Phys. A98, 529 (1967).
33. I. Bikit, J. Slivka, I. V. Anicin, L. Marinkov, A. Ruydic and W. D. Hamilton, Phys. Rev. C 35, 1943 (1987).
34. *The EGS4 Code System*, W. R. Nelson, H. Hirayama and d. W. O. Rogers, Stanford Linear Accelerator Center Report No. SLAC 265, 1985 (unpublished).
35. J. A. Anderson, C. D. Eberhard, K. N. Taylor, J. M. Carroll, J. J. Carroll, M. J. Byrd and C. B. Collins, IEEE Trans. Nucl. Sci. 36, 241 (1989).
36. M. Girod, J. P. Delaroche, D. Gogny and J. F. Berger, Phys. Rev. Lett. 65, 416 (1990).
37. P. M. Walker, F. Sletten, N. L. Gjørup, M. A. Bentley, J. Borggreen, B. Fabricius, A. Holm, D. Howe, J. Pedersen, J. W. Roberts and J. F. Sharpey-Schafer, Phys. Rev. Lett. 65, 416 (1990).
38. J. J. Carroll, K. N. Taylor, T. W. Sinor, C. Hong, J. D. Standifird and C. B. Collins, submitted to Nucl. Inst. Meth.
39. C. B. Collins, F. Davanloo, T. J. Lee, J. H. You and H. Park, Am. Ceram. Soc. Bull. 10, 1535 (1992).
40. "Thermal Economy of a Gamma-Ray Laser," C. B. Collins in the Center for Quantum Electronics: The Gamma-Ray Laser, Final Technical Report 1986-1989, p 1 (unpublished).
41. C. Kittel, Introduction to Solid State Physics, 6th Edition (Wiley, New York, 1986) p 106.

Experimental Preparations for the Excitation of Short-Lived Nuclear Isomers Pumped with the UTD-LINAC

by

K. N. Taylor, T. W. Sinor, J. D. Standifird, C. Hong,

J. J. Carroll, D. G. Richmond, and C. B. Collins

Center for Quantum Electronics

University of Texas at Dallas

P.O. Box 830688

Richardson, TX 75083

ABSTRACT

Experiments have been designed to populate Mössbauer levels of ^{57}Fe and ^{119}Sn by cascade from giant resonances pumped by bremsstrahlung radiation generated by the UTD-LINAC, the facility for which is currently under construction. In particular we have employed both resonant and non-resonant radiation transfer studies to aid in the design, construction, and characterization of a detection system for monitoring the signal electrons produced by the decay of the short-lived isomeric targets employed. Measurements utilizing conversion electron Mössbauer spectroscopy indicate that the detection system developed, convincingly approaches the level of performance considered mandatory for the harsh environment anticipated for the intended nuclear fluorescence experiments.

INTRODUCTION

Since 1986, gamma-ray laser research at the Center for Quantum Electronics has focused upon the photoexcitation of nuclei from their ground states to relatively long-lived metastable states. Current efforts have concentrated on extending the scope of this research to short-lived states. In particular, current experiments have been designed to populate the Mössbauer levels of ^{57}Fe and ^{119}Sn by cascade from giant resonances pumped by bremsstrahlung radiation generated by the UTD-LINAC. The UTD-LINAC facility is under construction and should be on-line in the spring of 1992.

In past experiments involving the photoexcitation of long-lived nuclear isomers pneumatic transfer systems were used to move the irradiated targets from the pumping environment to the detection systems. To study isomers with lifetimes less than 100 nsec, however, it will be necessary to develop experimental apparatus that allows nondestructive, in-situ detection of the fluorescence signal or some other emission proportional to it. The approach taken here to verify and measure the rate of population of the isomeric levels of the sample is to utilize it as a source of recoil-free radiation and Doppler modulate the energy of the Mössbauer emissions to pump a similar sample in an evacuated detector chamber. The second sample would then be monitored via conversion electron Mössbauer spectroscopy (CEMS) [1-6].

Research for the past six months has employed both resonant and non-resonant radiation transfer studies to aid in the design, construction, and characterization of the detection system needed to provide the capabilities for the measurements described above. Several phases of development and investigation have been involved in bringing the detection system to a level of maturity that closely approaches the design objectives. These goals include (1) an efficient transfer of resonance radiation from the external target, pumped by the bremsstrahlung radiation, to the sample, (2) an optimized collection/detector system for the signal electrons

emitted from the surface of the sample and (3) a minimum of scattering-induced background noise from the vacuum chamber and the components of the detection system within the chamber.

Extensive efforts were pursued to develop a system that optimized the transfer of the resonant radiation from the external target to the sample. To assure passage of the resonant γ rays into the target chamber a thin entrance window constructed of titanium was employed. This window had the added benefit of filtering many of the lower energy x rays that are products of the de-excitation process.

For a given solid angle, defined by the geometry of the external source, the sample and their separation, the next most significant factor affecting the efficiency of the resonant transfer process was the collimator. The collimator design that yielded the best performance for CEMS consisted of a lead plate having a circular aperture at its center. The aperture was shaped so that its diameter increased in the direction of propagation of the radiation. With the source located at the appropriate distance in front of the plate the desired collimation was achieved.

The significance of using the aperture-plate as opposed to a long mass of lead with a hole along its axis was that with the source backed away from the aperture, not only was the geometrical collimation defined (and therefore the scattering-induced background in the chamber limited) but a minimum of radiative scattering associated with the collimator itself occurred. Due to the extremely narrow linewidths encountered in Mössbauer spectroscopy any resonant photons scattered off the sides of the collimator would be shifted out of resonance and thus become potential sources of noise inside the chamber.

Closely allied with the rationale for developing an optimized transfer of the resonance radiation from the irradiated target to the sample is that of developing an efficient detection system for the resonant γ rays entering the chamber. An ideal γ-ray detector would possess a high throughput for the signal and a correspondingly low throughput for the noise. Due to the

nature of the resonance phenomena involved in CEMS, one is in an advantageous position for developing a detector that possesses, to a significant degree, these properties. Such a resonant detector has been constructed and it consists of the resonant target, which converts the incoming γ rays to signal electrons, an electron collection system and an electron detector.

Various efforts have been pursued to separately investigate the photoelectric emission generated from the entrance and exit windows of the target chamber, the holder for the sample target, the effect of the target itself, the walls of the chamber and the electron lens assembly responsible for collecting the signal electrons emitted by the target. Radioactive samples external to the chamber served as calibration sources of radiation to produce the scattering effects required for these evaluations. The radiation emitted from the sources was collimated to define the beam geometry and its path through the chamber.

A dual microchannel plate (MCP) assembly configured in the chevron tradition was chosen as the electron detector. (See Figure 1 for the chevron configuration and biases typical of our experiments.) A microchannel plate is an array of approximately 10^6 parallel channels that serve as miniature electron multipliers. Nominal diameters of the channels range from 10 to 100 μm and have typical length-to-diameter ratios ranging from 40 to 100. The channels are either normal to, or biased at a small angle of approximately eight degrees to, the input surface of the MCP. In our research efforts we use a 25 mm diameter Galileo Electro-Optic chevron. In the chevron arrangement [7,8], two plates are oriented so that the channel bias angles provide a sufficiently large directional change at the interface to inhibit positive ions produced near the output of the rear plate (by electron-residual-gas collisions) from migrating to the input of the front plate where, upon collision with the channel wall, they might cause indistinguishable noise pulses. The plates are separated normally by approximately 50 to 150 μm. Typical detection efficiencies of chevrons for various kinds of primary radiation are summarized in Table 1 [9].

The electron collection system consisted of the target, an aperture lens designed with the aid of computer simulations and a Faraday cage structure integrated with the lens and target in such a way as to shield the lens elements from the ground potentials of the chamber walls. The lens was designed to focus and accelerate the electron emissions from the target to the electron detector. Post-emission acceleration of the electrons enhanced the focusing power of the lens and produced and increased the energy of the electrons to a level more compatible with the energy-response region of the electron detector.

OVERVIEW OF CONVERSION ELECTRON MOSSBAUER SPECTROSCOPY

Evaluation of the resonant detection system described in the previous section was most effectively obtained by performing CEMS with an external source of ^{57}Co and an enriched target of ^{57}Fe inside the target chamber. Use of the Mössbauer effect in this evaluation was of considerable value for two reasons: (1) The method of measurement in the experiment with the LINAC will involve the emission and absorption of resonance radiation. The early incorporation of the Mössbauer effect thus serves to simulate to some degree that expectation. (2) Its use also allows for the simultaneous evaluation of signal and noise production in the detection system. The Mössbauer effect makes possible a high resolution nuclear spectroscopic technique applicable to certain transitions having γ-ray energies from 10 - 100 keV. The lifetimes of the nuclear states are typically 10^{-8} seconds, which is approximately the same order of magnitude as optical transitions in atomic states. However, due to the higher energy of the gamma radiation the Q ($=\Delta E/\Gamma$) of the resonance is about 10^{12}. This ratio of the transition energy to the natural linewidth is a measure of the accuracy of the determination of relative frequency or energy changes of the system. Therefore, the Mössbauer effect allows an intrinsic resolving power much

greater than any other form of spectroscopy. It is only through the existence of Mössbauer transitions that a practical source of very narrow line radiation can be produced and detected.

A nucleus resonantly excited by the recoil-free absorption of a γ ray can decay in various ways, involving either the re-emission of a γ ray or the ejection of an atomic electron via internal conversion. Typically, low energy isomeric states are characterized by internal conversion coefficients between 1 and 100 so that the resonant scattering of Mössbauer gamma radiation is dominated by the conversion process. Since all synchronous radiation emitted after the resonant decay of a nucleus can be employed to record a Mössbauer spectrum, the detection of conversion electrons and the subsequently emitted Auger and secondary electrons, can provide a low noise spectroscopic signal for the study of the de-excitation of short-lived nuclear isomers. CEMS necessarily imposes a scattering geometry upon the experimental arrangement and therefore the emission spectrum one observes is seen as an increase in count rate in the detector.

It is significant to point out that since only those electrons emitted from the surface can be detected, this, in a sense, places a natural limit on the effective thickness of the absorber. This limit on effective absorber thickness removes any saturation effects that might be related to the severe dependence of the resonant absorption coefficient on the energy of the incoming gamma ray. Hence, the natural linewidth of the transition is observed. Typical ranges for both the 7.3 keV conversion electrons and 5.4 keV Auger electrons in iron are approximately 57 nm and 36 nm, respectively.

The decay scheme and energy level diagram of the nuclear emission for ^{57}Co and its daughter isotope ^{57}Fe are shown in Figure 2. The ^{57}Co source decays by electron capture into an excited state of ^{57}Fe, with the 3/2 $\rightarrow$ 1/2 Mössbauer transition leading to either the emission of a 14.4 keV γ ray or a conversion electron. The mean lifetime of the isomer, τ, is 1.4×10^{-7} seconds. From Heisenberg's uncertainty principle, $\Delta E = \Gamma = \hbar/\tau$, it can be shown that the natural

linewidth of the transition is $\Gamma = 5 \times 10^{-9}$ eV. For ^{57}Co prepared as a resonant, single-line source in a palladium lattice the 14.4 keV γ-ray emission can occur without recoil, or measurable loss of energy, in about 62-66% of the decays. Hence, in the majority of cases resonant absorption can occur since the nuclear energy levels of the source and absorber match.

With the frequency of the resonant photons so well defined, an optical Doppler shift accomplished by moving the source relative to the absorber can be easily used to tune the single emission line of the source into and out of resonance with the absorber (which may be either single-line or possess hyperfine structure). The relative velocity of the source and absorber necessary to scan a full width, 2Γ, of the resonance line is given by

$$E_D = (v/c)E_\gamma \cos\theta \quad , \qquad (1)$$

where E is the energy of the γ ray, v is the relative velocity between the source and absorber, c is the speed of light and θ is the angle between the source velocity and the direction of the γ-ray propagation.

As previously mentioned, the de-excitation of a resonant nucleus in the absorber can proceed through the emission of a Mössbauer quantum or by internal conversion, and for ^{57}Fe the total electron conversion coefficient is 8.2. The relative intensities of the conversion and Auger electrons [1] are: (1) for conversion electrons: K(7.3 keV, 79%), L(13.6 keV, 8%), and M(5.4 keV, 1%); and (2) for Auger electrons: KLL(5.4 keV, 60%) and LMM (0.5 keV, 6%). As a practical matter, insofar as actual emission from the absorber is concerned, it has been shown that 50% of the signal electrons ejected from the target have energies below 15 eV because of scattering and thermalization effects [10-12].

The sensitivity of CEMS is determined by many factors that depend on the nuclear, atomic and solid state properties of the source and scatterer. For a thin, single-line source and resonant

scatterer the maximum resonant effect to be expected is given by the ratio of the number of conversion electrons ejected from the absorber to the number of photoelectrons ejected [1,2]. The expression for calculating this figure is given by

$$\eta_{cems} = \frac{N_0 - N_\infty}{N_\infty} = \frac{na\delta f_s f_a \alpha \sigma_0 \Omega}{2n\delta\,(\alpha + 1)\,\sigma_{ph}\Omega} = \frac{a f_s f_a \alpha \sigma_0}{2\,(\alpha + 1)\sigma_{ph}\Omega} \quad , \qquad (2)$$

where N_0, N_∞ are the count rates on and off resonance, n is the number of target nuclei per cm^3, a is the isotopic abundance of resonant nuclei, δ is the thickness of the target (on the order of several mean-free-paths of the conversion electrons in the absorber), σ_0 and σ_{ph} are the cross-sections for the Mössbauer and photoeffect and Ω is the relative solid angle (normalized to 4π) for detection of electrons, f_s and f_a are the recoil-free fractions for the source and absorber, and α is the total internal conversion coefficient. In actuality, the observed magnitude of the effect is significantly smaller than the value calculated from Equation 2. One major reason is that in the experiment conducted here a single-line emitter is used for the source but the absorber exhibits a multiplicity in which six allowed transitions having line intensities in the approximate ratios of 3:2:1:1:2:3 are present. The percent effect of the transitions are reduced by the ratio of the area under the resonances. Therefore, CEMS for the first transition would be about 20 using the values $\sigma_0/\sigma_{ph} = 400$, $\alpha = 8.2$ and $f_S = f_a = 0.7$.

OVERVIEW OF DESIGN AND DEVELOPMENT

Several distinct phases of design and testing were involved in bringing the target chamber to its present level of performance. For the earlier stages of development and evaluation a 12 mCi source of ^{57}Co was used to supply non-resonant radiation to the vacuum chamber and its

contents in order to simulate the scattering conditions to be expected in the latter steps of the evaluation process. The final stage of studies involved utilizing the CEMS procedure to determine the efficacy of the resonant detection system. The same source of radiation was used for both the nonresonant and resonant studies.

The physical layout of the system consisted of mounting the MCP, sample, electric feedthrough connectors and the Faraday cage as an integral unit on a six inch vacuum flange. As indicated in Figure 3, this provided for the convenient mounting and removal of the entire assembly from the vacuum chamber. The angular position of the target assembly with respect to the direction of the γ rays could be changed by rotating it about a vertical axis.

Chamber Background

To determine the contributions of the chamber itself to the scattered radiation arriving at the input of the electron detector, the MCP was replaced with a thin-window NaI detector placed in a shielded, custom mount that was located in the exact location of the MCP. It was found that radiation scattering from the chamber could be minimized by providing a radiation exit window diametrically opposite the entrance window. This window was constructed of mylar to minimize backscattering of the radiation and had a diameter of four inches. With proper collimation of the ^{57}Co source, the beam size could be optimized to illuminate only the target while not expanding to a diameter greater than the output window.

Detector Assembly Background

One of the initial experiments conceived to optimize the detector arrangement consisted of measuring the photoelectric contribution of the detector assembly excited by the external radioactive source. In part, to prevent contamination of these measurements by photoelectrons

produced by incident radiation striking and scattering off the walls of the vacuum chamber the MCP target assembly was enclosed in a Faraday cage which served as an opaque barrier to all but the most energetic photoelectrons.

To verify a consistent performance of the MCP for these background measurements an unsealed ^{57}Co source with a nominal activity of 11.6 microcuries was mounted inside the target chamber. A lead disk coupled to a rotary vacuum feedthrough served as a selective filter to pass either electrons and photons, γ rays and x rays only, or to block all direct radiation from the MCP. Since this source was mounted outside the Faraday cage, the effectiveness of the Faraday electrostatic shield against the inward migration of electrons could also be observed.

The relative photoelectric and Compton contributions from components inside the Faraday cage were determined in a series of experiments in which materials having different Z-values were employed. The basic experimental arrangement contained a chevron (with an electron lens) and a static external $^{57}Co(Pd)$ source for exciting the chamber. Once the chevron was shown to be operating at nominal sensitivity the internal reference source was blocked by the radiation filter. The radiation from the external Mössbauer source was, of course, collimated to define the beam. Data were collected in this arrangement with various combinations of the detector components assembled. The configurations included: (1) null, (2) Faraday cage, and (3) Faraday cage with target holder. In the final configuration, 5 cm by 5 cm targets of mylar, aluminum, copper, and tantalum were used. The results of these experiments are summarized in Table 2. In all of the configurations above, the operating bias across the chevron was -1400 V, and the protection grid and Faraday cage biases were -2400 V.

Relative Background Contributions of Target/Target Holder

As indicated previously, a collimator was used to control the spatial extent of the radiation beam entering the chamber. The most effective configuration for the background measurement was found to be a cylindrical collimator 5.4 cm in diameter and 21.3 cm long cast out of lead with a 0.7 cm bore machined to obtain the desired collimating effects. This collimator produced a spot size at the target center of 1.2 cm diameter and expanded to 1.8 cm at the radiation escape window. Since only the non-resonant processes were of interest at this stage, the frequency downconversion characteristic of a long collimator was not detrimental. To take proper advantage of this high level of collimation the collimator was mounted on a gimbal and coupled to a micrometer which allowed the radiation to be scanned horizontally over the target assembly (no Faraday cage or lens being present). To measure the angular deviation of the source about the normal to the entrance window a mirror epoxied to the rear of the collimator was illuminated with a He-Ne laser normally incident to the mirror. The angular separation of the incident and reflected beam, 2θ, was measured geometrically.

By scanning the radiation across the target assembly the sensitivity and value of this approach was confirmed by the extent of the relative photoelectron contributions observed for the holder and target. Again, data were collected for mylar, tantalum and null targets. Representative data for the tantalum and null targets are shown in Figure 4. As can be seen from the figure, photoelectrons from the target holder, constructed out of teflon, are clearly visible to the detector. While this signal is much smaller than that from a tantalum target, it was soon determined that it could still contribute a significant background in a CEM spectrum. To circumvent this source of noise, a new target holder was constructed out of delrin, which is a low-Z polymer having excellent vacuum properties.

Electron Lens Design and Construction

To increase the total detection efficiency for signal electrons by the chevron, an electrostatic, aperture lens was constructed to effectively increase the solid angle between the electron detector and the target foil. With a 1.2 cm spot size on the target foil, a chevron with a diameter of 2.5 cm and a separation distance of 9.5 cm, a geometrical solid angle of 1.3 steradians was defined. Numerous computer simulations using plane-wave and point-source electron configurations have shown that the electrostatic lens gives an effective solid angle of almost 2π steradians for electrons having appropriately low energies.

The structure and dimensions of the lens can be seen in Figure 3. It exhibits a standard two-stage ring configuration constructed from copper mesh with the potential difference between the two rings acting as the primary electron accelerator. It has an outside diameter of 12.7 cm, and a length of approximately 15 cm. The two annuli making up the rings have successively smaller apertures as the MCP is approached. The first annulus has an inside diameter of 3.2 cm while the second has an inside diameter of 2.5 cm. This was done to allow the electrostatic fields generated by the annuli to penetrate into the region occupied by the target foil, and so that the inside diameter of the second annulus matched the diameter of the MCP. This aided in preventing oversteering of the electrons so that a greater fraction of them were incident upon the face of the MCP.

Each lens segment is surrounded by copper wire cloth, fashioned in a simple weave, so as to simulate a Faraday cage. The Faraday cage used in earlier experiments proved the value of such structures in shielding the MCP from noise electrons produced outside the cage. Most importantly, however, the Faraday cage here serves to shield the various lens elements from the ground potentials of the chamber walls that would grossly distort the focusing fields. A fine mesh

endcap with 81% open area was placed over the portion of the lens next to the chevron input to complete the shield assembly.

The choice of copper wire cloth for the lens material was made for several reasons. First, it was very important that the mass inside the chamber be kept to a minimum since any mass can potentially be a source of photoelectric and Compton noise. Secondly, a mesh was needed so that openings would exist for the external radiation source to illuminate the target foil. The field disturbances caused by using a mesh instead of a continuous sheet of metal can easily be shown to be negligible [13].

The copper mesh has a wire diameter of approximately 250 μm and about 6 weaves per cm. Using simple formulae, it can be shown that this material has 69 percent open area. To increase the percent open area in the direct path of the radiation, alternate wires in the region of the lens within the path of the external radiation were removed. This reduced the mass present in the path of the radiation and, correspondingly, the photoelectric and Compton noise. The lens elements were then shaped and mounted on the MCP-target assembly. An annulus constructed from a low-Z polymer separated the two lens elements.

Once construction of the lens was completed and initial experimentation begun, it was necessary to find optimum potentials for the various parts of the lens so that maximum focusing could be achieved without putting "bright spots" on the face of the MCP which could physically damage the detector. This was accomplished using the EGUN2c electron optics software package traceable to SLAC. Once the initial boundary configuration was entered it was possible to test a variety of voltage arrangements, and plot corresponding electron trajectories. A set of representative trajectories is shown in Figure 5.

As indicated previously, about 50% of the signal electrons leaving the target have energies at or below 15 eV. Using this energy, various electron emission configurations such as plane

waves and point sources were simulated with electrons starting just off the surface of the foil. The overriding concern in the optimization process was that in order for an electron to be appreciably accelerated through the lens, it must, of course, be exposed to progressively higher potentials as it traverses the lens. However, the target foil is biased slightly less negatively than the first lens element to assist electrons near the edges in escaping from the target foil (see Fig. 3). The primary constraints on the optimum voltage selections were due to the fact that the chevron grid was being operated at -1870 V, and that the power supplies readily available were not capable of producing more than -3000 V. Nonetheless, suitable biases were found to achieve an effective collection solid angle of almost 2π steradians.

After optimizing the lens biases using computer simulations, further experimental refinement was performed by analyzing the count rates in multichannel scaler (MCS) spectra collected at various lens bias settings. The optimum operating biases for the lens were found to be V_{R1} = -2817 V, V_{R2} = -1967 V, and V_{Target} = -2757 V when the chevron was operated at -1616 V, and with the MCP grid at -1866 V.

It was expected that a small fraction of the signal electrons from the target foil would have energies approaching 7.3 keV. At these energies, the lens is almost completely ineffective due to limitations on its size imposed by the vacuum chamber and by restrictions on its bias values. The geometrical collection efficiencies for these electrons, having an effective solid angle defined solely by the geometry, prevented the experimental signal-to-noise ratios from reaching the full theoretical value.

CEMS EXPERIMENTAL ARRANGEMENT FOR DETECTOR EVALUATION

A block diagram of the experimental arrangement is shown in Figure 6. The source-target-detector was in a typical scattering geometry. A ^{57}Co(Pd) source was mounted on a velocity

transducer to Doppler shift the energy of the source. The intensity of the scattered radiation (conversion, Auger and secondary electrons) was monitored as a function of velocity.

The Mössbauer spectrometer employed made use of a velocity sweep system with an electromechanical driver on which the source was mounted and which was swept periodically through the range of interest. The spectrum was recorded by storing counts in memory channels of a multichannel scalar, that were addressed sequentially and synchronized with the velocity. By monitoring the Doppler motion of the source with an interferometer, velocity information was multiplexed into every 16th channel of the MCS. During the subsequent data analysis, a channel number could easily be converted into velocity units. This form of data collection is usually called a constant acceleration mode since a range of velocities are swept through at a linear rate.

To optimize the counts per second registered by the detector, useful information was obtained by difference measurements performed at constant velocity. In general, the Doppler velocity of the source was chosen to coincide with one of the Mössbauer resonances, then some parameter of the experiment was changed and the counting rate, (CPS), recorded. The experiment was repeated off-resonance to determine the noise contributed to the spectrum. This technique was used in our calibration work to monitor the intensity of a selected resonant emission as a function of the lens bias configuration.

Vacuum Pumping System for CEMS

Up to this point, for non-resonant studies of the environmental influences on the signal noise, the vacuum requirements were satisfied by using a turbo molecular pump (TMP) to maintain the appropriate pressure in the target chamber. But now, after having identified and reduced the sources of noise due to photoelectrons and scattered radiation, it became appropriate to proceed with the more precise Mössbauer experiments in which both resonant and non-

resonant signals could be observed. Unfortunately, however, since the Mössbauer effect is easily destroyed by spurious vibrations, the TMP could no longer be used to produce the vacuum of 2 X 10^{-6} Torr necessary for proper MCP operation.

To provide for vibrationless pumping, a 140 l/s Varian diode Vaclon pump was employed. Such pumps operate by ionizing gas in a magnetically confined cold-cathode discharge. Several mechanisms typically combine to pump the myriad of gases present in a vacuum chamber. These include the trapping of electrons in orbits by a magnetic field, ionization of gases by collision, sputtering of the titanium anodes by ion bombardment, gettering of active gases by the titanium, and diffusion of hydrogen and helium into the titanium. For the noble gases, the basic pumping mechanism is burial in the pump walls. These mechanisms combine to form an extremely harsh environment inside the Vaclon pump. Unless proper precautions are taken, neutral and charged particles as well as radiation (hard UV) can escape from the pump and seriously degrade the performance of the detector. To prevent contamination from the Vaclon from entering the target chamber, a line of sight baffle was inserted between the pump and target chamber. The baffle consisted of six successive plates having staggered apertures serving as choking orifices for the pump feedback.

Unfortunately, by using the baffle to reduce the noise from the pump to a negligible level, the efficiency of the pump was reduced to such a point that it could no longer maintain the chamber at the required pressure of 2 μTorr. To overcome this problem, an additional, smaller, ion pump was added to the pumping system. In this manner the contamination of the signal was reduced below observable limits and pressures as low as 1 μTorr could be maintained.

CEMS Evaluation of Detection System

The final test of the electron lens assembly was to collect a CEM spectrum at the optimum bias potentials. Since resonant effects were being studied at this point in the development the aperture collimator was introduced. The target was a 5.0 cm by 5.0 cm by 2 μm iron foil with an enriched abundance of ^{57}Fe nuclei of 93.55 percent. Data were collected with the electron lens in the active mode at the optimum biases previously mentioned and in the passive mode with the Faraday shield bias at -1866 V. These data are shown in Figure 7. In Figure 7a, with the lens in a passive mode, only those electrons falling within the geometric solid angle subtended by the target and chevron were collected. With the lens in the active mode, Figure 7b, the effective solid angle approaches 2π. The signal-to-noise of the spectrum, $(N_0 - N_\infty)/N_\infty$, was found to be 8.1; over an 800 percent effect in the #1 transition!

The maximum percent effect reported in the literature is η_{CEMS} = 3600 percent [1]. However, this was for a single line source and absorber. Since approximately 25 percent of the total resonance was under the #1 transition in our data, we can multiply the literature value η_{CEMS} = 3600 percent by 0.25 to estimate what their percent effect would have been if they had used a split absorber. This gives η_{CEMS} = 900 percent. Our data gave a percent effect only 10 percent lower than the maximum ever reported in the literature!

CONCLUSIONS

The substantial effort that has been contributed to the design, development and characterization of the target chamber being prepared for use with the UTD-LINAC has yielded a detector system that convincingly approaches the level of performance considered mandatory for the harsh environment anticipated for the intended nuclear fluorescence experiments conducted under more

nearly laser-like conditions. Certainly room for further refinement exists and efforts will continue to take us in that direction. Efforts toward improving the collecting ability of the electron lens toward higher energy electrons can be pursued, further reduction of background noise can be addressed, reliability standards of the microchannel plates can be established, and efforts toward determination of the total detection efficiency of the detector can be completed.

TABLE I

Detection efficiency of a chevron microchannel plate for various types of incident radiation.

Type of Radiation	Range	Detection Efficiency (%)
Electrons	0.2 - 2 keV	50 - 85
	2 - 50 keV	10 - 60
U. V. photons	300 - 11 A	5 - 15
	1100 - 1500 A	1 - 5
Soft γ rays and x rays	0,5 - 2 A	5 - 15

TABLE 2

Counts per second for various component configurations inside the chamber with the internal reference blocked.

Component	CPS with external source	CPS without source
Null	30.23 ± 1.62	3.14 ± 1.49
Cage	36.65 ± 1.88	2.56 ± 0.56
Cage/Holder	43.90 ± 1.87	1.65 ± 0.35
Mylar	42.02 ± 2.22	2.39 ± 0.44
Aluminum	41.41 ± 1.94	1.54 ± 0.40
Copper	46.20 ± 1.85	1.57 ± 0.38
Tantalum	67.55 ± 2.44	1.56 ± 0.35

REFERENCES

1. J. A. Sawicki, Industrial Applications of the Mössbauer Effect, ed by G. J. Long and J. G. Stevens. (Plenum Press, New York, 1986), p.83.
2. Gerd Weyer, Mössbauer Effect Methodology, Vol. 10, ed by I. J. Gruverman and Carl W. Seidel, p. 301 (1976).
3. K. R. Swanson and J. J. Spijkerman, J. Appl. Phys., 41, 3155 (1970).
4. R. Oswald and M. Ohring, J. Vac. Sci. Technol., 13, 40 (1976).
5. J. J. Spijkerman, Mössbauer Effect Methodology, Vol. 7, ed by J. Gruverman, p. 85 (1971).
6. J. A. Sawicki, Nucl. Instrum. and Meth., B16, 483, (1986).
7. R. W. Airey, T. T. Norton, B. L. Morgan, J. L. A. Fordham, D. A. Bone, and J. R. Powell, Electron Image Tubes and Image Intensifiers, SPIE 1243, 140 (1990).
8. O. H. W. Siegmund, K. Coburn, and R. F. Malina, IEEE Trans. Nucl. Sci., NS-32, 443 (1985).
9. P. Schagen, Advances in Image Pick-up and Display, Vol. 1. (Academic Press, New York, 1974), p.1
10. J. S. Zabinski and B. J. Tatrchuk, Nucl. Instrum. and Meth., B42 379 (1989).
11. W. Jones, J. M. Thomas, R. K. Thorpe, and M. J. Tricker, Appl. Surf. Sci. 1, 388 (1978).
12. J. A. Sawicki and T, Tyliszczak, Nucl. Instrum. and Meth., 216, 501 (1983).
13. R. P. Feynman, R. B. Leighton, and M. Sands, The Feynman Lectures in Physics, Vol II, (Addison-Wesley, Reading Massachusetts, 1964), p. 7-10.

CAPTIONS

Figure 1: Energy level diagram for ^{57}Co source and ^{57}Fe target showing (a) the emission process for the 14.4 keV gamma ray and (b) the nuclear Zeeman splitting of the nuclear energy levels due to the large internal magnetic fields in a ferromagnetic iron foil. Note: In (b) the energy scale is about 10^{13} smaller than in (a).

Figure 2: Schematic diagram of the experimental apparatus. For Mössbauer studies, the source-target-detector are in a backscatter geometry.

Figure 3: Circuit diagram of the supporting electronics for the chevron microchannel plate assembly electron detector.

Figure 4: Sweep data collected by scanning a highly collimated radiation beam across the target holder assembly containing (a) tantalum and (b) null targets. The contribution from the target holder is clearly seen in (c) after chamber background counts have been removed.

Figure 5: Drawing of the two-element electron lens. The steering of the electrons is performed primarily by the potential gradients established between R_1 and R_2.

Figure 6: The EGUN2c computer program was used to design the electron lens used in CEMS. In (a) the calculated electron trajectories for electrons emitted from a point source at the geometric center of the target are shown. A "plane-wave" of electrons emitted uniformly from the face of the target is shown in (b).

Figure 7: Conversion electron Mössbauer spectra for a 93.55% enriched ^{57}Fe target: (a) Lens in a passive mode possessing no focusing or accelerating properties and (b) Lens in a focusing or active mode.

Figure 1

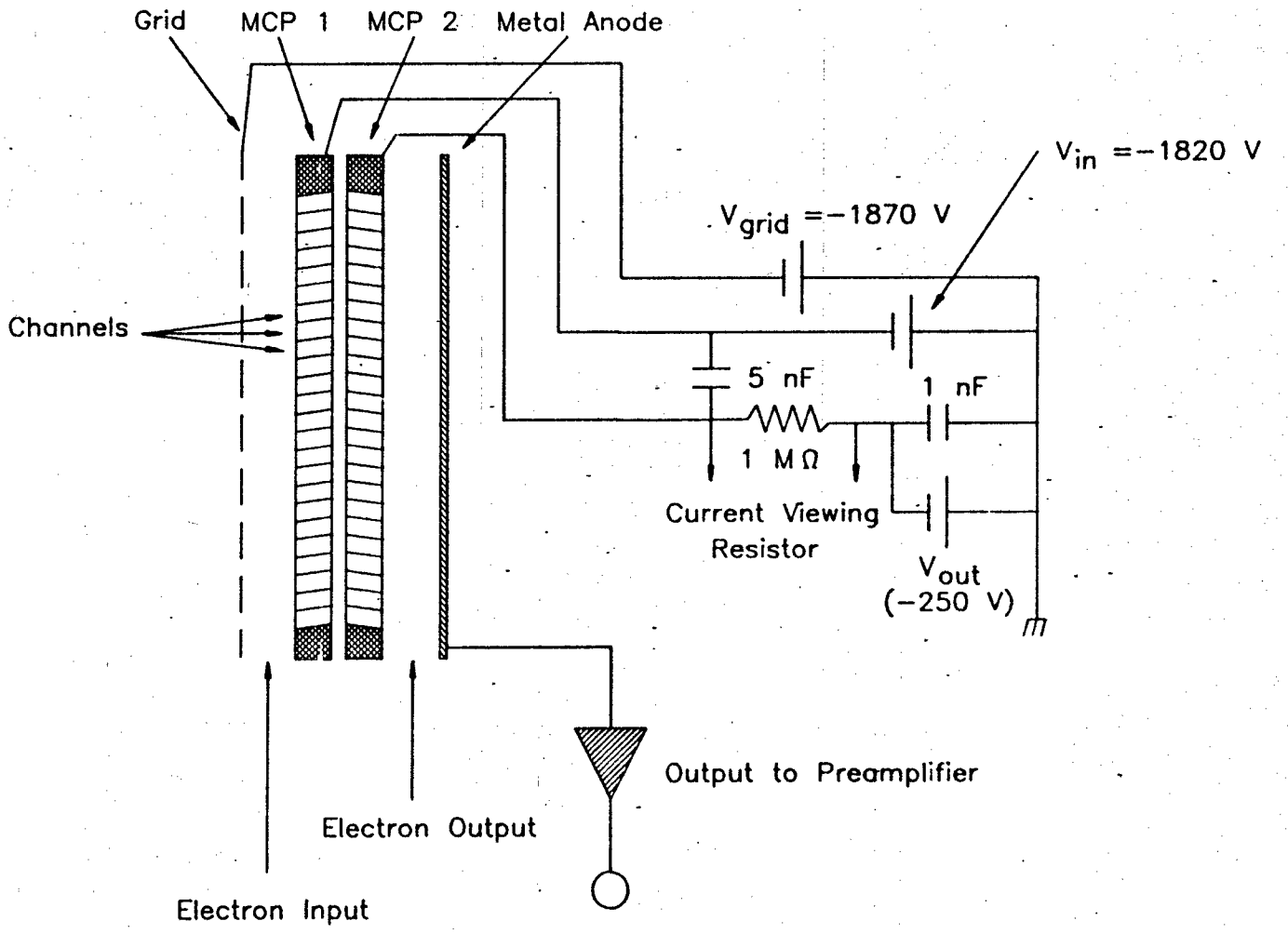

Chevron and Biasing Arrangement

Figure 2

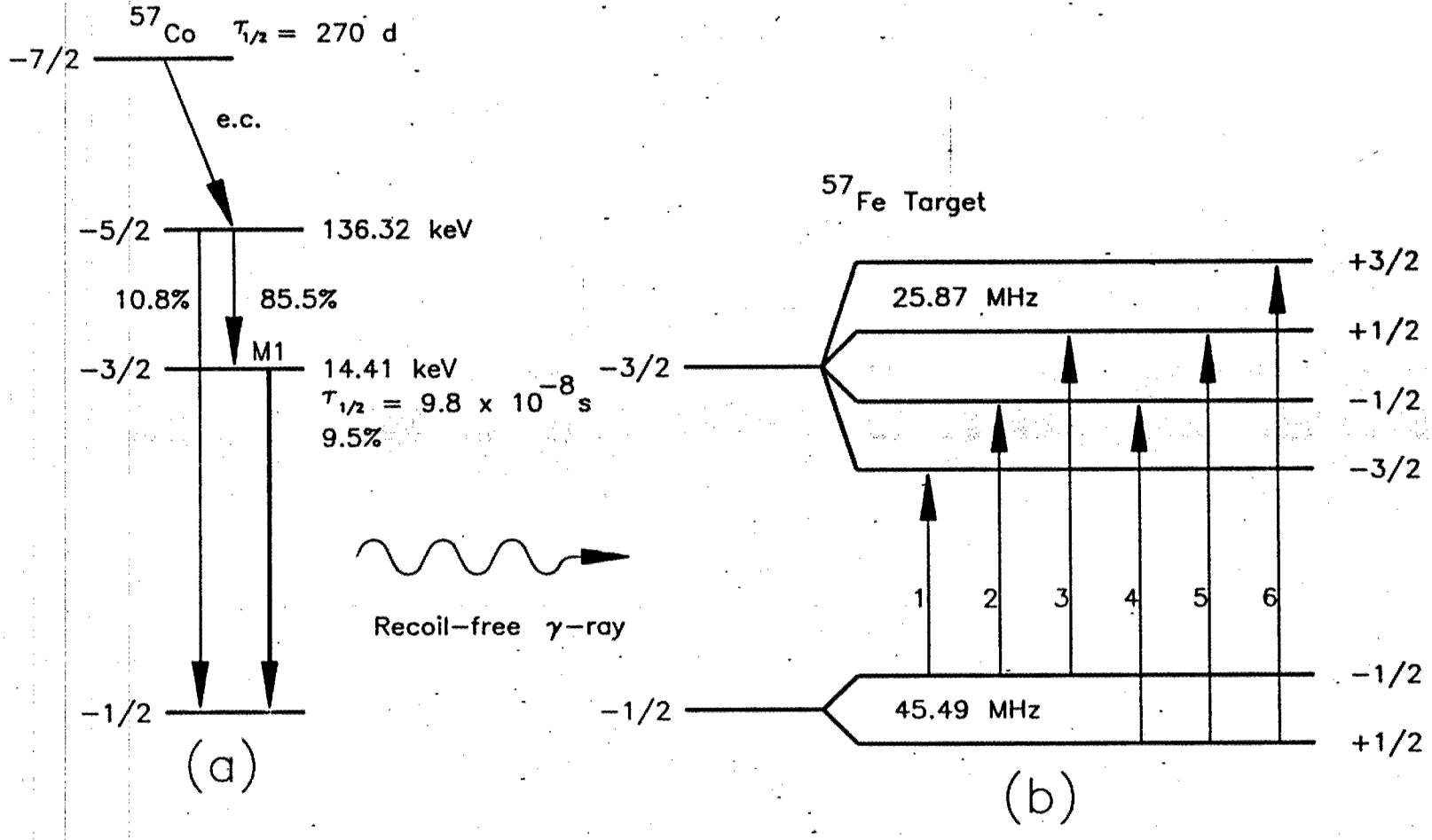
^{57}Co $\tau_{1/2}$ = 270 d
−7/2
e.c.
−5/2
136.32 keV
10.8%
85.5%
M1
−3/2
14.41 keV
$\tau_{1/2}$ = 9.8 x 10^{-8} s
9.5%
−1/2
(a)
Recoil−free γ−ray
^{57}Fe Target
25.87 MHz
+3/2
+1/2
−1/2
−3/2
−3/2
1
2
3
4
5
6
−1/2
45.49 MHz
−1/2
+1/2
(b)

Figure 3

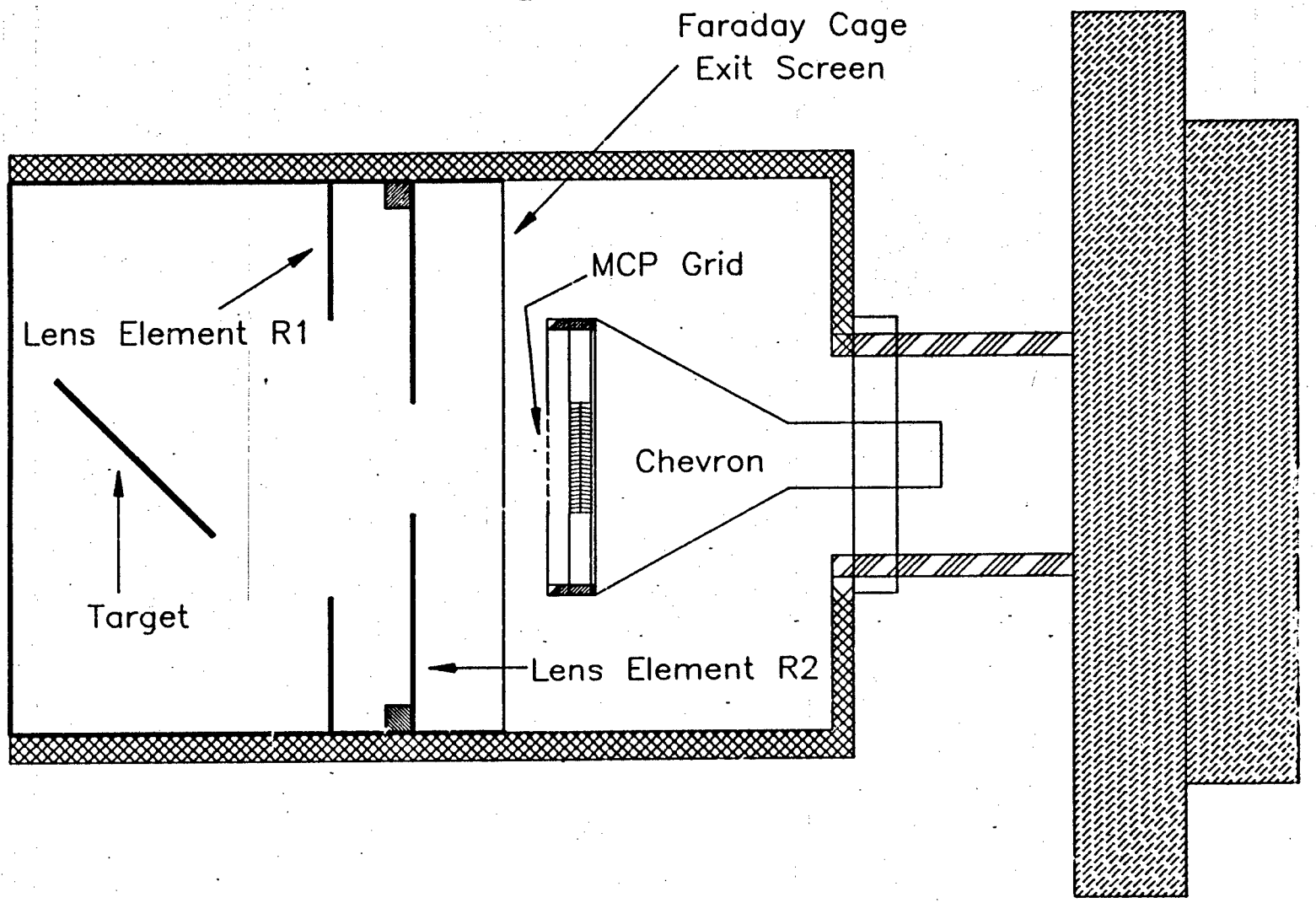
Faraday Cage
Exit Screen
MCP Grid
Lens Element R1
Chevron
Target
Lens Element R2

Figure 4

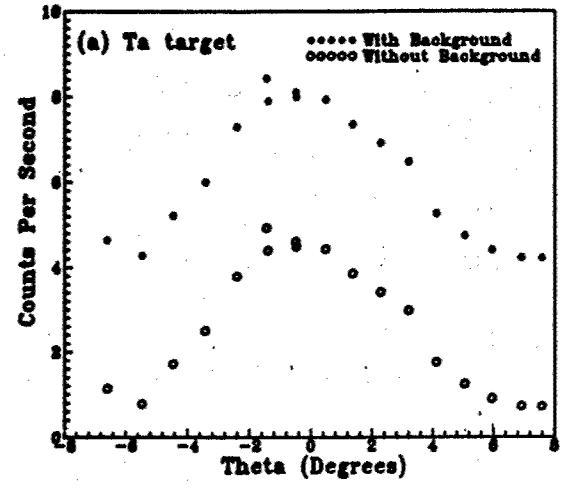
(a) Ta target
••••• With Background
ooooo Without Background
Counts Per Second
Theta (Degrees)

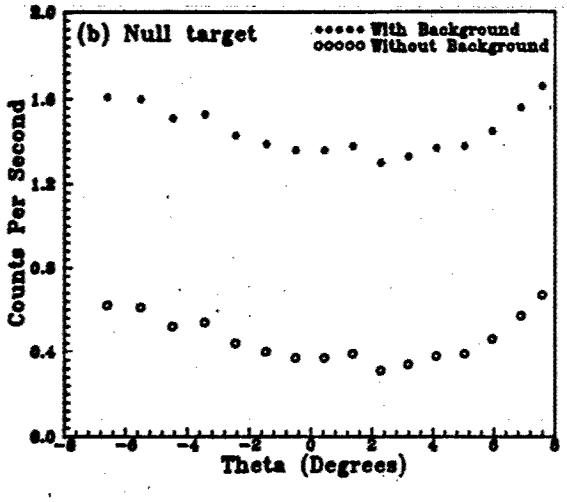
(b) Null target
••••• With Background
ooooo Without Background
Counts Per Second
Theta (Degrees)

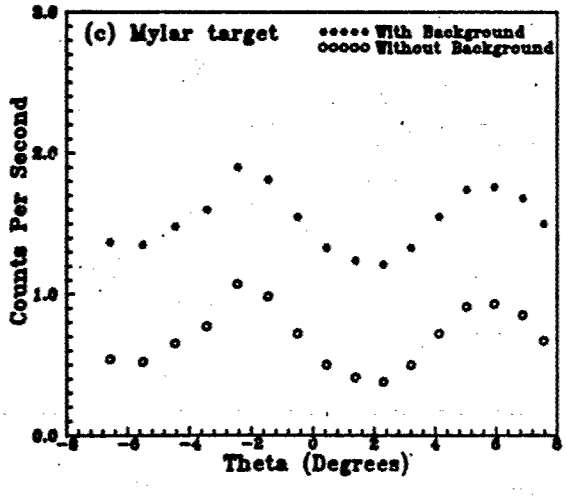
(c) Mylar target
••••• With Background
ooooo Without Background
Counts Per Second
Theta (Degrees)

Figure 5

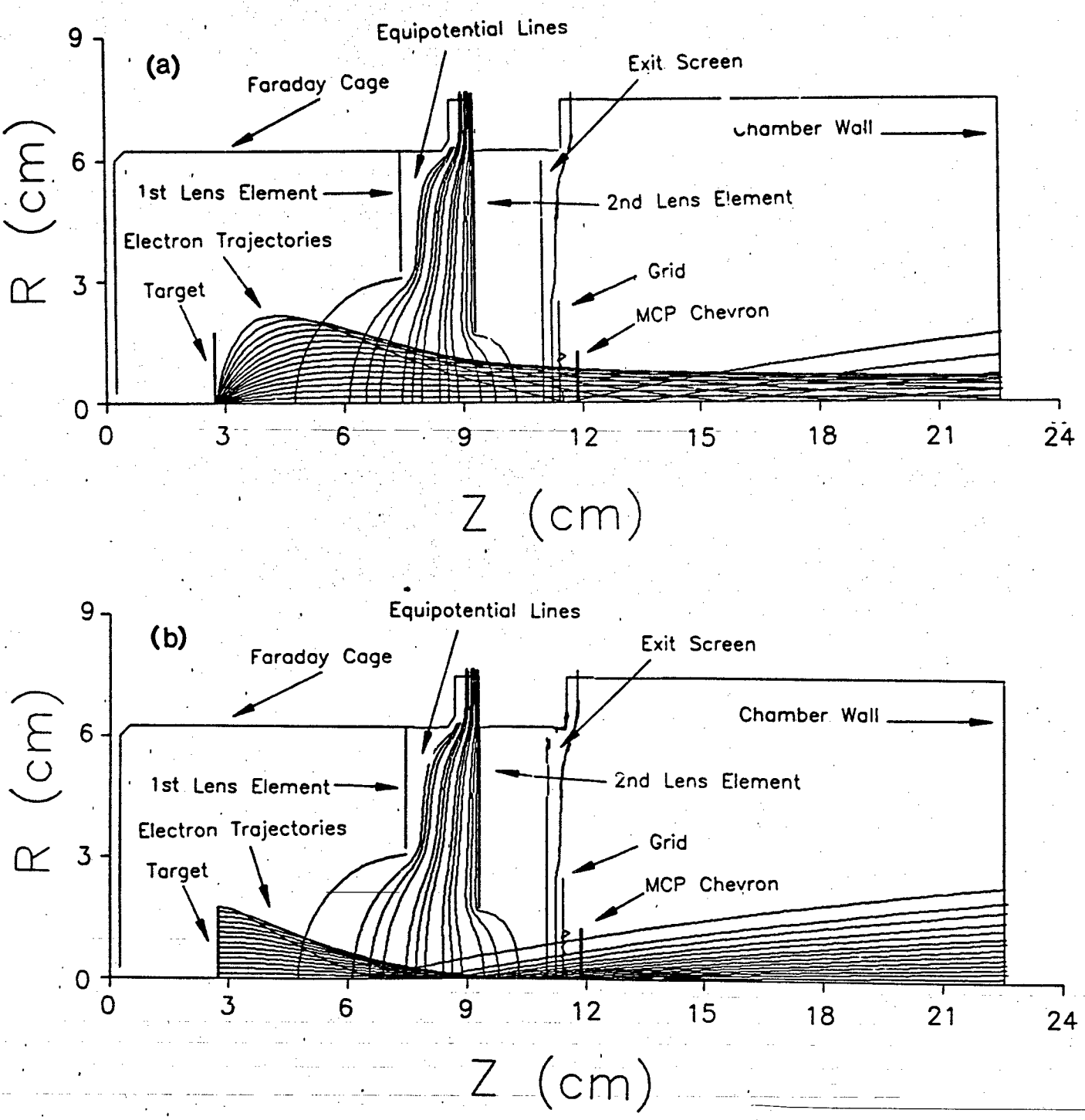
(a)
Equipotential Lines
Faraday Cage
Exit Screen
Chamber Wall
1st Lens Element
2nd Lens Element
Electron Trajectories
Target
Grid
MCP Chevron
R (cm)
Z (cm)
0
3
6
9
12
15
18
21
24
(b)
Equipotential Lines
Faraday Cage
Exit Screen
Chamber Wall
1st Lens Element
2nd Lens Element
Electron Trajectories
Target
Grid
MCP Chevron
R (cm)
Z (cm)

Figure 6

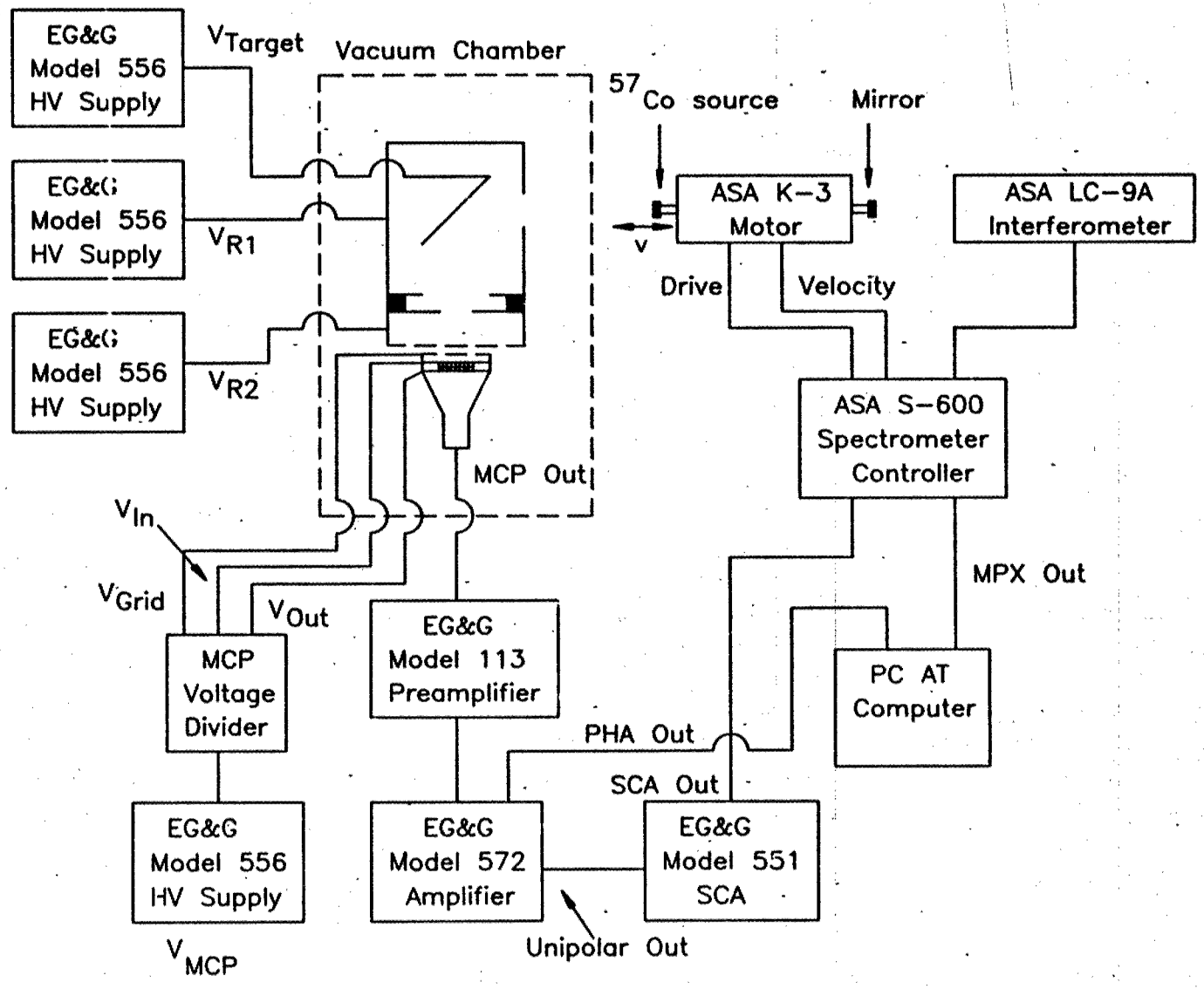
EG&G Model 556 HV Supply
V_{Target}
Vacuum Chamber
^{57}Co source
Mirror
EG&G Model 556 HV Supply
V_{R1}
ASA K-3 Motor
ASA LC-9A Interferometer
v
Drive
Velocity
EG&G Model 556 HV Supply
V_{R2}
ASA S-600 Spectrometer Controller
MCP Out
V_{In}
V_{Grid}
V_{Out}
MPX Out
MCP Voltage Divider
EG&G Model 113 Preamplifier
PC AT Computer
PHA Out
SCA Out
EG&G Model 556 HV Supply
EG&G Model 572 Amplifier
EG&G Model 551 SCA
V_{MCP}
Unipolar Out

Figure 7

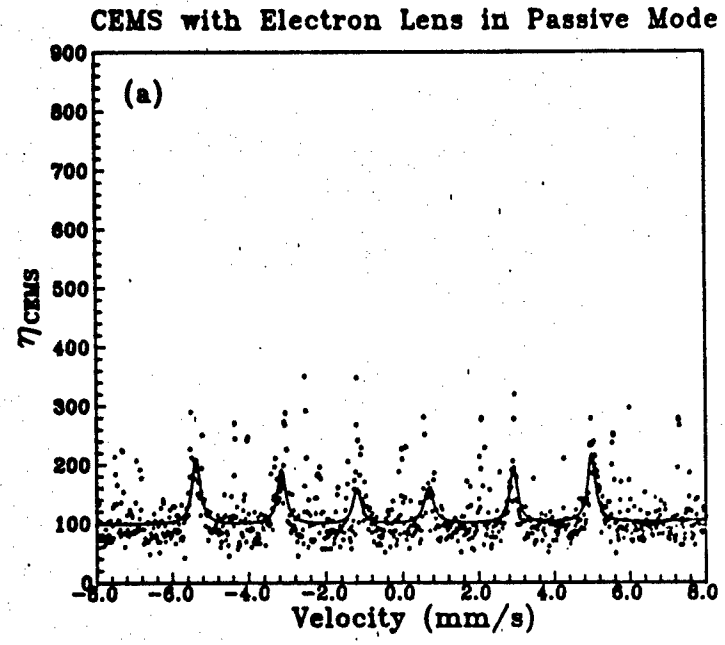
CEMS with Electron Lens in Passive Mode
(a)
η_{CEMS}
900
800
700
600
500
400
300
200
100
0
-8.0
-6.0
-4.0
-2.0
0.0
2.0
4.0
6.0
8.0
Velocity (mm/s)

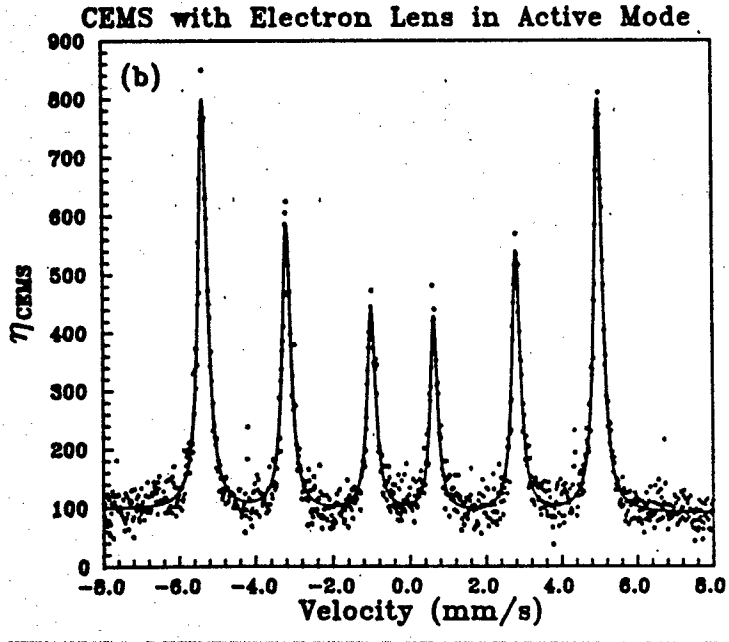
CEMS with Electron Lens in Active Mode
(b)
η_{CEMS}
900
800
700
600
500
400
300
200
100
0
-8.0
-6.0
-4.0
-2.0
0.0
2.0
4.0
6.0
8.0
Velocity (mm/s)

AN EVALUATION OF NANOPHASE DIAMOND FILM DOPED WITH ^{57}Fe FOR USE AS A NUCLEAR TARGET

T. W. Sinor, J. D. Standifird, J. J. Carroll,

K. N. Taylor, C. Hong and C. B. Collins

INTRODUCTION

The Mössbauer effect proves ideal for the sensitive characterization of implanted materials because it reveals the sharpest resonances occurring in nature. In this work we used it to investigate the properties of ^{57}Fe atoms implanted in nanophase (amorphic) diamond. The target had been prepared by depositing a 1 μm thick film of nanophase diamond on a Ti substrate. The film was then ion implanted with ^{57}Fe at an energy of 20 keV and a dose of 5×10^{16} atoms/cm^2. The ^{57}Fe atoms penetrated to a depth of approximately 200 A in the film and represented a concentration of about 10%.

The relatively low number of ^{57}Fe atoms implanted in the diamond film, combined with the presence of the Ti substrate, made the use of standard spectroscopic techniques impractical. To observe the resonant effects produced by the ^{57}Fe nuclei required the use of backscattering techniques. In Mössbauer spectroscopy two options for this are available, conversion electron Mössbauer spectroscopy (CEMS) and γ ray and conversion x ray Mössbauer spectroscopy.

The purpose of this work was to determine the utility of nanophase diamond films doped with micrograms of ^{57}Fe for use as nuclear targets in gamma-ray laser research. In these experiments the doped nanophase diamond would be used as the primary target excited by the bremsstrahlung radiation. Narrow-line fluorescence pumped through strong absorption resonances would be emitted with the best recoil-free fraction and the least amount of broad band background noise from scattering events in the target. Of secondary interest was the

potential for using doped diamond samples as efficient detectors for the resonance fluorescence emitted by the primary target. In this latter usage the electrons emitted from the detector as a result of the resonant absorption of the 14.4 keV component of the target fluorescence would be collected as signal.

CEMS MEASUREMENTS

Methods

Conversion electron Mössbauer spectroscopy has the advantage of being more sensitive to small concentrations of Mössbauer nuclei because of the large internal conversion coefficient of ^{57}Fe. The primary drawback to the use of CEMS is that it has a maximum depth of sensitivity in the sample equal to that for the escape of conversion and Auger electrons. Since most Mössbauer samples are much thicker than this depth which is typically around 50 nm, CEMS is not sensitive to most of the volume of the material being studied. In iron, the conversion and Auger electrons have mean escape depths of 57 nm and 36 nm respectively.[1] One question to resolve in this work was whether CEMS might nevertheless serve as a useful means of detecting a component of resonant fluorescence in a larger broad band background of scattered radiation.

Figure 1 shows the experimental arrangement for the CEMS measurements reported here. The absorbers under investigation were mounted on a rotatable holder so that samples could be changed without breaking the vacuum in which the experiments were done. The signal electrons emitted from the sample being illuminated were detected by a chevron microchannel plate (MCP) assembly. A two stage electrostatic lens was used to accelerate and steer the signal electrons from the target to the detector.[2] The Mössbauer source and Doppler motor assembly were external to the UHV chamber and the Mössbauer source illuminated the absorber assembly through a thin Ti entrance window.

The electrostatic lens assembly served several purposes. It was responsible for both focusing and accelerating the low energy ($\leq$ 15 eV) conversion and Auger electrons emitted from the absorber to the detector while shielding the various elements from the ground potentials of the chamber walls. A 700 V gradient increased the electron energies to values more compatible with the sensitivity of the input to the MCP.

Lower energy resonant electrons arise from both a surface and a bulk effect. In iron, the electrons sensitive to surface effects have a mean escape depth of approximately 4 nm, while electrons from the bulk have a mean escape depth of approximately 40 nm. For electron energies less than 15 eV, the ratio of the surface component to the bulk effect is reported[3] to be 8.5 to 12.5.

In this work spectra were obtained by CEMS for a variety of samples. They included foils of natural iron that contain 2.19% ^{57}Fe, 310 stainless steel enriched to 90.6% ^{57}Fe for the iron content of the alloy, and a 93.55% enriched iron absorber. These foils were used to generate an absolute calibration curve for the detection system. As seen in Fig. 1 each sample under investigation was mounted on a rotatable target holder inside the UHV chamber. A 310 stainless steel calibration foil placed on the opposite side of the holder could be rotated into the illumination to verify the reproducibility of the detection system without altering the experimental arrangement.

Analysis

The resulting calibration curve demonstrates the linear dependence of the resonant counting rate on the total illuminated mass of ^{57}Fe in each absorber that would be expected in a well-aligned system. The reproducibility of the detection system gives a high degree of confidence with respect to the placement of the data points on the calibration curve that is shown in Fig. 2. For each point on the curve, the counting rates in the corresponding spectra were normalized to

a spectrum taken when the calibration absorber on the opposite side of the holder was rotated into the illumination. The highlighted point in the figure corresponds to the ^{57}Fe implanted nanophase diamond sample. Direct comparison of this point with the calibration curve demonstrates that the emissivity of electrons from the nanophase diamond is greater than would be expected for a corresponding metallic absorber having the same number of Mössbauer nuclei. A typical spectrum taken with the nanophase diamond sample is shown in Fig. 3. The enhanced emissivity of resonant electrons from the nanophase diamond sample can be attributed to an increased Debye-Waller fraction.

The emission effects produced in nanophase diamond thin films were studied by overcoating the original sample with successive layers of nanophase diamond. Two layers having thicknesses of 230 A and 240 A, respectively, were deposited and calibration spectra were taken after each deposition. Analysis of the resonant counting rate from the sample versus the overcoat thickness could not be fit to a pure exponential due to an increase in the recoil-free fraction when the sample was overcoated with nanophase diamond. However, a numerical fit to the data yielded an estimated mean free path of 30 nm for the low energy signal electrons with energies of around 20 eV.

GAMMA-RAY AND CONVERSION X-RAY MEASUREMENTS

Methods

The CEMS data indicated that the nanophase diamond film may have a relatively large recoil-free fraction at room temperature after defects and voids created by the implantation were repaired with an overcoating layer of nanophase diamond. However, since CEMS provides only information about the surface layer of the nanophase diamond it cannot be used to determine the recoil-free fraction of the bulk material. Information about the bulk properties of the material

can be obtained from γ and conversion x ray fluorescence techniques.[4,5] Specifically this technique was used to verify linearity and to obtain a relative measurement of the recoil-free fraction of the nanophase diamond film.

For γ and conversion x-ray fluorescence measurements data were collected in a typical geometry with a scattering angle of 45°. A specially designed graded shield was used to reduce environmental scattering of the source radiation into the detector. In addition to the graded shield an x-ray filter was placed between the source and scattering target to reduce the number of low energy x rays which resulted from de-excitation processes in the source. These x rays were a major source of noise in the signal and by attenuating them with an appropriate filter, the signal to noise ratios of the Mössbauer spectra were greatly improved. The scattered γ and x rays from the various targets were detected by a thin window NaI(Tl)-PMT combination.

Analysis

Data were collected for a variety of iron targets and the total counts in the resonance lines were plotted as a function of the total mass of ^{57}Fe in the sample. The calibration curve is shown in Fig. 4. As expected the count rate increased linearly with the amount of ^{57}Fe in the sample. The total signal count rate for the ^{57}Fe implanted in the nanophase diamond film was plotted against the calibration curve and is shown in the inset of Fig. 4. As in the case of the CEMS measurement, direct comparison of this point with the calibration curve indicated that the fluorescent signal from the ^{57}Fe in the nanophase diamond was greater than would be expected for a corresponding metallic absorber having the same number of Mössbauer nuclei. This unambiguously indicated that the recoil-free fraction of the nanophase diamond at room temperature is greater than that for iron. From this data it was possible to estimate a lower limit of the recoil-free fraction of the nanophase diamond.

DETERMINATION OF THE RECOILLESS FRACTION OF NANOPHASE DIAMOND THIN FILMS

For the nuclear lifetimes usually encountered in the Mössbauer effect, the scattering process can be considered as a resonant absorption and subsequent re-emission. Under these conditions, the intensity of recoil-free resonant scattering will be proportional to the square of the Debye-Waller factor, while the intensity of recoil-free nonresonant scattering will be proportional to the first power of the Debye-Waller factor.[4] Multiple scattering, line width and interference effects are neglected in this analysis. Furthermore, the shapes of the lines after resonant scattering are assumed to be unaffected by self absorption. The recoilless fraction f of the nanophase diamond was determined from a measurement of the resonant scattering intensity calibrated against metallic iron foils with a known Debye-Waller fraction. A brief outline of the theory follows.

According to the Debye theory a solid may be considered to consist of a large number of linear oscillators with a distribution of frequencies ranging from zero to some maximum, ω_D. The total number of oscillators is equal to 3N, where N is the number of atoms in the solid. If the recoil energy of the nucleus is less than the quantum of energy necessary to excite the oscillator to the next higher energy level, the γ ray may be emitted without recoil. The probabilities of such recoilless emissions are, in most cases, governed by the Debye-Waller factor which is given by the Debye model as

$$f = \exp\left(- \frac{3E_R}{2k_B\theta_D} \left(1+4(T/\theta_D)^2 \int_0^{\theta_D/T} \frac{x}{e^x - 1}\, dx \right) \right) . \qquad (1)$$

In the limit of low or high temperatures Eq. 1 reduces to

$$f = \exp\left(-\frac{3E_R}{2k_B\theta_D}\right), \quad T \leq \theta_D$$

and (2)

$$f = \exp\left(-\frac{6E_R T}{2k_B\theta_D^2}\right), \quad T > \theta_D$$

where T is the absolute temperature, k_B is the Boltzman constant and Θ_D is the Debye temperature. The Debye temperature is a measure of the stiffness of the lattice and is defined by the expression $h\omega_D = k_B\Theta_D$.

Absolute measurements of f are difficult to make. However relative measurements of the recoil-free-fraction can be made by comparing the resonant scatterings from a target with a known value of f with the emissions of the material with an unknown f using the same source. For purposes of calibration, we used metallic iron foils with a recoil-free fraction[5] at room temperature of $f_{iron} = 0.69$. This corresponds to a Debye temperature calculated from Eq. 1 of about 335 K. The Debye temperature reported in the literature[6] for iron is 460 K. This indicates that the recoil-free fraction reported by Debrunner and Morrison[5] could possibly be low. However, O'Connor and Longworth[7] have reported the recoilless fractions of ^{57}Co in ^{56}Fe and natural iron absorbers to be 0.77 ± 0.02 and 0.76 ± 0.06 respectively. These measurements correspond to a Debye temperature of 400 K. Preston et al.[8] give $f = 0.90$ for iron at room temperature which corresponds to a Debye temperature of about 650 K.

This diverse range of f-values for metallic iron at room temperature indicates that the recoil-free fraction of thin films of the type usually used in Mössbauer spectroscopy are sensitive to the history of the foil, i.e., rolling procedure, annealing, etc. To obtain an absolute value for

the recoil-free fraction of the iron doped nanophase diamond it would have been necessary to determine f_{iron} for the calibration foils used in these experiments. However, as an approximation the value of $f = 0.69$ from Debrunner and Morrison[5] was used to obtain a lower limit for f_{dia} and the corresponding Debye temperature was calculated for Eq. 1.

If the recoil-free fraction for the source is f_s and the absorber is f_{abs}, the probability for resonant absorption is $f_s f_{abs}$ and the probability for resonant reemission is $f_s f_{abs}^2$. To relate this to an experimentally measured parameter we note that in a scattering geometry the total area under the lines of a Mössbauer spectrum is given by

$$A_{Theory} = \frac{\pi}{2} \sum_i \Gamma_i n_i \sigma_0 f_s f_{abs}^2 \quad , \tag{3}$$

where n_i is the number of Mössbauer nuclei per cm^2, Γ_i is the full-width half maximum of the i^{th} resonance line and σ_0 is the cross-section for resonance interaction.

The corresponding area of an experimental spectrum that has a Lorentzian shape is given by

$$A_{exp} = \frac{\pi}{2} \sum_i \varepsilon_i \Gamma_i^{exp} \tag{4}$$

where

$$\varepsilon_i = \frac{N_0 - N_-}{N_-} \quad . \tag{5}$$

Here N_0 is the total intensity of the resonantly scattered gamma rays and N_- is the nonresonant background.

If the resonant scatterings of two targets are compared, and if the recoil-free fraction of one of the materials is known we may take the ratio of the experimentally determined areas in the Mössbauer resonance and equate these to Eq. 4 to obtain

$$\frac{A_{1exp}}{A_{2exp}} = \frac{f_1^2}{f_2^2} \quad , \tag{6}$$

or more specifically,

$$f_{dia} = f_{iron} \sqrt{A_{dia}/A_{iron}} \quad . \tag{7}$$

Equation 7 provides an approximate value of the recoil-free fraction of the nanophase diamond film which is proportional to the area under the lines of the experimentally measured spectrum.

The determination of f from a measurement of the area of an experimental Mössbauer spectrum has been widely used. This method was developed by Shirley et al.[9] and later generalized by Lang.[10] In the present context it is important to notice that Eq. 7 is independent of the recoil-free fraction of the source. Furthermore by taking the ratio of the areas instrumental errors should cancel.

From the calibration data of Fig. 4 and using $f_{iron} = 0.69$ we obtained $f_{dia} = 0.94$ with a lower bound of 0.85. Using this measurement of f it is possible to determine the Debye temperature Θ_D by using Eq. 1 to make a plot of recoil-free fraction vs Debye temperature. This plot is shown in Fig. 5. As seen from the figure, the median value of the recoilless fraction of the nanophase diamond corresponds to a Debye temperature of 900 K.

CONCLUSION

In these experiments the Mössbauer properties of ^{57}Fe implanted nanophase diamond samples were investigated. The CEMS data indicates that the nanophase diamond film has a relatively large recoil-free-fraction at room temperature and that enhanced emission effects may

be produced in the amorphic diamond. Analysis of the resonant counting rate from the sample versus the overcoat thickness revealed the presence of both exponential and linear terms in the data. The exponential term is indicative of the attenuation of the electrons as they escape from the film. The linear term is believed to represent a small but definite growth of the resonant electron signal. Further analysis of the ^{57}Fe implanted nanophase diamond sample is necessary to fully understand the mechanisms responsible for its enhanced electron emissivity. Particular emphasis will be placed on re-implantation of the nanophase diamond sample so that more overcoating experiments can be performed to aid in the continuing study of resonant electron propagation and emission in nanophase diamond films.

Gamma and conversion x-ray Mössbauer spectroscopy has been used to experimentally determine the Debye-Waller fraction for the nanophase diamond film. The recoilless fraction f of the nanophase diamond film was determined from a measurement of the resonant scattering intensity calibrated against metallic iron foils with a known recoil-free fraction. Preliminary results give a median value of $f_{dia} = 0.94$ for the nanophase diamond film and a corresponding Debye temperature of 900 K for comparison with the value of 335 K indicated by recoil-free fractions of 0.69 in conventional iron Mössbauer foils. The large recoil-free fraction at room temperature makes nanophase diamond a promising substrate for micrograms of exotic nuclear materials that are of particular interest in gamma ray laser research.

REFERENCES

1. J. A. Sawicki, in Industrial Applications of the Mössbauer Effect. ed. G. J. Long and J. G. Stevens. (Plenum Press, New York, 1986), p. 83.
2. T. W. Sinor, J. D. Standifird, K. N. Taylor, C. Hong, J. J. Carroll and C. B. Collins, (submitted to Rev. Sci. Instrum.).
3. G. Klingelhöfer and E. Kankeleit, Hyperfine Interaction, 57, 1905 (1990).
4. J. K. Major, Nucl. Phys. 33, 323 (1962).
5. P. Debrunner and R. J. Morrison, Rev. Mod. Phys. 36, 463 (1962).
6. G. Burns, Solid State Physics, (Academic Press, Orlando, Florida, 1985) p. 354.
7. D. A. O'Connor and G. Longworth, Nucl. Instr. and Methods, 30, 290 (1964).
8. R. S. Preston, S. S. Hanna and J. Heberle, Phys. Rev. 128, 2207 (1962).
9. D. A. Shirley, M. Kaplan and P. Axel, Phys. Rev. 123, 816 (1961).
10. G. Lang, Nucl. Instr. and Methods, 24, 425 (1963).

CAPTIONS

Figure 1: Schematic diagram showing the arrangement of the sample holder and MCP detection assembly inside the UHV chamber. Note that the sample holder can be rotated to obtain calibration spectra without altering the experimental arrangement.

Figure 2: Calibration curve for the resonant counting rate of the metallic samples as a function of the number of micrograms of ^{57}Fe contained within them. The highlighted point at 8.5 micrograms corresponds to the implanted amorphic diamond sample. The increase in emissivity over the metallic absorbers can be seen clearly.

Figure 3: CEMS spectrum of the ^{57}Fe implanted nanophase diamond sample. The partially resolved doublet is due to quadruple splitting in the sample.

Figure 4: Calibration data for signal count rate vs. amount of ^{57}Fe. The inset shows the datum for iron in amorphic diamond. From this data the lower limit on the recoil-free-fraction of amorphic diamond is $f = 0.85$.

Figure 5: Plot of recoil-free-fraction vs Debye temperature. Using the measured value of $f = 0.94$ the corresponding Debye temperature of nanophase diamond was 900 K.

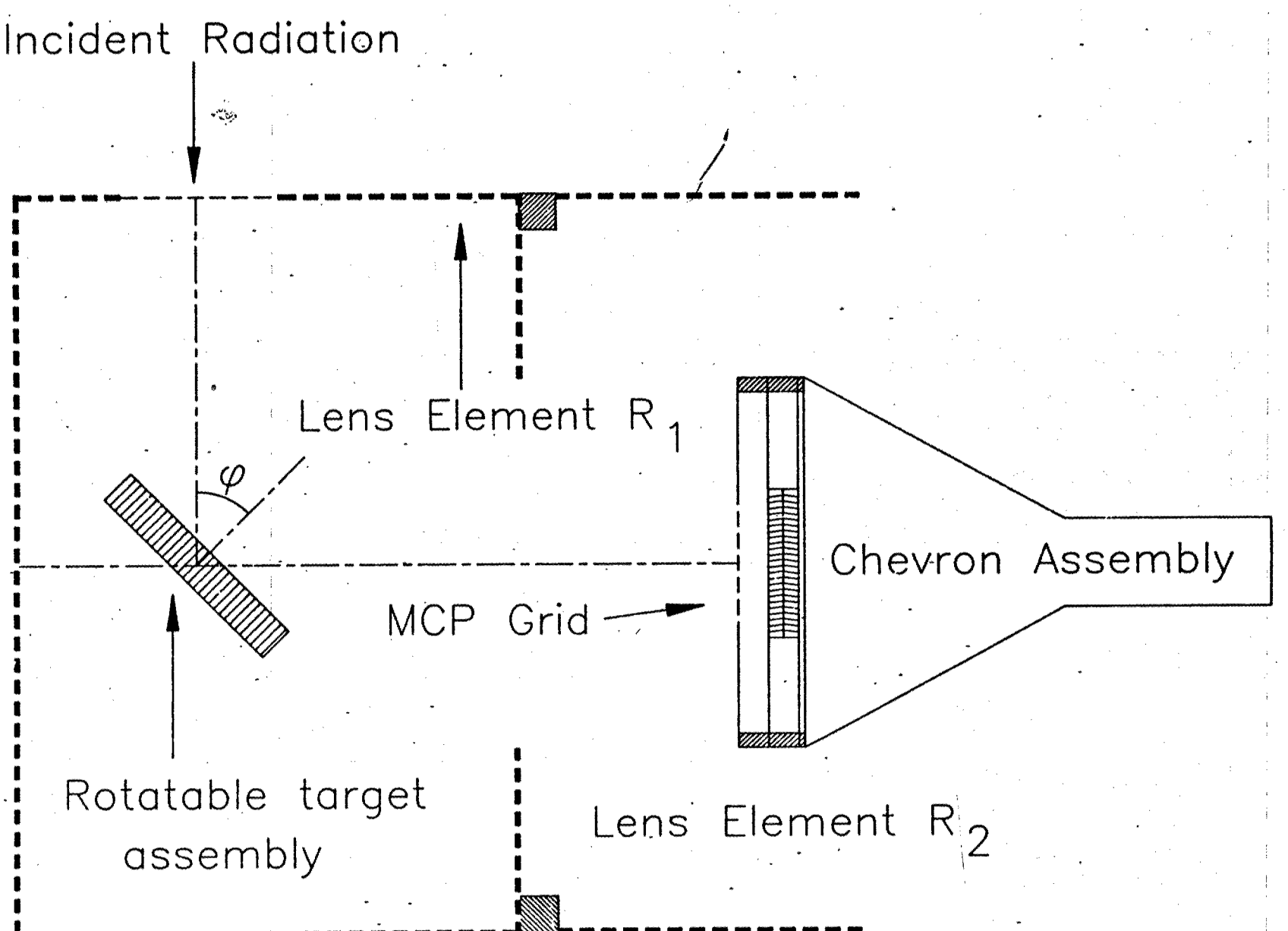
Incident Radiation
Lens Element R 1
φ
Chevron Assembly
MCP Grid
Rotatable target assembly
Lens Element R 2

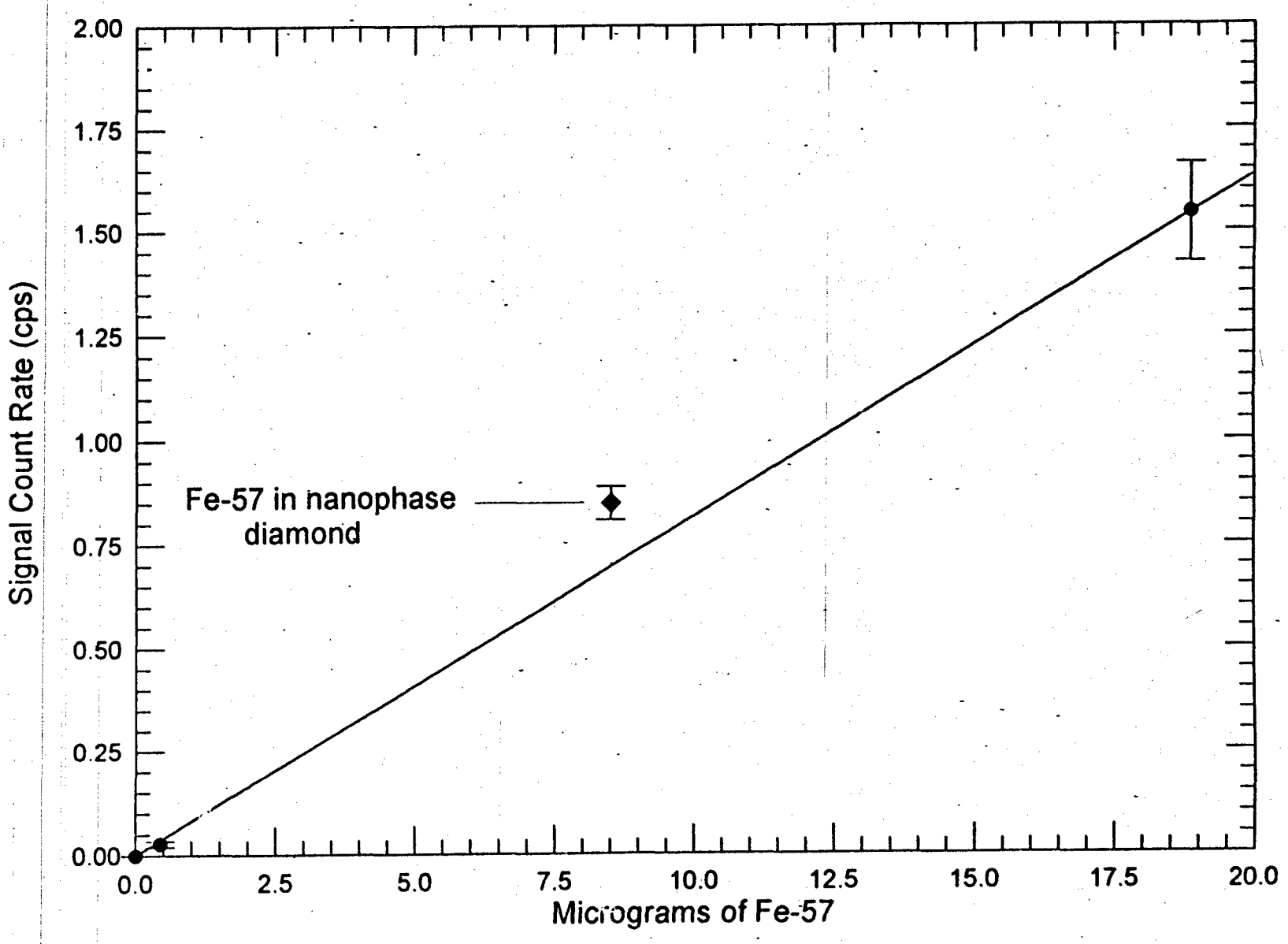
2.00
1.75
1.50
1.25
1.00
0.75
0.50
0.25
0.00
Signal Count Rate (cps)
Fe-57 in nanophase diamond
0.0
2.5
5.0
7.5
10.0
12.5
15.0
17.5
20.0
Micrograms of Fe-57

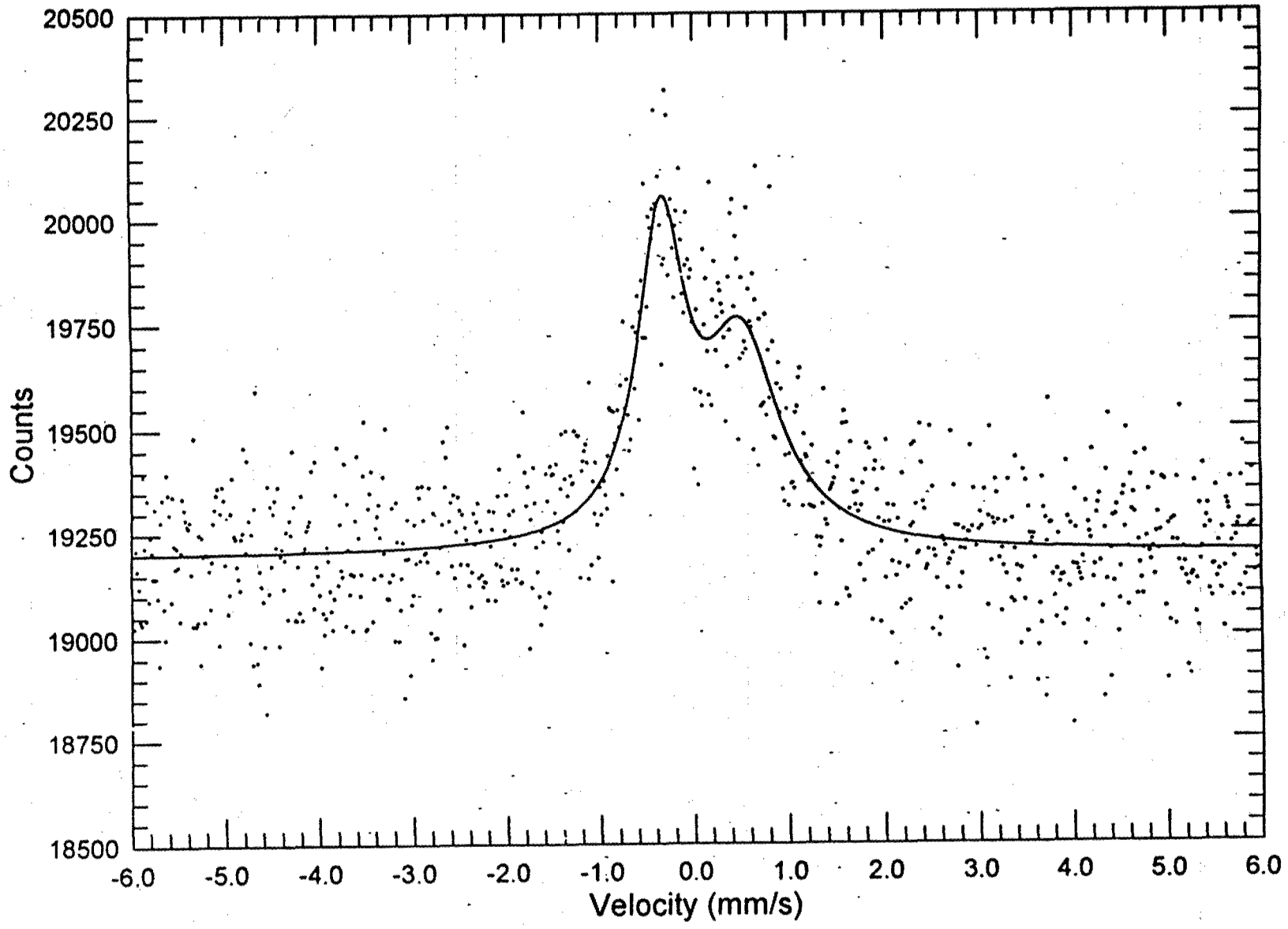
20500
20250
20000
19750
19500
19250
19000
18750
18500
Counts
-6.0
-5.0
-4.0
-3.0
-2.0
-1.0
0.0
1.0
2.0
3.0
4.0
5.0
6.0
Velocity (mm/s)

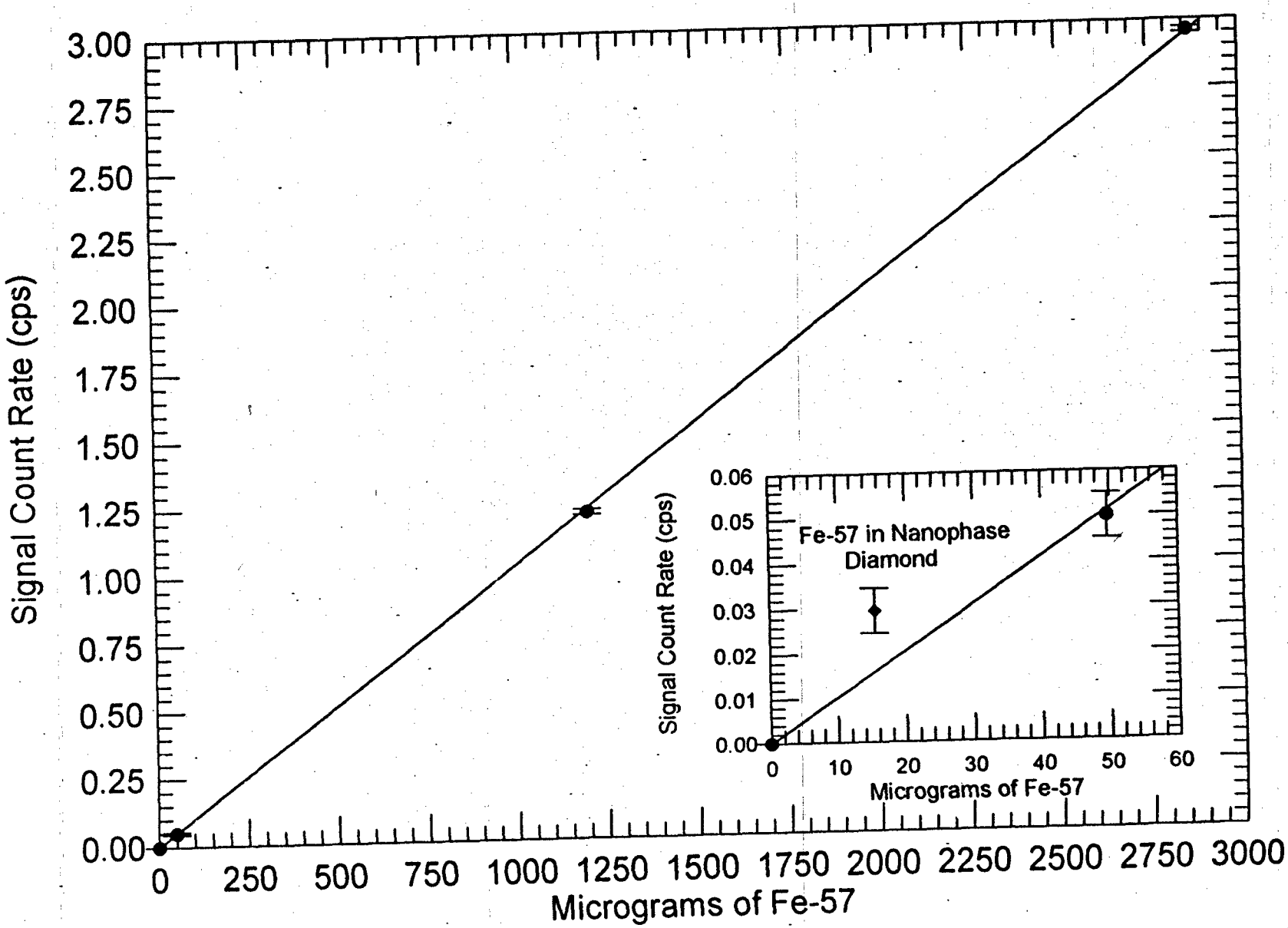
Signal Count Rate (cps)
3.00
2.75
2.50
2.25
2.00
1.75
1.50
1.25
1.00
0.75
0.50
0.25
0.00
0
250
500
750
1000
1250
1500
1750
2000
2250
2500
2750
3000
Micrograms of Fe-57
Fe-57 in Nanophase Diamond
Signal Count Rate (cps)
0.06
0.05
0.04
0.03
0.02
0.01
0.00
0
10
20
30
40
50
60
Micrograms of Fe-57

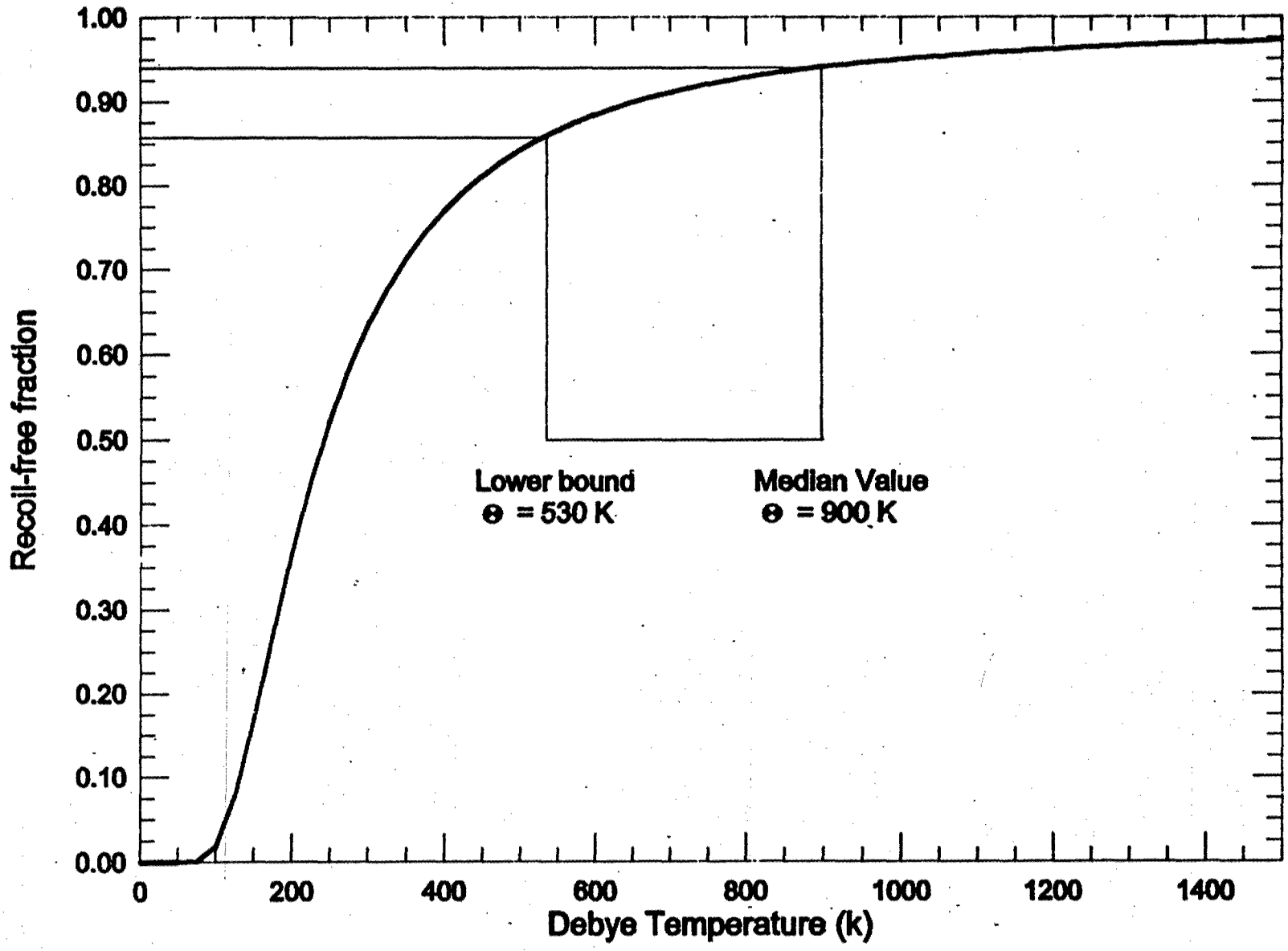
1.00
0.90
0.80
0.70
0.60
0.50
0.40
0.30
0.20
0.10
0.00
Recoil-free fraction
Lower bound
Θ = 530 K
Median Value
Θ = 900 K
0
200
400
600
800
1000
1200
1400
Debye Temperature (k)

INSTALLATION OF THE TEXAS-X RESEARCH LINEAR ACCELERATOR

K. N. Taylor, C. Hong, T. W. Sinor, J. J. Carroll,

J. D. Standifird, D. G. Richmond, and C. B. Collins

INTRODUCTION

The previous chapter of this report reviewed the motivations and successes in studies conducted at the Center for Quantum Electronics on the feasibility of a gamma-ray laser. It was emphasized there that the next level of investigation would involve the study of isomers possessing laserlike nuclear states having lifetimes on the order of one to several microseconds and that this would be done with an in-house linac. The intent of the following material is to detail the various phases of the construction, installation, testing, optimizations and initial experiments that have gone into bringing the Texas-X research linear accelerator on line and into the fruitful research endeavors described here.

UNDERGROUND FACILITIES AND INSTALLATION OF TEXAS-X

Preparations for installation and operation of the Texas-X linear accelerator began with construction of the dedicated shielding chamber which was designed for housing the device and constructed at university expense. Excavation for this construction began adjacent to the High Energy Laser Laboratory of the Center for Quantum Electronics on Nov. 7, 1991. Construction by a State of Texas agency is complex and highly regulated and the final designs for the building called for an underground facility that would derive its shielding capacity from both concrete and groundcover. With prevailing considerations of ground water and soil instability the foundation called for a pier and beam support structure reaching to bedrock (Figure 1). Following construction of the piers and a mud slab, the main floor, which was one foot thick and laced very heavily with reinforcement bars, was poured on Dec. 16, 1991. As seen in

Figs. 2 and 3, this was followed by construction of the walls, ceiling, and installation of conduits for power, accelerator control, and signal cables, etc. Toward the end of February 1992 soil had been moved into place about the walls and packed to attain proper densities for meeting the shielding specifications and temporary soil cover had been placed over the ceiling (Figs. 4 and 5). The final phases of construction occurred during March and early April of 1992. These included such items as electrical wiring, plumbing, installation of the air exchange system, heating and cooling devices, safety interlocks, and personnel safety alarms. Figure 6 shows an interior view of the chamber and also the future location of the accelerator (as demonstrated by the wooden simulation frame). Following sodding of the ground cover with bermuda grass, installation of a chain link fence enclosing the chamber was begun on April 10 (Figure 7). Tasks relating to cleanup and small oversights, etc., were completed in May, 1992.

Final acceptance of the accelerator system itself was completed during the spring and the device was shipped to the University of Texas at Dallas at the end of May 1992. Representatives from the manufacturer accompanied the system and supervised placement of its various components. As indicated in Fig. 8, the control console and modulator were separated from the underground accelerating unit and placed inside the main laboratory. The control unit was accessibly located inside the copper mesh screen room which also contains the controlling and processing electronics for the experiments. The modulator, which contains the power distribution system, switching elements and pulse forming network was placed near the door leading downstairs to the accelerator chamber. The cable run conducting the power pulses from the modulator to the linac is on the order of 50 feet. The process of installing, testing and adjusting the machine took approximately 3 to 4 weeks. The university began operation of the machine the last week of June. Characterization studies of its output began on June 23, 1992. Following these studies, as described below, an involved series of efforts was initiated to develop

an operating environment in which noise levels, and other concerns, permitted the observation of delayed nuclear emissions from target isomers possessing laserlike energy levels. This objective required the optimization, and even the development of technology, in three areas: the fluorescence detection system, EMI and RFI noise control, and data acquisition and processing.

DETECTION SYSTEM

The critical core of the detection system for nuclear fluorescence was a fast scintillation crystal having a very low residual phosphorescence. After evaluating the many alternatives, the rather obscure CsF material was concluded to offer the best figure of merit when measured against these unusual requirements.

A CsF crystal having cylindrical dimensions of 2.5 cm diameter and length of 2.5 cm and coupled to an RCA 8850 photomultiplier tube served to detect the delayed fluorescent emissions from the target nuclei irradiated by the bremsstrahlung radiation from the linear accelerator. This combination of a fast scintillator and fast photomultiplier tube yielded a composite detector capable of fast speeds, good charge production and high gain.[1] Because of the typically short lifetimes concerned with in our work and, also, the expected high background count rates, CsF was chosen over the more popular, but slower NaI. The significant increase in count rate capability of CsF, whose principal decay constant[2] is 4.4 ns, over that of NaI (230 ns decay constant[3]) outweighed concerns over nearly commensurate losses in light output (CsF output[2] about 5 to 10 % of NaI). Furthermore, losses in energy resolution were of minor consideration due to the energy and temporal simplicity of the spectra being observed.

By far, the most intense emissions that the detection system had to contend with were those due to the nonresonant, Compton scattered photons produced during irradiation of the sample by the pumping x rays. Fortunately, the delayed nuclear fluorescence was temporally

resolved from the pumping pulse and a gating scheme designed to minimize the deleterious effects of the scattered radiation was implemented. Without gating the detector OFF during irradiation of the sample, the photomultiplier tube would be driven into saturation and premature deterioration of the photocathode would ensue. The scintillator itself cannot be gated, of course. Therefore, in order to minimize exposure of the scintillator to the scattered radiation a high degree of shielding and collimation was employed. These efforts helped minimize concerns about scintillator afterglow or phosphorescence[4] (another property for which CsF is superior to NaI).

The gating technique employed consisted of driving the focusing electrode of the photomultiplier tube into an OFF condition prior to each onset of a pumping pulse from the accelerator. At termination of the pulse, the operating potential of the focusing electrode was restored and normal operation of the photomultiplier tube resumed. This scheme is depicted in Fig. 9 in which it can be seen that an appropriately negative potential applied to the focusing electrode results in an effective OFF condition for the tube. Gating the focusing electrode[5-10] of an 8850 tube provides for a high contrast ratio (i.e., the quotient of the tube's ON gain to its OFF gain) and short gating transition times (on the order of 80 ns here).

An inherent drawback of gating a photomultiplier tube by direct switching of any of the electrode potentials is the generation of switching transients, caused by the capacitive coupling between the gated electrode and the anode of the tube, that may be inadvertently mistaken for signal photocurrents. In the case of an approximately rectangular gating pulse the corresponding transient output is a set of oppositely polarized spikes caused by differentiation of the original pulse. The precise shape of the transient output is, of course, determined by the shape of the gating pulse and the RC parameters of the differentiating output (which consists of the stray, coupling capacitance between the focusing electrode and the anode and the effective output

impedance of the detection system). Naturally, one seeks to minimize the effects of this output transient, and this can, in part, be done by adjusting, where possible, the parameters that influence its shape and magnitude. For fluorescent emissions sufficiently delayed, the gating transients do not present a problem.

NOISE CONTROL

One of the most serious concerns to affect efforts directed toward detecting and measuring delayed fluorescent emissions is that of electrical interference[11] produced by the operation of the linear accelerator itself. This form of interference has directly influenced the nature of the processing electronics, the physical arrangement and nature of signal cables, and, in fact, all electrical elements involved in the collection, transmission and processing of the detected signal. The principal sources of electrical noise are the high current and high voltage pulses that propagate along transmission lines from the pulsed power source (i.e., the modulator) to the accelerator unit itself. These pulses are delivered into an unshielded network of wires and components adjacent to the accelerating section of the linac. It has not proven practical to provide individual shielding of the networks and a more tractable approach of shielding the signal collection system has been pursued.

Following efforts to minimize conductive interference via ground loops, etc., Fourier decomposition of the power pulses was undertaken and it was found that the principal spectral components had frequencies below several hundred kHz. Due to these relatively lower frequencies and the confining dimensions of the signal collection system the most significant propagated contributions to the electromagnetic noise were seen to result from the inductive components[11,12] rather than the radiative components of the field. These inductive components result from both magnetic and electric contributions. In an effort to identify the precise sources and

nature of this mode of interference the photomultiplier tube, which acts as a high impedance current source, was disconnected from the signal cable leading from the accelerator chamber to the processing electronics and replaced with a resistor across the input to the cable as shown in Fig. 10. Figure 11 shows the resulting peak noise amplitude detected at the processing end of the cable as the input impedance of the cable was increased. It is interesting to note that the signal does not extrapolate to zero for large input resistances but instead tends to a constant level. The nature of this dependence on impedance suggests that the primary concern with the photomultiplier tube connected to the system is electrostatic coupling.

An effective approach taken to decouple the signal system from the noise source was that of placing a large sheet of copper (5 ft. x 6 ft.) on the chamber wall from which the signal cables entered the room for connection to the detector output. With an appropriate aperture through which the cables could emerge, the sheet surrounded the terminating ends of the cables and thus presented a substantial baffle to interfering fields. A copper box was constructed over the aperture with bulkhead cable connectors mounted on it for connection to the cables from inside in the chamber. The thickness of the copper sheet (approximately 0.7 mm) was sufficient to account for the skin depths of the significant frequencies encountered in the noise spectrum. In addition to the electrostatic baffle, high quality, double shielded coaxial cable was employed for transmission of the signal. With the implementation of this scheme significant reduction of the noise could be demonstrated as seen in Fig. 12.

Further refinement of the signal received by the processing electronics was achieved by constructing and inserting a passive, 50 ohm bandstop filter having band edges at approximately 200 kHz and 1200 kHz (Figure 13). This filtering action enhanced the baseline restoration of the signal following termination of the accelerator power pulse and gating of the detector by removing contaminating components that contained little or no useful information.

The efforts described thus far have addressed the issues of enhancing the signal to noise ratio of the detector output by minimizing the rf noise contents of the signal. Another effort that tends toward the same end is to minimize contamination of the original photon signal by contributions from possible delayed, but unrelated, emissions from the sample itself or from environmental materials exposed to the bremsstrahlung pulse. As indicated in Fig. 14 the output of the accelerator was spatially defined by a collimator constructed of lead and having dimensions of 14 inches length and an exit aperture of 1 inch. The photomultiplier tube/CsF detector was contained inside a graded cylindrical housing constructed of copper, tin and lead. Radiation entering the photomultiplier tube housing was restricted by a 4-inch length of collimation that terminated at the face of the crystal. To minimize noise photons having energies less than about 200 keV a lead filter 1/16 inch thick was placed at the entrance to the detector collimator. The significance of this filter was that it could limit the input of low energy photons at all times and not just during the periods of signal input. This limitation would help minimize[13] any slightly residual effects of afterglow in the crystal due to the tremendous burst of scattered radiation occurring during the pumping phase of the cycle.

DATA ACQUISITION, CONTROL AND PROCESSING

The anode timing output from the 8850 tube was inserted into a double shielded coaxial cable that connected to the cover box on the chamber wall. This fed, in turn, to the double shielded 50 ohm cable mentioned earlier that led to the processing electronics housed in a copper mesh screen room. The pulse handling electronics were fast, 50 ohm devices designed for high pulse rate data sources (Fig. 15).

The block diagram shown in Fig. 15 illustrates both the logic layout for synchronizing and controlling the gating electronics and the signal processing and timing electronics used for

recording the timing spectrum of the decaying isomer. As seen in the diagram, the reference signal for initiating the gating process was derived from a synchronizing pulse provided at the modulator when the main thyratron was triggered into commutation. This analog pulse was converted to a TTL pulse with a nonretriggerable 74121 multivibrator chip. The TTL pulse then served as an external trigger for the DG 535 digital delay pulse generator. Two independent, logical outputs of the DG 535 were time-adjusted to initiate two independent sequences of events. The first of these events was that of triggering the HV pulse generator into producing a gating pulse for the focusing electrode of the photomultiplier. Upon arrival of this appropriately shaped negative pulse at the focusing electrode of the photomultiplier tube the ON bias at the electrode supplied by the dc power supply was canceled. The HV power supply maintained the normal +1800 V bias for the photomultiplier tube and the dc power supply biased the focusing electrode to an ON voltage of +650 V. The gating pulse was typically set to -820 V and had a typical width of 10 microseconds.

The second event triggered by the DG 535 output was the timing sequence for recording the decaying fluorescence spectrum being emitted by the irradiated sample. This timing sequence began with arrival of the START pulse from the DG 535 at the input of the time-to-amplitude converter (TAC). This signal was, of course, delayed until termination of the linac pulse and until any residual, nontractable noise had sufficiently decayed to acceptable levels. The TAC measured the time interval between arrival of the START pulse and a STOP pulse. The STOP pulse was derived from the processed signals coming from the detector output. With this technique only one timing count could be recorded per linac pulse. So the timing spectrum was accumulated over many cycles of linac operation. The output of the TAC (an analog signal whose amplitude is proportional to the measured timing interval) was fed into a multichannel analyzer whose response was calibrated to indicate time per channel. The method is similar to that of

delayed coincidence techniques except that here an artificial reference pulse, synchronized to the irradiation cycle, was used for initiating the timing sequence. The multichannel analyzer displayed counts vs time.

As indicated in the previous chapter, the success of the efforts, and the validity of the techniques described here have been beautifully demonstrated for the cases of ^{181}Ta and ^{176}Hf. Figure 16, reproduced from chapter one, demonstrates the delayed emissions obtained from the two isomers. The statistics and simplicity of the spectra were sufficient to allow derivation of the characteristic relaxation times by the straightforward slope technique frequently employed in delayed coincidence measurements.

ACCELERATOR MODIFICATIONS

Unfortunately, before isomers having shorter lifetimes could be studied, and prior to any further refinements of the data acquisition and processing systems, a sequence of accelerator problems which would eventually remove the linac from operation for a period of more than seven months began to develop. Following approximately fifty hours of beam-time operation a loss of vacuum by the accelerator waveguide was incurred due to a failure of the electron beam exit window. This failure necessitated a return of the waveguide under warranty to the manufacturer for repair of the window. They elected to replace, as a normal course for such failures, the electron gun at the input end of the guide and to replace the previously .002 inch thick copper/berylium exit window with .001 inch thick 310 stainless steel. Unfortunately, this window failed within one hour of operation following its return and installation. The machine was once again returned under warranty to the manufacturer. This time a major reconsideration of the failure modes of the exit windows was undertaken without cost to our contract. Following a substantial number of consultations with university personnel, outside consultants

contracted by the manufacturer, and their own staff, a reengineering effort was begun that would address three major issues relating to durability of the exit window. The first, and most significant of these, was the optimum thickness and material for the exit window. The second concerned the most practical cooling methods for the window and the third, which eventually involved reengineering the output, addressed the incorporation of a maintenance program in which the exit window could be replaced prior to failure.

The eventual selection of appropriate window material, and more importantly, window thickness was governed by failure modes that were critically dependent on the energy deposited in the window by the beam, by eddy currents driven by residual accelerating fields emanating from the resonant standing waveguide and by considerations of exit beam divergence caused by electron beam scattering within the window. The residual fields were removed from the drift space leading to the exit window by the incorporation of absorption pads designed for efficient operation at microwave frequencies. A more difficult problem to address was the dissipation of the excess energy deposited in the window by the pulsed electron beam. All three modes of heat transfer were considered as to their effectiveness in removing excess energy from the window. It was determined that efforts to maintain an oxide-free surface was very important for maintaining an optimum radiative component of heat transfer and that direct cooling of the surface with either water or a flow of compressed air was critical. The third method of heat transfer, viz., that of conduction, was perhaps the most significant in determining the optimum thickness of the window. Not surprisingly, opposing mechanisms strongly influenced the consideration of thickness. For example, the thicker the window, the greater the conductive removal of energy, but also the greater the deposition of energy by the electron beam.

After much consideration two proposals were presented to the university: (1) an exit window cooled by the direct flow of a 1 mm thick layer of water between two surfaces of

.002 inch thick layers of stainless steel and (2) a .003 inch thick copper/berrylium window cooled directly by a jet of compressed air and indirectly by a water cooled coil placed at the circumference of the window. The final selection from these two proposals was based on three considerations : (1) the effect on beam brightness (i.e., beam divergence), (2) the energy removed from the beam and (3) the final dose from the photon beam following energy conversion at the bremsstrahlung target. After tests performed on location at the manufacturing site in California by both the manufacturer and our university personnel the air cooled copper/berrylium window was chosen for final placement on the machine. This window was mounted on the reengineered output section of the guide that provided for routine maintenance of the accelerator by prescheduled replacement of the window.

The guide was returned to the University of Texas at Dallas in mid-February, 1993. Unfortunately, it was damaged during shipment and had to once again be returned to the manufacturer. This necessitated another round of repairs and tests. The guide was finally returned to UTD on April 7, 1993. A representative from the manufacturer reinstalled the guide and began a series of tests to optimize performance. During this operation, the pulse transformer that drives both the e-gun and magnetron failed. A replacement transformer was installed and tests resumed on May 25, 1993. A successful reinstallation and series of test runs was finally completed on May 27, 1993.

All aspects of repair and reengineering of the accelerator have been performed under warranty at no additional cost to the contract. The parties involved have been most cooperative in adapting the machine from the reasonably light duties customary for medical-like applications to those requiring long, intensive machine runs. As presently configured, the UTD linear accelerator will play a well-defined and central role in the gamma-ray laser research effort at the Center for Quantum Electronics.

REFERENCES

1. RCA 8850 Photomultiplier Tube Specifications Sheets (unpublished).
2. Introductory Nuclear Physics, First Edition, K. L. Krane (John Wiley & Sons, Inc., New York, 1988).
3. Harshaw/Filtrol Scintillation Phosphor Specifications Sheets (unpublished).
4. Scintillation Crystals Performance Specification Booklet (unpublished, Solon Tech. Inc.).
5. N. Klein and T. J. Rock, Rev. Sci. Instrum. 41, 1671 (1970).
6. D. G. Jameson and J. J. Martin, J. Phys. E. : Sci. Instrum. 8, 635 (1975).
7. T. M. Yoshida, T. M. Jovin and B. G. Barisas, Rev. Sci. Instrum. 60, 2924 (1989).
8. U. Fairnelli and R. Malvano, Rev. Sci. Instrum. 29, 699 (1958).
9. K. B. Keller and B. M. K. Nefkens, Rev. Sci. Instrum. 35, 1359 (1964).
10. B. L. Elphick, J. Phys. E. 2, 953 (1969).
11. Electrical Interference, Rocco F. Ficchi (Hayden Book Co. Inc., New York, 1964).
12. Principles of Electromagnetic Compatibility, Third Edition, Bernhard Keiser (Artech House Inc., 1987).
13. V. Ponomarev, A. P. Dubenskiy, V. P. Dubenskiy and E. A. Boykova, J. Phys. G. : Nucl. Part. Phys. 16, 1727 (1990).

CAPTIONS

Figure 1: Pier drilling following excavation.

Figure 2: Installation of reinforcement bars for ceiling.

Figure 3: View of chamber from northeast with laser lab in left background.

Figure 4: Packed soil surrounding walls.

Figure 5: View from the east --- soil placed on top of chamber.

Figure 6: Simulation frame showing accelerator location inside chamber.

Figure 7: Posts installed for chain link fence.

Figure 8: Placement of accelerator system.

Figure 9: (a) PMT focusing electrode and dynode potentials in the ON and OFF states. (b) Corresponding gating voltage to focusing electrode.

Figure 10: Test arrangement for studying EMI.

Figure 11: Noise amplitude vs resistance for test system of Figure 10.

Figure 12: Noise levels into 50 ohm scope showing effectiveness of shielding. (a) Noise without copper sheet rf shielding and with common coaxial cable. (b) Noise without copper sheet rf shielding and with double shielded cable. (c) Noise with copper sheet rf shielding and with double shielded cable.

Figure 13: 50 ohm tee bandstop filter.

Figure 14: Experimental arrangement for detecting fluorescent emissions from irradiated sample.

Figure 15: Block diagram for control and processing electronics.

Figure 16: Timing spectra showing fluorescence from microsecond excited states of (a) ^{181}Ta and (b) ^{176}Hf.

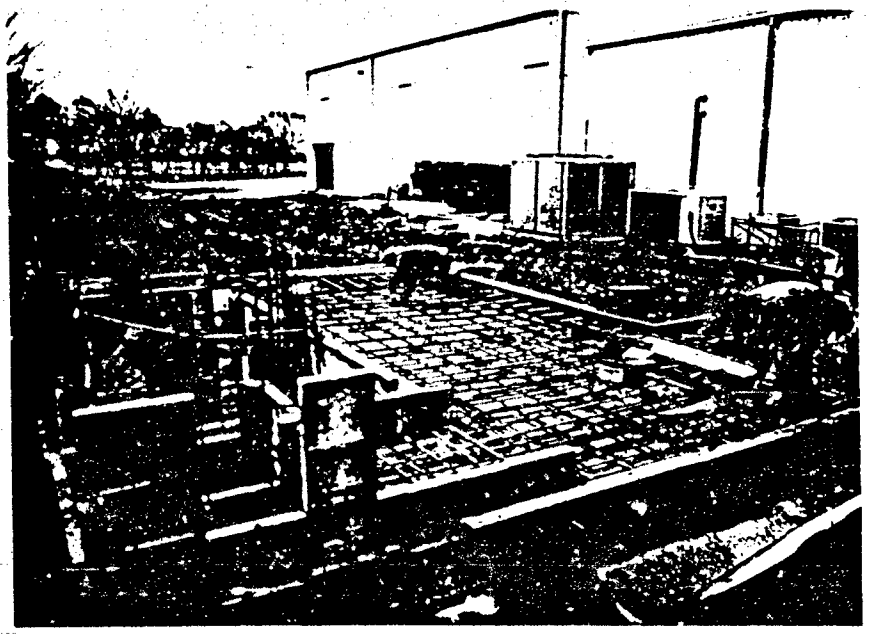

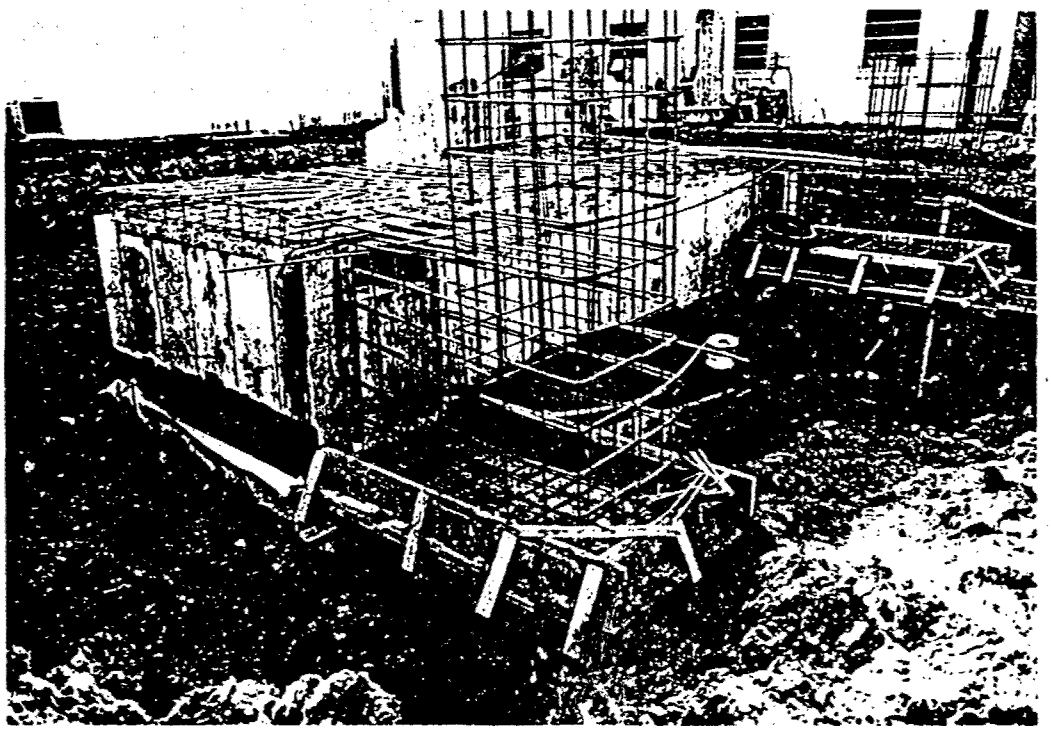

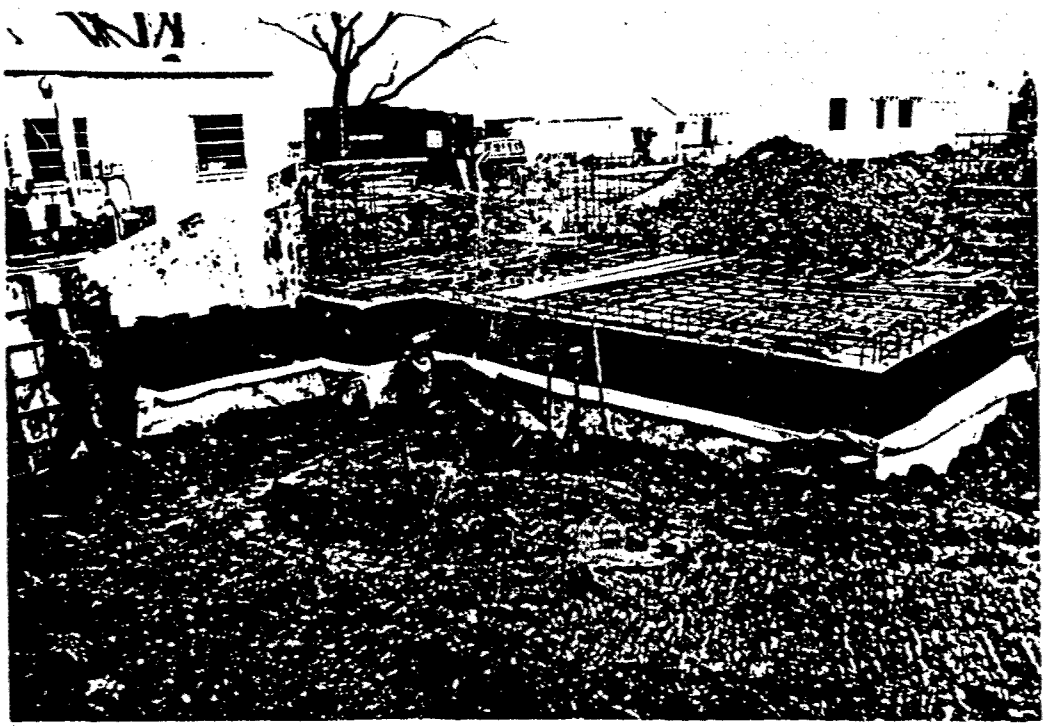

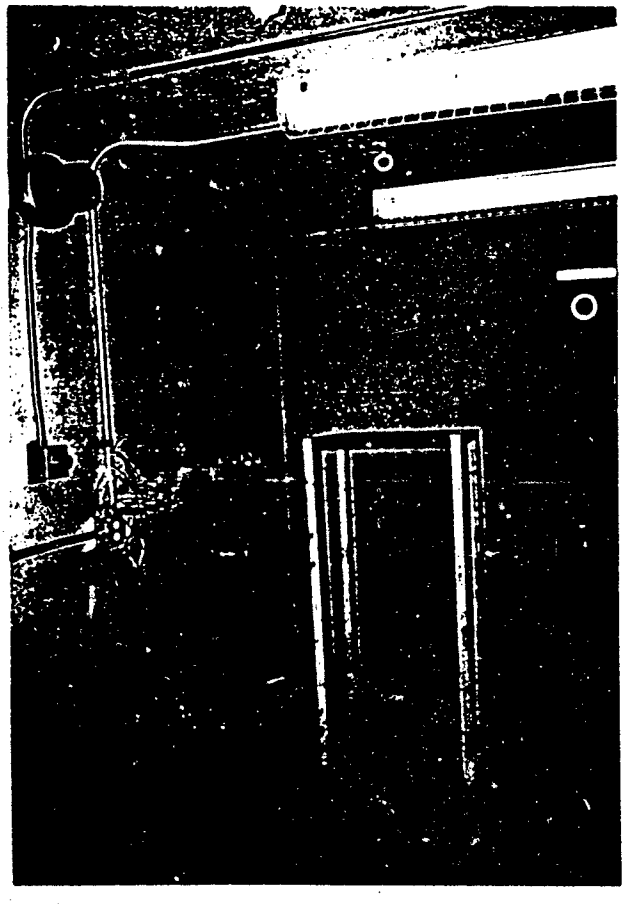

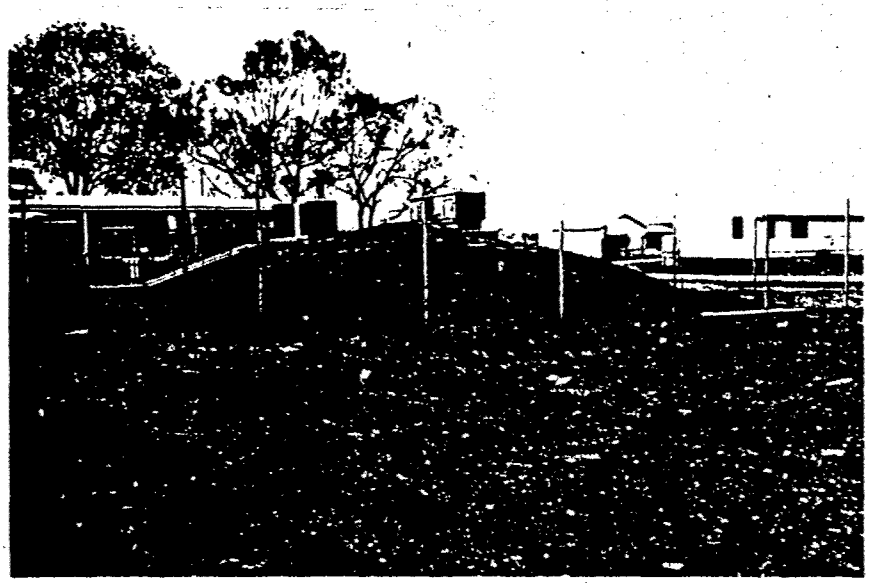

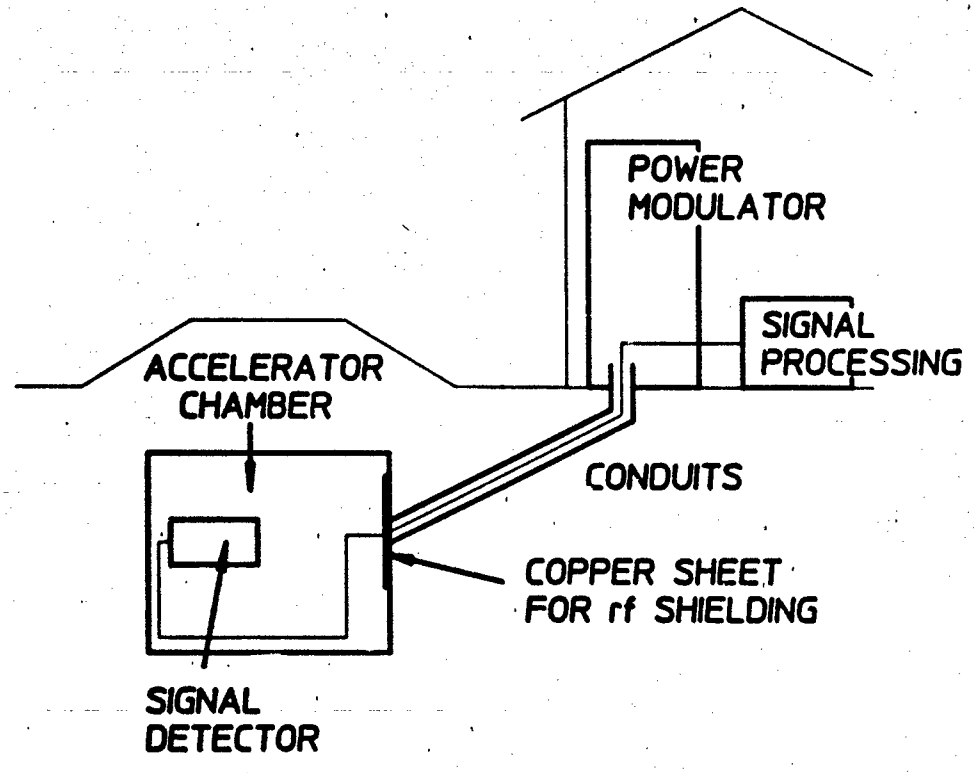
POWER
MODULATOR
SIGNAL
PROCESSING
ACCELERATOR
CHAMBER
CONDUITS
COPPER SHEET
FOR rf SHIELDING
SIGNAL
DETECTOR

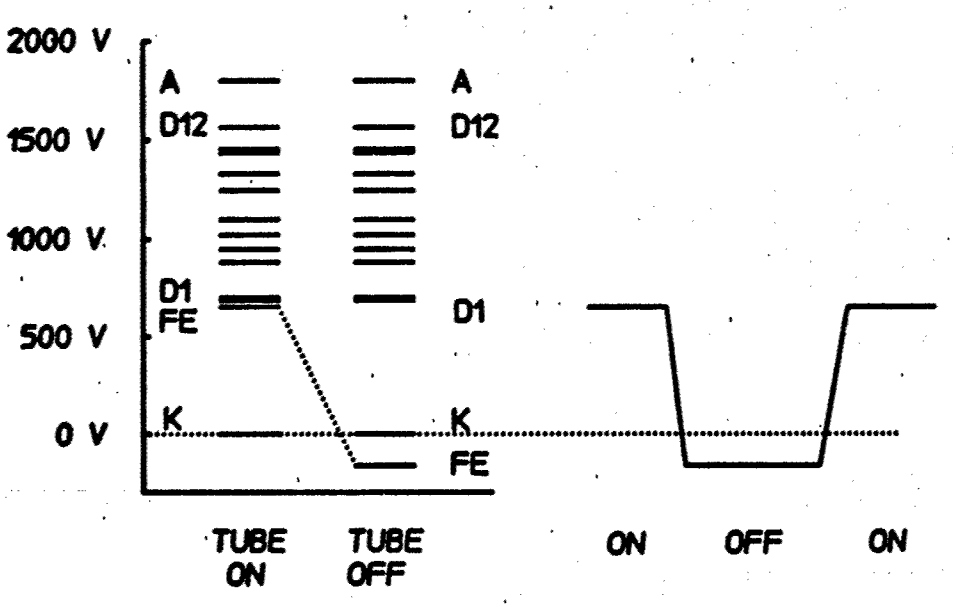
2000 V
1500 V
1000 V
500 V
0 V
A
D12
D1
FE
K
A
D12
D1
K
FE
TUBE ON
TUBE OFF
ON
OFF
ON

(a) (b)

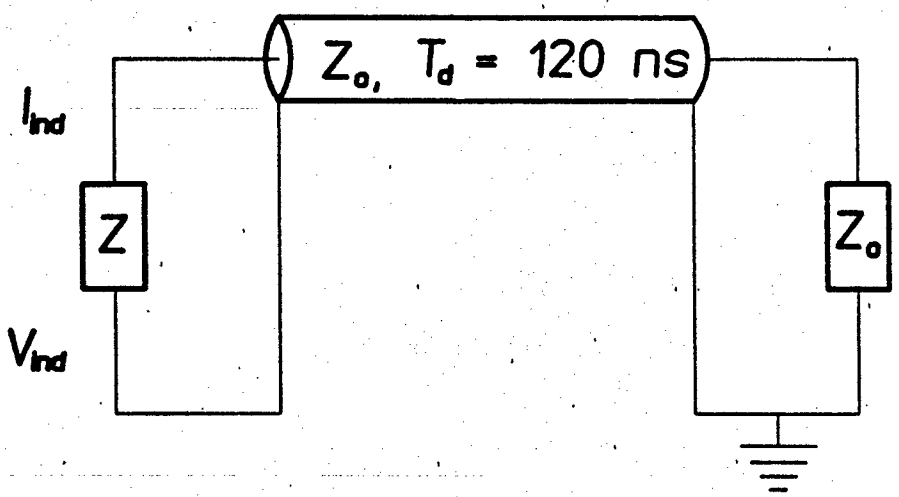

PICKUP DETECTION

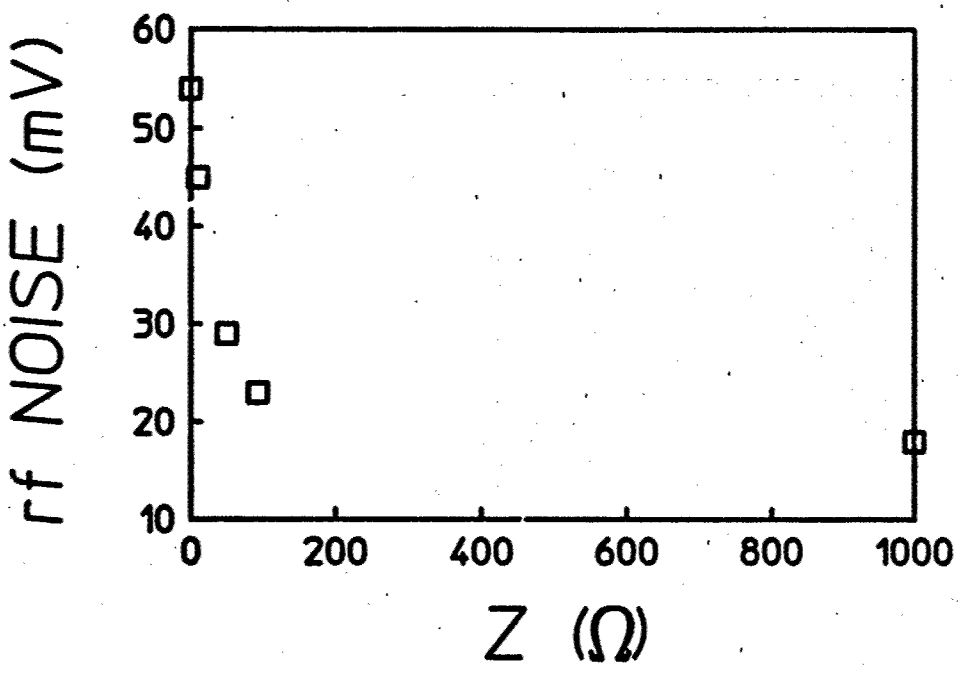
rf NOISE (mV)
60
50
40
30
20
10
0
200
400
600
800
1000
Z (Ω)

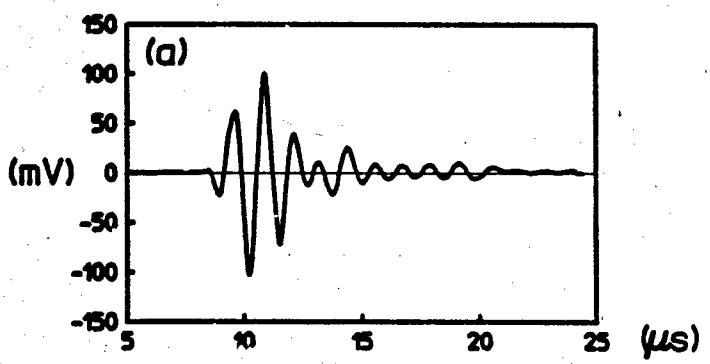
(a)
150
100
50
(mV) 0
-50
-100
-150
5
10
15
20
25
(μs)

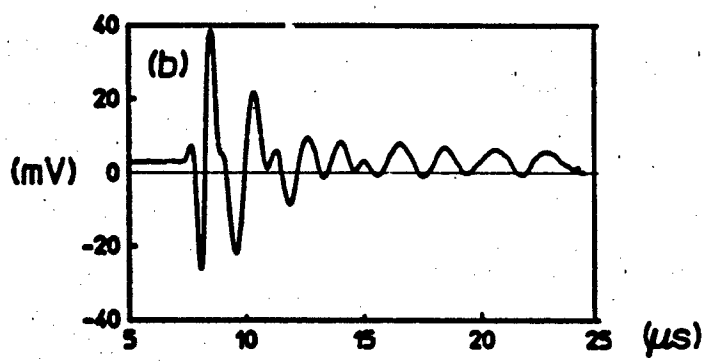
(b)
40
20
(mV) 0
-20
-40
5
10
15
20
25
(μs)

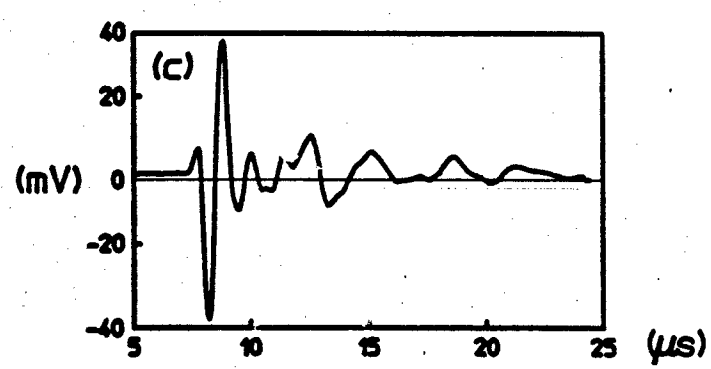
(c)
40
20
(mV) 0
-20
-40
5
10
15
20
25
(μs)

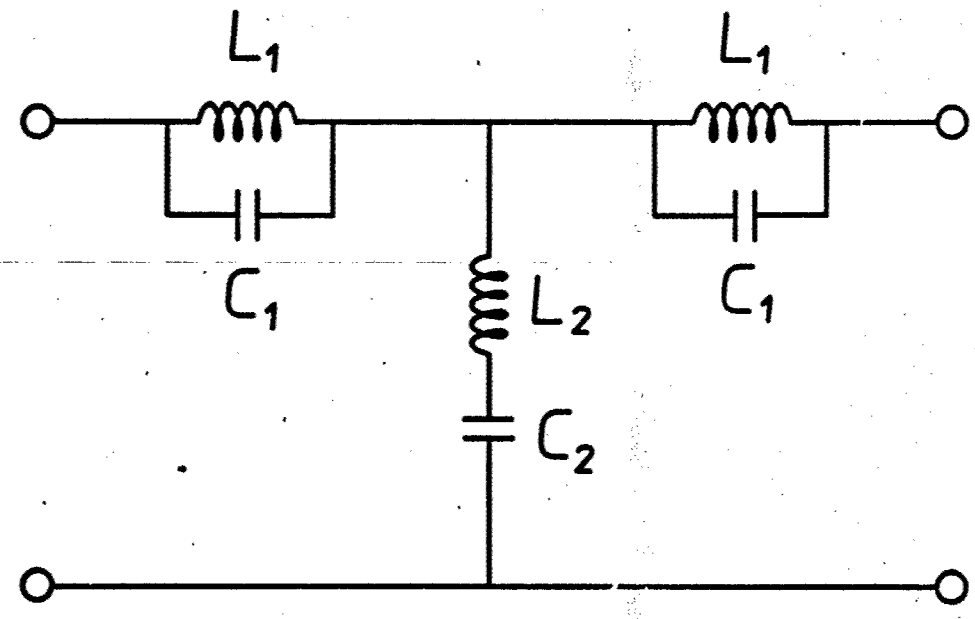
L1
L1
C1
L2
C1
C2

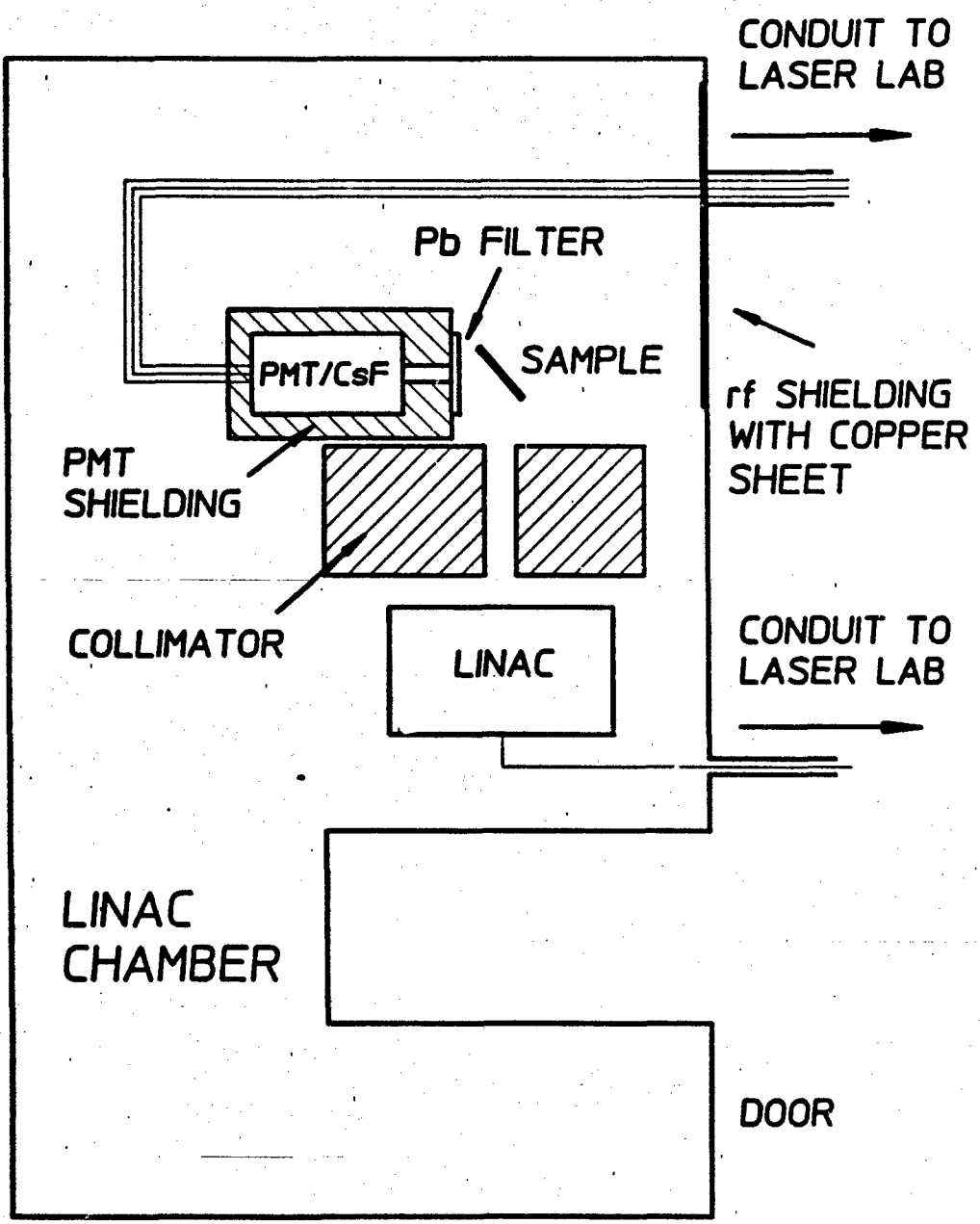
CONDUIT TO
LASER LAB
Pb FILTER
SAMPLE
PMT/CsF
rf SHIELDING
WITH COPPER
SHEET
PMT
SHIELDING
COLLIMATOR
LINAC
CONDUIT TO
LASER LAB
LINAC
CHAMBER
DOOR

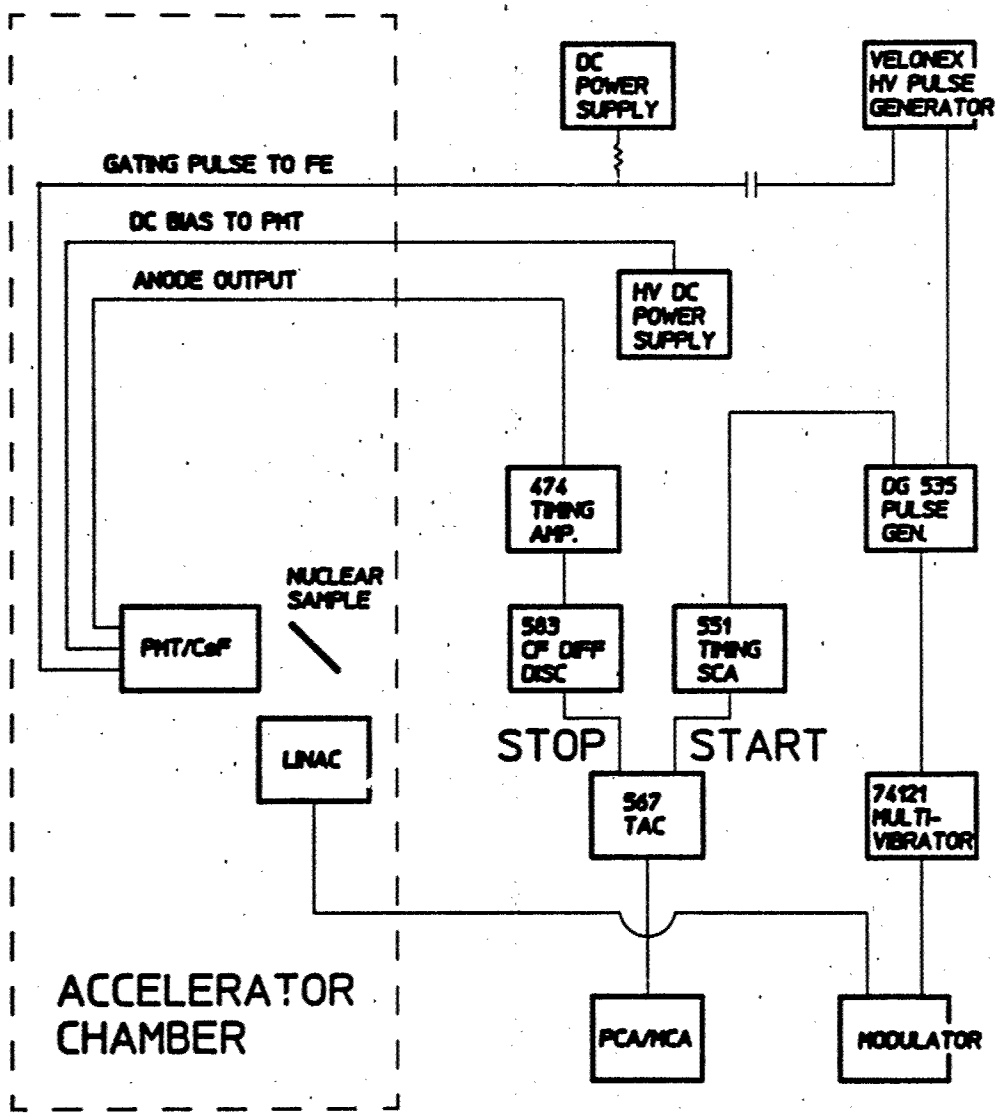
DC POWER SUPPLY
VELONEX HV PULSE GENERATOR
GATING PULSE TO FE
DC BIAS TO PMT
ANODE OUTPUT
HV DC POWER SUPPLY
474 TIMING AMP.
DG 535 PULSE GEN.
NUCLEAR SAMPLE
PMT/CaF
583 CF DIFF DISC
551 TIMING SCA
LINAC
STOP
START
567 TAC
74121 MULTI-VIBRATOR
ACCELERATOR CHAMBER
PCA/MCA
MODULATOR

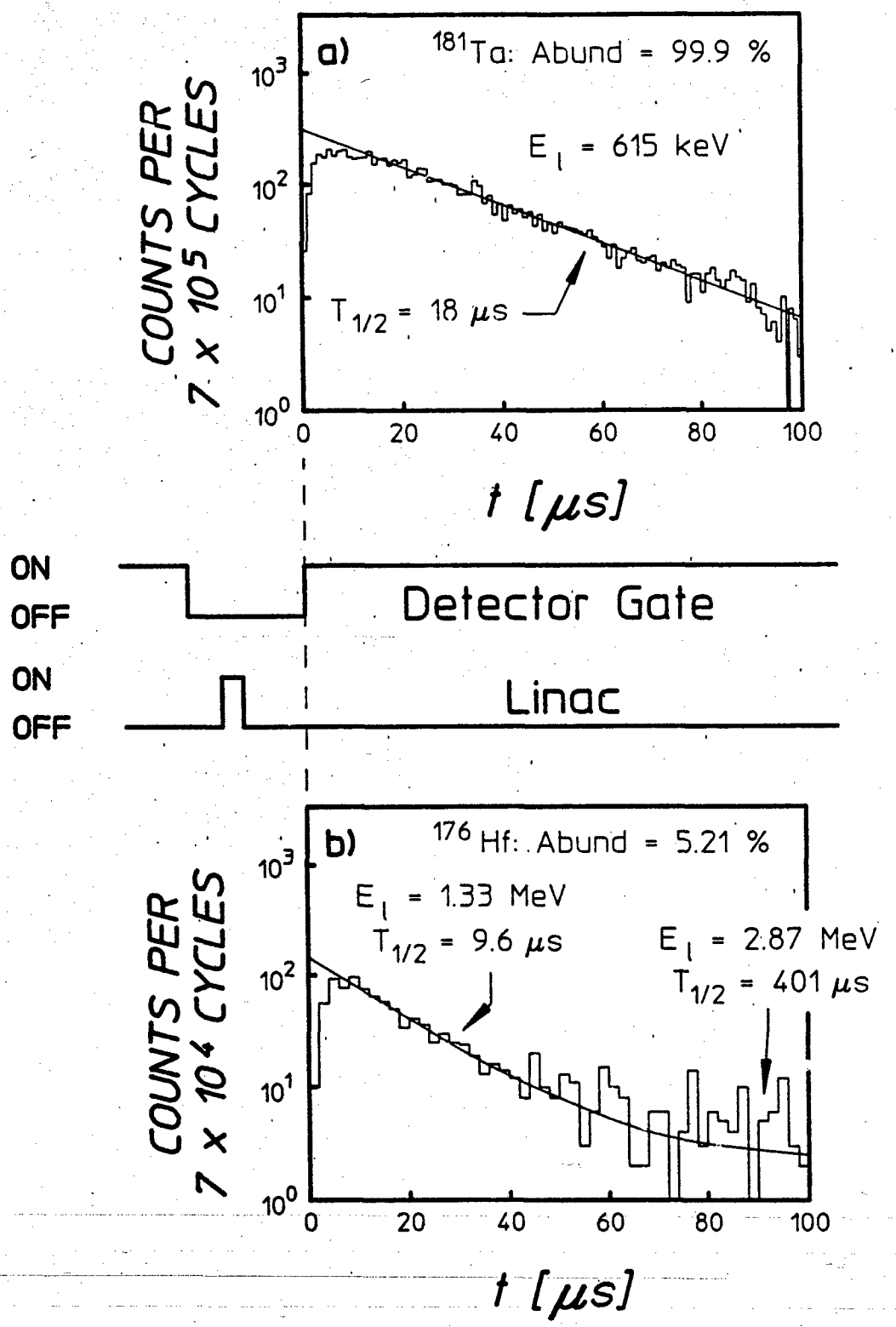
a)
^{181}Ta: Abund = 99.9 %
E_l = 615 keV
$T_{1/2}$ = 18 μs
COUNTS PER 7 x 10^5 CYCLES
10^3
10^2
10^1
10^0
0
20
40
60
80
100
t [μs]
ON
OFF
Detector Gate
ON
OFF
Linac
b)
^{176} Hf: Abund = 5.21 %
E_l = 1.33 MeV
$T_{1/2}$ = 9.6 μs
E_l = 2.87 MeV
$T_{1/2}$ = 401 μs
COUNTS PER 7 x 10^4 CYCLES
10^3
10^2
10^1
10^0
0
20
40
60
80
100
t [μs]